GEORGIA INSTITUTE OF TECHNOLOGY — OFFICE OF CONTRACT ADMINISTRATION

PROJECT ADMINISTRATION DATA SHEET

[x] ORIGINAL [ ] REVISION NO. _____

Project No. E-23-624 DATE 4/15/82

Project Director: Dr. J. T. S. Wang School/~~Lab~~XXX ESM

Sponsor: Lockheed - Georgia Company

Type Agreement: Purchase Order No. CY48335

Award Period: From 1/16/82 To ~~9/15/82~~ 12/30/83 (Performance) 9/15/82 (Reports)

Sponsor Amount: $40,000 Contracted through: 12/31/83

Cost Sharing: $23,250 (E-23-350) GTRI/~~GUXX~~

Title: Damage of Composite Structures

ADMINISTRATIVE DATA

OCA Contact Faith G. Costello x-4820

QUARTERLY PROGRESS REPORTS

1) Sponsor Technical Contact:

Mr. John N. Dickson
Advanced Structures Department
Lockheed-Georgia Company
Marietta, GA 30063

2) Sponsor Admin/Contractual Matters:

W. R. Britton, Senior Buyer
Direct Charge Group
Department 52-25, Zone 383
Lockheed-Georgia Company
Marietta, GA 30063

Phone: 424-5250

Defense Priority Rating: N/A

Security Classification: N/A

RESTRICTIONS

See Attached N/A Supplemental Information Sheet for Additional Requirements.

Travel: Foreign travel must have prior approval – Contact OCA in each case. Domestic travel requires sponsor approval where total will exceed greater of $500 or 125% of approved proposal budget category.

Equipment: Title vests with Sponsor; however, none proposed

COMMENTS:

APR 1982 RECEIVED Research Reports Office

COPIES TO:

Research Admin. Network
Research Property Management
Accounting
Procurement/EES Supply Services
Research Security Services
~~Reports Coordinator (OCA)~~
Legal Services (OCA)
Library
EES Public Relations (2)
Computer Input
Project File
Other _____

FORM OCA 4:781

GEORGIA INSTITUTE OF TECHNOLOGY OFFICE OF CONTRACT ADMINISTRATION

SPONSORED PROJECT TERMINATION/CLOSEOUT SHEET

Date 2/10/84

Project No. E-23-624 School/~~XXX~~ ESM

Includes Subproject No.(s)

Project Director(s) Dr. J. Wang GTRI / ~~XXX~~

Sponsor Lockheed - Georgia Company

Title Damage of Composite Structures

Effective Completion Date: 12/31/83 (Performance) 12/31/83 (Reports)

Grant/Contract Closeout Actions Remaining:

- [ ] None
- [x] Final Invoice ~~XXXXXXXXXXXXXXXX~~
- [ ] Closing Documents
- [x] Final Report of Inventions
- [ ] Govt. Property Inventory & Related Certificate
- [ ] Classified Material Certificate
- [ ] Other

Continues Project No. Continued by Project No.

COPIES TO:

Project Director (Wang)
Research Administrative Network
Research Property Management
Accounting
Procurement/EES Supply Services
Research Security Services
Reports Coordinator (OCA)
Legal Services

Library
GTRI
Research Communications (2)
Project File
Other

Form OCA 60:1028

E23-624

ENGINEERING COLLEGE
GEORGIA INSTITUTE OF TECHNOLOGY

SCHOOL OF ENGINEERING SCIENCE
AND MECHANICS
225 NORTH AVENUE, N.W.
ATLANTA, GEORGIA 30332

April 20, 1982

Mr. John N. Dickson
Department 72-77
Mail Zone 415
Lockheed-Georgia Company
Marietta, Georgia 30063

Subject: Research Grant P. O. No. CY48335
Progress Report (1/16/82 thru 4/15/82)
(Georgia Tech Project No. E-23-624)

Dear Mr. Dickson:

During the subject period, emphasis has been focused on literature reviews, exploratory types of studies, identification and formulation of problems related to the dynamic response, wave propagation, damage characterization and prediction of residual strength of composite laminates subjected to transverse normal impact. The following represents a summary of the progress of research under the subject grant, and more detailed discussions on various aspects are also enclosed:

(1) Dynamic response of orthotropic laminates subjected to impulse loading based on the modal analysis is examined. The analysis concerning the flexural wave only could be suitable for low speed impact investigation. Numerical results may also be used for future comparison to more exact wave propagation analysis. Examples for a simply supported composite laminate subjected to a central point impact and impact of a uniformly distributed loading are enclosed. Numerical results indicate that in the limit of delta function impulse impact, large strain occurs before the flexural wave reaches the boundary when the plate is under the point impact. Consequently, boundary conditions will not be important for this case.

(2) For exploring the through-thickness response, a discrete model consisting of a system of springs and concentrated masses is considered. While the effective mass and stiffness of springs for each ply (or ply group) can not be adequately established, relative magnitudes are used to give qualitative indications of the wave phenomenon including the relative instances at which the maximum response of each point mass and peak tension waves occur. Examples for a three degrees of freedom system are enclosed.

(3) The transient impact problem concerning the propagation of stress wave in elastic composite plates consisting of a number of layers of different properties has been formulated with sufficient generality. Inasmuch as the boundary effect is not important for a laminate under central impact as indicated under (2), it is intended that Laplace transform in time and

Fourier transform in space will be applied to the set of resulting differential equations for interfacial stresses and displacements, and the inverse transformation will be determined numerically.

(4) Delamination is generally considered to be the dominant energy absorbing mechanism in fracture of impacted laminates. Estimation of the residual strength of an impact-damaged laminate required an analysis of delamination growth. We observe that when delamination reaches an existing transverse matrix crack, it is likely to shift from the original interlaminar plane to an inner interlaminar plane. Subsequent delamination growth is investigated by solving a buckling problem of a stepped delamination layer. There are indications that, compared to the delamination growth along the original interlaminar plane, our stepped layer model yields a larger strain energy release rate and assigns a more prominent role to the mode II fracture behavior. The result of this analysis can be a critical factor in the residual strength prediction of an impact-damaged laminate.

Sincerely yours,

R. K. Kunz, Assistant Professor

J. T. S. Wang, Professor

W.-L. Yin, Associate Professor

ew

Enclosure

1. Dynamic Response of Orthotropic Laminates

The general solution subject to classical laminated plate theory for a simply supported rectangular composite plate subjected to transverse loading, and data used in the examples are summarized on the next page. The results for the first example concerning the response of the plate to central point impact are shown in Fig. (1). It indicates that severe flexural strains have occurred before t = 0.0001 sec., and the wave is still far from the boundary line. Consequently, the boundary effect is not important for this case. The response for the plate under uniformly distributed impact loading is shown in Fig. (2), and the boundary conditions will affect the dynamic response. While only response curves are shown in Figs. (1) and (2), interfacial stresses may be subsequently computed according to the laminated plate theory.

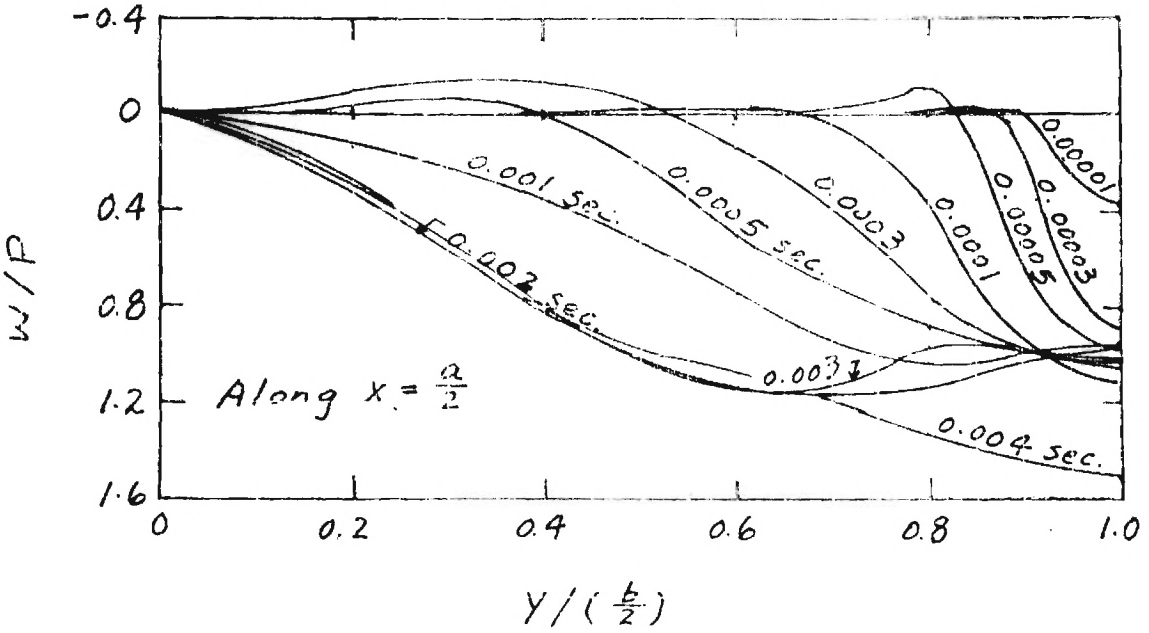

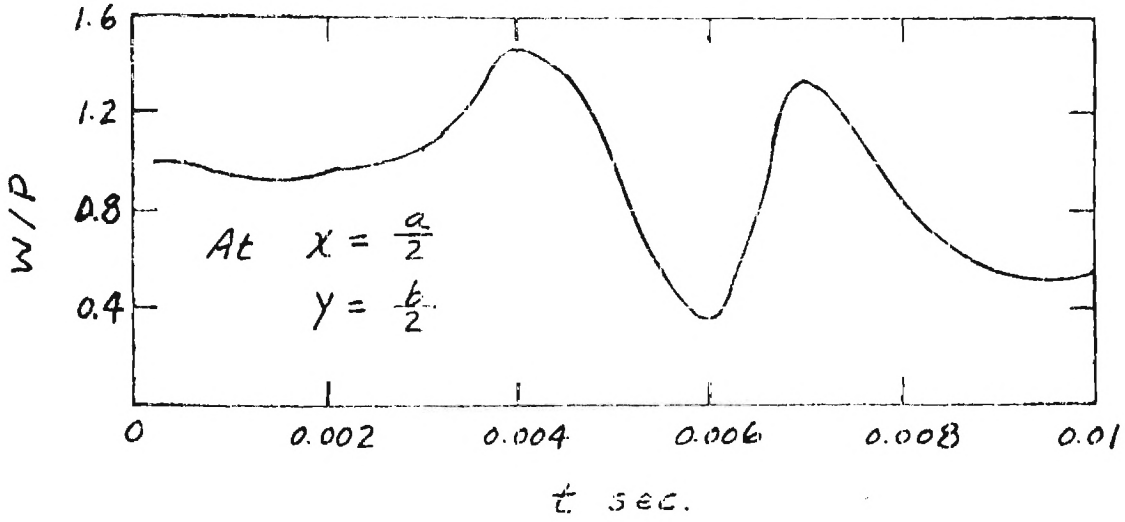

Fig. 1

Response under Point Load

$q = P\,\delta(x - \frac{a}{2})\,\delta(y - \frac{b}{2})\,\delta(t)$

with $N_x = N_y = 0$

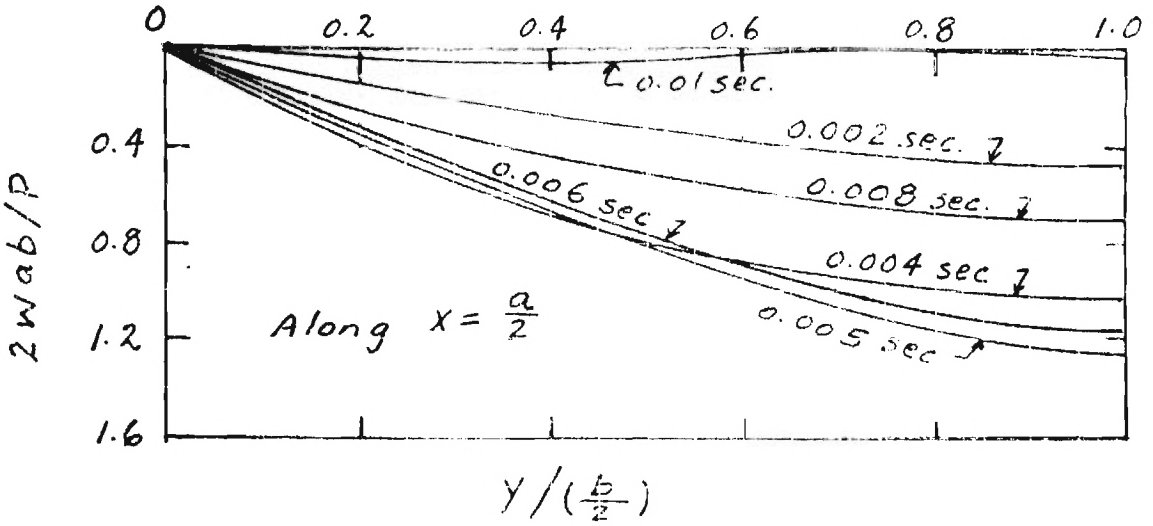

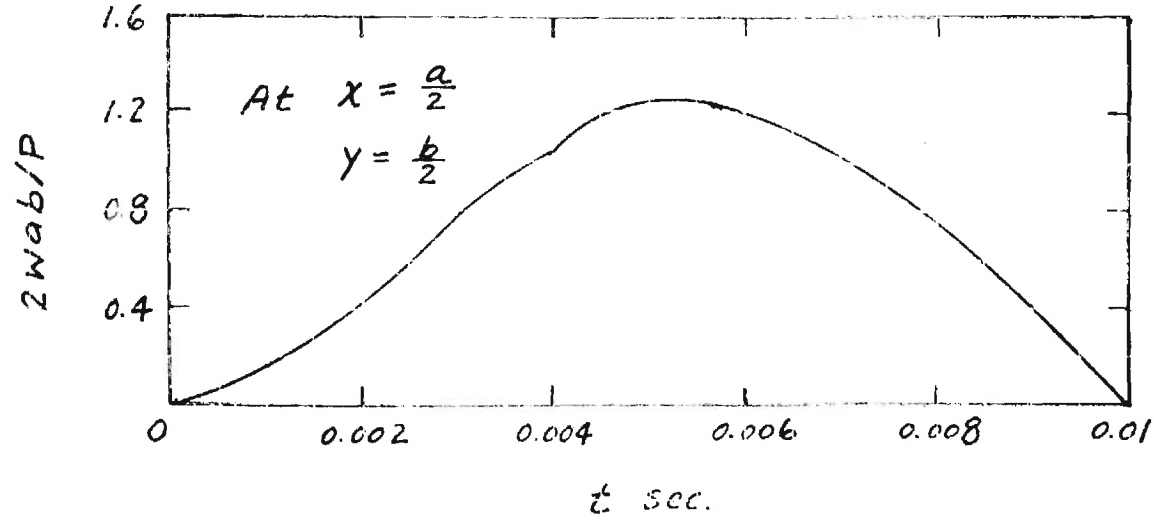

Fig. 2

Response under Uniform Load

$q = \frac{P}{ab}\delta(t)$

with $N_x = N_y = 0$

2. Discrete Models

To qualitatively explore the through-thickness dilatational wave motion, systems of point masses connected by linear springs, as shown in Fig. (3), are modelled to represent the layered construction of composite laminates. The structural stiffness of a general ith ply or lamina is characterized by K_i, and the interfacial stiffness is characterized by k_i. Non-zero k_n may represent that the region under consideration is at the support. Otherwise, k_n should be zero. Numerical examples for a three degrees of freedom system with numbering system shown in Fig. (3b) are considered. While it is difficult to establish adequate values for K_i, k_i and m_i, relative magnitudes are used. Responses for the example problems plotted against the dimensionless time are shown in Figs. (4) and (5). The shaded regions represent occurrence of tension waves, and the bold vertical lines represent peak interfacial tensile forces when multiplied by k_i. While the peak tension may occur at one interface earlier than the peak occurs at another interface, the magnitude of the peak tension occurring at the later time may be larger. It is therefore important that a reliable failure criterion must be established first before the location of damage initition can be determined.

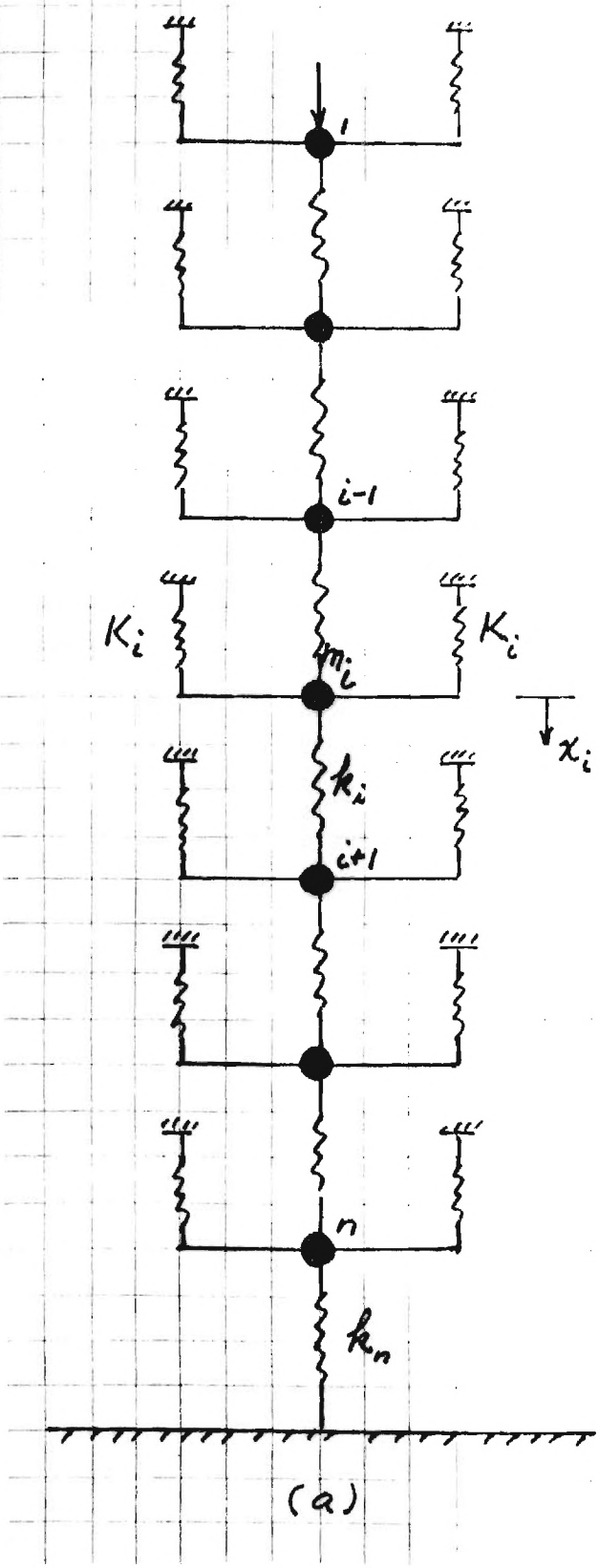

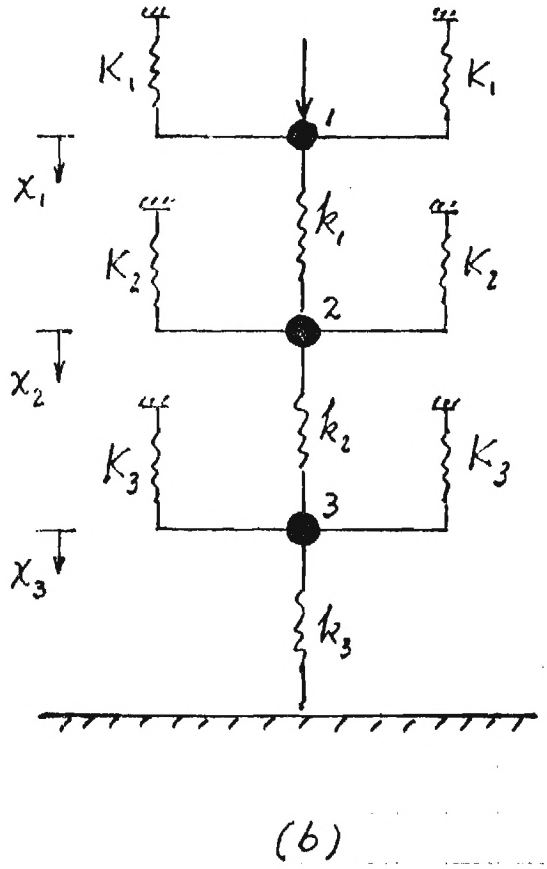

Fig. 3 Discrete Models

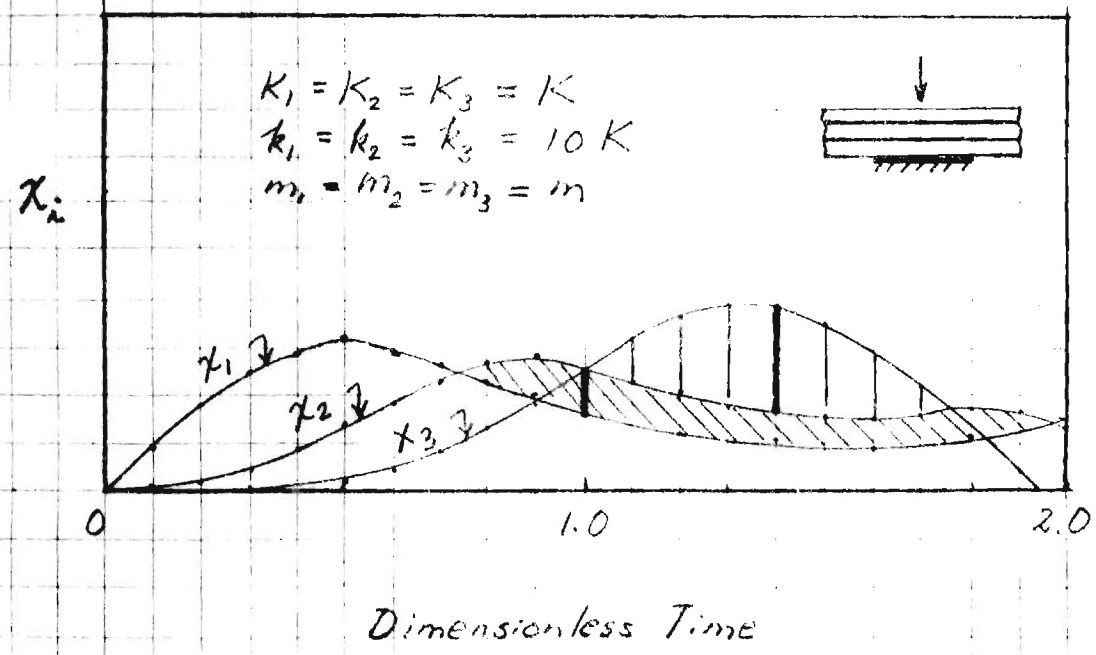

Fig. 4 Response of a Discrete Model

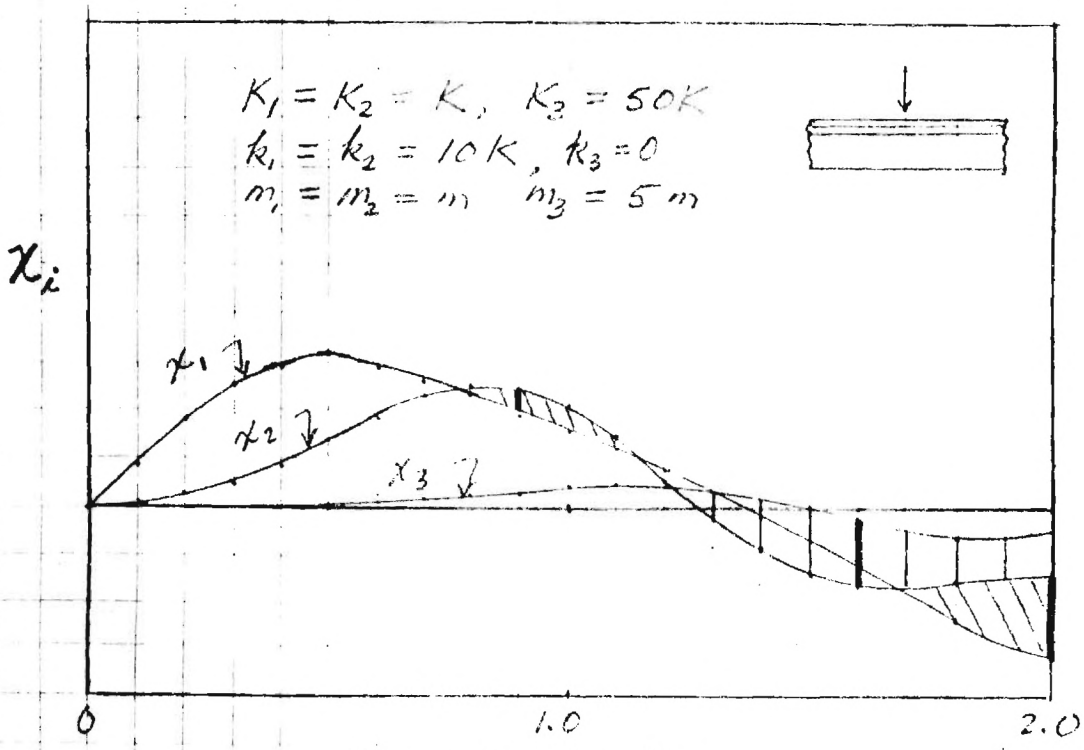

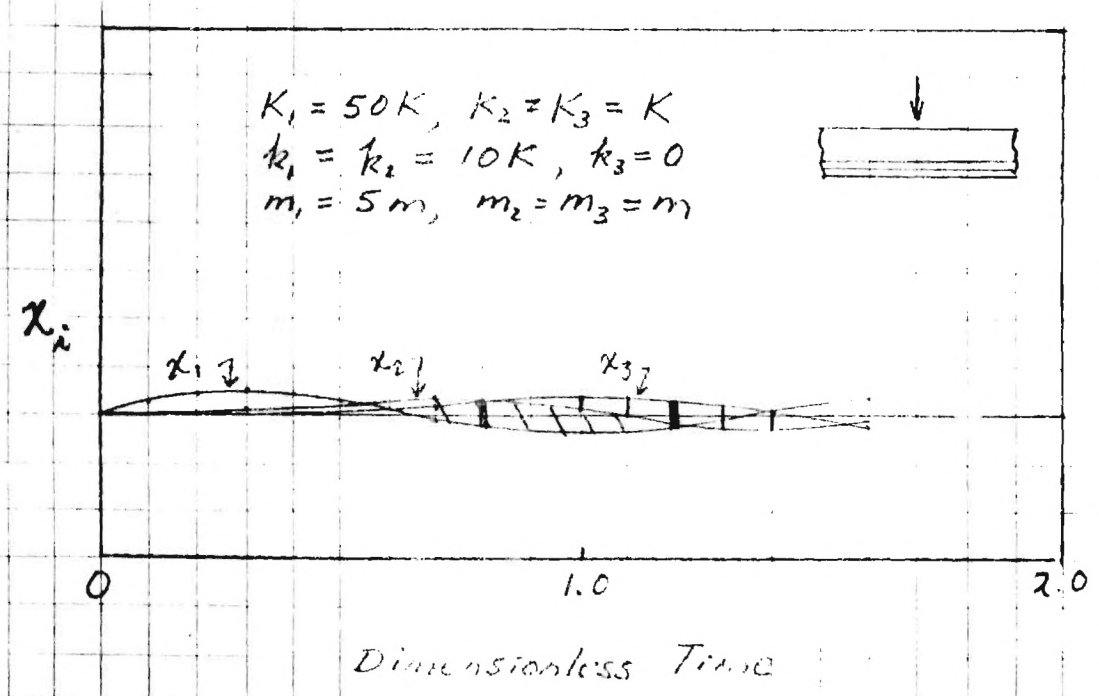

Fig. 5 Response of Discrete Models

3. Wave Propagation Due to Impact in Laminated Composite Plates

The primary emphasis in the work described in this section is the analytical determination of the propagation of stress waves in elastic composite plates, generated due to impact on the plate surface. In order to examine the initiation of impact-induced delaminations, the interlaminar stresses as functions of position and time are of fundamental interest. It is hoped that, when completed, the analysis will provide for the investigation of the influence of material properties and stacking sequence on the propagation of elastic-waves.

This basic problem has attracted some previous analytical research efforts in recent years. Dong and Nelson [1] and Kubo and Nelson [2] employ a finite element-normal mode method in which the displacement components in each lamina are approximated by a quadratic function of position in the thickness direction. Upon assembling the laminae into a plate, the free vibration problem is solved, yielding natural frequencies, mode shapes, and the associated dispersion relations. The transient impact problem is then solved as a linear combination of the normal modes. The primary disadvantage of this approach is the requirement that, due to the nature of the impact loading, a large number of modes must be obtained to insure accuracy.

In an approach by Moon [3,4,5] and Kim and Moon [6], displacements in each layer are represented by a Legendre polynomial expansion in the thickness direction. A set of equations of motion is obtained for each layer, and the layers are assembled to yield a set of equations in which interfacial displacements and stresses are explicit unknowns. Equations are solved using integral transform techniques. The advantage of this method is that the use of integral transforms enables the efficient determination of transient solutions without the necessity of first

obtaining modal solutions. In the work described in [6], however, the results are restricted to the case of line impact on a plate consisting of a series of orthotropic layers, all of which are identical as to material properties and orientation.

In this work, the basic approach of Moon will be followed, due to its efficiency in the handling of the transient impact problem. However, the formulation will be generalized to include full three-dimensional impact on a plate consisting of a series of orthotropic layers, each of which may have its axes of material symmetry oriented in an arbitrary direction with respect to the plate axes. This last generalization is of particular significance in the study of delamination. Takeda, Sierakowski, Ross, and Malvern [7] observed experimentally that delaminations occur in $[(0^{\circ})_5/\ (90^{\circ})_5/(0^{\circ})_5]$ laminates only at the two interfaces where the fiber directions change. Furthermore, a study of the effects of fiber lay-up and stacking sequence on magnitudes of interlaminar stresses requires this generality in the formulation.

Analysis of a Layer

The coordinate system for a layer of the plate is shown in Figure 6. The infinitesimal strain tensor

$$\varepsilon_{k\ell} = \tfrac{1}{2}\left(u_{k,\ell} + u_{\ell,k}\right) \tag{1}$$

is related to the stress tensor by

$$\tau_{ij} = C_{ijk\ell}\,\varepsilon_{k\ell}, \quad \text{or} \quad \tau_i = C_{ij}\,\varepsilon_j \tag{2}$$

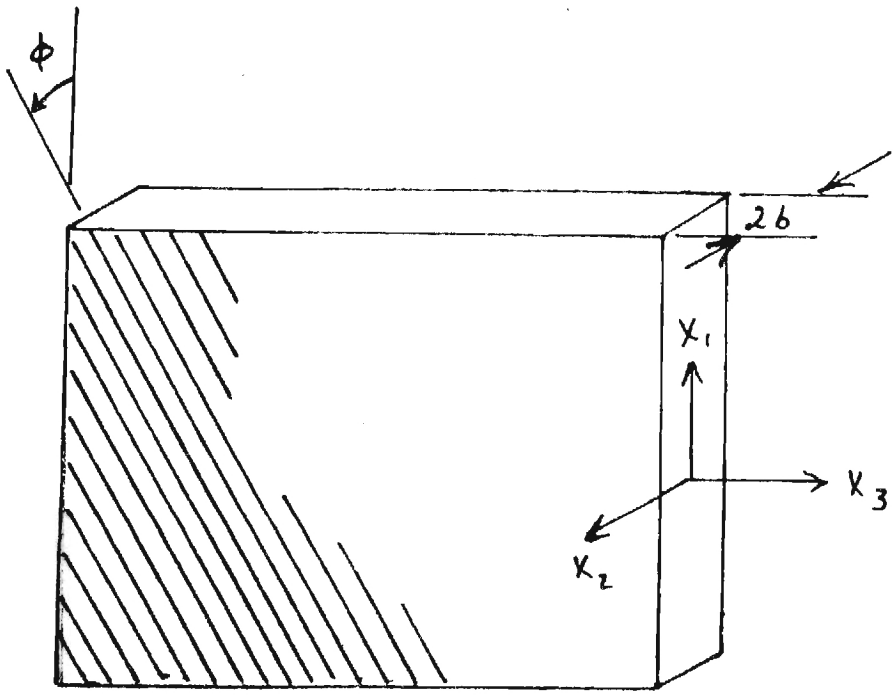

Figure 6. Layer coordinates.

The layer is assumed to be orthotropic; hence, there are 9 independent elastic constants. However, since the principal material axes do not in general coincide with the x_1 and x_3 directions (x_2 is a principal material direction - fibers lie in x_1 - x_3 plane), the non-zero C_{ij}'s are

$$C_{ij} = \begin{bmatrix} C_{11} & C_{12} & C_{13} & 0 & C_{15} & 0 \\ & C_{22} & C_{23} & 0 & C_{25} & 0 \\ & & C_{33} & 0 & C_{35} & 0 \\ & \text{Symmetric} & & C_{44} & 0 & C_{46} \\ & & & & C_{55} & 0 \\ & & & & & C_{66} \end{bmatrix} \tag{3}$$

where C_{ij} are functions of the 9 independent constants and the lay-up angle ϕ.

Displacement components u_i are expanded in terms of Legendre polynomials in the thickness direction,

$$u_i(x_1, x_2, x_3, t) = \sum_{n=0}^{\infty} u_i^{(n)}(x_1, x_3, t)\, P_n(\eta), \quad \eta = \frac{x_2}{b}. \tag{4}$$

From the variational formulation of the equations of motion,

$$\int_A \int_{-b}^{b} (\tau_{ij,i} - \rho \ddot{u}_j)\, \delta u_j \, dx_2 \, dA = 0, \tag{5}$$

Equation (4) is substituted into (5) for the u_j, and integration is performed in the x_2 - direction to yield the stress equations of motion of order n

$$b\,\tau_{\alpha j,\alpha} + \left[\tau_{2j}\,P_n(\eta)\right]_{-1}^{1} - \sum_{m=1,3,\ldots}^{n} D_{mn}\,\tau_{2j}^{(n-m)} = \rho\, b\,\frac{2}{2n+1}\,\ddot{u}_j^{(n)} \qquad (6)$$

$$(\alpha = 1,3;\ j = 1,2,3)$$

where $$\tau_{ij}^{(n)} = \int_{-1}^{1} \tau_{ij}\,P_n(\eta)\,d\eta$$

$$D_{mn} = 2(n-m) + 1.$$

By substituting stress-strain equation (2) with kinematic equations (1) and displacement expansion (4) into (6), an infinite set of equations of motion in terms of $u_1^{(0)}$, $u_2^{(0)}$, $u_3^{(0)}$, $u_1^{(1)}$, ..., are obtained. In order to reduce the complexity, terms through n = 2 only are retained. Furthermore, in the equations for the second mode, all second derivatives of $u_i^{(2)}$ are set to zero, as in [6]. This eliminates coupling with modes higher than n = 2. Note that x_2 dependence of field quantities may be well approximated by the remaining terms, providing the plate is divided into a sufficient number of layers; the approach is reminiscent of a finite element approximation in the thickness direction. The equations of motion for n = 2 are then solved for $u_1^{(2)}$, $u_2^{(2)}$, and $u_3^{(2)}$, substituted in the equations for n = 0, 1, to yield the following six equations of motion for the layer:

$$C_{11}u_{1,11}^{(0)} + \tfrac{3}{2}C_{15}u_{1,13}^{(0)} + \tfrac{1}{2}C_{55}u_{1,33}^{(0)} + \tfrac{1}{2}C_{15}u_{3,11}^{(0)} + \left(C_{13} + \tfrac{1}{2}C_{55}\right)u_{3,13}^{(0)} + C_{35}u_{3,33}^{(0)} + \tfrac{1}{b}C_{12}u_{2,1}^{(1)} + \tfrac{1}{b}C_{25}u_{2,3}^{(1)} + \tfrac{1}{b}\left(\tau_{12}^{+} - \tau_{12}^{-}\right) = \rho\,\ddot{u}_1^{(0)} \qquad (7a)$$

$$\tfrac{1}{2}C_{66}u_{2,11}^{(0)} + C_{46}u_{2,13}^{(0)} + \tfrac{1}{2}C_{44}u_{2,33}^{(0)} + \tfrac{1}{2b}C_{46}u_{3,1}^{(1)} + \tfrac{1}{2b}C_{66}u_{1,1}^{(1)} + \tfrac{1}{2b}C_{44}u_{3,3}^{(1)} + \tfrac{1}{2b}C_{46}u_{1,3}^{(1)} + \tfrac{1}{2b}\left(\tau_{22}^{+} - \tau_{22}^{-}\right) = \rho\,\ddot{u}_2^{(0)} \qquad (7b)$$

$$C_{15}u_{1,11}^{(0)} + \left(\tfrac{1}{2}C_{55} + C_{13}\right)u_{1,13}^{(0)} + \tfrac{1}{2}C_{35}u_{1,33}^{(0)} + \tfrac{1}{2}C_{55}u_{3,11}^{(0)} + \tfrac{3}{2}C_{35}u_{3,13}^{(0)} + C_{33}u_{3,33}^{(0)} + \tfrac{1}{b}C_{25}u_{2,1}^{(1)} + \tfrac{1}{b}C_{23}u_{2,3}^{(1)} + \tfrac{1}{2b}\left(\tau_{23}^{+} - \tau_{23}^{-}\right) = \rho\,\ddot{u}_3^{(0)} \qquad (7c)$$

$$\hat{C}_{11} u_{1,11}^{(1)} + \frac{3}{2}\hat{C}_{15} u_{1,13}^{(1)} + \frac{1}{2} C_{55} u_{1,33}^{(1)} + \frac{1}{2}\hat{C}_{15} u_{3,11}^{(1)} + \left(\hat{C}_{13} + \frac{1}{2}\hat{C}_{55}\right) u_{3,13}^{(1)}$$
$$+ \hat{C}_{35} u_{3,33}^{(1)} - \frac{3}{2b} C_{46} u_{2,3}^{(0)} - \frac{3}{2b} C_{66} u_{2,1}^{(0)} - \frac{3}{2b^2} C_{46} u_3^{(1)} - \frac{3}{2b^2} C_{66} u_1^{(1)} \qquad (8a)$$
$$+ \frac{1}{2}\frac{C_{12}}{C_{22}}\left(\tau_{22}^{+} - \tau_{22}^{-}\right)_{,1} + \frac{1}{2}\frac{C_{25}}{C_{22}}\left(\tau_{22}^{+} - \tau_{22}^{-}\right)_{,3} + \frac{3}{2b}\left(\tau_{12}^{+} + \tau_{12}^{-}\right) = \rho \ddot{u}_1^{(1)}$$

$$-\frac{3}{b} C_{12} u_{1,1}^{(0)} - \frac{3}{b} C_{23} u_{3,3}^{(0)} - \frac{3}{2b}\left(u_{1,3}^{(0)} + u_{3,1}^{(0)}\right) C_{25} - \frac{3}{b^2} C_{22} u_2^{(1)} \qquad (8b)$$
$$+ \frac{1}{2}\left(\tau_{12}^{+} - \tau_{12}^{-}\right)_{,1} + \frac{1}{2}\left(\tau_{23}^{+} - \tau_{23}^{-}\right)_{,3} + \frac{3}{2b}\left(\tau_{22}^{+} + \tau_{22}^{-}\right) = \rho \ddot{u}_2^{(1)}$$

$$\hat{C}_{15} u_{1,11}^{(1)} + \left(\frac{1}{2}\hat{C}_{55} + \hat{C}_{13}\right) u_{1,13}^{(1)} + \frac{1}{2}\hat{C}_{35} u_{1,33}^{(1)} + \frac{1}{2}\hat{C}_{55} u_{3,11}^{(1)} + \frac{3}{2}\hat{C}_{35} u_{3,13}^{(1)}$$
$$+ \hat{C}_{33} u_{3,33}^{(1)} - \frac{3}{2b} C_{44} u_{2,3}^{(0)} - \frac{3}{2b} C_{46} u_{2,1}^{(0)} + \frac{1}{2}\frac{C_{25}}{C_{22}}\left(\tau_{22}^{+} - \tau_{22}^{-}\right)_{,1} \qquad (8c)$$
$$+ \frac{1}{2}\frac{C_{23}}{C_{22}}\left(\tau_{22}^{+} - \tau_{22}^{-}\right)_{,3} - \frac{3}{2b^2} C_{44} u_3^{(1)} - \frac{3}{2b^2} C_{46} u_1^{(1)} + \frac{3}{2b}\left(\tau_{23}^{+} + \tau_{23}^{-}\right) = \rho \ddot{u}_3^{(1)}$$

where $$\hat{C}_{ij} = C_{ij} - \frac{C_{i2} C_{j2}}{C_{22}} \qquad (9)$$

In the above equations, + and - denote stresses on the $\eta = +1$ and -1 surfaces, respectively.

It should be noted that, for the case of plane strain ($u_3 = 0$, $\frac{\partial}{\partial x_3} = 0$), corresponding to impact loading independent of x_3, equations (7a, b) and (8a, b) reduce to the equations of motion given in [6]. However, in contrast to [6], [7c] and [8c] are not identically zero in this case; rather, they yield relations for τ_{23}^{+} and τ_{23}^{-} which are non-zero in this more general case of arbitrary fiber orientation.

Plate Analysis

Equations (7) and (8) for a single layer are now assembled to yield a set of equations for the plate. Since

$$u_i = u_i^{(0)} P_0(\eta) + u_i^{(1)} P_1(\eta) + u_i^{(2)} P_2(\eta),$$

expressions for the interlaminar displacement components may be written as

$$u_i^{\pm} = u_i^{(0)} \pm u_i^{(1)} + u_i^{(2)} , \qquad (10)$$

where $u_i^+ = u_i(\eta = +1)$ and $u_i^- = u_i(\eta = -1)$. Substituting (10) into (7) and (8) yields the equations of motion for a layer explicitly in terms of interlaminar normal and shear stresses and interlaminar displacements. When the corresponding equations for each layer in the plate are assembled, the required continuity conditions for interfacial stresses and displacements are automatically satisfied.

Solution Technique

In order to complete the analysis, a Laplace transform in time and a Fourier transform in space will be applied to the set of governing equations for interfacial stresses and displacements. Stress boundary conditions corresponding to an impact-type loading will be applied, and the solution for the transformed variables will be obtained. Inverse transformations will then be numerically determined. This work is underway at this writing.

4. Delamination Damage Growth

Low velocity impact on composite laminates generally causes fiber breaking, matrix cracking and delamination. Among these three, delamination appears to be the dominant energy absorbing mechanism in dynamic fracture [7]. Furthermore, it is associated with the significant reduction in the residual strength of the laminate to subsequent compressive static loading or cyclic loading. Damage characterization and the prediction of the residual strength, which form the main objective of the present study, should therefore be based on an analysis of delamination growth.

Two studies on the criteria of delamination growth have appeared recently [8, 9]. These works are based, respectively, on analytical and finite element methods applied to a one-dimensional buckling problem of a delaminated layer. In the latter work, the mode I and mode II energy release rates are calculated numerically for various combinations of the delamination lengths and compressive loads. The former work yielded an analytical expression for the energy release rate, but the rates associated with the two fracture modes were not separated. In so far as the results of these two works can be compared, their conclusions appear to be in general agreement.

Both works assumed or implied continued growth of delamination within a single interlaminar plane. The possibility that the growth of delamination may shift from one interlaminar plane to another when the delamination flaw reaches and intersects an existing transversal matrix crack was not considered. Such a matrix crack may exist as an initial flaw but could be, and more likely was, generated by impact. That delamination growth with an abrupt shift of the delamination face is not only possible but probably a common phenomenon is suggested by some recent observations on experimental results [10].

According to the results of [9], the (dominant) mode I energy release rate first increases and subsequently decreases as the delaminate length continues to increase. It is also clear that for a thinner delaminated layer, the peak energy release rate is reached earlier. Hence if the growth of delamination is confined to the original interlaminar plane, it usually tends to become stable or is eventually arrested. However, if delamination growth shifts from one interlaminar plane to an inner plane, then the thickness of newly delaminated portion abruptly

increases and a larger amount of strain energy is released per unit area of delamination. Furthermore, in this case the lack of symmetry implies that the mode II energy release rate, which does not decrease with delamination growth [9], may become significant. These two factors can contribute to an accelerated and unstable delamination growth.

The foregoing arguments suggest that a correct prediction of the laminate residual strength should be based on (i) a damage characterization including delamination shape and size, delaminated layer thickness, and distance to the impact generated matrix crack, (ii) an analysis of the buckling of a delaminated layer with a thickness discontinuity (stepped layer model) and the calculation of energy release rate associated with this model.

Let a stepped delaminated layer consist of two portions with lengths a and b and thicknesses h_1 and h_2 ($h_2 > h_1$), respectively. Let x and ξ be the distances of a cross-section of the layer from the two fixed ends of the layer, so that $x = a$ and $\xi = b$ at the junction of the two portions. Then, under a compressive force P per unit width of the layer, the lateral deflections of the two portions may be expressed, respectively, in the form

$$\left.\begin{aligned} v(x) &= A\mu\left(x - \frac{1}{\lambda}\sin\lambda x\right) - \left\{\mu(a+b)A + B + \frac{h_2 - h_1}{2}\right\}(1-\cos\lambda x) \\ &\qquad \text{for } 0 \le x \le a, \\ W(\xi) &= A(\sin\mu\xi - \mu\xi) - B(1-\cos\mu\xi) \\ &\qquad \text{for } 0 \le \xi \le b. \end{aligned}\right\} \quad (1)$$

where λ and μ are proportional to $P^{\frac{1}{2}}$

$$\frac{P}{\lambda^2} = \frac{E h_1^3}{12(1-\nu^2)}, \qquad \frac{P}{\mu^2} = \frac{E h_2^3}{12(1-\nu^2)}. \quad (2)$$

and, for simplicity, the buckled layer is assumed to be isotropic with

elastic moduli E and ν. Anisotropic layers may be considered by introducing additional elastic moduli. The coefficients A and B in the expressions of $v(x)$ and $w(\xi)$ are given by

$$A = \frac{1}{\Delta} 2\lambda(h_2-h_1) \sin\frac{\lambda a}{2} \sin\frac{\mu b}{2} \left(\lambda \cos\frac{\lambda a}{2} \sin\frac{\mu b}{2} - \mu \sin\frac{\lambda a}{2} \cos\frac{\mu b}{2}\right),$$

$$B = \frac{1}{\Delta} 2\lambda(h_2-h_1) \sin\frac{\lambda a}{2} \cos\frac{\mu b}{2} \left\{ \frac{\lambda\mu}{2}(a+b) \cos\frac{\lambda a}{2} / \cos\frac{\mu b}{2} \right. \qquad (3)$$

$$\left. - \lambda \cos\frac{\lambda a}{2} \sin\frac{\mu b}{2} - \mu \sin\frac{\lambda a}{2} \cos\frac{\mu b}{2} \right\}.$$

where

$$\Delta = 2\lambda\mu(1-\cos\lambda a \cos\mu b) + (\lambda^2+\mu^2) \sin\lambda a \sin\mu b$$
$$- \lambda\mu(a+b)(\lambda \cos\mu b \sin\lambda a + \mu \sin\mu b \cos\lambda a). \qquad (4)$$

Substituting the expressions (2), (3) and (4) into (1), we find that the lateral deflection of the delaminated layer depends on the compressive load per unit width of the layer, P, and the given geometric and material parameters E, ν, a,b, h_1 and h_2.

P is related to the compressive strain ϵ_o in the unbuckled portion of the laminate by the relation

$$\epsilon_o(a+b) = \frac{P}{E}\left(\frac{a}{h_1}+\frac{b}{h_2}\right) + \frac{1}{2}\int_0^a v'(x)^2 dx + \frac{1}{2}\int_0^b w'(\xi)^2 d\xi. \qquad (5)$$

The most critical condition of delaminate growth proceeds with an increase in the length of the thicker portion. Hence, for a given compressive strain ϵ_o in the main body of the laminate and for a fixed length a, the total strain energy of the delaminated portion should be expressed as a function of the length of the thicker portion b. The analytical expression requires complicated functional inversion. The strain energy release rate, which is the derivative of the total strain energy with

respect to b, may be obtained numerically for each given pair of (ϵ_o, b). In an actual composite laminate, the functional relation depends on layer anisotropy and ply orientation.

It is expected that numerical calculation may yield an appreciably larger energy release rate for the stepped delaminated layer at given values of ϵ_o, a and b, compared to the energy release rate of a uniform layer of thickness h_1 and length $a + b$. The maximum value of ϵ_o under which the delamination growth of the stepped layer is arrested or becomes stable will be used as a measure of the residual strength of a laminate with delamination flaws.

In summary, delamination growth has been identified as the major factor affecting or determining the residual strength. It is pointed out that the shifting of delamination growth from one interlaminar plane to an inner plane may occur along an existing transverse matrix crack. This enhances the strain energy release rate as well as the importance of its mode II component. The one-dimensional buckling problem of a stepped delamination layer has been formulated and the solution procedure outlined. The execution of the procedure will deliver quantitative measures of the residual strength under static and cyclic loading, when reasonable fracture criteria are incorporated. In a more detailed formulation the effects of layer anisotropy and ply orientation on thedelamination growth of a stepped layer model can be examined. Progress in these activities will be reported in subsequent communications.

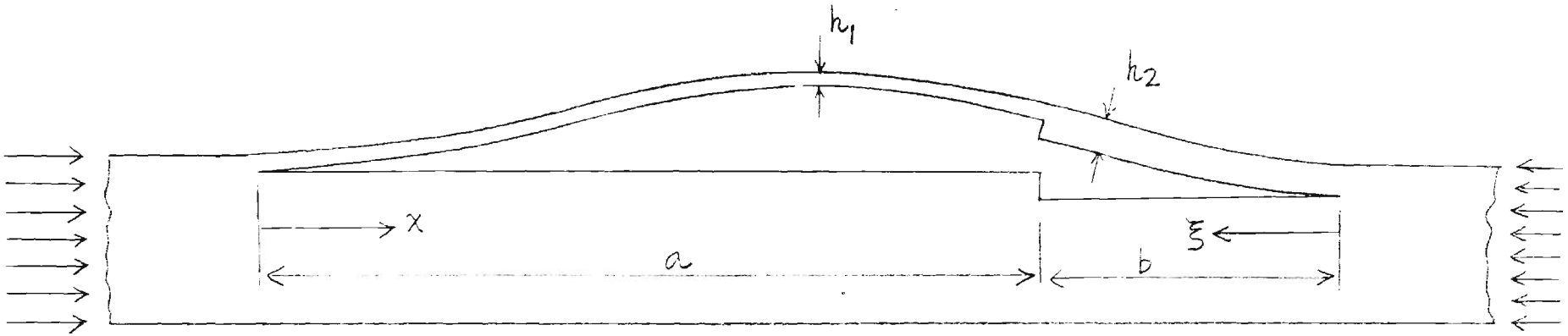

Figure : The stepped delaminated layer

References

1. Dong, S. B. and Nelson, R. B., "On Natural Vibrations and Waves in Laminated Orthotropic Plates," Trans. ASME, J. Appl. Mech., Sept., 1972, pp. 739-745.

2. Kubo, J. T. and Nelson, R. B., "Modal Analysis for Impact of Layered Plates," ASCE, J. Eng. Mech. Div., Feb., 1975, pp. 45-57.

3. Moon, F. C., "Wave Surfaces Due to Impact on Anisotropic Plates," J. Comp. Mat., Jan., 1972, pp. 62-79.

4. Moon, F. C., "One-Dimensional Transient Waves in Anisotropic Plates," Trans. ASME, J. Appl. Mech., June, 1973, pp. 485-490.

5. Moon, F. C., "Stress Wave Calculations in Composite Plates Using the Fast Fourier Transform," Computers and Structures, Vol. 3, pp. 1195-1204.

6. Kim, B. S. and Moon, F., "Impact Induced Stress Waves in an Anisotropic Plate," AIAA Journal, Oct., 1979, pp. 1126-1133.

7. Takeda, N., Sierakowski, R. L., Ross, C. A., and Malvern, L. E., "Delamination-crack propagation in Ballistically Impacted Glass/Epoxy Composite Laminates," Exp. Mech., Jan., 1982, pp. 19-25.

8. Chai, H., Babcock, C. D., and Knauss, W. G., "One dimensional modelling of failure in laminated plates by delamination buckling," Intl. J. Solids Structures, 17, pp. 1069-1083 (1981).

9. Whitcomb, J. D., "Finite element analysis of instability related dalamination growth," J. Composite Materials, 15, pp. 403-426 (1981).

10. Reifsnider, K. L. and Talug, A., "Analysis of fatigue damage in composite laminates," Int. J. Fatigue, Jan., 1980, pp. 3-11.

E-23-624

ENGINEERING COLLEGE
GEORGIA INSTITUTE OF TECHNOLOGY

SCHOOL OF ENGINEERING SCIENCE
AND MECHANICS
225 NORTH AVENUE, N.W.
ATLANTA, GEORGIA 30332

June 15, 1982

Mr. John N. Dickson
Department 72-77
Mail Zone 415
Lockheed-Georgia Company
Marietta, Georgia 30063

Subject: Research Grant P. O. No. CY48335 (Ga. Tech Project No. E-23-624)
Progress Report (4/16/82 through 6/15/82)

Dear Mr. Dickson:

During the subject period, emphasis has been made in seeking solutions of the problems based on the general formulations discussed in the previous progress report (1/16/82 thru 4/15/82) for the propagation of stress wave in elastic composite plates, and for the delamination of the stepped-layer model. The following represents a summary of the progress of research under the subject grant, and more detailed discussions are also enclosed:

(1) As indicated in the last progress report for the transient impact problem concerning the propagation of stress wave in elastic composite plates, Laplace transform in time and Fourier transform in space will be considered in determining interfacial stresses and displacements. The transformed equations exhibit a heavily banded coefficient matrix; an effective scheme for determining the transformed variables as the first step of the analysis has been used and tested with satisfaction. It is commonly known that the numerical determination of the inverse transformation is a difficult task. Efforts are being made to explore, evaluate, and/or extend the existing schemes, procedures as well as computer programs concerning fast Fourier transform suitable for the present problem.

(2) Stepped thin film delamination model has been formulated. While the general solution for determining the deformation and strain energy can be obtained explicitly, it becomes extremely complex to arrive at an explicit expression for determining the strain energy release rate, G_a. The effect of

misalignment of the middle planes of the two portions of the stepped layer which was thought to be negligible, has been neglected. The general solution for calculating G_a has been obtained. Inasmuch as the resulting expression for calculating G_a is lengthy, the derivation is being checked independently, and a computational scheme is being planned for subsequent computer programming. A separate attempt to determine G_a through numerical differentiation is being made also. Limited numerical results generated from an Apple II microcomputer show favorable agreement with our conjecture.

Sincerely yours,

R. K. Kunz, Assistant Professor

S. T. S. Wang, Professor

L. Yin, Associate Professor

ew
Enclosure

Supplement to Summary of Progress Report

for

Lockheed-Georgia Research Grant P. O. No. CY48335
(Georgia Tech Project No. E-23-624)

for

The Period April 16 through June 15, 1982

by

R. K. Kunz, J. T. S. Wang, and W. L. Yin
School of Engineering Science and Mechanics
Georgia Institute of Technology
Atlanta, Georgia 30332

1. Wave Propagation Due to Impact in Laminated Composite Plates

Analytical and numerical work aimed at studying the propagation of impact-generated transient stress waves in a laminated plate has been continued. As described in the previous report, an approach developed by Kim and Moon [1] has been adopted and generalized in order to calculate interlaminar stresses and displacements in a plate with arbitrary material properties and stacking sequence. The ability to determine interlaminar stresses under a variety of impact conditions and plate designs is of primary importance in predicting the onset and extent of impact induced delamination.

1.1 Analysis of a Layer

In the previous report, the basic equations of motion of a layer were obtained in terms of displacement functions. In this formulation, displacement components u_i were expanded in terms of Legendre polynomials in the thickness (x_2) direction,

$$u_i(x_1, x_2, x_3, t) = \sum_{n=0}^{\infty} u_i^{(n)}(x_1, x_3, t)\, P_n(\eta) \quad , \quad \eta = x_2/b \qquad (1.1)$$

where 2b is the layer thickness and x_1, x_3 are the in-plane coordinates. By truncating the series (1.1) after n = 2, the approximate equations of motion for a single layer were obtained in terms of $u_i^{(0)}$, $u_i^{(1)}$ (i = 1,2,3), and the stress components τ_{12}, τ_{22}, τ_{23} on the layer surfaces. These equations were recorded in the previous report as equations (7) and (8).

The next step requires re-writing the equations for each layer in a form such that they may be assembled into a set of equations for the plate. From equation (1.1), after truncation, the displacements at the layer surfaces

may be written as

$$u_i^{\pm} = u_i^{(0)} \pm u_i^{(1)} \tag{1.2}$$

where $u_i^{\pm} = u_i(\eta = \pm 1)$. Hence, by using equations (1.2), $u_i^{(0)}$ and $u_i^{(1)}$ may be eliminated from the layer equations of motion in favor of the surface displacements of the layer. The resulting equations for layer n are as follows:

$$\begin{aligned} &C_{11}^n (u_n + u_{n-1})_{,11} + \tfrac{3}{2} C_{15}^n (u_n + u_{n-1})_{,13} + \tfrac{1}{2} C_{55}^n (u_n + u_{n-1})_{,33} + \tfrac{1}{2} C_{15}^n (w_n + w_{n-1})_{,11} \\ &+ (C_{13}^n + \tfrac{1}{2} C_{55}^n)(w_n + w_{n-1})_{,13} + C_{35}^n (w_n + w_{n-1})_{,33} + \tfrac{1}{b} C_{12}^n (v_n - v_{n-1})_{,1} \\ &+ \tfrac{1}{b} C_{25}^n (v_n - v_{n-1})_{,3} + \tfrac{1}{b} (\tau_{12}^n - \tau_{12}^{n-1}) = \rho (\ddot{u}_n + \ddot{u}_{n-1}) \end{aligned} \tag{1.3a}$$

$$\begin{aligned} &\tfrac{1}{2} C_{66}^n (v_n + v_{n-1})_{,11} + C_{46}^n (v_n + v_{n-1})_{,13} + \tfrac{1}{2} C_{44}^n (v_n + v_{n-1})_{,33} \\ &+ \tfrac{1}{2b} C_{46}^n (w_n - w_{n-1})_{,1} + \tfrac{1}{2b} C_{66}^n (u_n - u_{n-1})_{,1} + \tfrac{1}{2b} C_{44}^n (w_n - w_{n-1})_{,3} \\ &+ \tfrac{1}{2b} C_{46}^n (u_n - u_{n-1})_{,3} + \tfrac{1}{b} (\tau_{22}^n - \tau_{22}^{n-1}) = \rho (\ddot{v}_n + \ddot{v}_{n-1}) \end{aligned} \tag{1.3b}$$

$$\begin{aligned} &C_{15}^n (u_n + u_{n-1})_{,11} + (\tfrac{1}{2} C_{55}^n + C_{13}^n)(u_n + u_{n-1})_{,3} + \tfrac{1}{2} C_{35}^n (u_n + u_{n-1})_{,33} \\ &+ \tfrac{1}{2} C_{55}^n (w_n + w_{n-1})_{,11} + \tfrac{3}{2} C_{35}^n (w_n + w_{n-1})_{,13} + C_{33}^n (w_n + w_{n-1})_{,33} + \tfrac{1}{b} C_{25}^n (v_n - v_{n-1})_{,1} \\ &+ \tfrac{1}{b} C_{23}^n (v_n - v_{n-1})_{,3} + \tfrac{1}{b} (\tau_{23}^n - \tau_{23}^{n-1}) = \rho (\ddot{w}_n + \ddot{w}_{n-1}) \end{aligned} \tag{1.3c}$$

$$\begin{aligned} &\hat{C}_{11}^n (u_n - u_{n-1})_{,11} + \tfrac{3}{2} \hat{C}_{15}^n (u_n - u_{n-1})_{,13} + \tfrac{1}{2} \hat{C}_{55}^n (u_n - u_{n-1})_{,33} + \tfrac{1}{2} \hat{C}_{15}^n (w_n - w_{n-1})_{,11} \\ &+ (\hat{C}_{13}^n + \tfrac{1}{2} \hat{C}_{55}^n)(w_n - w_{n-1})_{,13} + \hat{C}_{35}^n (w_n - w_{n-1})_{,33} - \tfrac{3}{2b} C_{46}^n (v_n + v_{n-1})_{,3} \\ &- \tfrac{3}{2b} C_{66}^n (v_n + v_{n-1})_{,1} - \tfrac{3}{2b^2} C_{46}^n (w_n - w_{n-1}) - \tfrac{3}{2b^2} C_{66}^n (u_n - u_{n-1}) \\ &+ C_{12}^n / C_{22}^n (\tau_{22}^n - \tau_{22}^{n-1})_{,1} + C_{25}^n / C_{22}^n (\tau_{22}^n - \tau_{22}^{n-1}) + \tfrac{3}{b} (\tau_{12}^n + \tau_{12}^{n-1}) = \rho (\ddot{u}_n - \ddot{u}_{n-1}) \end{aligned} \tag{1.4a}$$

$$-\tfrac{3}{b}C^n_{12}(u_n+u_{n-1})_{,1}-\tfrac{3}{b}C^n_{23}(w_n+w_{n-1})_{,3}-\tfrac{3}{2b}C^n_{25}(u_n+u_{n-1})_{,3}$$
$$-\tfrac{3}{2b}C^n_{25}(w_n+w_{n-1})_{,1}-\tfrac{3}{b^2}C^n_{22}(v_n-v_{n-1})+(\tau^n_{12}-\tau^{n-1}_{12})_{,1}+(\tau^n_{23}-\tau^{n-1}_{23})_{,3} \qquad (1.4b)$$
$$+\tfrac{3}{b}(\tau^n_{22}+\tau^{n-1}_{22})=\rho(\ddot{v}_n-\ddot{v}_{n-1})$$

$$\hat{C}^n_{15}(u_n-u_{n-1})_{,11}+(\tfrac{1}{2}\hat{C}^n_{55}+\hat{C}^n_{13})(u_n-u_{n-1})_{,3}+\tfrac{1}{2}\hat{C}^n_{35}(u_n-u_{n-1})_{,33}$$
$$+\tfrac{1}{2}\hat{C}^n_{55}(w_n-w_{n-1})_{,11}+\tfrac{3}{2}\hat{C}^n_{35}(w_n-w_{n-1})_{,13}+\hat{C}^n_{33}(w_n-w_{n-1})_{,33}-\tfrac{3}{2b}C^n_{44}(v_n+v_{n-1}) \qquad (1.4c)$$
$$-\tfrac{3}{2b}C^n_{46}(v_n+v_{n-1})_{,1}-\tfrac{3}{b^2}C^n_{44}(w_n-w_{n-1})-\tfrac{3}{2b^2}C^n_{46}(u_n-u_{n-1})+\hat{C}^n_{25}/\hat{C}^n_{22}(\tau^n_{22}-\tau^{n-1}_{22})_{,1}$$
$$+\hat{C}^n_{23}/\hat{C}^n_{22}(\tau^n_{22}-\tau^{n-1}_{22})_{,3}+\tfrac{3}{b}(\tau^n_{23}+\tau^{n-1}_{23})=\rho(\ddot{w}_n-\ddot{w}_{n-1})$$

In equations (1.3) and (1.4), u_n, v_n, w_n are the x_1, x_2, x_3 displacements at the nth interface (the zeroth interface being the top surface of the plate); C^n_{ij} are the elastic constants of the nth layer; and τ^n_{ij} represent the stresses on the nth interface.

Equations (1.3) and (1.4) are the final approximate equations of motion for a layer in the form of difference-differential equations. Variation of all field qualities has been discretized through the thickness; in-plane coordinates and time remain as continuous variables to which integral transforms will be applied. Since the unknowns appearing in equations (1.3) and (1.4) are the surface displacements and surface stresses for layer n, the required continuity of interlaminar displacements and stresses is automatically satisfied when the sets of equations for all N layers are assembled.

1.2 Transformation and Solution Technique

Equations (1.3) and (1.4) are now transformed, using the Laplace transformation in time and the Fourier transformation in space. By using the properties of the transforms of derivatives, the equations are reduced to a set of linear algebraic difference equations in terms of transformed interfacial stresses and displacements, and the transform variables. The initial conditions and the boundary conditions at infinity are incorporated into the set of transformed equations.

Upon transforming, the following set of equations results for layer n:

$$[R_n]\{X_n\} + [Q_n]\{X_{n-1}\} = \{0\} \tag{1.5}$$

$$\{X_n\}^T = \{U_n, V_n, W_n, T_{22}^n, T_{12}^n, T_{23}^n\} \tag{1.6}$$

$$\begin{aligned}
R_{11}^n &= C_{11}^n k_1^2 + \tfrac{3}{2} C_{15}^n k_1 k_3 + \tfrac{1}{2} C_{55}^n k_3^2 + \rho s^2 & Q_{11}^n &= R_{11}^n \\
R_{12}^n &= \tfrac{1}{b} C_{12}^n i k_1 + \tfrac{1}{b} C_{25}^n i k_3 & Q_{12}^n &= -R_{12}^n \\
R_{13}^n &= \tfrac{1}{2} C_{15}^n k_1^2 + (C_{13}^n + \tfrac{1}{2} C_{55}^n) k_1 k_3 + C_{35}^n k_3^2 & Q_{13}^n &= R_{13}^n \\
R_{15}^n &= -\tfrac{1}{b} & Q_{15}^n &= -R_{15}^n \\
R_{21}^n &= \tfrac{1}{2b} C_{66}^n i k_1 + \tfrac{1}{2b} C_{46}^n i k_3 & Q_{21}^n &= -R_{21}^n \\
R_{22}^n &= \tfrac{1}{2} C_{66}^n k_1^2 + C_{46}^n k_1 k_3 + \tfrac{1}{2} C_{44}^n k_3^2 + \rho s^2 & Q_{22}^n &= R_{22}^n \\
R_{23}^n &= \tfrac{1}{2b} C_{46}^n i k_1 + \tfrac{1}{2b} C_{44}^n i k_3 & Q_{23}^n &= -R_{23}^n \\
R_{24}^n &= -\tfrac{1}{b} & Q_{24}^n &= -R_{24}^n \\
R_{31}^n &= C_{15}^n k_1^2 + (\tfrac{1}{2} C_{55}^n + C_{13}^n) k_1 k_3 + \tfrac{1}{2} C_{35}^n k_3^2 & Q_{31}^n &= R_{31}^n \\
R_{32}^n &= \tfrac{1}{b} C_{25}^n i k_1 + \tfrac{1}{b} C_{23}^n i k_3 & Q_{32}^n &= -R_{32}^n \\
R_{33}^n &= \tfrac{1}{2} C_{55}^n k_1^2 + \tfrac{3}{2} C_{35}^n k_1 k_3 + C_{33}^n k_3^2 + \rho s^2 & Q_{33}^n &= R_{33}^n \\
R_{36}^n &= -\tfrac{1}{b} & Q_{36}^n &= -R_{36}^n
\end{aligned} \tag{1.7}$$

$$R_{41}^n = \hat{C}_{11}^n k_1^2 + \tfrac{3}{2}\hat{C}_{15}^n k_1 k_3 + \tfrac{1}{2}\hat{C}_{55}^n k_3^2 + \tfrac{3}{2b^2}C_{66}^n + \rho s^2$$

$$R_{42}^n = -\tfrac{3}{2b}C_{46}^n ik_3 - \tfrac{3}{2b}C_{66}^n ik_1$$

$$R_{43}^n = \tfrac{1}{2}\hat{C}_{15}^n k_1^2 + (\hat{C}_{13}^n + \tfrac{1}{2}\hat{C}_{55}^n) k_1 k_3 + \hat{C}_{35}^n k_3^2 + \tfrac{3}{2b^2}C_{46}^n$$

$$R_{44}^n = C_{12}^n/C_{22}^n ik_1 + C_{25}^n/C_{22}^n ik_3$$

$$R_{45}^n = -\tfrac{3}{b}$$

$$R_{51}^n = -\tfrac{3}{b}C_{12}^n ik_1 - \tfrac{3}{2b}C_{25}^n ik_3$$

$$R_{52}^n = \tfrac{3}{b^2}C_{22}^n + \rho s^2$$

$$R_{53}^n = -\tfrac{3}{b}C_{23}^n ik_3 - \tfrac{3}{2b}C_{25}^n ik_1$$

$$R_{54}^n = -\tfrac{3}{b}$$

$$R_{55}^n = ik_1$$

$$R_{56}^n = ik_3$$

$$R_{61}^n = \hat{C}_{15}^n k_1^2 + (\tfrac{1}{2}\hat{C}_{55}^n + \hat{C}_{13}^n) k_1 k_3 + \tfrac{1}{2}\hat{C}_{35}^n k_3^2 + \tfrac{3}{2b^2}\hat{C}_{46}^n$$

$$R_{62}^n = -\tfrac{3}{2b}C_{44}^n ik_3 - \tfrac{3}{2b}C_{46}^n ik_1$$

$$R_{63}^n = \tfrac{1}{2}\hat{C}_{55}^n k_1^2 + \tfrac{3}{2}\hat{C}_{35}^n k_1 k_3 + C_{33}^n k_3^2 + \tfrac{3}{2b^2}C_{44}^n + \rho s^2$$

$$R_{64}^n = C_{25}^n/C_{22}^n ik_1 + C_{23}^n/C_{22}^n ik_3$$

$$R_{66}^n = -\tfrac{3}{b}$$

$$Q_{41}^n = -R_{41}^n$$

$$Q_{42}^n = R_{42}^n$$

$$Q_{43}^n = -R_{43}^n$$

$$Q_{44}^n = -R_{44}^n$$

$$Q_{45}^n = R_{45}^n$$

$$Q_{51}^n = R_{51}^n$$

$$Q_{52}^n = -R_{52}^n$$

$$Q_{53}^n = R_{53}^n$$

$$Q_{54}^n = R_{54}^n$$

$$Q_{55}^n = -R_{55}^n$$

$$Q_{56}^n = -R_{56}^n \qquad (1.7)$$

$$Q_{61}^n = -R_{61}^n \qquad \text{(cont'd}$$

$$Q_{62}^n = R_{62}^n$$

$$Q_{63}^n = -R_{63}^n$$

$$Q_{64}^n = -R_{64}^n$$

$$Q_{66}^n = R_{66}^n$$

$$R_{14}^n = R_{16}^n = R_{25}^n = R_{26}^n = 0$$

$$R_{34}^n = R_{35}^n = R_{46}^n = R_{65}^n = 0$$

$$Q_{14}^n = Q_{16}^n = Q_{25}^n = Q_{26}^n = 0$$

$$Q_{34}^n = Q_{35}^n = Q_{46}^n = Q_{65}^n = 0$$

In equations (1.5-1.7), k_1 and k_3 are the Fourier transform variables, s is the Laplace transform variable. A capital letter denotes a transformed quantity, e.g.

$$U_n(k_1,k_3,s) = \int_0^\infty \int_{-\infty}^{\infty} \int_{-\infty}^{\infty} u_n(x_1,x_3,t)\exp[-st+i(k_1x_1+k_3x_3)]dx_1dx_3dt \qquad (1.8)$$

Equations (1.5) represent the transformed equations of motion for the nth layer. When the resulting set of equations for an N layered plate are assembled, the result has the banded form:

$$\begin{bmatrix} [Q_1] & [R_1] & & \\ & [Q_2] & [R_2] & \\ & & \ddots & \ddots \\ & & & [Q_N] \quad [R_N] \end{bmatrix} \begin{Bmatrix} \{X_0\} \\ \{X_1\} \\ \vdots \\ \{X_N\} \end{Bmatrix} = \begin{Bmatrix} 0 \end{Bmatrix} \qquad (1.9)$$

Equation (1.9) represents a set of 6N equations for 6(N + 1) unknowns. For the case of known normal impact loading, the boundary conditions at the free surfaces of the plate assume the form

$$\begin{aligned} \tau_{22}^0 &= \sigma(x_1,x_3,t) \\ \tau_{12}^0 = \tau_{23}^0 &= \tau_{12}^N = \tau_{23}^N = \tau_{22}^N = 0 \end{aligned} \qquad (1.10)$$

where σ is the known loading function. These boundary conditions, when transformed, provide the 6 additional equations necessary to complete the system.

The simplicity of equations (1.10) allows one to directly eliminate

T^{o}_{22}, T^{o}_{12}, T^{o}_{23}, T^{N}_{12}, T^{N}_{22}, T^{N}_{23} from equations (i.9), leaving a set of 6N equations in 6N unknowns having the general form:

$$\begin{bmatrix} [B_0] & [C_0] & & & & \\ [A_1] & [B_1] & [C_1] & & & \\ & [A_2] & [B_2] & [C_2] & & \\ & & \ddots & \ddots & \ddots & \\ & & & [A_{N-2}] & [B_{N-2}] & [C_{N-2}] \\ & & & & [A_{N-1}] & [B_{N-1}] & [C_{N-1}] \\ & & & & & [A_N] & [B_N] \end{bmatrix} \begin{Bmatrix} \{X_0^*\} \\ \{X_1\} \\ \{X_2\} \\ \vdots \\ \{X_{N-2}\} \\ \{X_{N-1}\} \\ \{X_N\} \end{Bmatrix} = \begin{Bmatrix} \{D_0^*\} \\ \{D_1\} \\ \{D_2\} \\ \vdots \\ \{D_{N-2}\} \\ \{D_{N-1}\} \\ \{D_N\} \end{Bmatrix} \quad (1.$$

In equation (1.11) the submatrices have the following dimensions:

$A_1 : 6\times 3$	$B_0 : 3\times 3$	$C_0 : 3\times 6$
$A_i : 6\times 6 \quad (i=2,N-1)$	$B_i : 6\times 6 \quad (i=1,N-1)$	$C_i : 6\times 6 \quad (i=1,N-2)$
$A_N : 3\times 6$	$B_N : 3\times 3$	$C_{N-1} : 6\times 3$

In addition,

$$\{X_0^*\}^T = \{U_0, V_0, W_0\}, \qquad \{X_N^*\}^T = \{U_N, V_N, W_N\}$$

$$\{D_0^*\}^T = \{0, R'_{24}\Sigma, 0\}, \qquad \{D_1\}^T = \{R'_{44}\Sigma, -R'_{54}\Sigma, R'_{64}\Sigma, 0, 0, 0\}$$

(where Σ is the transform of the loading function σ), and all other elements on the right-hand side of (1.11) are zero.

Equation (1.11) is in a form referred to as "block-tridiagonal" for which an efficient solution algorithm exists [2]. The algorithm involves factorizing the coefficient matrix in (1.11) into lower and upper diagonal

factors, before solving for the unknowns. By using this factorization technique, no more than six equations at a time need be solved simultaneously.

In order to solve for the interlaminar stresses, then, the following procedure must be implemented: equations (1.13) must be solved repeatedly for ranges of values of the transform variables k_1, k_3, and s; solutions, in the form of transformed interfacial stresses and displacements, are stored; actual interfacial stresses and displacements must then be obtained by numerically inverting the transforms. This last step will be accomplished using the Fast-Fourier Transform (Cooley-Tukey) algorithm [3]. Progress made to date in effecting such a solution is described in the next section.

1.3 Plate Subjected to Line Loading

In order to test the general procedure on a more manageable set of cases than the general problem of central impact, the two-dimensional analogue-a plate subjected to line-impact loading - will be investigated first. It is hoped that this will have the advantage of bringing to light early some of the numerical pitfalls to be encountered in the more complicated three-dimensional case, as well as possibly providing numerical results of some practical interest. By considering the simpler case first, much of the numerical testing can be done on a smaller system of equations, thus saving on computation time. Computation costs for the general 3-D problem may then be estimated from those encountered in the 2-D test cases. Once the simpler case has been successfully implemented, it should not be a difficult matter to expand the program to handle central impact problems.

In the two-dimensional, or line-impact, case, the loading function is independent of x_3; $u_3 = 0$; and all partial derivatives with respect to x_3 are zero. The governing equations for this subset of problems may be easily obtained directly from those recorded above for the three-dimensional analysis,

and will not be listed here. The essential differences are that the sub-matrix blocks in the two-dimensional analogue to equations (1.11) are 4 x 4 rather than 6 x 6; the unknowns are U_n, V_n, T_{22}^n, T_{12}^n, n = 0, N; and the coefficients depend on s and the single space-transform variable k_1, rather than on k_1 and k_3.

At the writing of this report, a FORTRAN computer program for determining the interlaminar stresses and displacements for the 2-D case is being developed. A subroutine for solving the two-dimensional analogue to the block-tridiagonal system (1.11) has been written and tested. Work is currently progressing on the development of a routine to calculate the inverse transforms.

2. Delamination Growth and Residual Strength

2.1 Stepped thin film delamination

In the previous report, it was pointed out that impact-generated delamination plays a significant role in the reduction of the residual strength of the laminate under compressive static and cyclic loads. The analytical studies available in the current literature [4-6] are restricted to the growth of a delaminated layer of constant thickness. Typically, a fracture criterion is used in which the energy release rate associated with the growth of delamination is compared with a critical value. This experimentally determined critical value determines whether delamination continues to grow under a fixed static or cyclic load.

Results obtained by Chai et al. [4] and by Whitcomb [6] indicate that for a laminate under fixed compressive load (or strain), the energy release rate of a delaminated film reaches a maximum value at a certain delamination length. The energy release rate is small if the delamination length is either too small or too large. Therefore, an impact-generated delamination with relatively small length-to-thickness ratio will not grow, and one with relatively large length-to-thickness ratio will grow at first and then cease to grow (or will grow stably under cyclic load) when the energy release rate decreases below the critical value If this is the case, the theory presumes that the specified laminate compressive load (or strain) does not exceed the laminate residual strength.

However, we point out in our previous report that, if the delamination face intersects an existing transverse matrix crack at a certain stage of delamination growth, further growth of delamination may shift from one interlaminar face to an interior one. The stepped delamination layer which is used to model this type of growth will yield a higher value of the energy release rate, as compared

to the continued growth of the uniform layer along the original interlaminar plane, because the delamination of a thicker layer is associated with a larger amount of released strain energy. This implies that, under a given laminate load, the uniform layer model may predict lack of growth of an existing delamination but the stepped-layer model may predict continued growth. Therefore, the residual strength of an impact-damaged laminate may be governed by the conclusions of a stepped-layer mode.

2.2 Formulation of the stepped-layer model

Formulation of the stepped-layer model requires an elastic post-buckling analysis which is considerably more complicated than the corresponding analysis of a uniform layer. A preliminary outline of the analysis procedure was given in the previous report. In the following, we develope and discuss the analysis with some detail.

The post-buckling analysis of the stepped layer may be greatly simplified by introducing an approximation, i.e. by ignoring the non-alignment of the middle planes of the two portions of the layer. Under this assumption, the axial force in the buckled layer remains constant, while the lateral deflection of the layer increases with the compressive strain in the main body of the laminate. If the two portions of the stepped layer have thicknesses h_1 and h_2, lengths a and b, and effective elastic moduli E_1, ν_1, E_2 and ν_2, respectively, and if we define

$$\beta = \left\{ \frac{E_1 h_1^3 (1-\nu_2^2)}{E_2 h_2^3 (1-\nu_1^2)} \right\}^{1/2} \qquad (2.1a)$$

$$\chi = a \left\{ \frac{12(1-\nu_1^2) P}{E_1 h_1^3} \right\}^{1/2} \qquad (2.1b)$$

$$y = b \left\{ \frac{12(1-\nu_2^2) P}{E_2 h_2^3} \right\}^{1/2} \qquad (2.1c)$$

then the buckling load P (force per unit film width) is determined by the equatio

$$\Delta \equiv 2\beta(1-\cos x\cos y)+(1+\beta^2)\sin x\sin y$$

$$-(\beta x+y)(\sin x\cos y+\beta\cos x\sin y)=0 \qquad (2.2)$$

This equation can be solved numerically for P. Then x and y are obtained from Eq. (2.1 b, c).

When the compressive strain ϵ_0 in the laminate is sufficiently large, the stepped layer buckles. We assume that the delamination thickness is considerably smaller than the laminate thickness so that the buckling of the layer does not cause bending deformation in the remaining portion of the laminate. The strain energy of the buckled layer consists of a part due to membrane compression and another part due to bending:

$$U = U_M + U_B$$

$$= \frac{P^2}{2}\left(\frac{a}{E_1h_1}+\frac{b}{E_2h_2}\right)+\left\{(a+b)\epsilon_0 P-P^2\left(\frac{a}{E_1h_1}+\frac{b}{E_2h_2}\right)\right\}\frac{T-S}{T+S} \qquad (2$$

where

$$S = \frac{\sin 2x}{2\beta}(\beta^2-Q^2)+\frac{\sin 2y}{2}(1-R^2)-Q\cos 2x+R\cos 2y,$$

$$T = \frac{x}{\beta}Q^2+yR^2$$

$$Q = \frac{\beta\sin x+\sin y-(\beta x+y)\cos y}{\cos x-\cos y}$$

$$R = Q-(\beta x+y) = \frac{\beta\sin x+\sin y-(\beta x+y)\cos x}{\cos x-\cos y}$$

2.3 Calculation of the strain energy release rate

The strain energy release rate G_a is given by

$$G_a = \frac{1}{2} E_2 h_2 \epsilon_0^2 - \frac{dU}{db} \qquad (2.4)$$

Since in Eq. (3) U is given in terms of two variables P and b which are related by Eq. (2.2), an analytical expression for dU/db must be obtained by using the chain rule of differentiation. We obtain

$$G_a = \frac{1}{2} E_2 h_2 \epsilon_0^2 - \left.\frac{\partial U}{\partial b}\right|_P + 2\left(\mu P \left.\frac{\partial U}{\partial P}\right|_b\right) \frac{\frac{1}{\mu}\frac{\partial \Delta}{\partial b}}{2P\frac{\partial \Delta}{\partial P}} \qquad (2.5)$$

where

$$\left.\frac{\partial U}{\partial b}\right|_P = \frac{P^2}{2E_2 h_2} + \left(\epsilon_0 P - \frac{P^2}{E_2 h_2}\right)\frac{T-S}{T+S}$$

$$+ \frac{2\beta\chi}{(T+S)^2}\left\{\left(1+\frac{b}{a}\right)\epsilon_0 P - P^2\left(\frac{1}{E_1 h_1} + \frac{b}{aE_2 h_2}\right)\right\}\left(S\frac{\partial T}{\partial y} - T\frac{\partial S}{\partial y}\right),$$

$$\mu P \left.\frac{\partial U}{\partial P}\right|_b = \beta\chi P^2\left(\frac{1}{E_1 h_1} + \frac{b}{aE_2 h_2}\right) + \beta\chi\left\{\left(1+\frac{b}{a}\right)\epsilon_0 P - 2P^2\left(\frac{1}{E_1 h_1} + \frac{b}{aE_2 h_2}\right)\right\}\frac{T-S}{T+S}$$

$$+ \frac{\beta\chi}{(T+S)^2}\left\{\left(1+\frac{b}{a}\right)\epsilon_0 P - P^2\left(\frac{1}{E_1 h_1} + \frac{b}{aE_2 h_2}\right)\right\}\cdot$$

$$\cdot\left\{S\left(x\frac{\partial T}{\partial x} + y\frac{\partial T}{\partial y}\right) - T\left(x\frac{\partial S}{\partial x} + y\frac{\partial S}{\partial y}\right)\right\},$$

$$\frac{1}{\mu}\frac{\partial \Delta}{\partial b} = \cos\chi\sin y + \beta\sin\chi\cos y - \left(\chi + \frac{y}{\beta}\right)\left(\beta\cos\chi\cos y - \sin\chi\sin y\right),$$

$$2P\frac{\partial \Delta}{\partial P} = \left(\frac{\chi}{\beta} + y\right)\left(\cos\chi\sin y + \beta\sin\chi\cos\beta\right)$$

$$-\left(\chi + \frac{y}{\beta}\right)\left\{(\chi+\beta y)\cos\chi\cos y - (\beta\chi + y)\sin\chi\sin y\right\}$$

With given material elastic moduli and given values of h_1, h_2, a and ϵ_o, we calculate the buckling load P of the stepped layer as a function of the length b by using Eq. (2.2). From Eq. (2.5), we then calculate Ga as a function of b. The results are then compared with the energy release rate G'_a of a uniform -thick layer:

$$G'_a(b) = \frac{E_1 h_1}{2}\left\{\epsilon_o - \frac{\pi^2}{3}\left(\frac{h_1}{a+b}\right)^2\right\}\left\{\epsilon_o + \pi^2\left(\frac{h_1}{a+b}\right)^2\right\} \qquad (2.6)$$

To give some indication of the validity of our conjecture, an example based on the following data is considered:

$$a = 1\ in.,\quad h_1 = 0.01\ in.,\quad h_2 = 0.02\ in.,$$
$$E_1 = E_2,\quad \nu_1 = \nu_2 = 0.3,\quad 8\beta^2 = 1.$$

Based on numercial differentiation, results presented in Fig. 1 show favorable agreement with our conjecture.

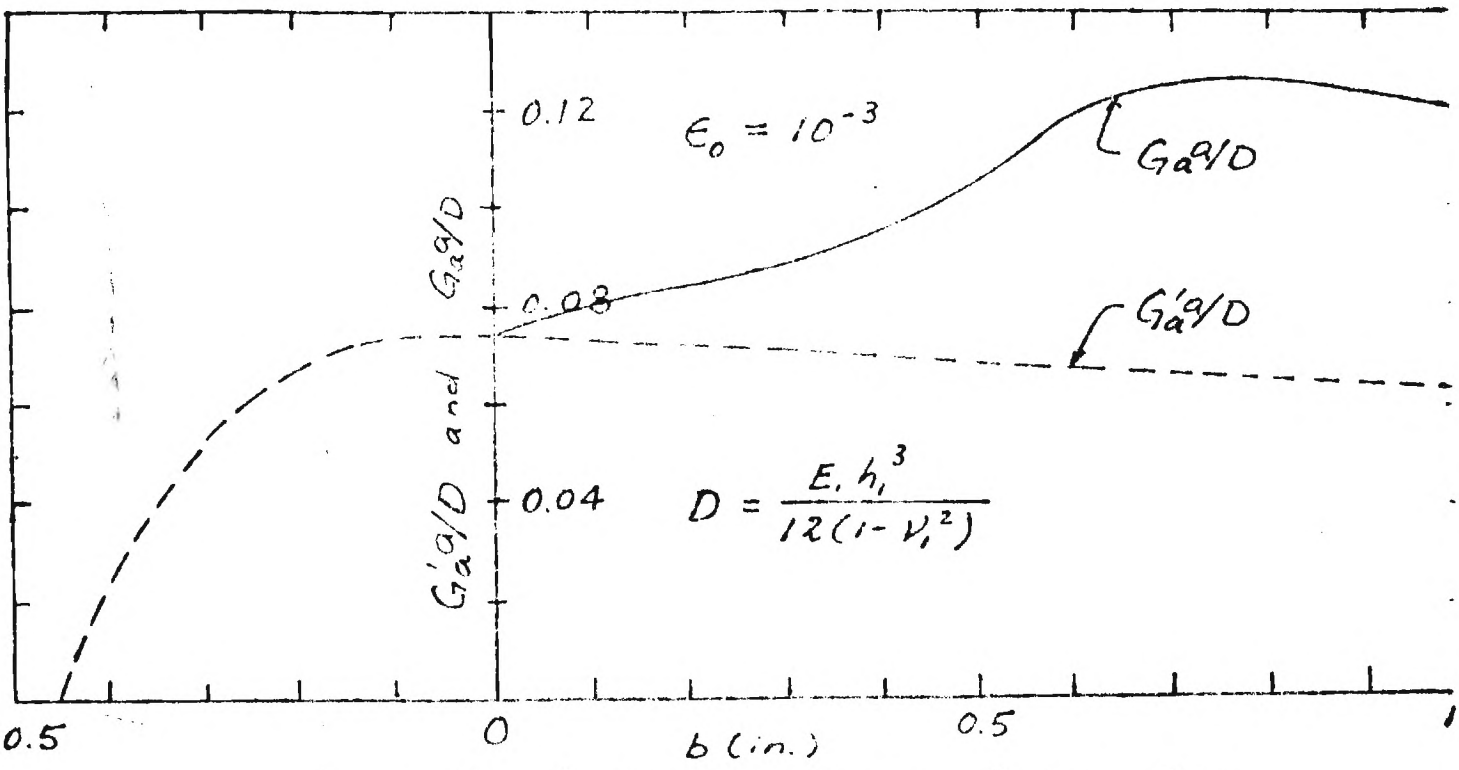

Fig. 1 Strain Energy Release Rate

2.4 Multiple delamination

Impact of foreign object on a composite laminate may cause delamination in more than one interlaminar faces. When the laminate is subsequently subjected to compressive strain ϵ_o, parallel thin layers separated by delamination may buckle independently or interactively. These layers may be considered together as a single relatively thick layer whose bending stiffness is considerably reduced by the existence of internal delamination. Analysis of multiple delamination resembles in many aspects the analysis of a stepped layer, and may also predict continued growth of damage under a laminate compressive load which, on the basis of a single uniform-thickness layer analysis, is presumed smaller than the residual strength.

REFERENCES

1. Kim, B. S. and Moon, F., "Impact Induced Stress Waves in an Anisotropic Plate," AIAA Journal, Oct., 1979, pp. 1126-1133.

2. Isaacson, E. and Keller, H. B., Analysis of Numerical Methods, John Wiley and Sons, Inc., 1966.

3. Cooley, J. W. and Tukey, J. W., "An Algorithm for the Machine Calculation of Complex Fourier Series," Mathematics of Computation, Vol. 90, No. 19, Apr. 1965, pp. 297-301.

4. Chai, H., Babcock, C. D., and Knauss, W.G., "One dimensional modelling of failure in laminated plates by delamination buckling," Int. J. Solids Structures, 17, pp. 1069-1083 (1981).

5. Whitcomb, J. D., "Finite element analysis of instability related delamination growth," J. Composite Materials, 15, pp. 403-426 (1981).

6. Whitcomb, J. D., "Approximate analysis of postbuckled through-width delaminations", NASA Technical Memorandum TM-83147, June 1981.

E-23-624

Georgia Institute of Technology
Atlanta, Georgia 30332

College of Engineering
School of Engineering Science and Mechanics

April 19, 1983

Mr. John N. Dickson
Department 72-77
Mail Zone 415
Lockheed-Georgia Company
Marietta, Georgia 30063

SUBJECT: Research Grant P.O. No. CA08738
Georgia Tech Project No. E-23-624
Progress Report (2/1/83 through 4/15/83)

Dear Mr. Dickson:

During the subject period, emphasis has been made to extend research work completed in the first phase of the research grant under P.O. No. CY48335 for the period from January 16 through September 15, 1982. With reference to the list of proposed areas of investigation attached to our letter to you on November 16, 1982, the present studies have been directed to the three-dimensional analysis of laminates under point load, general one-dimensional delamination, and growth of two-dimensional delaminations. The following represents a summary of the progress made under the subject grant during the subject period, and more detailed discussions are also enclosed:

I. Wave Propagation Due To Impact:

Three-dimensional wave propagation in laminates under point impact load has been initiated. The basic procedure using Fourier and Laplace transforms in the analysis of the two-dimensional case reported previously is followed with appropriate extensions. A Fortran computer code is being generated. As the source of difficulty lies in computer execution time and storage limitations, it is necessary to extensively modify the program written for the line impact problem. However, no limitation on the usefulness of the solution technique is expected.

II. Damage Growth:

In the second phase of the research activity on analytical models of delamination growth, the following three topics were identified as the subjects of primary interest:

(i) Study of the growth of general one-dimensional delamination on the basis of strain energy release rates by taking into account the buckling-induced bending and axial deformation in the main body of the laminate.

(ii) Parametric study of the growth characteristics of one-dimensional delamination.

(iii) Determination of the strain energy release rate associated with the growth of a two-dimensional delamination.

Beginning with the implementation of the second phase of this research project, significant analytical progress and conceptual generalizations have been achieved during the last quarter. Specifically, the following results were obtained:

(1) Closed-form expression of the strain energy release rate G associated with the growth of a general one-dimensional delamination (Eq. (2.8) of the new report).

(2) Separation of G into mode I and mode II components (Eqs. (3.6) and (3.5), containing an undetermined function of the thickness ratio) by means of dimensional analysis.

(3) Closed-form expressions of G associated with uniform expansion growth of a two dimensional thin-film delamination of circular shape (Eq. (4.7)) and of arbitrary shape (Eq. (5.3) and (5.2)). The expressions were obtained by means of the surface-independent M-integral of Eschelby, Knowles and Sternberg.

Furthermore, our expression of G for a general one-dimensional delamination includes the known formula for a thick-column model (Chai, Babcock and Knauss) and the formula for a symmetric double-cantilever beam as special cases. Our expression of G for the uniform expansion growth of a two-dimensional delamination suggests corresponding results in more general modes of growth.

As a consequence of these achievements, the strain energy release rate associated with delamination growth can be evaluated straightforwardly in terms of the post-buckling solution of the delamination. The procedure of numerical differentiation of the total potential energy with respect to geometrical parameters is rendered completely unnecessary.

We intend to implement extensive computation and parametric study on the basis of the foregoing analytical results to investigate the conditions and characteristics of delamination growth and thereby to provide a basis for evaluating damage tolerance of composite structures.

Sincerely yours,

R. K. Kunz, Assistant Professor

J. C. S. Wang, Professor

W. L. Yin, Associate Professor

vt

Lockheed-Georgia Company

Research Grant P. O. No. CA 08738

(Georgia Tech Project No. E-23-624)

Damage of Composite Structures

Progress Report (2/1/83 - 4/15/83)

April , 1983

by

R. K. Kunz

J. T. S. Wang

W. L. Yin

School of Engineering Science and Mechanics

Georgia Institute of Technology

Atlanta, Georgia 30032

Part I

Wave Propagation Due to Impact in Laminated Composite Plates

R. K. Kunz

The primary emphasis of this segment of the project has been toward an analytical and numerical study of the transient dynamic stresses in composite laminates subject to impact. Calculations of the transverse and longitudinal propagation of interlaminar stresses subsequent to impact are expected to yield critical information on the initiation and the extent of impact-induced delamination in composite laminates. Principal objectives of this phase of the project are the identification of those material and geometric parameters which are critical to the delamination phenomenon, and the explanation of experimentally observed delamination patterns in specimens subject to impact testing.

Previous reports [1,2] have dealt with the formulation of a set of difference-differential equations approximately governing the dynamic propagation of stresses in a multi-layer plate, of which each layer is orthotropic with principal material axes lying at an arbitrary orientation in the plane of the plate. This generality, which is absent in prior investigations into the problem [3], enables one to fully investigate the effects of stacking sequence on the transient behavior. The governing equations may be transformed into a set of linear algebraic equations by employing the Fourier transform in the in-plane spatial coordinates and the Laplace transform in time; the unknowns in this set of equations are the interlaminar stresses and displacements in the transform space. Upon specification of the impact boundary conditions on the free surfaces of the plate, the algebraic equations are solved. Finally, the inverse transforms are calculated numerically using the Fast Fourier Transform technique, to

yield the interlaminar stresses and displacements at discrete values of position and time subsequent to impact.

These techniques were employed successfully for the case of line-impact loading, or two-dimensional propagation, and the results reported in [4]. The principal conclusions obtained from that study may be briefly summarized as follows:

i) Immediately subsequent to impact on the top surface of the plate, a compressive wave propagates through the thickness; when it reaches the bottom surface, it is reflected as a tensile wave. It appears from this that delamination is initiated, and will be most extensive, directly underneath the impact zone at the interface furthest from the impact surface, due to these reflected tensile stresses. This conclusion is consistent with experimental results.

ii) As these tensile stresses do not propagate longitudinally, the spread of the delaminated area in the longitudinal direction must be due to the propagation of slower flexural waves generated subsequent to impact. This too agrees with certain experimental findings [5].

The numerical solution of the equations governing line impact has thus provided some useful results, and has established some measure of confidence in the approximations made in the derivation of the governing equations and in the numerical techniques employed for their solution. However, several unanswered questions remain, particularly concerning the directional dependence of longitudinal propagation of the delaminated areas on fiber orientation, which cannot be resolved on the basis of a two-dimensional analysis. Therefore, the present work has been directed toward extending the solution to the case of central impact, or three-dimensional propagation of stresses due to point loading.

Solution of the central impact problem is of interest because it corresponds physically to the most probable type of impact loading. Due to the generality incorporated into the mathematical problem formulation, results may be obtained for arbitrary material properties and layer stacking sequences. Numerical results obtained from this work for the dynamic interlaminar stresses should thus aid in the identification of critical material and geometric parameters influencing the extent of delamination caused by impact.

The approximate equations governing the three-dimensional propagation of stresses in a multi-layer plate were presented in detail in [2]; only their basic forms and considerations necessary for their solution will be given here. The transformed set of governing equations for the nth layer (n = 1 to N) have the form

$$[A_n]\{X_n\} + [B_n]\{X_{n-1}\} = 0, \quad n = 1, 2, \ldots, N \tag{1}$$

where

$$\{X_n\}^T = \{U_n, V_n, W_n, T_{22}^n, T_{12}^n, T_{23}^n\} \tag{2}$$

are the transformed interlaminar displacements and stresses at the nth interface, defined from the physical components of displacement and stress through a transformation of the form

$$U_n = \int_0^\infty \int_{-\infty}^{\infty} \int_{-\infty}^{\infty} u_n(x_1, x_3, t) \exp[-st + i(k_1 x_1 + k_3 x_3)]\, dx_1\, dx_3\, dt; \tag{3}$$

x_1 and x_3 are the in-plane coordinates; $[A_n]$ and $[B_n]$ are each 6 x 6 submatrices whose elements are complex, and depend on the orthotropic elastic constants of layer n, layer thickness and density, and the

variables k_1, k_3 and s. Boundary conditions corresponding to normal impact on the top surface (n = 0) have the form

$$T_{22}^{0} = H(k_1, k_3, s) \tag{4}$$
$$T_{12}^{0} = T_{23}^{0} = T_{22}^{N} = T_{12}^{N} = T_{23}^{N} = 0$$

where H is the transform of the loading function, presumed known. When equation (4) is incorporated into (1) to eliminate stresses at the top and bottom surfaces, the result is a set of 6N equations for the remaining 6N unknown stresses and displacements. This set of equations has a so-called block-tridiagonal form, for which a reasonably efficient solution algorithm may be implemented.

The solution procedure for the final determination of the interlaminar stresses as functions of position and time for the analogous two-dimensional case was discussed in detail in [2] and [4]. This basic procedure is also followed in the three-dimensional case, with appropriate extensions, and may be summarized as follows:

(i) Elastic constants for each layer are computed, based on the fiber orientation and the orthotropic constants for that layer.

(ii) Coefficients in $[A_n]$ and $[B_n]$, equation (1), are calculated for a specific value of each of the transform variables k_1, k_3, and s.

(iii) The linear algebraic equations are solved for the unknown, transformed interlaminar stresses; the solution is stored.

(iv) Values of k_1, k_3 and s are varied, and steps (ii) and (iii) are repeated until appropriate ranges of the three transform variables have been covered. Step sizes for the transform variables are determined by the time and spatial intervals over which changes are to be observed.

(v) The stored solutions for each of the transformed interlaminar stresses corresponding to discrete values of the transform variables k_1, k_3 and s are used in the Fast Fourier Transform algorithm to obtain the physical interlaminar stresses at discrete values of position and time.

This basic solution procedure was successfully implemented in the numerical solution of the line impact problem. Hence, many of the difficulties and pitfalls to be faced in solving the central impact problem have already been encountered in the solution of the two-dimensional case. The primary source of potential difficulty in the implementation of the above solution procedure for the three-dimensional case lies in computer execution time and storage limitations. However, it is felt that, with efficient programming, and by taking advantage of certain symmetries and antisymmetries in the governing equations, these limitations will not impose binding constraints on the usefulness of the solution technique.

At this writing, a Fortran computer code is being generated for the implementation of the solution algorithm outlined above. To accomplish this, it necessary to extensively modify the program written for the line impact problem, in order to generate and solve the larger set of equations, and to incorporate the additional spatial dimension into the Fourier transform inversion.

In addition to the completion of the numerical work for the study of three-dimensional wave propagation, a few other areas demand further attention in order to extend our understanding of the impact-induced delamination phenomenon. It would be useful to search the literature for a suitable dynamic delamination-failure criterion which could be incorporated into the wave propagation study; together, these could perhaps yield more

quantitative information as to the extent of the delamination as a result of a specific impact event. In addition, the effects of compressive in-plane pre-loading on a plate subject to impact should be investigated. These are both areas of potential future investigation which may yield valuable information on the factors affecting delamination.

References

1. Kunz, R. K., Wang, J. T. S., and Yin, W. -L., "Damage of Composite Structures", Progress Report for Lockheed Research grant P.O. No. CY48335, April, 1982.

2. Kunz, R. K., Wang, J. T. S., and Yin, W.-L., "Damage of Composite Structures", Progress Report for Lockheed Research Grant P.O. No. CY48335, June, 1982.

3. Kim, B. S. and Moon, F. C., "Impact Induced Stress Waves in an Anisotropic Plate", AIAA Journal, Oct. 1979, pp. 1126-1133.

4. Kunz, R. K., Wang, J. T. S., and Yin, W.-L., "Damage of Composite Structures", Final Report for Lockheed Research Grant P.O. NO. CY48335, September, 1982.

5. Takeda, N., Sierakowski, R. L., Ross C. A., and Malvern, L. E., "Delamination-crack Propagation in Ballistically Impacted Glass-Epoxy Composite Laminates," Experimental Mechanics, Vol. 22, No. 1, Jan. 1982, pp. 19-25.

Part II

Strain Energy Release Rate in Delamination Growth

J. T. S. Wang and W. L. Yin

Abstract Extending the work of our previous report, the strain energy release rate associated with the growth of a general one-dimensional delamination is obtained by evaluating the J-integral while taking into account the bending deformation of the laminate. Partition of the energy release rate into its mode I and mode II components is achieved by means of dimensional analysis and the resulting expressions contain an undetermined function of the ratio of the thickness of the delamination to that of the laminate. Buckling and uniform expansion growth of a thin-film circular delamination is analyzed in detail. By evaluating the M-integral, we obtain an expression of the strain energy release rate associated with uniform expansion growth of a two-dimensional delamination of arbitrary shape in terms of the laminate strain and the normal and tangential forces and the bending and twisting moments acting on the boundary of the delamination.

Table of Contents

1. Introduction

In the previous report, we adopted an approach based on the critera of critical energy release rates to determine the growth characteristics of one-dimensional delamination in a composite laminate subjected to compressive strain. There are many compelling reasons for preferring an energy release rate criterion. The first is its utmost mathematical simplicity, since the strain energy release rate is a scalar quantity. Secondly, although the energy release rate essentially depends on the singular stress field near the boundary of delamination, it is a global quantity and as such is not entirely determined by the local condition at any particular position. Furthermore, the energy release rate is not merely a function of the present geometry of delamination and of the distribution of stress; it depends also on the instantaneous mode of damage growth. The last feature is particularly valuable because it suggests the feasibility of predicting the actual mode of damage growth by comparing the energy release rates associated with various possible modes of growth.

In the special case of one-dimensional delamination, the strain energy release rate associated with delamination growth can be evaluated straightforwardly, in terms of the laminate strain and the axial force and the bendng moment at the moving front of delamination, by using the method of J-integral. Thus a solution of the post-buckling problem of the delaminated layer immediately yields the energy release rate associated with the growth of a one-dimensional delamination, and the procedure of analytical or numerical differentiation as required in the analysis of Chai et al. [1] is rendered completely unnecessary. The method of J-integral was used in our previous report [2] to evaluate the energy release rate of

a thin-film delamination. In Section 2 of he present report, we apply the same method to obtain the energy release rate of a general one-dimensional delamnation which takes into account the bending deformation of the main body of the laminate. It has been demonstrated [1] that there may be significant discrepancies between the energy release rates associated with thin-film delaminations on the one hand and general one-dimensional delaminations on the other hand.

There are evidences that the mode I and mode II components of the energy release rate have different effects upon the growth of delamination. In the previous report, a theory of separating these two components of the energy release rate was developed for a one-dimensional thin-film delamination on the basis of the invariance of solutions under similarity transformatons. The resulting expressions contained an undetermined material parameter. In Section 3 of the present report, the method is applied, with slight modification in detail, to general one-dimensional delaminations. The resulting expressions for mode I and mode II energy release rates contain an undetermined function of the ratio of the thickness of the delamination to that of the laminate.

In the practically important case of two-dimensional delamination, the postbuckling solution of the delaminated layer requires the application of von Karman's geometrically non-linear theory of plates. The edge forces and moments along the boundary of a two-dimensional thin-film delamination are determined by the post-buckling solution. Then the energy release rate associated with uniform expansion growth of the delamination can be evaluated and expressed in terms of the edge forces and moments and the compressive strain in the laminate. In deriving this expression we make

use of a surface-independent integral called the M-integral. The expression is obtained in Section 4 for the special case of unifom expansion of a circular delamination under an axisymmetric laminate load; it is obtained in Section 5 for uniform expansion growth of a thin-film delamination of arbitrary shape.

Since the actual mode of growth of a two-dimensional delamnatior is assumed to proceed in such a manner as to maximize the energy release rate at each stage of growth, it generally deviates from uniform expansion growth. Hence the energy release rate associated with uniform expansion (as obtained by evaluation of the M-integral) is a lower bound of the actual energy release rate.

The analytical results presented in this report offer a simple and rational procedure for studying and predicting the growth of delamination damage in a compressed laminate. Following this procedure, extensive computation and parametric study may be undertaken in subsequent research activity to determine the conditions and phenomena of delamination growth and to provide a basis for evaluating the damage-tolerance characteristics of composite structures.

Part A General One-Dimensional Delamination

2. Strain energy release rate associated with delamination growth

Consider a laminated plate, with the middle plane y = 0 and thickness t, and containing a delamination which runs across the entire width of the plate. The laminate is subjected to an average compressive strain ϵ_o in the longitudinal direction (the x-direction). The geometry of the problem and the loading on the plate are both independent of the z-coordinate. The laminate is unrestrained in the z-direction, so that the average value of the stress σ_z vanishes. When the compressive strain ϵ_o is sufficiently large, the delaminated layer buckles. This induces extensional and bending deformation in the main body of the laminate, as shown in Fig. 1. Such induced deformations caused by the buckling of the delaminated layer are negligibly small if the thickness h of the delaminated layer is small composed to that of the laminate, $h \ll t$. This situation defines the "thin-film model" introduced in the work of Chai et al. [1], and adopted in our previous report [2]. In the present report, general one-dimensional delamination models are analyzed by taking into account buckling induced deformation in the laminate. Numerical solutions of [1] showed that such deformation may produce appreciable and even significant effects on the calculated strain energy release rate associated with the growth of delamination.

Although our analytical method can be straightforwardly applied to orthotropic plates and plates with layered structures, the present analysis has been worked out in the simpler case of an isotropic plate for the sake of conciseness and clarity. Consequently, the linearly elastic behavior of

the material is characterized by two elastic moduli, E and ν. The post-buckling deformation and the axial forces and the bending moments in the various portions of the laminate can be calculated by using the classical beam-plate theory, as was done by Chai et al. [1]. This solution gives the compressive axial forces P_i and bending moments M_i (i = 1,2,3), per unit width of the plate, acting on the cross-section of the delamination and of the laminate at the front of delamination (Fig. 2). Equilibrium of forces and moments requires that

$$P_1 = P_2 + P_3 \ , \quad M_1 = M_2 + M_3 + P_3 H/2 - P_2 h/2 \ , \tag{2.1}$$

where H = t-h.

2.1 Two independent load parameters.

We decompose the system of forces and moments shown in Fig. 2 into subsystems:

$$M_i = M_i' + M_i'' \ , \quad P_i = P_i' + P_i'' \qquad (i = 1,2,3) \tag{2.2}$$

where the first subsystem is given by

$$\begin{aligned} &P_1' = 0 \ , \quad P_2' = -P_3' = \bar{h}\{P_1 + 6((1-\bar{h})M_1/t\} - P_3 \ , \\ &M_1' = 0 \ , \quad M_2' = M_2 - M_1(1-\bar{h})^3 \ , \quad M_3' = M_3 - M_1 \bar{h}^3 \ , \end{aligned} \tag{2.3}$$

where $\bar{h} = h/t$.

The second subsystem (P_i'' and M_i'') produces a continuous stress field near the delamination front:

$$\sigma_x = -\frac{P_1}{t} - \frac{12 M_1 y}{t^3} \ , \quad \tau_{xy} \approx 0 \qquad \left(-\frac{t}{2} \le y \le \frac{t}{2}\right)$$

The stress intensity factors associated with this subsystem of loading are $K_I'' = K_{II}'' = 0$. Consequently, the stress intensity factors associated with the total loading system (P_i and M_i) are the same as those associated with the first subsystem of loading:

$$K_I = K_I', \qquad K_{II} = K_{II}'.$$

It follows that the total loading system (P_i and M_i) and the first subsystem (P_i' and M_i') also yield the same mode I and mode II strain energy release rates during the growth of delamination:

$$G_I = \frac{K_I^2}{E} = \frac{K_I'^2}{E} = G_I', \quad G_{II} = \frac{K_{II}^2}{E} = \frac{K_{II}'^2}{E} = G_{II}'.$$

As a general rule, when evaluating the strain energy release rates associated with the growth of delamination, any component system of loading which generates a continuous stress field near the line of singularity may be completely ignored.

The subsystem of loading given by Eq. (2.3) leaves the undelaminated portion free from axial force and bending moment. Under this subsystem of loading, the two delaminated layers on the left side of Fig. 2 carry equal and opposite axial force

$$P^* = \bar{t}_h \{ P_1 + 6(1-\bar{t}_h) M_1/t \} - P_3 . \tag{2.4}$$

The thinner layer carries tensile load, $P_3' = P^*$ and the thicker layer carries a compressive load, $P_2' = -P^*$. The bending moments in the two layers are given respectively by

$$M^* = M_3 - M_1 \bar{h}^3 \tag{2.5}$$

and

$$M_2' = P^* t/2 - M^* = M_2 - M_1 (1-\bar{h})^3.$$

Hence the first subsystem (Eq. (2.3)) contains only two independent loading parameters P^* and M^*, defined respectively by Eqs. (2.4) and (2.5). The stress intensity factors and the mode I and mode II energy release rates are determined by these two loading parameters.

2.2 Calculation of the energy release rate

Under the tensile axial loading P^* and bending moment M^*, the thinner delaminated layer is subjected to the stress

$$\sigma_x = \frac{P^*}{h} - \frac{12 M^* \eta}{h^3}, \quad \sigma_y = 0 \qquad \left(-\frac{h}{2} \le \eta \le \frac{h}{2}\right). \tag{2.6}$$

Since there is no stress and strain in the non-delaminated portion, we have

$$\epsilon_z = 0 = (\sigma_z - \nu \sigma_x) / E .$$

It follows that

$$\begin{aligned} \sigma_z &= \nu \sigma_x , \\ \epsilon_x &= \frac{\sigma_x - \nu \sigma_z}{E} = \frac{1-\nu^2}{E} \sigma_x . \end{aligned} \tag{2.7}$$

Hence

$$\begin{aligned} dJ &= \frac{1}{2} (\sigma_x \epsilon_x + \sigma_z \epsilon_z) dy + \sigma_x \epsilon_x ds \\ &= \frac{1}{2} (\sigma_x \epsilon_x - \sigma_z \epsilon_z) ds = \frac{1-\nu^2}{2E} \left(\frac{P^*}{h} - \frac{12 M^* \eta}{h^3} \right)^2 , \end{aligned}$$

and the contribution to the J-integral from this layer is

$$\int_{-h/2}^{h/2} dJ = \frac{1-\nu^2}{2E} \left\{ \frac{(P^*)^2}{h} + \frac{12 (M^*)^2}{h^3} \right\} .$$

Similarly, the thicker delaminated layer, which is loaded by axial force $-P^*$ and bending moment $P^*t/2 - M^*$, contributes the following term to the J-integral

$$\int_{-H/2}^{H/2} dJ = \frac{1-\nu^2}{2E}\left\{\frac{(P^*)^2}{H} + \frac{12\,(P^*t/2 - M^*)^2}{h^3}\right\}.$$

The strain energy release rate associated with delamination growth equals the J-integral along a path in the x-y plane enclosing the tip of delamination. It is given by the sum of the last two integrals since the remaining portions of the path make no contribution:

$$G = \frac{1-\nu^2}{2E}\left\{\frac{(P^*)^2}{h} + \frac{(P^*)^2}{H} + \frac{12\,(M^*)^2}{h^3} + \frac{12\,(P^*t/2 - M^*)^2}{H^3}\right\}$$

$$= \frac{1-\nu^2}{2Et^3}\left\{\frac{(tP^*)^2}{\bar{h}(1-\bar{h})} + \frac{12\,(M^*)^2}{\bar{h}^3} + \frac{12\,(tP^*/2 - M^*)^2}{(1-\bar{h})^3}\right\}, \quad (2.8)$$

where $\bar{h} = h/t$ and P^* and M^* are defined in terms of the original loading P_i and M_i $(i = 1,2,3)$ by Eqs. (2.4) and (2.5).

2.3 Results for the thick column model

In their study of one-dimensional delamination growth, Chai et al. [1] considered a "thick-column model" in which the bending deformation is restricted to the thin delaminated layer, while each of the remaining parts of the laminate is subjected only to a compressive strain. They obtained a closed-form expression for the strain energy. The strain energy release

rate was then derived by direct differentiation. Their result can be obtained from our Eq. (2.8) by setting $M_1 = 0$. We have, from Eqs. (2.4) and (2.5),

$$P^* = \bar{h} P_1 - P_3 \quad , \quad M^* = M_3 \, .$$

Hence Eq. (2.8) reduces to

$$G = \frac{1-\nu^2}{2Et} \left\{ \frac{(\bar{h} P_1 - P_3)^2}{\bar{h}(1-\bar{h})} + \frac{12}{\bar{h}^3} \left(\frac{M_3}{t}\right)^2 + \frac{12}{(1-\bar{h})^3} \left(\frac{\bar{h}}{2} P_1 - P_3 - \frac{M_3}{t}\right)^2 \right\},$$

where the force P_1, the compressive load in the non-delaminated portion, and P_3 and M_3, the axial force and the bending moment at the ends of the delaminated layer, can be obtained from the solution of the buckling problem. We have

$$\frac{P_1}{Et} = \frac{(1-\bar{h})\,\epsilon_0 + \bar{h}\,\bar{\ell}\,\epsilon_{cr}}{1-\bar{h}+\bar{h}\,\bar{\ell}} \quad , \quad \frac{P_3}{Et} = \frac{\bar{h}\,\epsilon_{cr}}{1-\bar{h}+\bar{h}\,\bar{\ell}} \, ,$$

$$\left(\frac{M_3}{Et^2}\right)^2 = \frac{\bar{h}^4}{3} \frac{1-\nu^2\,\bar{h}(1-\bar{\ell})}{1-\bar{h}+\bar{h}\,\bar{\ell}} \epsilon_{cr}(\epsilon_0 - \epsilon_{cr})$$

where $\bar{\ell} = \ell/L$ is the ratio of the delamination length to the total laminate length, ϵ_0 is the average compressive strain of the laminate, and

$$\epsilon_{cr} = \frac{\pi^2}{3(1-\nu^2)} \left(\frac{h}{\ell}\right)^2$$

Substituting P_1, P_3 and M_3 into the expression of G, we obtain precisely Eq. (27) in Chai et al. [1].

However, our Eqs. (2.8), (2.4) and (2.5) also deliver the strain energy release rates for the general case when the other portions of the laminate suffer bending deformations under bending moments M_2 and M_3.

3. Partition of the strain energy release rate into mode I and mode II components

In the previous report, we used dimensional analysis to obtain separate expressions of the mode I and mode II energy release rates associated with the growth of a thin-film delamination. The expressions contain an undetermined material constant which should be evaluated by means of a numerical solution of the singular stress field or an experimental measurement. In the present report, a similar dimensional analysis is used to partition the strain energy release rate of a general one-dimensional delamination into its mode I and mode II components. The resulting expressions contain an undetermined material function of $\bar{h} = h/t$, which may be determined by a series of numerical solutions with varying ratios $\bar{h}$.

Let the subsystem of loading (Fig. (3a))

$$P_1' = 0, \quad P_2' = -P_3' = P^*,$$
$$M_1' = 0, \quad M_2' = tP^*/2 - M^*, \quad M_3' = M^*, \tag{3.1}$$

be further decomposed into two equilibrium component systems as shown in Figs. 3(b) and 3(c). Under the first component loading system, the thinner layer is subjected only to the axial force P^*. The stress component σ_y ahead of the delamination is proportional to $P^* r^{-1/2}$, where r is the distance from the tip of the delamination. We write

$$\sigma_y = \sigma(r; h, t) = \frac{f(h,t)}{\sqrt{r}} P^*.$$

We next consider a geometrically similar problem with t,h and H = t-h replaced by αt, αh and αH, respectively, where α is a positive constant.

Let the axial load P^* be replaced by αP^*. Then the stress distribution σ_y ahead of the delamination front in the new problem is related to that in the original problem by the relation

$$\sigma(\alpha r;\ \alpha h,\ \alpha t) = \sigma(r;\ h, t),$$

or,

$$\frac{f(\alpha h, \alpha t)}{\sqrt{\alpha r}}\ \alpha p^* = \frac{f(h,t)}{\sqrt{r}}\ p^*.$$

Hence,

$$f(\alpha h, \alpha t) = \frac{f(h,t)}{\sqrt{\alpha}}\ .$$

Assuming f to be a differentiable function of its arguments, the last equation may be differentiated with respect to α. Setting $\alpha = 1$ in the result of differentiation, we obtain

$$h\frac{\partial f}{\partial h} + t\frac{\partial f}{\partial t} = -\frac{f}{2},$$

or

$$\frac{\partial(\ln f)}{\partial(\ln h)} + \frac{\partial(\ln f)}{\partial(\ln t)} = -\frac{1}{2}.$$

Hence

$$\ln f = -\frac{1}{2}\ln h + \ln \alpha,$$

where α is an arbitrary function of $\bar{h} = h/t$. Consequently,

$$\sigma_y = \frac{f(h,t)}{\sqrt{r}}\ p^* = \frac{\alpha(\bar{h})}{\sqrt{hr}}\ p^*.$$

Similarly, the shearing stress distribution ahead of the tip of the delamination has the following expression

$$\tau_{xy} = \frac{\gamma(\bar{h})}{\sqrt{hr}}\ p^*.$$

Next consider the effect of the loading shown in Fig. 3(c), The stress component σ_y ahead of the delamination is given by

$$\sigma_y = \sigma(r; h, t) = \frac{g(h,t)}{\sqrt{r}} M^*.$$

Comparison with a geometrically similar problem yields the functional equation

$$\frac{g(\alpha h, \alpha t)}{\sqrt{\alpha r}} \alpha^2 M^* = \frac{g(h,t)}{\sqrt{r}} M^*.$$

The solution of this equation is

$$g(h,t) = \frac{\beta(\bar{h})}{h^{3/2}}.$$

Hence

$$\sigma_y = \frac{\beta(\bar{h})}{(hr)^{3/2}} M^*,$$

and similarly

$$\tau_{xy} = \frac{\delta(\bar{h})}{(hr)^{3/2}} M^*.$$

Combining the effects of the two component loading systems, we obtain the following expressions of the mode I and mode II stress intensity factors

$$K_I = \frac{\alpha(\bar{h})}{\sqrt{h}} P^* + \frac{\beta(\bar{h})}{h^{3/2}} M^*, \quad K_{II} = \frac{\gamma(\bar{h})}{\sqrt{h}} P^* + \frac{\delta(\bar{h})}{h^{3/2}} M^*. \quad (3.2)$$

Hence the total strain energy release rate is given by

$$G = \frac{K_I^2 + K_{II}^2}{E} = \frac{1}{hE}\left\{(\alpha^2+\gamma^2)(P^*)^2 + \frac{\alpha\beta+\gamma\delta}{h} 2P^*M^* + \frac{\beta^2+\delta^2}{h^2}(M^*)^2\right\}. \quad (3.3)$$

Equating the two expressions of G as given by Eqs. (2.8) and (3.3), we obtain an identity valid for various combinations of the load parameters P^* and M^*. This implies that the respective coefficients of $(P^*)^2$, P^*M^* and $(M^*)^2$ in the two expressions of G are identical. Hence,

$$\frac{2}{1-\nu^2}(\alpha^2+\gamma^2) = \frac{1+\bar{h}+\bar{h}^2}{(1-\bar{h})^3},$$

$$\frac{2}{1-\nu^2}(\alpha\beta+\gamma\delta) = -\frac{6\bar{h}^2}{(1-\bar{h})^3},$$

$$\frac{2}{1-\nu^2}(\beta^2+\delta^2) = 12\,\frac{1-3\bar{h}+3\bar{h}^2}{(1-\bar{h})^3}.$$

The general solution of this system of algebraic equations is given by

$$\begin{aligned}
(1-\bar{h})^{3/2}\left(\frac{2}{1-\nu^2}\right)^{1/2}\alpha &= -(1+\bar{h}+\bar{h}^2)^{1/2}\sin\omega,\\
(1-\bar{h})^{3/2}\left(\frac{2}{1-\nu^2}\right)^{1/2}\gamma &= (1+\bar{h}+\bar{h}^2)^{1/2}\cos\omega,\\
(1-\bar{h})^{3/2}\left(\frac{2}{1-\nu^2}\right)^{1/2}\beta &= \{12(1-3\bar{h}+3\bar{h}^2)\}^{1/2}\cos\chi,\\
(1-\bar{h})^{3/2}\left(\frac{2}{1-\nu^2}\right)^{1/2}\delta &= \{12(1-3\bar{h}+3\bar{h}^2)\}^{1/2}\sin\chi,
\end{aligned} \tag{3.4}$$

where $\omega = \omega(\bar{h})$ is some function of h and $\chi = \chi(\bar{h})$ is determined by the relation

$$\sin(\chi-\omega) = -\frac{6\bar{h}^2}{\sqrt{12(1+\bar{h}+\bar{h}^2)(1-3\bar{h}+3\bar{h}^2)}}. \tag{3.5}$$

Substituting Eq. (3.4) into (3.2) and using the relations between the energy release rates and the stress intensity factors, we obtain the following expressions of the mode I and mode II energy release rates:

$$G_I = \frac{K_I^2}{E} = \frac{1-\nu^2}{2Eh(1-\bar{h})^3}\left\{-\sqrt{1+\bar{h}+\bar{h}^2}\,P^*\sin\omega+\sqrt{12(1-3\bar{h}+3\bar{h}^2)}\,\frac{M^*}{h}\cos\chi\right\}^2,$$

$$G_{II} = \frac{K_{II}^2}{E} = \frac{1-\nu^2}{2Eh(1-\bar{h})^3}\left\{\sqrt{1+\bar{h}+\bar{h}^2}\,P^*\cos\omega+\sqrt{12(1-3\bar{h}+3\bar{h}^2)}\,\frac{M^*}{h}\sin\chi\right\}^2, \quad (3.6)$$

where one material function $\omega(\bar{h})$ is undetermined and the other $\chi(\bar{h})$ is related to the first according to Eq. (3.5). The material function $\omega(\bar{h})$ can be determined by solving a sequence of singular stress distributions near the delamination tip for various values of $\bar{h}$, or by using simpler methods such as the crack closure integral.

For a thin-film delamination, $\bar{h}$ approaches the limiting value 0 and both ω and χ reduce to the same constant, $\omega=\chi$. The expressions of Eq. (3.6) also reduce to the form given in the previous report.

Another special case, $\bar{h}$ = 1/2, corresponds to a symmetric double cantilever beam-plate. For this case Eq. (3.5) yields

$$\omega-\chi = \sin^{-1}\left(\sqrt{3/7}\right), \quad (3.7)$$

and Eq. (3.6) reduces to

$$G_I = \frac{1-\nu^2}{Eh}\left\{-\sqrt{7}\,P^*\sin\omega+\sqrt{12}\,\frac{M^*}{h}\cos\chi\right\}^2,$$

$$G_{II} = \frac{1-\nu^2}{Eh}\left\{\sqrt{7}\,P^*\cos\omega+\sqrt{12}\,\frac{M^*}{h}\sin\chi\right\}^2. \quad (3.8)$$

Although Eqs. (3.7) and (3.8) are valid for different combinations of loading parameters P^* and M^*, in buckling problems associated with delamination where $h = H = t/2$, the force $P^* = P_3' = -P_2'$ vanishes because of the symmetry condition $P_2' = P_3'$. Hence Eq. (3.8) reduces to

$$G_I = \frac{12(1-\nu^2)}{E h^3}(M^* \cos\chi)^2, \quad G_{II} = \frac{12(1-\nu^2)}{E h^3}(M^* \sin\chi)^2.$$

The condition of symmetry also implies that $G_{II} = 0$. Consequently, $\chi = 0$ and

$$G_I = \frac{12(1-\nu^2)}{E h^3}(M^*)^2.$$

The last result is well-known.

Part B. Uniform Expansion of a Two-dimensional Delamination

In this part of the report, we consider a two-dimensional thin-film delamination in a plate subjected to compressive loading. When the compressive strain is sufficiently large, the delaminated layer buckles. Although the buckling load (or the corresponding strain in the plate) are determined by the classical plate theory, the post-buckling solution of the delaminated layer requires the application of von Karman's geometrically non-linear theory of plates. When the post-buckling solution is obtained by appropriate numerical methods, the normal and shearing forces and the bending and twisting moments along the curved boundary of the delamination may be calculated. The pattern of delamination growth cannot be predicted without introducing certain fracture criteria. Chai [3], for example, postulated that an elliptical delamination grows in such a manner as to maximize the strain energy released per unit incremental area of delamination at each stage of growth. He calculated the total strain energy release rate by numerical differentitation of the total potential energy.

In the present work, we calculate the strain energy release rate associated with uniform expansion growth of a two-dimensional thin-film delamination of arbitrary shape by means of the M-integral. The result is expressed as a line integral (along the boundary of the delaminated region) of a quadratic function of the normal and shearing forces and bending and twisting moments. Although the actual growth pattern of the delamination is generally not a uniform expansion, the present result yields a lower bound estimate of the (maximum) energy release rate associated with the actual growth pattern, and therefore can be useful in predicting the growth of delamination.

The M-integral is first applied to the uniform growth of a circular delamination under axi-symmetric in-plane compression (Section 4). The extension of the method to the uniform growth of a two-dimensional delamination of arbitrary shape under axi-symmetric compression is shown in Section 5.

4. Uniform expansion of a circular delamination under axi-symmetric compression

4.1 Critical buckling load and post-buckling solution

The critical buckling load of a two-dimensional delaminated layer can be obtained by applying linear buckling equations. For a clamped isotropic circular delamination under axi-symmetric compression, the transverse deflection as a function of the radial coordinate satisfies Bessel's equation of zeroth order. The critical radial compressive force P_{cr} per unit arc length on the boundary of the delamination is determined by the first zero of Bessel's function of first order, i.e.,

$$J_1(\sqrt{P_{cr}/D}\, a) = 0, \quad \text{or} \quad \sqrt{P_{cr}/D}\, a = 3.83171, \qquad (4.1)$$

where a is the radius of the circular delamination and $D = Eh^3/12(1-\nu^2)$.

Generally, a reasonably accurate post-buckling analysis of the delaminated layer requires the application of non-linear plate theory. In contrast to the linear theory, the membrane stresses in the non-linear buckling theory are not uniform over the plate. For the case of a clamped circular plate under axi-symmetric compression, the radial compressive force

per unit circumferential length depends on the radial coordinate, $P = P(r)$. Let $\varphi(r) = w'(r)/r$ where w is the transverse displacement. Then the buckling problem is described by the following system of differential equations and boundary conditions [4]

$$r^{-3}(r^3 P')' = Eh\,\varphi^2/2, \quad r^{-3}(r^3 \varphi')' = -P\varphi/D, \tag{4.2}$$

$$P'(0) = 0, \quad \varphi'(0) = 0, \quad \varphi(a) = 0. \tag{4.3}$$

If the compressive loading on the boundary $r = a$ produces a radial displacement $u_r = -a\epsilon_0$, then

$$-a\epsilon_0 = \int_0^a \epsilon_r\,dr - \int_0^a \frac{(w')^2}{2}\,dr$$

$$= \frac{1}{Eh}\int_0^a \{-P + \nu(rP)'\}\,dr - \frac{1}{2}\int_0^a (r\varphi)^2\,dr. \tag{4.4}$$

For given ϵ_0, Eqs. (4.2) - (4.4) can be solved numerically for the functions $P(r)$ and $\varphi(r) = w'(r)/r$. This solution yields the radial force $P(a)$ and bending moment $M_r(a)$ per unit arc length of the boundary, where $M_r = D \times (w'' + \frac{\nu}{r}w')$.

4.2 Strain energy release rate associated with uniform expansion

Consider a plate, containing a thin-film delamination of radius a, subjected to uniform biaxial compressive strain ϵ_0. When ϵ_0 is sufficiently large so that the delamination buckles, the radial compressive force $P(a)$ and the bending moment $M(a)$ along the edge of the delamination can be computed numerically by solving Eqs. (4.2) - (4.4). In the fol-

lowing, we evaluate the M-integral to obtain the strain energy release rate associated with uniform expansion of the circular delamination in terms of ϵ_0, P(a) and M(a).

Let a constant biaxial stress field

$$\sigma_x = \sigma_y = \frac{E}{1-\nu}\epsilon_0 \ , \quad \sigma_z = 0 \ , \quad \tau_{ij} = 0 \tag{4.5}$$

be superposed on the (non-linear) buckling solution. Since the constant stress field is continuous, it produces no effect on the stress intensity factor and energy release rate. With the superposition of the constant stress field, the exterior boundary of the main body of the laminate becomes stress-free and the edge of the delamination is subjected to a bending moment M^* and a tensile radial force P^*, per unit arc length, given respectively by

$$M^* = M(a) \ , \quad P^* = \frac{Eh}{1-\nu}\epsilon_0 - P(a) \ . \tag{4.6}$$

Hence, along the edge of delamination r=a, we have

$$\sigma_r = \frac{P^*}{h} - \frac{12\,M^*\eta}{h^3} \qquad \left(-\frac{h}{2} \le \eta \le \frac{h}{2}\right) ,$$

$$E\,\epsilon_\theta = \sigma_\theta - \nu\,\sigma_r = 0 \ , \quad \epsilon_r = \frac{1-\nu^2}{E}\sigma_r \ ,$$

$$W\,x_j\,n_j = -\frac{1-\nu^2}{2E}\,a\,\sigma_r^2 \ , \quad -\sigma_{jk}\,n_k\,u_{j,i}\,x_i = \frac{1-\nu^2}{E}\,a\,\sigma_r^2 \ ,$$

where W is the strain energy density. The circular edge of the delamination yields the following contribution to the M-integral:

$$M = \iint \left(W x_i n_i - \sigma_{jk} n_k u_{j,i} x_i - \frac{1}{2} \sigma_{ik} n_k u_i \right) dA$$

$$= 2\pi a \int_{-h/2}^{h/2} \frac{1-\nu^2}{2E} a \sigma_r^2 \, d\eta$$

$$= \frac{\pi a^2 (1-\nu^2)}{E} \left\{ \frac{(P^*)^2}{h} + \frac{12 (M^*)^2}{h^3} \right\} .$$

Budiansky and Rice [5] have shown the following relation between the M-integral and the rate of energy release in uniform expansion of a crack:

$$M = a \frac{d\Pi}{da} .$$

Hence

$$\frac{d\Pi}{d(\pi a^2)} = \frac{M}{2\pi a^2} = \frac{1-\nu^2}{2Eh} \left\{ (P^*)^2 + 12 \left(\frac{M^*}{h} \right)^2 \right\}$$

$$= \frac{1-\nu^2}{2Eh} \left[\left\{ \frac{Eh}{1-\nu} \epsilon_0 - P(a) \right\}^2 + 12 \left\{ \frac{M(a)}{h} \right\}^2 \right] \qquad (4.7)$$

gives the strain energy release rate per unit increment of area of delamination, as the delamination grows uniformly under a biaxial compressive laminate strain ϵ_0. As was mentioned previously, P(a) and M(a) may be evaluated from the solution of Eqs. (4.2) - (4.4).

5. Strain energy release rate associated with uniform expansion of a two-dimensional delamination of arbitrary shape

Sufficiently large compressive loading on a plate containing a two-dimensional delamination of arbitrary shape may produce buckling of the delaminated layer and growth of delamination. In general, the solution of the non-linear buckling problem requires approximate numerical methods. The solution determines the normal and shearing forces and bending and twisting moments acting along the boundary of the delamination. When the distribution of these forces and moments are obtained, the strain energy release rate associated with uniform expansion growth of the delamination can be evaluated by means of the M-integral. As mentioned previously, the actual growth of the delamination is assumed to proceed in such a manner as to maximize the rate of energy release at each stage of growth and therefore it generally deviates from uniform expansion growth. Thus the energy release rate calculated in the following gives a lower bound of the maximum energy release rate.

For simplicity we consider the case when the main body of the laminate is subjected to a uniform biaxial strain $\epsilon_x = \epsilon_y = -\epsilon_0$. Let P(s), Q(s), $M_n(s)$ and $M_{ns}(s)$ denote the normal compressive force, shearing force, bending moment and twisting moment acting on a segment of unit arc length of the boundary of delamination, where all four quantities are expressed as functions of the arc length parameter s. Let the constant biaxial stress field of Eq. (4.5) be superimposed so that the exterior boundary of the laminate becomes stress-free. Then the normal, circumferential and shearing stresses on the boundary of delamination are given respectively by

$$\sigma_n = \frac{E}{1-\nu}\epsilon_0 - \frac{P}{h} - \frac{12 M_n}{h^3}\eta \ ,$$

$$\sigma_s = \nu \sigma_n \ ,$$

$$\tau_{ns} = \frac{Q}{h} - \frac{12\, M_{ns}}{h^3}\eta \qquad \left(-\frac{h}{2} \le \eta \le \frac{h}{2}\right).$$

Let $\xi(s)$ be the perpendicular distance from the origin of the x-y plane to the tangent line of the delamination boundary at the point with the parameter value s. Then

$$A = \frac{1}{2}\oint \xi(s)\, ds \tag{5.1}$$

is the area of delamination and $\frac{1}{2}\xi(s)ds$ is the contribution to that area from a boundary element of arc length ds. The integrand of the M-integral is given by

$$W x_i n_i - \sigma_{jk} n_k u_{j,i} x_i - \frac{1}{2}\sigma_{ik} n_k u_i$$
$$= -\left\{\frac{1-\nu^2}{2E}\sigma_n^2 + \frac{1+\nu}{E}\tau_{ns}^2\right\}\xi + 2\left\{\frac{1-\nu^2}{2E}\sigma_n^2 + \frac{1+\nu}{E}\tau_{ns}^2\right\}\xi$$

Hence,

$$M = \oint \left[\frac{1-\nu^2}{2Eh}\left\{\left(\frac{Eh}{1-\nu}\epsilon_0 - P(s)\right)^2 + 12\left(\frac{M_n(s)}{h}\right)^2\right\}\right.$$
$$\left. + \frac{1+\nu}{Eh}\left\{Q(s)^2 + 12\left(\frac{M_{ns}(s)}{h}\right)^2\right\}\right]\xi(s)\, ds \tag{5.2}$$

and the strain energy released per unit increment of delamination area is

$$\frac{d\Pi}{dA} = \frac{M}{2A} \tag{5.3}$$

In the special case of a circular delamination, $Q(s)$ and $M_{ns}(s)$ vanish identically because the laminate is subjected to axi-symmetric compressive loading. It is easily found that Eqs. (5.2) and (5.3) reduce to Eq. (4.7).

References

[1] Chai, H., Babcock, C. D. and Knauss, W. G., "One dimensional modelling of failure in laminated plates by delamination buckling," Int. J. Solids Structures, 17, 1069-1083 (1981).

[2] Kunz, R. K., Wang, J. T. S. and Yin, W.-L., "Damage of Composite Structures. Part II: Analytical Models of Delamination Growth", Georgia Tech Project No. E-23-624 Final Report, September, 1982.

[3] Chai, H., Ph.D. Thesis, The Growth of Impact Damage in Compressively Loaded Laminates, California Institute of Technology, Pasadena, California, 1982.

[4] Bodner, S. R., "The post-buckling behavior of a clamped circular plate", Quart. Appl. Math., 12, 397-401 (1954).

[5] Budiansky, B. and Rice, J. R., "Conservation laws and energy-release rates", J. Appl. Mech., 40, 201-203 (1973).

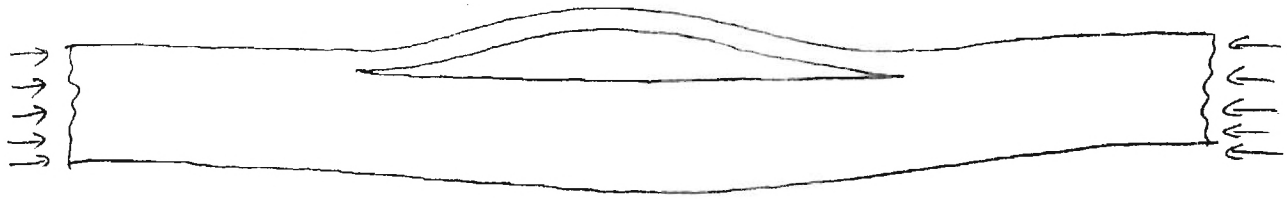

Fig. 1

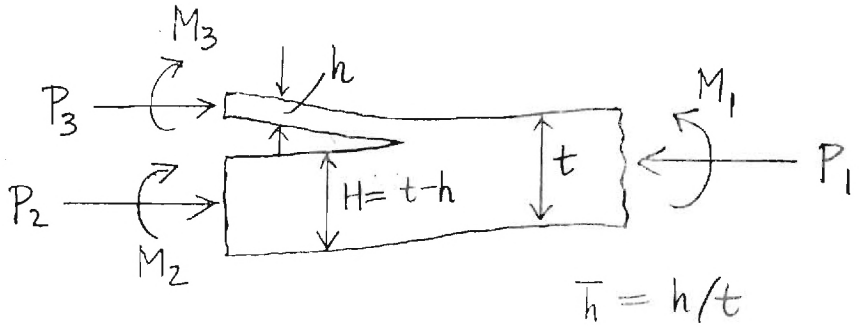

Fig. 2

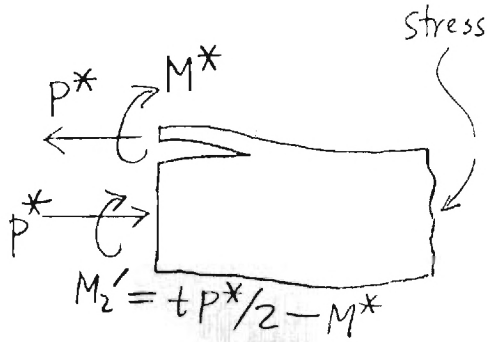

Fig. 3a

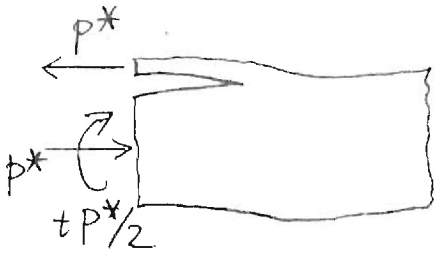

Fig. 3b

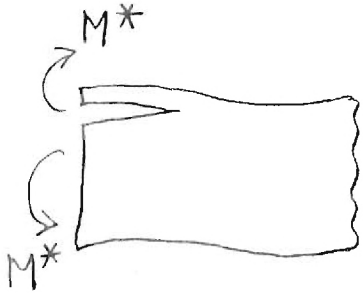

Fig. 3c

Georgia Institute of Technology
Atlanta, Georgia 30332

College of Engineering
School of Engineering Science and Mechanics

April 19, 1983

Mr. John N. Dickson
Department 72-77
Mail Zone 415
Lockheed-Georgia Company
Marietta, Georgia 30063

SUBJECT: Research Grant P.O. No. CA08738
Georgia Tech Project No. E-23-624
Progress Report (2/1/83 through 4/15/83)

Dear Mr. Dickson:

During the subject period, emphasis has been made to extend research work completed in the first phase of the research grant under P.O. No. CY48335 for the period from January 16 through September 15, 1982. With reference to the list of proposed areas of investigation attached to our letter to you on November 16, 1982, the present studies have been directed to the three-dimensional analysis of laminates under point load, general one-dimensional delamination, and growth of two-dimensional delaminations. The following represents a summary of the progress made under the subject grant during the subject period, and more detailed discussions are also enclosed:

I. Wave Propagation Due To Impact:

Three-dimensional wave propagation in laminates under point impact load has been initiated. The basic procedure using Fourier and Laplace transforms in the analysis of the two-dimensional case reported previously is followed with appropriate extensions. A Fortran computer code is being generated. As the source of difficulty lies in computer execution time and storage limitations, it is necessary to extensively modify the program written for the line impact problem. However, no limitation on the usefulness of the solution technique is expected.

II. Damage Growth:

In the second phase of the research activity on analytical models of delamination growth, the following three topics were identified as the subjects of primary interest:

(i) Study of the growth of general one-dimensional delamination on the basis of strain energy release rates by taking into account the buckling-induced bending and axial deformation in the main body of the laminate.

(ii) Parametric study of the growth characteristics of one-dimensional delamination.

(iii) Determination of the strain energy release rate associated with the growth of a two-dimensional delamination.

Beginning with the implementation of the second phase of this research project, significant analytical progress and conceptual generalizations have been achieved during the last quarter. Specifically, the following results were obtained:

(1) Closed-form expression of the strain energy release rate G associated with the growth of a general one-dimensional delamination (Eq. (2.8) of the new report).

(2) Separation of G into mode I and mode II components (Eqs. (3.6) and (3.5), containing an undetermined function of the thickness ratio) by means of dimensional analysis.

(3) Closed-form expressions of G associated with uniform expansion growth of a two dimensional thin-film delamination of circular shape (Eq. (4.7)) and of arbitrary shape (Eq. (5.3) and (5.2)). The expressions were obtained by means of the surface-independent M-integral of Eschelby, Knowles and Sternberg.

Furthermore, our expression of G for a general one-dimensional delamination includes the known formula for a thick-column model (Chai, Babcock and Knauss) and the formula for a symmetric double-cantilever beam as special cases. Our expression of G for the uniform expansion growth of a two-dimensional delamination suggests corresponding results in more general modes of growth.

As a consequence of these achievements, the strain energy release rate associated with delamination growth can be evaluated straightforwardly in terms of the post-buckling solution of the delamination. The procedure of numerical differentiation of the total potential energy with respect to geometrical parameters is rendered completely unnecessary.

We intend to implement extensive computation and parametric study on the basis of the foregoing analytical results to investigate the conditions and characteristics of delamination growth and thereby to provide a basis for evaluating damage tolerance of composite structures.

Sincerely yours,

vt

Georgia Institute of Technology
Atlanta, Georgia 30332

E-23-624

College of Engineering
School of Engineering Science and Mechanics

July 20, 1983

Mr. John N. Dickson
Department 72-77
Mail Zone 415
Lockheed-Georgia Company
Marietta, Georgia 30063

SUBJECT: Research Grant P.O. No. CA 08738
Georgia Tech Project No. E-23-624
Progress Report (4/16/83 through 6/30/83)

Dear Mr. Dickson:

The following represents a summary of the progress made under the subject grant during the subject period, and more detailed discussions are also enclosed:

I. Wave Propagation Due to Impact:

Work has been directed toward the generation of a Fortran program to perform the complex numerical calculations. The subroutines for solution of the block-tridiagonal system of equations with complex coefficients have been completed and tested. Work on routines to assemble the coefficient matrix to take advantage of symmetries in the solution over ranges of values of the transform variables is progressing.

II. Damage Growth:

A substantial amount of computation and analysis has been made to test the previously developed theory of delamination buckling and the method of evaluating energy release rates. Predictions of our formulae for the total energy release rate and for its mode I component were compared with the existing finite-element results generated by means of the closure integral. Good agreement was observed as shown in the attached figures of this report. The difference between our theory and Whitcomb's approximate analysis is discussed. It is pointed out that the prediction of the present theory appears to be more uniformly in agreement with the complete set of finite-element results.

Sincerely yours,

Lockheed-Georgia Company

Research Grant P. O. No. CA 08738

(Georgia Tech Project No. E-23-624)

DAMAGE OF COMPOSITE STRUCTURES

Progress Report (4/16/83 - 6/30/83)

July, 1983

by

R. K. Kunz

J. T. S. Wang

W. L. Yin

School of Engineering Science and Mechanics

Georgia Institute of Technology

Atlanta, Georgia 30332

Part I

Wave Propagation Due to Impact in Laminated Composite Plates

R. K. Kunz

Efforts devoted to the analytical determination of dynamic interlaminar stresses in a laminated composite plate due to central impact are continuing. The mathematical analysis and numerical techniques required have been outlined in previous reports. The analysis is sufficiently general to enable the calculation of interlaminar stresses for arbitrary material properties and layer stacking sequence. Results obtained from this work are expected to shed some light on the initiation of impact-induced delamination.

Current work has been directed toward the generation of a Fortran program to perform the complex numerical calculations required in the determination of interlaminar stresses as functions of position and time. The numerical techniques employed are entirely analogous to those used in the successful implementation of the line impact problem reported previously. However, due to the presence of the additional spatial dimension in the central impact case, additional difficulties arise which must be overcome. In particular, computer storage requirements and execution time required to perform the calculations become a major consideration in the three-dimensional case. As a result, special attention must be paid to optimizing the program with respect to these criteria. In addition, each segment of the program requires extensive testing during development in order to ensure its correct functioning when assembled with the remainder of the program.

At this writing, the subroutines for solution of the block-tridiagonal system of algebraic equations with complex coefficients has been completed and tested. It is crucial that these subroutines be as efficient as possible, since it is required to solve the system of equations for each combination of the

transformed spatial and time variables. Work is currently progressing on routines to assemble the coefficient matrix of the linear system and to take advantage of symmetries in the solution over ranges of values of the transform variables. Finally, routines to invert the Fourier transform in the two in-plane spatial dimensions and the Laplace transform in time must be implemented for the case of central impact. When completed, the program will yield the interlaminar normal and shear stresses at discrete values of the in-plane coordinates and time subsequent to impact.

Part II

Analytical Models of Delamination Growth

J.T.S. Wang and W.-L. Yin

Abstract The procedure for evaluating the energy-release rate and its mode I and mode II components in the growth of a general one-dimensional delamination, as developed in the last report, takes into account the bending deformation of the laminate and the resulting formulae involve a single undetermined parameter. In the present report, the total energy release rate as predicted by our theory is compared with the available finite-element results for a specific problem and reasonable agreement is observed. Furthermore, a procedure is worked out for evaluating the undetermined parameter on the basis of selected data from finite-element solutions. With this parameter value, our theory delivers mode I and mode II energy-release rates that are in satisfactory agreement with the remaining finite-element solutions. In spite of the formal semblance between our formula for the mode I energy release-rate and an empirical formula proposed by Whitcomb, there are important differences in structure and rational justification. Futhermore, the prediction of the present theory appears to be more uniformly in agreement with the complete set of finite-element results.

1. Introduction

A theory for evaluating the energy-release rate in the growth of a one-dimensional delamination and, furthermore, for separating this energy-release rate into its mode I and mode II components, has been developed in two previous reports [1,2]. In the present report, the validity of the theory is tested by application to a specific one-dimensional problem whose finite-element solutions are available in the literature [3]. Satisfactory agreement is found between the total energy-release rate according to finite-element analysis and that according to the present theory. The discrepancy between the two types of results appears to be reasonable in view of the different assumptions underlying the respective postbuckling solutions.

Our theory of separating the energy-release rate yields a pair of formulae, containing a single undetermined parameter, for evaluating the mode I and mode II energy-release rates. The value of the parameter may be inferrred from the mode I energy-release rate associated with a small, selected set of finite-element solutions. When the parameter is so evaluated, our formulae deliver mode I and mode II energy-release rates that are in satisfactory agreement with the remaining finite-element results. This agreement not only verifies the applicability of the theory, it also suggests that the validity of the results is unaffected by structural and material inhomogeneities in the laminate, since the laminate under consideration is composed of graphite-epoxy layers and an aluminum plate. In view of the intended application of the present thoery to composite laminates, this broader scope of applicability is indeed a most important and desirable feature.

While our formula for the mode I energy-release rate bears some formal semblance to an empirical formula proposed by Whitcomb [4], it is essentially different in its rationale and structure. The former is based on the knowledge of the total energy release rate as delivered by the postbuckling solution of the laminate and the J-integral method; the latter is guided by intuitive arguments and mainly based on curve-fitting the finite-element data. The former gives a consistent treatment of the end rotation of the delamination by taking into account the bending deformation in the main body of the laminate, the latter ignores laminate bending and deals with the end rotation of the delamination by introducing an "effective delamination length" based on finite-element solution of critical buckling loads. Furthermore, the number of undetermined parameters and the force and moment variables occurring in the respective formulae are different. The present theory not only furnishes a theoretical justification of the resulting formulae, it also appears to deliver results more uniformly in agreement with that of the finite-element analysis.

2. Postbuckling solution and the energy release rate

In the finite-element model of one-dimensional delamination studied by Whitcomb [3,4], a unidirectional graphite-expoxy coupon of thickness h is bonded to an aluminum plate of thickness H = 6 mm, except for a segment of length 2a. Figure 1 shows one half of the laminate. Let $w(\xi)$ and $v(\xi)$ denote respectively the transverse deflections of the unbonded segments of the composite layer and of the aluminum plate, and let $u(\eta)$ denote the transverse deflection of the bonded portion, where $0 \le \xi \le a$ and $0 \le \eta \le b$. Then

$$u(\eta) = -A(1 - \cos \varkappa\eta),$$

$$v(\xi) = -A\left[\frac{\varkappa \sin \varkappa b}{\lambda \sin \lambda a} (\cos \lambda\xi - \cos \lambda a) + 1 - \cos \varkappa b\right] \qquad (1)$$

$$w(\xi) = -A\left[\frac{\varkappa \sin \varkappa b}{\mu \sin \mu a} (\cos \mu\xi - \cos \mu a) + 1 - \cos \varkappa b\right]$$

In these expressions

$$\varkappa^2 = P_1/D_1, \quad \lambda^2 = P_2/D_2, \quad \mu^2 = P_3/D_3 \qquad (2)$$

and P_i and D_i $(i = 1,2,3)$ are the compressive axial forces and the bending rigidities per unit width of the various parts which undergo deflections $u(\eta)$, $v(\xi)$ and $w(\xi)$, respectively, in the buckled state. The amplitude A is determined by the compressive load P_1 in the following manner.

The elastic modulus of the composite layer in the axial direction, E_1, is different from that of the aluminum plate, E. Hence the effective neutral axis of the combined laminate is located at a distance e above the geometrical center of the cross-section, where

$$e = \frac{(E_1 - E)h\,H}{2(E_1 h + EH)} \qquad (3)$$

At the delamination front ($\xi = a$ or $\eta = b$), the axial forces P_1, P_2 and P_3 and the bending moments

$$M_1 = D_1\, u''(b),\quad M_2 = D_2\, v''(a),\quad M_3 = D_3\, w''(a) \tag{4}$$

satisfy the equilibrium equations

$$P_2 + P_3 = P_1,\quad M_1 = M_2 + M_3 - P_2\, h/2 + P_3\, H/2 - P_1\, e. \tag{5}$$

Furthermore, by comparing the deformed curve lengths of the unbonded segments of the graphite-epoxy layer and of the aluminum plate, one obtains the relation

$$\frac{P_3}{E_1 h}\, a + \frac{1}{2}\int_0^a (w')^2\, d\xi = \frac{P_2}{EH}\, a + \frac{1}{2}\int_0^a (v')^2\, d\xi + \frac{h+H}{2}\, w'(a). \tag{6}$$

Substituting Eq. (1) and (5a) into (6) yields the following equation

$$\left(\frac{P_3}{E_1 h} - \frac{P_1 - P_3}{EH}\right) - \frac{h+H}{a}\,\theta + \theta^2\left(\frac{1}{\sin^2 Z} - \frac{1}{Z\tan Z} - \frac{1}{\sin^2 Y} + \frac{1}{Y\tan Y}\right) = 0, \tag{7}$$

where

$$\theta \equiv (A\,\varkappa \sin \varkappa\, b)/2, \tag{8}$$

$$Y \equiv \left\{(P_1 - P_3)/D_2\right\}^{\frac{1}{2}} a,\quad Z \equiv \left(P_3/D_3\right)^{\frac{1}{2}} a. \tag{9}$$

Furthermore, Eqs. (1) to (5) deliver

$$\theta = \frac{\{(2e+h)\,P_1 - (h+H)P_3\}/(2b)}{\dfrac{P_1}{\varkappa b \tan \varkappa\, b} + \dfrac{a}{b}\left(\dfrac{P_1 - P_3}{Y\tan Y} + \dfrac{P_3}{Z\tan Z}\right)}. \tag{10}$$

For any given value of total axial load P_1, Eqs. (7) and (10) furnish two algebraic equations for two unknowns P_3 and θ. Solution of this system of equations yeids the amplitude A via Eq. (8). Then the transverse deflections and the bending moments can be obtained from Eqs. (1) and (4). Let P* and M* be defined by

$$P^* = \frac{E_1 h}{E_1 h + EH}\, P_1 - P_3 + \frac{E_1 h}{D_1}\left(\frac{H}{2} - e\right) M_1,\quad M^* = M_3 - \frac{D_3}{D_1}\, M_1. \tag{11}$$

The energy-release rate is given by

$$G = \frac{(P^*)^2}{2E_1 h} + \frac{(P^*)^2}{2EH} + \frac{(M^*)^2}{2D_3} + \frac{\{P^*(h+H)/2 - M^*\}^2}{2D_2} \tag{12}$$

$$= (\alpha P^*)^2 + (\beta M^*)^2 - 2\alpha\beta P^* M^* \sin\delta$$

where

$$\alpha = \left\{\frac{1}{2E_1 h} + \frac{1}{2EH} + \frac{(h+H)^2}{8D_2}\right\}^{\frac{1}{2}},$$

$$\beta = \left\{\frac{1}{2D_3} + \frac{1}{2D_2}\right\}^{\frac{1}{2}}, \tag{13}$$

$$\sin\delta = \frac{h+H}{4\alpha\beta D_2}.$$

The mode I and mode II components of G are given respectively by

$$G_I = \left\{-P^*\alpha \sin\omega + M^*\beta\cos(\omega - \delta)\right\}^2$$

$$G_{II} = \left\{P^*\alpha\cos\omega + M^*\beta\sin(\omega - \delta)\right\}^2 \tag{14}$$

The last expressions contain only one undetermined parameter ω. This parameter will be evaluated by using the data from Whitcomb's finite-element computation.

3. Comparison with finite-element results

If the geometrical and material parameters characterizing a one-dimensional delamination are specified, then under any supercritical laminate load P_1 the energy-release rate per unit increment of delamination length can be evaluated by using Eq. (12). For the laminate considered in Whitcomb's finite-element analysis, it was found that the total energy-release rate obtained from the finite-element computation was in reasonable agreement with the prediction of Eq. (12), as shown in Fig. 2 and 3. The former is generally larger than the latter, except in a range of laminate load wherein the mode I energy-release rate (from finite-element analysis) attains or is close to its maximum value. Since the buckling and postbuckling solutions of the present theory are based on the Euler-Bernoulli equations of beam-plates, their underlying kinematical assumptions overestimate the stiffness of the structure. Consequently, the present theory should deliver a higher critical buckling load (and smaller values of G_1 in the initial postbuckling range) as compared to the finite-element solution. This relation is clearly visible in Fig. 2 and 3.

The inherent discrepancy between the prediction of eq. (12) and the results of finite-element analysis necessarily implies a similar discrepancy between Eq. (14) and the values of G_I and G_{II} as delivered by finite-element analysis. Therefore, no specific value of the parameter ω in Eq. (14) will ever make the prediction of that equation completely in agreement with the finite-element results. The best one can hope is that, by choosing the ω-value appropriately, Eq. (14) will agree with the finite-element results as closely as possible, in certain average sense, over the full range of laminate load corresponding to positive values of

mode I stress-intensity factor. With this in mind, we develop a procedure for evaluating the parameter ω of Eq. (14) by inference from a selected set of finite-element results.

Figures 11-13 in Reference [14] show the mode I energy-release rates as functions of the laminate load, obtained from finite-element computation with various combinations of delamination thickness and length. For each combination of thickness and length, the laminate load P_T corresponding to the maximum value of G_I can be estimated from the appropriate curve in one of these figures. Since G_I has a stationary value at laminate load P_T, Eq. (14) implies that

$$-\{P^*(P_T') - P^*(P_T)\}\,\alpha \sin\omega + \{M^*(P_T') - M^*(P_T)\}\,\beta \cos(\omega - \delta) \approx 0,$$

provided that P_T' is very close to P_T. Hence

$$\tan\omega \approx \frac{\{M^*(P_T') - M^*(P_T)\}\,\beta \cos\delta}{\{P^*(P_T') - P^*(P_T)\}\alpha - \{M^*(P_T') - M^*(P_T)\}\,\beta \sin\delta} \qquad (15)$$

Since P_T can only be estimated from Fig. 11, 12 or 13 of Reference [4], using this approximate value and an adjacent value P_T' in Eq. (15) may or may not deliver a good choice of ω. However, this tentative value of ω may be used in Eq. (14a) to generate values of G_I and the results may be compared with all available G_I values from finite element analysis. If the discrepancy is not uniformly small, then the pair of laminate loads P_T' and P_T are shifted in such a way that the new value of ω delivered by Eq. (15) results in uniformly small discrepancies.

By implementing this procedure for various combinations of delamination thickness and length, we obtain the ω-values shown in Table 1. According to our theory, ω should be independent of the delamination length.

This appears to be substantiated by the results in Table 1, except for some moderate deviation in cases of relatively short delaminations. When ω is chosen to be 43.5°, 46.5° and 51.0°, corresponding respectively to delamination thickness 0.254 mm, 0.508 mm and 0.762 mm, Eq. (14a) delivers G_I values as shown by solid curves in Fig. 4-6. The corresponding results from Whitcomb's finite-element analysis are indicated in the same figures by broken lines. As was mentioned in the foregoing discussion, the total energy release rate obtained in finite-element analysis was generally greater than the prediction of eq. (12), except in a range of the laminate load wherein G_I attains its maximum value. Figures 4-6 show that the mode I energy release rate obtained from finite-element analysis is likewise greater than the prediction of Eq. (14a), except in a similar range of the laminate load. The discrepancies between the two sets of results for G_I appear to be consistent with the discrepancies between the two sets of results for the total energy release rate. In view of the approximations inherent in a postbuckling solution based on the Euler-Bernoulli equations, the separation of the energy-release rate according to Eq. (14) may be considered as in reasonable agreement with the results of finite-element analysis.

h	δ	Delamination Length, 2a				
		12.7 mm	25.4 mm	31.8 mm	38.1 mm	50.8mm
0.254 mm	0.33°	44.6°	42.3°			
0.508 mm	1.20°		47.3°	46.4°	46.6°	46.4°
0.762 mm	2.49°		51.7°		50.3°	

Table 1: ω-values inferred from the finite-element solutions with various combinations of delamination thickness and length (blank spaces indicate no finite-element results available)

4. Difference between the present theory and Whitcomb's approximate analysis

As was pointed out in an earlier report [1], our formula for the mode I energy release rate (Eq. (14a) of the present report) bears some formal semblance to eq. (11) in Reference [4]. However, there are significant differences in detail, including the number of independent parameters involved in the expressions. Our earlier report was concerned with the various types of thin-film delamination, where the deformation of the main body of the laminate is not affected by buckling and growth of the delamination. In this and the last report, the restriction to thin-film delamination was removed, the induced bending deformation in the main body of the laminate was considered, and the validity of Eq. (14) has been confirmed by comparison with finite-element results. It is now meaningful to examine the difference between Eq. (14) of the present theory with Eq. (11) in Whitcomb's work, with a view to elucidate the respective assumptions, methodology, and accuracy of prediction.

The main difference in structure between our formula (Eq. (14a)) and whitcomb's formula is that the former contains only one underdetermined parameter ω whereas the latter contains two (C_1 and C_2). In our theory, the total energy release rate is already determined from the postbuckling solution via Eq. (12); it need not be calculated by means of finite-element computation although it may be checked by the latter result. In Whitcomb's approximate analysis, the total energy release rate is not directly considered and his empirical formula for G_I is to be established solely by curve-fitting the finite-element results. Since the total energy-release rate can be obtained from he postbuckling solution, and since the

stress-intensity factors depend linearly on the forces and moments at the delamination front, our Eq. (12) directly implies Eq. (14) with only one undetermined parameter ω, provided that G_I and G_{II} depend only on their respective stress-intensity factors. Therefore, in case of a homogeneous laminate the number of undetermined parameters in the expressions for G_I and G_{II} should in principle be one, not two. The parameter C_2 in Whitcomb's formula is determinable by considering the total energy-release rate, which is given by Eq. (12) of this report.

Secondly, the various forces and moments occuring in Whitcomb's formula were calculated by an approximate analysis which ignored the bending deformation of the main body of the laminate. Our theory includes the bending effect and therefore takes into account the rotation of the ends of the delamination in a way consistent with the Euler-Bernoulli theory. In contrast, Whitcomb accounted for the rotation of the ends by introducing an "effective length" of the delamination based on the finite-element solution of the critical buckling load. Thus, for each new problem (say, with a new length of delamination) the finite-element computation should in principle be executed anew to compute the new "effective length". Although he found the effective delamination length to be greater than the actual length by approximately twice the delamination thickness, this is again an empirical formula based on fitting the finite-element results and its general validity cannot be assured.

Furthermore, the substitution of the "effective delamination length" for the actual length essentially shifts the curve of G_I vs laminate load toward the left so that this curve contacts the corresponding curve for finite-element results in a range of laminate load greater than but still

close to the critical buckling load (see Figs. 12 and 13 of Reference [4]). This merely improves the prediction of his formula for relatively small laminate loads; the discrepancy between his formula and the finite-element results becomes even greater at large laminate loads.

It appears that the introduction of an additional undetermined parameter C_2 in Whitcomb's formula, which is unjustified by theory, fails to give a uniform agreement with the finite-element results. The reason appears to be because the bending deformation of the main body of the laminate is ignored in his analysis. The two load parameters P* and M* occurring in our Eq. (14) were defined by Eq. (11). Although M* is approximately equal to M_3, the last term on the right hand side of Eq. (11a) is not negligible compared to the other two terms. The absence of this term in Whitcomb's formula (Eq. (11) of [4]) might have introduced effects which, in the case of a relative thick delamination, cannot be compensated by including an additional undetermined parameter C_2.

References

1. Kunz, R. K., Wang, J.T.S. and Yin, W.-L., "Damage of Composite Structures", Final Report for Lockheed Research grant P.O. No CY48335, September, 1982.

2. Wang, J.T.S. and Yin, W.-L. "Damage of Composite Structures, Part II: Analytical Models of Delamination Growth", Progress Report for Lockheed Research Grant P.O. No. CA 08738, April, 1983.

3. Whitcomb, J.D., "Finite element analysis of instability related delamination growth", J. Composite Materials, 15, 403-426 (1981).

4. Whitcomb, J.D., "Approximate analysis of postbuckled through-width delaminations", NASA Technical Memorandum TM-83147 (1981).

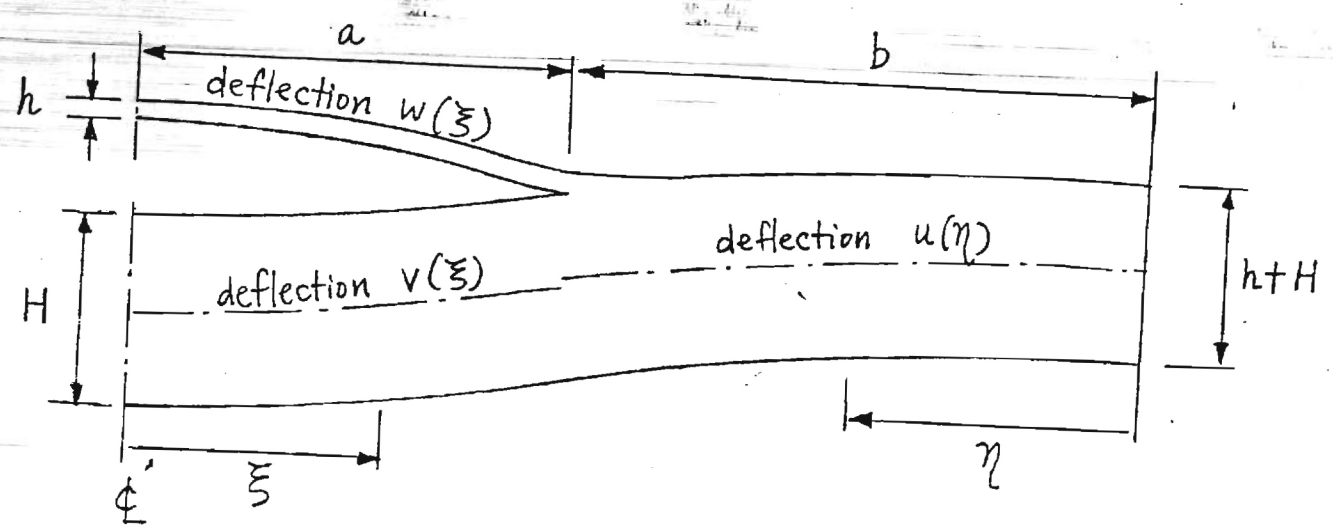
a
b
h
deflection w(ξ)
H
deflection v(ξ)
deflection u(η)
h+H
ξ
η

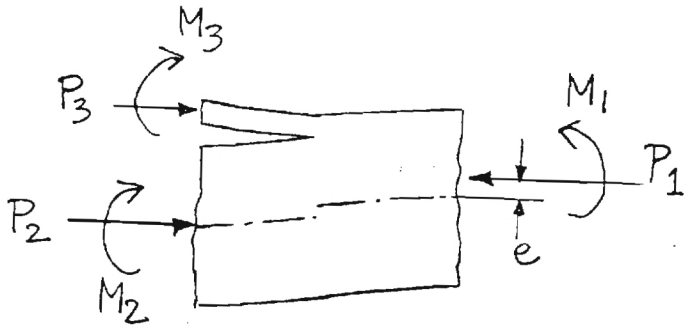
M3
P3
M1
P1
P2
e
M2

Fig. 1

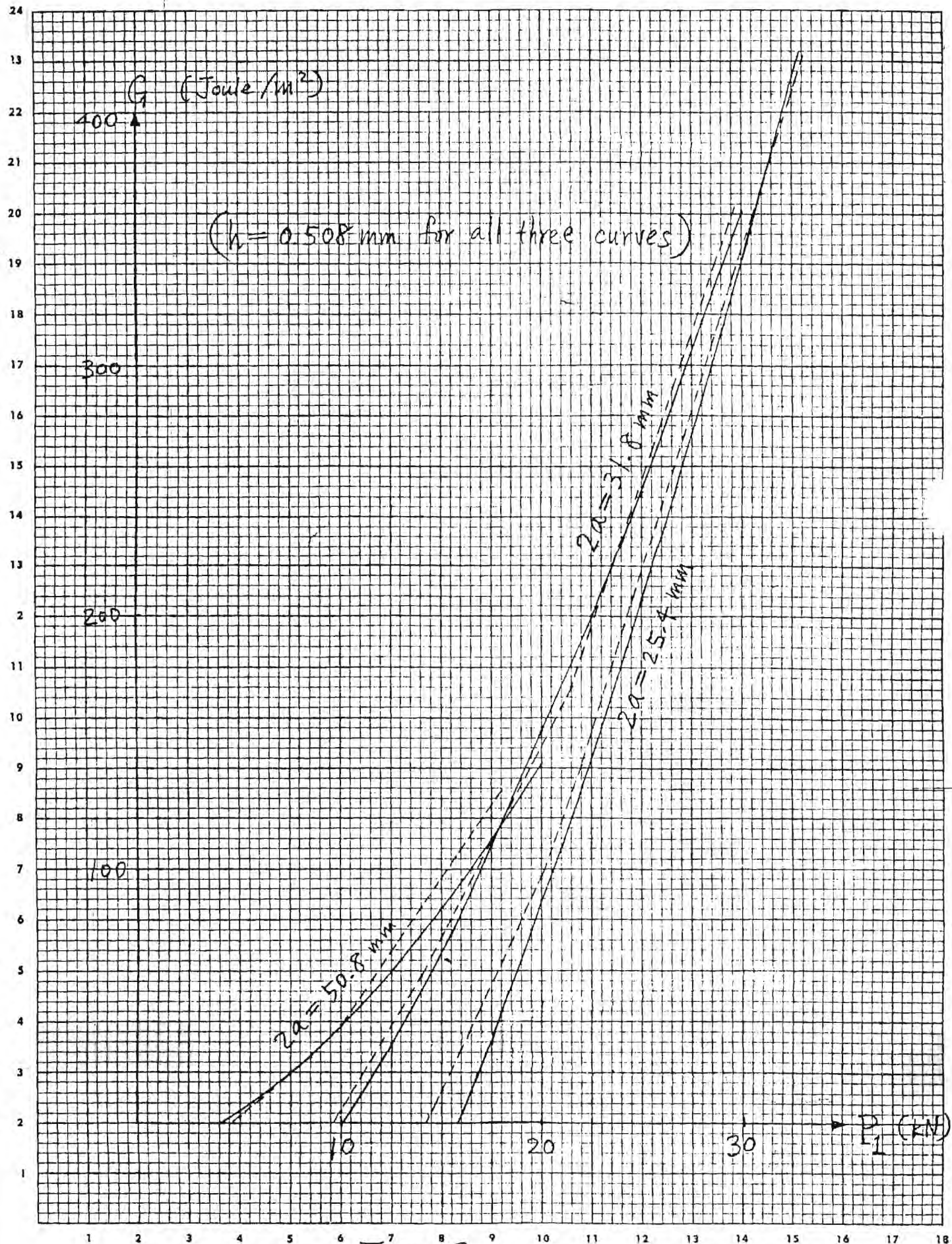
G (Joule/m²)
400
300
200
100
(h = 0.508 mm for all three curves)
2a = 31.8 mm
2a = 25.4 mm
2a = 50.8 mm
10
20
30
P1 (KN)

Fig. 2

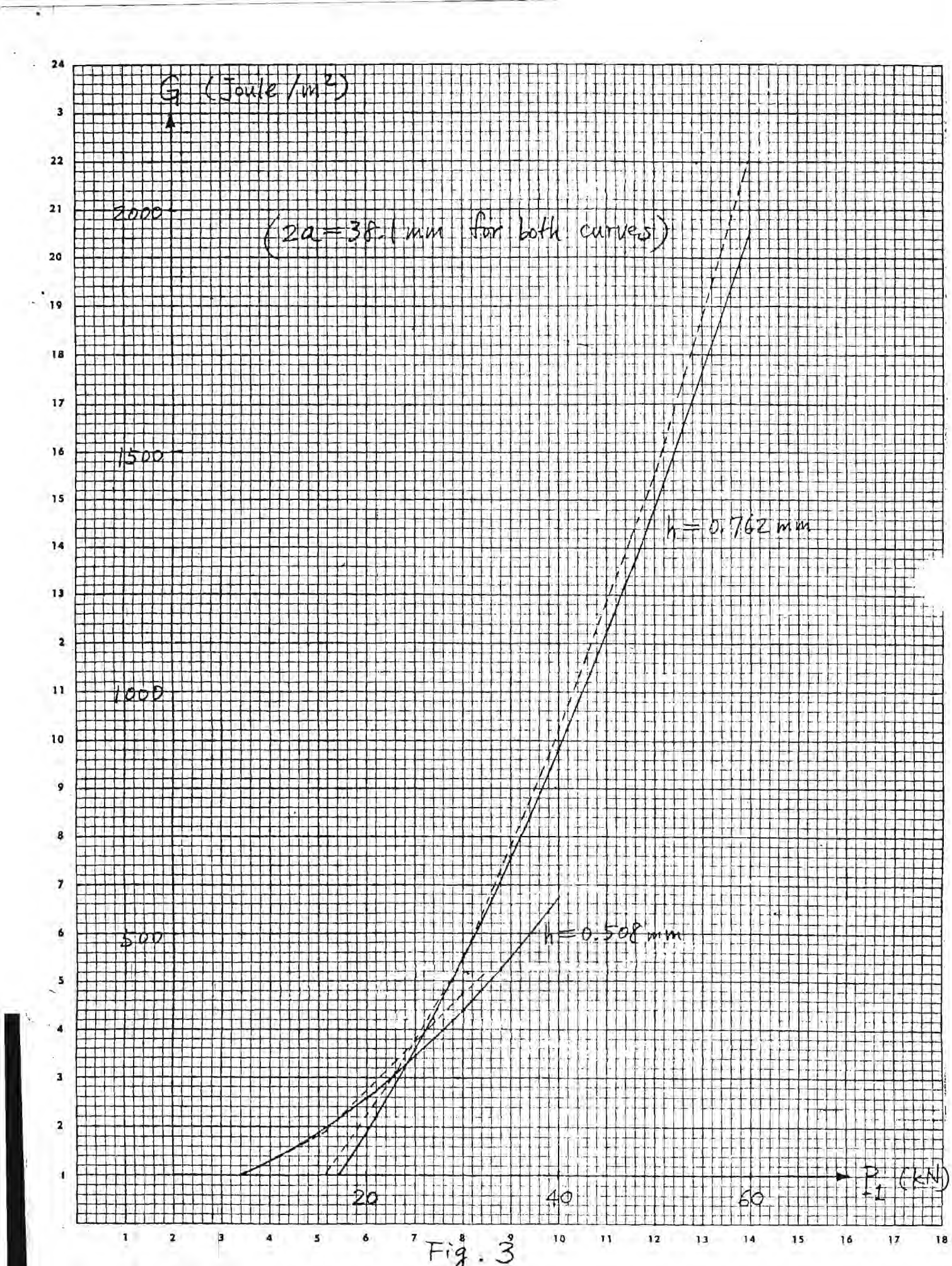
G (Joule/m²)
2000
1500
1000
500
(2a = 38.1 mm for both curves)
h = 0.762 mm
h = 0.508 mm
20
40
60
P (kN)

Fig. 3

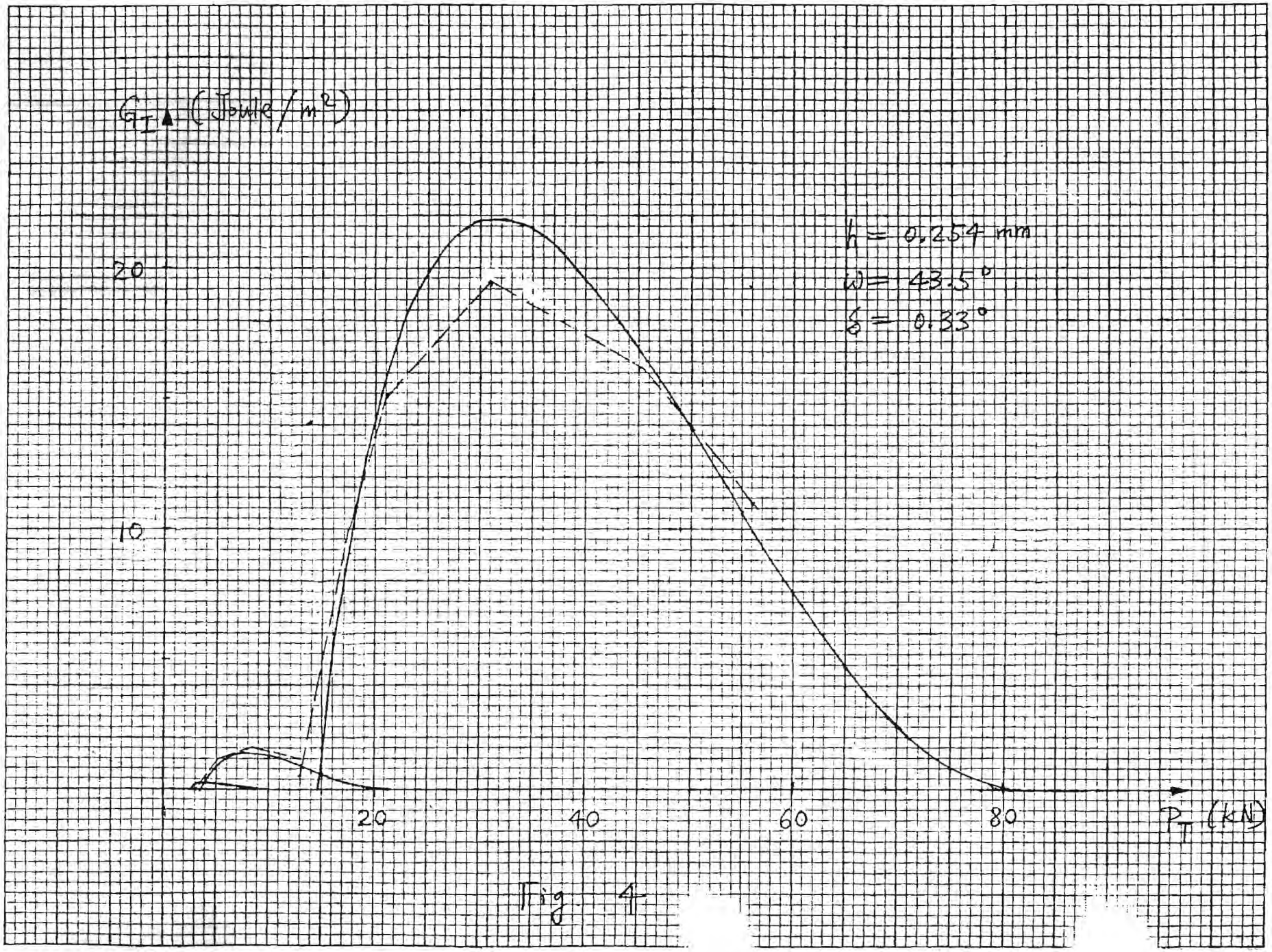

Fig 4

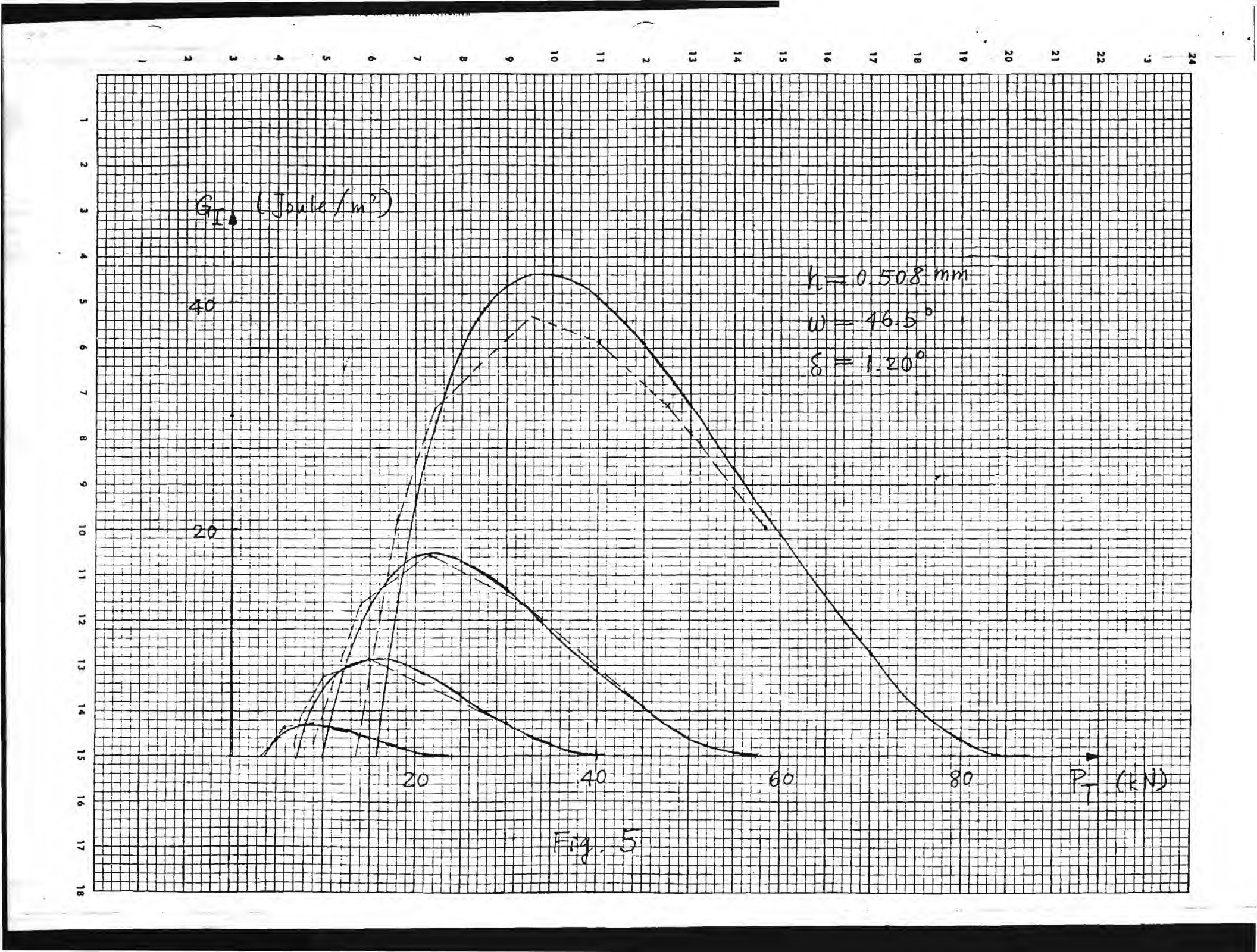

Fig. 5

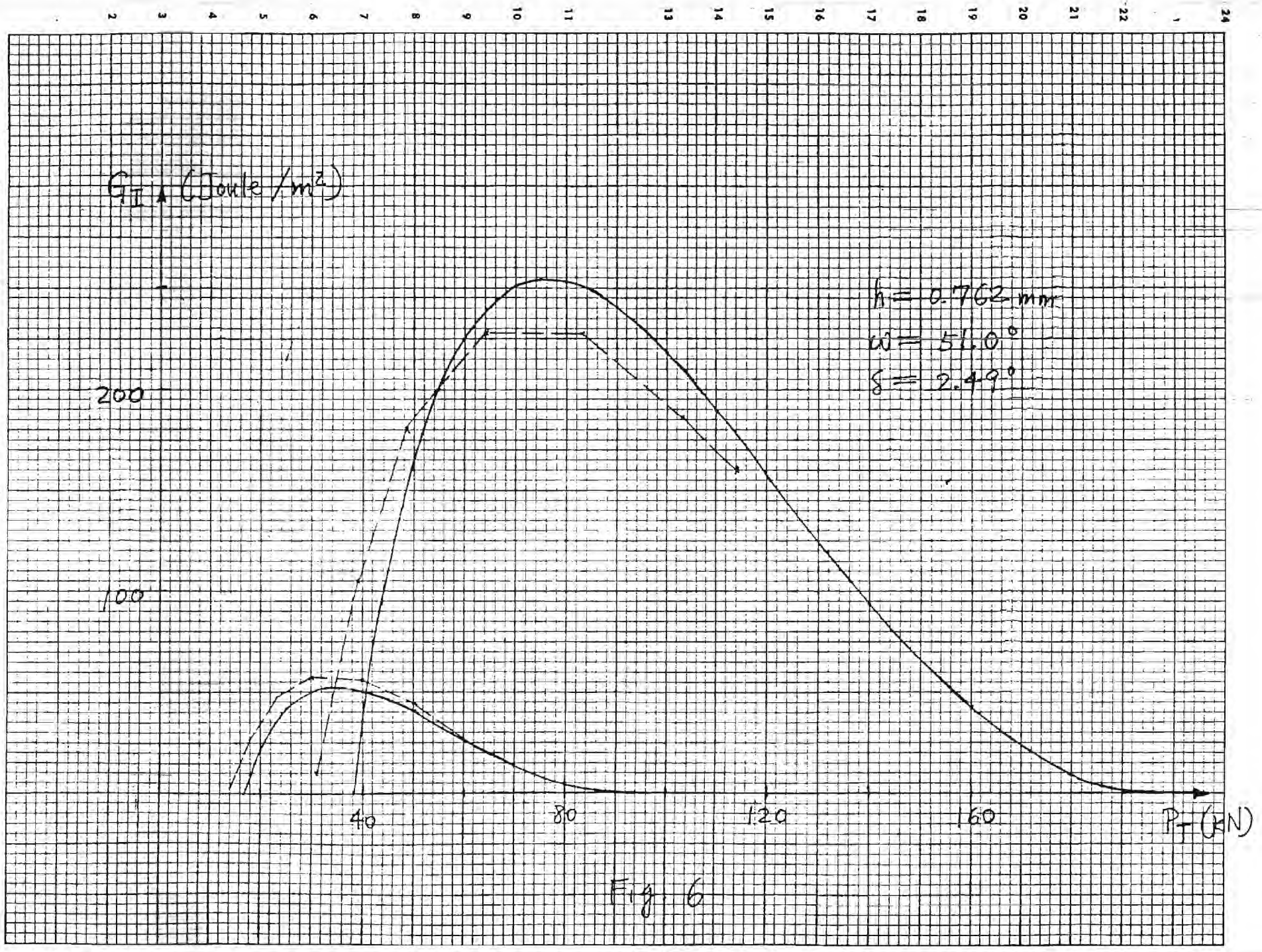

Fig. 6

E-23-624

Lockheed-Georgia Company
Research Grant P.O. No. CA 08738
(Georgia Tech Project NO. E-23-624)

DAMAGE OF COMPOSITE STRUCTURES

Progress Report (7/1/83 - 9/30/83)
October, 1983

by

R. K. Kunz
J. T. S. Wang
W. L. Yin

School of Engineering Science and Mechanics
Georgia Institute of Technology
Atlanta, Georgia 30332

Part I

Wave Propagation Due to Impact in Laminated Composite Plates

R. K. Kunz

1. Introduction

During the subject period, efforts have been focused on the development and implementation of Fortran computer code for the purpose of determining the dynamic interlaminar stresses in a laminated composite plate subject to central normal impact loading on a free surface. This study is motivated by the conviction that impact-induced delamination is initiated as a result of the stresses which act on interlaminar surfaces exceeding a critical value. Hence, a study of the three-dimensional propagation of stress waves in the vicinity of the impact loading zone will potentially yield valuable information as to the nature of, and the parameters affecting, the delamination phenomenon. By making the analysis sufficiently general, dynamic interlaminar stresses may be calculated for arbitrary geometrical and material parameters, and for arbitrary layer stacking sequences. As a result, the effects of these parameters on interlaminar stress levels, and therefore on the initiation of delamination, may be studied.

Results previously reported for the case of a composite plate subject to line impact loading, and the ensuing two-dimensional propagation of stress waves, have served to verify the analytical and numerical models employed in this work, and to suggest some preliminary conclusions as to the mechanisms involved in the onset of delamination. These results are summarized in [3]. How-

ever, due to the nature of the two-dimensional analysis, only certain stacking sequences may be employed, and some fundamental questions remain unanswered. The present work is aimed toward the more general and realistic case of central impact loading and the resulting three-dimensional wave propagation. Therefore, the limitations inherent in the two-dimensional analysis have been removed, and it is expected that the results obtained will yield additional information on the critical parameters affecting the generation of impact-induced delaminations.

2. Problem Formulation and Numerical Solution Procedure

The geometry of the problem under consideration is shown in Figure 1. The plate consists of N orthotropic layers, each with its principal orthotropic axes at an arbitrary orientation in the x_1-x_3 plane. There are M = N + 1 interlaminar planes, with m = 0 corresponding to the impact surface, and m = N corresponding to the bottom free surface. A general layer n is bounded by interfaces m = n − 1 and m = n.

The analysis leading up to the numerical calculations has been developed in detail in previous reports [1,2], and will be summarized here for the sake of completeness:

i) A set of six approximate equations of motion for layer n are obtained. These are cast in the form of differential equations in terms of the interlaminar stresses and displacements on the bounding surfaces m = n − 1 and m = n. Hence, the unknowns are the three displacement components u_1, u_2, u_3 and the three stress components τ_{22}, τ_{12}, τ_{23} on each of the two surfaces. Each of the unknowns is a function of x_1, x_3, and t.

Figure 1. Plate Geometry

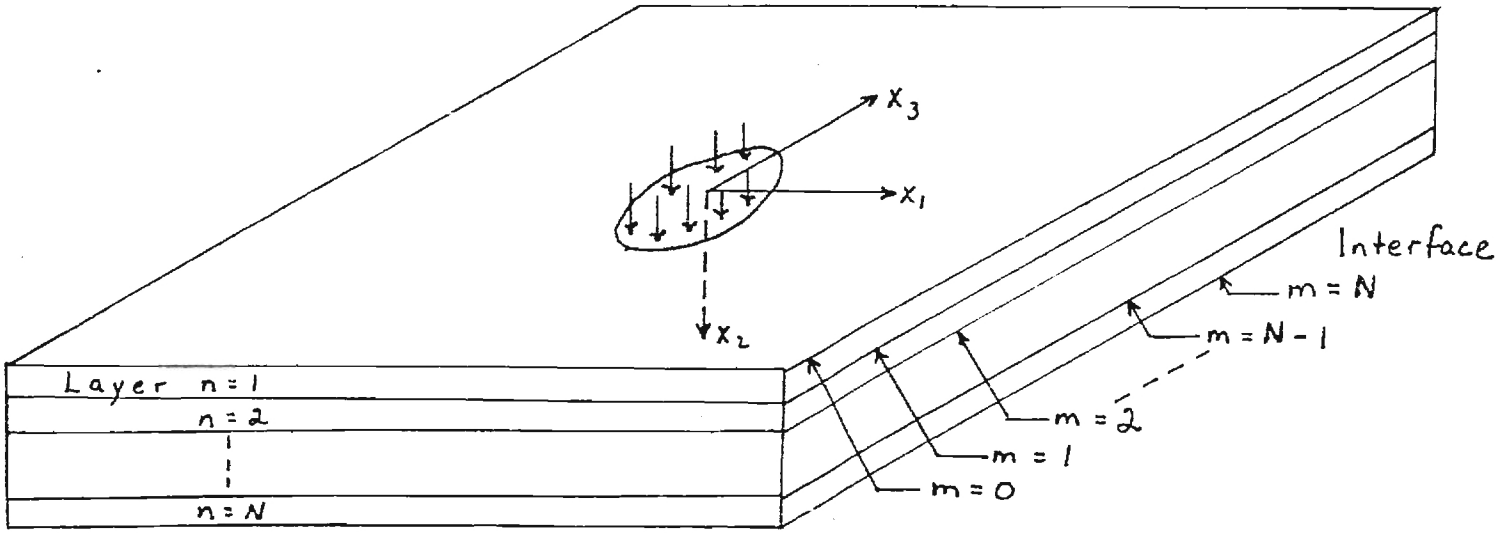

ii) This set of differential equations is transformed using the Laplace transformation in time, and the Fourier transformation in both the x_1 and x_3 directions. The result is a set of six linear algebraic equations corresponding to layer n for the transformed interlaminar stresses and displacements on surfaces m = n - 1 and m = n. The transformed unknowns are related to the physical stresses and displacements through transformations of the form

$$U(k_1, k_3, s) = \int_0^\infty \int_{-\infty}^{\infty} \int_{-\infty}^{\infty} u(x_1, x_3, t) \exp[-st + i(k_1 x_1 + k_3 x_3)] dx_1 dx_3 dt \qquad (1)$$

where k_1, k_3, s are the transform variables. It should be noted that, during the process of transforming the equations, boundary conditions at x_1 and $x_3 = \pm\infty$ (stresses and displacements vanish) and initial conditions at t = 0 (stresses, displacements, and velocities zero) are explicitly satisfied.

iii) The sets of equations for all N layers are assembled, resulting in a set of 6N algebraic equations for the 6(N + 1) transformed interlaminar stresses and displacements. Continuity of stresses and displacements at the internal interfaces (m = 1 to N - 1) are automatically satisfied.

iv) Boundary conditions at the top and bottom surfaces are appended. These are: on m = N, transformed stresses $T_{12} = T_{13} = T_{23} = 0$; on m = 0, $T_{12} = T_{23} = 0$, $T_{22} = \Sigma$, where Σ is the transform of the impact loading function.

At this point, the problem is completely formulated, and numerical methods must be employed to determine the interlaminar stresses as functions of position and time. These may be briefly summarized as follows:

v) The set of linear algebraic equations is solved repeatedly for the transformed interlaminar stresses and displacements at selected discrete combinations of the transform variables k_1, k_3, and s.

vi) The inverse transforms of the transformed interlaminar stresses are numerically calculated to yield the true interlaminar stresses at discrete values of x_1, x_3, and t.

3. Implementation of Numerical Procedures

3.1 Loading Function. The function chosen to model the applied surface traction on the free surface m = 0 due to normal impact is

$$\sigma(x_1,x_3,t)=\begin{cases} -p_0/2\left(1-2\frac{r^2}{a^2}+\frac{r^4}{a^4}\right)\left(1-\cos\frac{2\pi t}{t_0}\right), & 0<r<a \\ & 0<t<t_0 \\ 0, & r>a \\ & t>t_0,\ t<0 \end{cases} \tag{2}$$

where $r^2 = x_1^2 + x_3^2$. By inspection, the maximum normal compressive load is p_0, which occurs at r = 0, t = $t_0/2$. For numerical reasons, the function was chosen to have continuous first derivatives with respect to both position and time at its boundaries (r = a, t = 0 and t_0). It is expected that this function will adequately model the applied load due to foreign object impact normal to the plate surface. When transformed by equation (1), the result is

$$\Sigma(k_1,k_3,t) = 8\pi\frac{p_0}{k^2}\left[\frac{4}{(ak)^2}J_0(ak)+\left(\frac{1}{ak}-\frac{8}{(ak)^3}\right)J_1(ak)\right]\times \left(1-e^{-st_0}\right)\left(\frac{1}{s}-\frac{s}{s^2+(2\pi/t_0)^2}\right) \tag{3}$$

where $k^2 = k_1^2 + k_3^2$, and J_0 and J_1 are Bessel functions of the first kind of order zero and one.

3.2 Solution of equations. The set of linear algebraic equations to be solved is in so-called block-tridiagonal form; each group of six equations for a given layer contains only the six unknowns on each of its corresponding bounding surfaces. Because of this form, an efficient algorithm is available for their solution, as discussed in [2]. This is fortunate, since the set of equations must be solved repeatedly in order to obtain the transformed interlaminar stresses for all combinations of the chosen values of k_1, k_3, and s. (Considerations necessary for the selection of the discrete values of the transform variables are defined in the next sub-section). Specifically, if it is desired to obtain values for the stresses at the nodes of an $N_F \times N_F$ grid in the x_1-x_3 plane, for N_L time intervals, solutions to the algebraic equations must be obtained for $N_F^2 N_L$ combinations of k_1, k_3, and s. However, due to certain observed symmetries and antisymmetries in the solutions of the equations, they need be explicitly solved only $N_F^2 N_L/4$ times. The solutions for the remaining $3N_F^2 N_L/4$ combinations of the transform variables are obtained through the aforementioned symmetries.

3.3 Transform inversion. In order to obtain the interlaminar stresses as functions of position and time, the inverse transforms of the solutions to the algebraic systems must be obtained. That is, to determine a physical quantity from its transform as defined in equation (1), an inversion of the form

$$u(x_1,x_3,t) = \frac{1}{8\pi^3 i}\int_{c-i\infty}^{c+i\infty}\int_{-\infty}^{\infty}\int_{-\infty}^{\infty} U(k_1,k_3,s)\exp[st - i[k_1x_1+k_3x_3]]\,ds\,dk_1\,dk_3 \qquad (4)$$

must be calculated. Since the transformed functions have been obtained as outlined above at discrete values of the transform

variables, the so-called Fast Fourier Transform (FFT) algorithm [4] may be used to determine the inverses. This involves the approximation of equation (4) by a triple finite summation which may be manipulated into the form of a sequence of Inverse Discrete Fourier Transforms. Details of this manipulation are obtained as an extension to the techniques reported previously in [3], and will not be presented here; however, the consequences of this approach deserve some mention.

If significant changes in the interlaminar stresses are expected to occur only over distances greater than λ, and over times greater than τ, then the transformed stresses must be calculated at the following values of k_1 and k_3:

$$k_1, k_3 = \frac{4\pi}{\lambda N_F}\left(I - \tfrac{1}{2}\right), \quad I = 1, 2, \ldots, N_F \tag{5}$$

and at the following values of s:

$$s = c + i\left(\frac{4\pi}{\tau N_L}\right)\left(I - \tfrac{1}{2}\right), \quad I = 1, 2, \ldots, N_L \tag{6}$$

This defines the combinations of k_1, k_3, and s for which the solutions for the transformed stresses must be obtained. As before, N_F is the number of intervals in each of the x_1 and x_3 directions; N_L is the number of time intervals. The result of the FFT computation gives the stresses at the following discrete values of x_1, x_3, and t:

$$x_1, x_3 = \tfrac{\lambda}{2}(J-1), \quad J = 1, 2, \ldots, N_F \tag{7}$$

$$t = \tfrac{\tau}{2}(J-1), \quad J = 1, 2, \ldots, N_L \tag{8}$$

Considerations for the selection of c in equation (6) were discussed in [3]. It should also be noted that, due to the nature of the FFT algorithm and the symmetry of loading, of the N_F^2

points at which stresses are calculated, only those for which $J = 1, 2, \ldots, N_F/2$ (equation (7)) are of use.

3.4 Programming considerations. The principal effort during the period of this report has been in the development, testing, and refinement of a Fortran computer program, IMP3D, to carry out the numerical procedures described above. This program is similar in principle to IMP2D, the program for the case of line impact reported previously [3]. However, certain major modifications to the original program were necessitated by the additional complexity of the three-dimensional problem. In particular, computer storage limitations, which were not a critical factor in the two-dimensional case, became a prime consideration in the development of the present program. At this writing, development and testing of IMP3D are completed, and several test cases have been run, with some preliminary results summarized below. In its present form, IMP3D can perform the necessary interlaminar stress calculations for a plate of up to six layers ($N = 6$), with up to 8 steps in the x_1 and x_3 directions ($N_F = 16$), and 16 steps in time ($N_L = 16$). While it is acknowledged that most composites contain far more than 6 layers, the purposes of this study should be adequately served by consideration of a relatively small number of layers. For the limiting values of N, N_F, and N_L, approximately 200 K of computer core is required, with an execution time of 300 CPU seconds on Georgia Tech's Cyber computer system.

4. Preliminary Results

The table on the following page summarizes a sampling of the results obtained in a typical run of IMP3D. The results presented are for the interlaminar normal stress σ_{22} on each interface at the location $x_1 = x_3 = 0$ (directly underneath the center of the impact region). These results are consistent with those of the two-dimensional case reported previously. As can be observed from examination of the table, a compressive wave propagates through the thickness to the bottom surface, and is reflected back as a tensile wave. As before, the calculated speed of propagation is very close to the theoretical dilatational wave velocity.

This small sample of numerical results serves to establish some measure of confidence in the numerical techniques and in their implementation in IMP3D. While considerably more results have been generated, it would be premature at this time to attempt to draw any definite conclusions from them. At this writing, the results of several runs are being examined not only for the interlaminar normal stress propagating through the thickness, but also for interlaminar shear stress propagating both longitudinally and transversely. By varying the time and distance parameters, certain features of the propagation patterns may be brought into sharper focus. In addition, various stacking sequences should be examined to determine their effects on stress levels. It is hoped that, by examining, evaluating, and comparing the results of several sets of calculations, a suitable criterion for the initiation of impact-induced delamination can be identified, and the parameters influencing the extent of the delamination as observed

Table 1

Transverse Propagation of Normal Stress

Time Step ↓ / τ_{22}/p_0 →	Interface Number 0	1	2	3	4	5	6
0	0.00	0.02	0.07	0.11	0.04	-0.03	0.00
1	-0.50	0.03	0.08	0.06	0.10	0.10	0.00
2	-1.00	-0.51	0.04	0.09	0.11	0.11	0.00
3	-0.50	-1.06	-0.57	0.11	0.13	-0.01	0.00
4	0.00	-0.44	-0.95	-0.61	0.00	0.06	0.00
5	0.00	0.03	-0.37	-0.99	-0.74	0.01	0.00
6	0.00	-0.02	-0.10	-0.39	-0.88	-0.90	0.00
7	0.00	-0.12	-0.09	-0.10	-0.53	-0.72	0.00
8	0.00	-0.48	-0.13	-0.32	0.01	0.49	0.00
9	0.00	-0.03	-0.30	0.05	0.70	0.59	0.00
10	0.00	-0.30	0.27	0.75	0.56	0.19	0.00
11	0.00	0.37	0.67	0.69	0.31	0.01	0.00
12	0.00	0.92	0.78	0.25	0.18	0.17	0.00
13	0.00	0.25	0.54	0.34	0.10	0.18	0.00
14	0.00	-0.34	-0.20	0.36	0.38	-0.09	0.00
15	0.00	-0.42	-0.46	-0.22	0.11	0.32	0.00

Calculations based on the following:

Material constants $E_1 = 20 \times 10$ psi $E_2 = 2 \times 10$ psi
$\nu_{12} = 0.30$ $\nu_{23} = 0.40$
$G_{12} = 2 \times 10$ psi $\rho = 0.055$ lb/in^3

Loading function Duration of load = 1.53 μsec
Radius of loaded region = 0.60 in.

Time step = 0.38 μsec.

experimentally can be ascertained.

References

1. Kunz, R. K., Wang, J. T. S., and Yin, W.-L., "Damage of Composite Structures", Progress Report for Lockheed Research Grant P.O. No. CY48335, April, 1982.

2. Kunz, R. K., Wang, J. T. S., and Yin, W.-L., "Damage of Composite Structures", Progress Report for Lockheed Research Grant P.O. No. CY48335, June, 1982.

3. Kunz, R. K., Wang, J. T. S., and Yin, W.-L., "Damage of Composite Structures", Final Report for Lockheed Research Grant P.O. No. CY48335, September, 1982.

4. Cooley, J. W., and Tukey, J. W., "An Algorithm for the Machine Calculation of Complex Fourier Series", Mathematics of Computation, Vol. 90, No. 19, April, 1965, pp.297-301.

Part II: Stability and Residual Strength of a Delaminated Plate

by W.-L. Yin, J. T. S. Wang and Z.- Z. Fei

1. Introduction

It has been shown in our previous reports that the energy release rate associated with the growth of a one-dimensional or circular delamination may be expressed in terms of the axial or in-plane forces and the bending moments acting across the cross-sections of the various portions of a plate at the front of the delamination. This expression of the energy release rate was obtained by means of the J-integral or M-integral. When the load or displacement applied to the boundary of the plate is sufficiently large so that the energy-release rate exceeds the fracture toughness of the material, the delamination starts to grow and the geometry of the laminte undergoes continuous and irreversible change. In order to follow the history of delamination growth and to predict the load-carrying capacity of a plate with inital delamination, it is in principle necessary to solve a sequence of postbuckling problems with successively increased length or radius of delamination.

The general procedure and the underlying theory for such an analysis has been outlined in the previous reports. In the present report, we present certain important details of the implementation of the procedure, as well as certain conclusions of the analysis with regard to the ultimate load capacity of the delaminated plate, i.e., the residual strength of the impact-damaged plate. In Section 2, we calculate the critical buckling load of a fixed-end plate with a symmetrically positioned one-dimensional delamination. The results are useful as the starting point of the sequence of postbuckling solutions, which will determine the character of delamina-

tion growth. Furthermore, it is shown that if the delamination is thin and the slenderness ratio of the plate is larger than the slenderness ratio of the delamination then the critical axial load of the delaminated plate is a good approximation to the load-capacity of the plate. In Section 2, we determine the critical in-plane load of a clamped circular plate containing a concentric circular delamination. When the results are normalized with respect to the critical load of a perfect plate otherwise identical to the delaminated plate, they are remarkably similar to the corresponding results for the case of a one-dimensinal delamination. In Section 4, we present two typical sets of results of postbuckling analysis, each corresponding to a fixed delamination length and to increasing axial strain in the plate. Qualitative differences between the two sets of postbuckling deformation histories are discussed. In the final section, we draw certain tentative conclusions concerning the residual strength of a delaminated plate on the basis of the present analysis.

2. One-Dimensional Delamination Buckling

In the analysis of the buckling of a delaminated plate and the ensuing growth of delamination, it is useful to know the critical axial load or the critical axial strain which defines the initiation of the postbuckling process. Delaminations induced in a laminate by low velocity impact usually have a small thickness compared to that of the laminate. If the delamination is relatively short so that the slenderness ratio of the laminate is larger than the slenderness ratio of the thin delaminated layer, then the global buckling of the laminate precedes the local buckling of the delamination. In this case the critical axial load (P_{cr}) of the delaminated laminate is nearly equal to the corresponding critical axial load (P_{cr}^{o}) of a perfect laminate which does not contain the delamination, and the delaminated laminate cannot cary much additional load beyond P_{cr}. The critical axial load is, in this case, a good approximation to the ultimate load-carrying capacity of the laminate. On the other hand, if the slenderness ratio of the laminate is smaller than that of the delaminated layer, then local buckling of thin layer occurs at a laminate load P_{cr} (or laminate strain) significantly below P_{cr}^{o}, but such local buckling affects very little the deformation in the main body of the laminate. When the laminate load or laminate strain is increased, the transverse deflection of the delaminated layer becomes more pronounced until delamination grows spontaneously when the strain-energy-release rate exceeds the fracture toughness of the material. In order to follow the complete course of delamination growth and to evaluate the maximum load-carrying capacity of the laminate, it may be necessary to obtain a sequence of postbuckling solutions corresponding to increasing delamination lengths and increasing

axial strains in the laminate. In such an analysis, the critical axial load P_{cr} is the starting point of the sequence of postbuckling solutions.

In this section, we calculate the critical axial load, P_{cr}, of a homogeneous beam-plate containing a one-dimensional delamination, located symmetrically with respect to the two clamped edges of the plate. The results are normalized with respect to the critical axial load of the corresponding perfect beam-plates, P_{cr}^{o}. Let $\bar{a}$ denote the ratio of delamination length to the total length of the plate, and let $\bar{h}$ be the ratio of delamination thickness to the total thickness. Then, for each value of $\bar{h}$, the dependence of the normalized critical axial load $P \equiv P_{cr}/P_{cr}^{o}$ upon the dimensionaless length parameter $\bar{a}$ has the character as shown in Fig. 1. If $\bar{h}$ is small (thin delamination), then P is close to unity as long as $\bar{a} < \bar{h}$ and P drops rapidly as $\bar{a}$ exceeds $\bar{h}$. For larger values of $\bar{h}$, the variation of P with $\bar{a}$ is similar in kind, although the decrease of the normalized critical axial load with the increase of delamination length is more gradual.

To compute the critical axial load P_{cr}, we consider the transverse deflections $u(\eta)$, $v(\xi)$ and $w(\xi)$ of the three portions of the delaminated plate in the buckled state, as shown in Fig. 2. Let P_1, P_2, P_3 and D_1, D_2, D_3 be the compressive axial loads and bending stiffness (per unit width of the plate) in the respective portions. Then

$$u'(\eta) = -A\kappa \sin \kappa\eta \ , \quad v'(\xi) = A_2 \lambda \sin \lambda\xi \ , \quad w'(\xi) = A_3 \mu \sin \mu\xi$$

where

$$\kappa = \sqrt{P_1/D_1} \ , \quad \lambda = \sqrt{P_2/D_2} \ , \quad \mu = \sqrt{P_3/D_3} \ .$$

Continuity of the slope $-u'(b) = v'(a) = w'(a)$ determines the ratios among the coefficients A, A_2 and A_3. It follows that

$$u''(b) = -A\kappa^2 \cos \kappa b \ , \quad v''(a) = A\lambda\kappa \sin \kappa b \ \text{ctn} \ \lambda a \ ,$$

$$w''(a) = A\mu\kappa \sin \kappa b \operatorname{ctn} \mu a .$$

Equilibrium of the moments at the front of delamination requires that

$$-D_1 A \kappa^2 \cos \kappa b = P_2 A \lambda \kappa \sin \kappa b \operatorname{ctn} \lambda a + D_3 A \mu \kappa \sin \kappa b \operatorname{ctn} \mu a + (P_3 H - P_2 h)/2 ,$$

where h is the thickness of delamination and H + h is the total thickness of the laminate. Comparison of the deformed curve lengths of the upper and lower delaminated portions yields

$$\frac{a}{E}\left(\frac{P_3}{h} - \frac{P_2}{H}\right) = \frac{H+h}{2} A\kappa \sin \kappa b + \frac{1}{2}\int_0^a v'(\xi)^2 d\xi - \frac{1}{2}\int_0^a w'(\xi)^2 d\xi .$$

Immediately after buckling, the terms $-(1/2)\int w'^2 d\xi$ and $(1/2)\int v'^2 d\xi$ are of the order A^2 and may be neglected in comparison with the term $-\frac{1}{2}(H + h) A\kappa \sin \kappa b$. Hence the last two equations deliver

$$\kappa a \operatorname{ctn} \kappa b + (1-\bar{h})^3 \lambda a \operatorname{ctn} \lambda a + \bar{h}^3 \mu a \operatorname{ctn} \mu a + 3(1-\nu^2)\bar{h}(1-\bar{h}) = 0 ,$$

where we have used

$$D_1 = \frac{E(H+h)^3}{12(1-\nu^2)} , \quad D_2 = \frac{EH^3}{12(1-\nu^2)} , \quad D_3 = \frac{Eh^3}{12(1-\nu^2)} .$$

At the initiation of buckling, we have

$$\mu = \sqrt{\frac{P_3}{D_3}} = \sqrt{\frac{P_3}{P_1}\frac{D_1}{D_3}}\sqrt{\frac{P_1}{D_1}} = \sqrt{\bar{h}\,\frac{1}{\bar{h}^3}}\,\kappa = \frac{\kappa}{\bar{h}} ,$$

$$\lambda = \sqrt{\frac{P_2}{D_2}} = \frac{\kappa}{1-\bar{h}} = \frac{\bar{h}}{1-\bar{h}}\mu .$$

Define $X \equiv \kappa a = \sqrt{\frac{P_1}{D_1}}\, a$. Then the preceding equations yield

$$-\operatorname{ctn}\left\{\left(\frac{1}{a}-1\right)\bar{h}X\right\} = \frac{3(1-\nu^2)(1-\bar{h})}{X} + \bar{h}^2 \operatorname{ctn}\left(\frac{X}{\bar{h}}\right) + (1-\bar{h})^2 \operatorname{ctn}\left(\frac{\bar{h}X}{1-\bar{h}}\right) , \quad (1)$$

where $\bar{a} \equiv a/(a+b)$. For specified $\bar{h}$ and $\bar{a}$, X can be calculated from the last equation by iteration. Then the normalized critical axial load is given by

$$P \equiv \frac{P_{cr}}{P_{cr}^{o}} = \frac{P_1 (a+b)^2}{\pi^2 D_1} = \frac{P_1 a^2}{D_1} \frac{(a+b)^2}{\pi^2 a^2} = \left(\frac{\bar{h} X}{\pi \bar{a}}\right)^2. \qquad (2)$$

The results of computation are shown in Fig. 1 for $\bar{h} = 0.1$, 0.2, 0.3, 0.4 and 0.5. A similar procedure to obtain these curves without numerical iteration is to evaluate $\bar{a}$ successively corresponding to a sequence of specified values of X.

Fig. 3 shows the axial load in the delaminated layer at the initiation of buckling of the delaminated plate, normalized with respect to the buckling load of an identical layer subjected to clamped end conditions:

$$Q \equiv \frac{P_3}{\pi^2 D_3 / a^2} = \left(\frac{\mu a}{\pi}\right)^2 = \left(\frac{X}{\pi}\right)^2 = \left(\frac{\bar{a}}{\bar{h}}\right)^2 P. \qquad (3)$$

For a thin delamination ($\bar{h} \leq 0.1$), Q is found to be close to unity whenever $\bar{a} > \bar{h}$. Hence

$$P = \left(\frac{\bar{h}}{\bar{a}}\right)^2 Q \lessapprox \left(\frac{\bar{h}}{\bar{a}}\right)^2,$$

and $(\bar{h}/\bar{a})^2$ is a close upper bound of the normalized critical axial load P_{cr}/P_{cr}^{o}, provided that $\bar{h}$ is small and $\bar{a} > \bar{h}$.

3. Buckling Load of a Clamped Circular Plate with a Concentric Circular Delamination

A more appropriate analytical model of impact generated delamination is furnished by a clamped, homogeneous isotropic circular plate of radius R containing a concentric circular delamination of radius $a = \bar{a}R$. For simplicity we assume that the plate is subjected to axisymmetric in-plane

compressive load P_1 per unit arc length of the boundary. In the pre-buckling states and immediately following the buckling of the plate the membrane compression is constant and transverely isotropic, as may be shown from the equations of equilibrium. When P_1 exceeds the critical value, the three portions of the plate undergo transverse deflections u(r), v(r) and w(r), respectively, as shown in Fig. 4. Let P_2 and P_3 be the in-plane compressive loads in the two delaminated portions. Then

$$u'(r) = -A\kappa\left\{J_1(\kappa r) - \frac{J_1(\kappa R)}{Y_1(\kappa R)}\,Y_1(\kappa r)\right\},$$

$$v'(r) = -A_2\lambda\,J_1(\lambda r), \quad w'(r) = -A_3\mu\,J_1(\mu r),$$

where J_1 and Y_1 denote, respectively, first order Bessel and Neumann functions and where κ, λ and μ are <u>dimensionless</u> load parameters defined by

$$\kappa = a\sqrt{P_1/D_1}, \quad \lambda = a\sqrt{P_2/D_2}, \quad \mu = a\sqrt{P_3/D_3}.$$

Continuity of the slope at r = a determines the ratios among the coefficients A, A_2 and A_3. It follows that

$$-\frac{a\,u'(r)}{\kappa A} = J_1(\kappa r/a) - \frac{J_1(\kappa/\bar{a})}{Y_1(\kappa/\bar{a})}\,Y_1(\kappa r/a),$$

$$-\frac{a\,v'(r)}{\kappa A} = \left\{J_1(\kappa) - \frac{J_1(\kappa/\bar{a})}{Y_1(\kappa/\bar{a})}\,Y_1(\kappa)\right\}\frac{J_1(\lambda r/a)}{J_1(\lambda)},$$

$$-\frac{a\,w'(r)}{\kappa A} = \left\{J_1(\kappa) - \frac{J_1(\kappa/\bar{a})}{Y_1(\kappa/\bar{a})}\,Y_1(\kappa)\right\}\frac{J_1(\mu r/a)}{J_1(\mu)}.$$

Differentiating the preceding formulae and using the identity

$$\frac{d\,J_1(\alpha z)}{dz} = \alpha J_0(\alpha z) - \frac{J_1(\alpha z)}{z},$$

one obtains

$$-\frac{a^2 u''(a)}{\kappa A} = \kappa J_0(\kappa) - J_1(\kappa) - \frac{J_1(\kappa/\bar{a})}{Y_1(\kappa/\bar{a})}\{\kappa Y_0(\kappa) - Y_1(\kappa)\},$$

$$-\frac{a^2 v''(a)}{\kappa A} = \left\{J_1(\kappa) - \frac{J_1(\kappa/\bar{a})}{Y_1(\kappa/\bar{a})} Y_1(\kappa)\right\}\left\{\frac{\lambda J_0(\lambda)}{J_1(\lambda)} - 1\right\},$$

$$-\frac{a^2 w''(a)}{\kappa A} = \left\{J_1(\kappa) - \frac{J_1(\kappa/\bar{a})}{Y_1(\kappa/\bar{a})} Y_1(\kappa)\right\}\left\{\frac{\mu J_0(\mu)}{J_1(\mu)} - 1\right\}.$$

Comparison of the deformed meridional curve lengths of the two delaminated portions yields

$$\frac{(1-\nu) P_3 a}{Eh} + \frac{(\kappa A/a)^2}{2\{J_1(\mu)\}^2}\left\{J_1(\kappa) - \frac{J_1(\kappa/\bar{a})}{Y_1(\kappa/\bar{a})} Y_1(\kappa)\right\}\int_0^a \{J_1(\mu r/a)\}^2 dr$$

$$= \frac{(1-\nu) P_2 a}{EH} + \frac{(\kappa A/a)^2}{2\{J_1(\mu)\}^2}\left\{J_1(\kappa) - \frac{J_1(\kappa/\bar{a})}{Y_1(\kappa/\bar{a})} Y_1(\kappa)\right\}\int_0^a \{J_1(\lambda r/a)\}^2 dr$$

$$+ \frac{H+h}{2}\frac{\kappa A}{a}\left\{J_1(\kappa) - \frac{J_1(\kappa/\bar{a})}{Y_1(\kappa/\bar{a})} Y_1(\kappa)\right\}.$$

Neglecting the terms involving A^2 in the last equation and substituting the result into the equilibrium equation of the bending moments

$$D_1 u''(a) = D_2 v''(a) + D_3 w''(a) + (P_2 h - P_3 H)/2,$$

one obtains, at the initiation of buckling

$$\frac{Y_1(\kappa/\bar{a})}{J_1(\kappa/\bar{a})} = \frac{\kappa Y_0(\kappa) - Y_1(\kappa) F(\kappa, \bar{h})}{\kappa J_0(\kappa) - J_1(\kappa) F(\kappa, \bar{h})},$$

$$F(\kappa, \bar{h}) \equiv 6\bar{h}(1-\bar{h}) + \bar{h}^3 \frac{\frac{\kappa}{\bar{h}} J_0(\kappa/\bar{h})}{J_1(\kappa/\bar{h})} + (1-\bar{h})^3 \frac{\frac{\kappa}{1-\bar{h}} J_0\left(\frac{\kappa}{1-\bar{h}}\right)}{J_1\left(\frac{\kappa}{1-\bar{h}}\right)}. \tag{4}$$

where the relation $\kappa = (1-\bar{h})\lambda = \bar{h}\mu$ has been used. Let $\bar{h}$ be specified. Then, for any specified value of the load parameter κ, the right hand side of the last equation may be evaluated. Then the ratio of the radii $\bar{a} = a/R$ occuring in the left hand side can be obtained by iteration. Corresponding to the delamination radius $a = \bar{a}R$, the normalized critical in-plane load is given by

$$\frac{P_{cr}}{P_{cr}^{o}} = \frac{P_1 R^2}{(3.831706)^2 D_1} = \left(\frac{K}{3.831706\ \bar{a}}\right)^2.$$

Here the number 3.831706 is the first zero of Bessel's function of the first order. The results of computation are shown in Fig. 5 for $\bar{h}$ = 0.1, 0.2, 0.3, 0.4 and 0.5. Fig. 6 shows the in-plane load in the delaminated layer at the initiation of buckling, normalized with respect to the buckling load of an identical circular layer subjected to clamped edge conditions at r = a.

The similarity and even the quantitative closeness between the curves in Fig. 1 and 3, on the one hand, and Figs. 5 and 6, on the other, is noteworthy. In both cases, it is seen that if the dimension (length or radius) of a thin delamination is sufficiently small so that the slenderness ratio of the laminate is larger than the slenderness ratio of the delaminated layer (i.e., $\bar{a}<\bar{h}$), then the normalized critical axial or in-plane load is close to unity. In such cases the existence of the small delaminated region does not significantly reduce the critical axial or in-plane load nor does it significantly impair the load-carrying capacity of the laminate. On the other hand, if $\bar{a}>\bar{h}$, then the critical axial or in-plane load may be significantly smaller than the ultimate load capacity of the laminate. The determination of the ultimate load capacity requires a sequence of postbuckling solutions corresponding to increasing delamination length or radius. Procedure of postbuckling analysis for the case of one-dimensional delamination is shown in the next section along with the characteristic features of postbuckling deformaton.

4. Postbuckling Solution and Energy Release Rate of a One-Dimensional Delamination

The procedure for computing postbuckling solutions of a buckled plate containing a one-dimensional delamination, and for evaluating the energy-release rate associated with delamination growth, has been presented in our previous report. In this section, we examine the results of two sample calculations to show the change of postbuckling deformation with increasing axial strain. Although the axial load in the laminate first increases with the axial strain in a range immediately following buckling, for certain types of delamination geometry there is a maximum value of the axial load beyond which the load decreases even though the axial strain continues to increase. In such cases the maximum value is the ultimate load-carrying capacity of the laminate.

Immediately following the buckling, the delaminated plate deflects transversely toward the side of thin delamination. The intact segments of the plate near the two fixed ends bend with a curvature toward one side while the two delaminated portions of the middle segment are concave toward the opposite side (Fig. 7). There is a discontinuity of curvature at the front of delamination because the reduced axial force in the thin layer of delamination contributes to an unbalanced bending moment at the front. In the case of a relatively short and thick delamination, this deformation pattern persists until the plate collapses under a maximum axial load or until delamination starts to grow with a sufficiently large energy-release rate. However, in the case of a long thin delamination the postbuckling deformation of the plate shows a qualitatively different later phase in which the curvatures of the intact segments and of the thick delaminated portion decrease as the compressive axial strain of the plate and the

deflection of the thinner delaminated portion continue to increase. Eventually the curvatures reverse their algebraic signs and the deformation of the plate assume a pattern as shown in Fig. 8.

Two sample histories of a postbuckling deformation are shown in Tables 1 and 2. Table 1 refers to a relatively short delamination for which the later phase of postbuckling behavior is entirely absent. Table 2 refers to a relatively long delamination. In this case the later phase of the postbuckling deformation is characterized by wider separation of the two delaminated portions and larger peeling moments at the delamination front. This enchances the growth tendency of the delamination, and as the delamination grows the fracture mode has a pronounced mode I component.

Computation of the postbuckling deformation is based on the following analysis. Let $w(\xi)$ and $v(\xi)$ denote respectively the transverse deflections of the thinner and thicker delaminated segments, where the coordinate ξ is such that $\xi = 0$ at the midpoint of the segments and $\xi = a$ at the front of delamination. Furthermore, let $u(\eta)$ denote the transverse deflection of the intact segment of the plate, where $\eta = 0$ at the fixed end and $\eta = b$ at the front of delamination, then

$$
\begin{aligned}
u(\eta) &= -A(1-\cos \kappa\eta), \\
v(\xi) &= -A\left[\frac{\kappa \sin \kappa b}{\lambda \sin \lambda a}(\cos \lambda\xi - \cos \lambda a) + 1 - \cos \kappa b\right], \qquad (5) \\
w(\xi) &= -A\left[\frac{\kappa \sin \kappa b}{\mu \sin \mu a}(\cos \mu\xi - \cos \mu a) + 1 - \cos \kappa b\right].
\end{aligned}
$$

where

$$
\kappa^2 = P_1/D_1, \quad \lambda^2 = P_2/D_2, \quad \mu^2 = P_3/D_3.
$$

Let

$$X = \tau a/\bar{h}, \quad Y = \lambda a, \quad Z = \mu a.$$

Then the equilibrium conditions

$$P_1 = P_2 + P_3, \quad D_1 u''(b) = D_2 v''(b) + P_3 w''(a) - P_2 h/2 + P_3 H/2$$

and the compatibility condition

$$\frac{P_3}{Eh} a + \frac{1}{2}\int_0^a (w')^2 d\xi = \frac{P_2}{EH} a + \frac{1}{2}\int_0^a (v')^2 d\xi + \frac{h+H}{2} w'(a)$$

yield the following relations

$$Y = \bar{h}\sqrt{(X^2 - \bar{h} Z^2)/(1-\bar{h})^3}, \tag{6}$$

$$\Lambda^* \sin \tau b = \frac{h+H}{a} \frac{\bar{h}^2}{\varphi} (X^2 - Z^2), \tag{7}$$

$$-\frac{1}{3(1-\nu^2)(1-\bar{h})} \varphi^2 - \varphi + \frac{\bar{h}^2}{4}(X^2 - Z^2)\left\{\frac{1}{\sin^2 Z} - \frac{1}{Z \tan Z} - \left(\frac{1}{\sin^2 Y} - \frac{1}{Y \tan Y}\right)\right\} = 0, \tag{8}$$

where

$$\varphi \equiv X \operatorname{ctn}\left\{\left(\frac{1}{\bar{\alpha}} - 1\right)\bar{h} X\right\} + \frac{(1-\bar{h})^3}{\bar{h}} Y \operatorname{ctn} Y + \bar{h}^2 Z \operatorname{ctn} Z. \tag{9}$$

The quantities X and Z are related, respectively, to the normalized axial load of the whole plate $P = P_1 a^2/(\pi^2 \bar{a}^2 D_1)$ and the normalized axial load of the delaminated layer, $Q = P_3 a^2/(\pi^2 D_3)$, according to

$$\frac{X}{\pi} = \frac{\bar{a}}{\bar{h}}\sqrt{P}, \quad \frac{Z}{\pi} = \sqrt{Q}. \tag{10}$$

For any specified supercritical value of P, X is evaluated from Eq. (10a) and Y, Z and φ are computed iteratively from Eqs. (6), (8), and (9).

Equation (7) yields the coefficient A in the expressions of Eq. (5). Let t = H+h denote the total thickness of the plate and let

$$\beta = \frac{\bar{h}^2 (X^2 - Z^2)}{2\varphi} .$$

Then the following expressions characterize the normalized deflection, separation and curvature of the postbuckling solution:

$$\begin{aligned}
\frac{v(0)}{t} &= -\beta \left[\frac{\tan (Y/2)}{Y/2} + \frac{\tan\left\{\left(\frac{1}{a}-1\right)\bar{h}X/2\right\}}{\bar{h}X/2} \right], \\
\frac{w(0)-v(0)}{t} &= \beta \left[\frac{\tan (Y/2)}{Y/2} - \frac{\tan (Z/2)}{Z/2} \right], \\
\frac{a^2 w''(0)}{2t} &= \beta Z/\sin Z, \qquad \frac{a^2 w''(a)}{2t} = \beta Z/\tan Z, \\
\frac{a^2 v''(0)}{2t} &= \beta Y/\sin Y, \qquad \frac{a^2 v''(a)}{2t} = \beta Y/\tan Y, \\
\frac{a^2 u''(0)}{2t} &= -\beta \frac{\bar{h}X}{\sin\left\{\left(\frac{1}{a}-1\right)\bar{h}X\right\}}, \\
\frac{a^2 u''(a)}{2t} &= -\beta \frac{\bar{h}X}{\tan\left\{\left(\frac{1}{a}-1\right)\bar{h}X\right\}} .
\end{aligned} \tag{11}$$

The bending moments at the delamination front are

$$M_1 = D_1 u''(b) = -\beta \frac{t}{a} D_1 \frac{\kappa}{\tan \kappa b},$$

$$M_3 = D_3 w''(a) = \beta \frac{t}{a} D_3 \mu \operatorname{ctn} \mu a .$$

Let $\bar{P}$ and $\bar{M}$ denote the dimensionless quantities

$$\bar{P} = \frac{\bar{h}^3(X^2-Z^2)}{\bar{a}^2\varphi}\left[\varphi - 3(1-\nu^2)(1-\bar{h})\frac{\bar{h}X}{\tan\left\{\left(\frac{1}{\bar{a}}-1\right)\bar{h}X\right\}}\right],$$

$$\bar{M} = \frac{\bar{h}^3(X^2-Z^2)}{\bar{a}^2\varphi}\left[\frac{Z}{\tan Z} + \frac{\bar{h}X}{\tan\left\{\left(\frac{1}{\bar{a}}-1\right)\bar{h}X\right\}}\right]. \qquad (12)$$

Then the energy-release rate is expressed by

$$G = \frac{Et^5}{96(1-\nu^2)(a+b)^4}\left[\frac{\bar{P}^2}{3(1-\nu^2)\bar{h}(1-\bar{h})} + \bar{h}\,\bar{M}^2 + \frac{1}{(1-\bar{h})^3}(\bar{P}-\bar{h}^2\bar{M})^2\right]. \qquad (13)$$

The results shown in Table 1 correspond to the case $\bar{h} = 0.1$ and $\bar{a} = 0.05$. Buckling occurs at normalized axial load P = .99751696. Separation between the midpoints of the delaminated segments reaches a maximum value when P = .997535. The maximum value attained by the normalized axial load is P_{MAX} = .99753683. Further increase in the axial strain of the laminate is accompanied by a reduction in the axial load. When the normalized axial load decreases to .997535, the two delaminated portions contact each other and thereafter our postbuckling analysis, which is based on the assumption of non-contact between the delaminated portions, ceases to be applicable. For this case the collape load is extremely close to the buckling load

($P_{collapse} = 1.00002\ P_{cr}$), and the transition from the first phase of post-buckling deformation to the second phase does not take place.

The results shown in Table 2 correspond to the case $\bar{h} = 0.1$ and $\bar{a} = 0.125$. The normalized axial load is 0.638223 at the instant of buckling. When it reaches the value 0.6504, transition from the initial to the later phase of postbuckling deformation occurs. Furthermore, the maximum value of the normalized axial load, 0.9236824, is considerable greater than its value at the instant of buckling.

5. Conclusion

For a homogeneous plate with fixed boundary conditions containing a thin delamination ($\bar{h} \leq 0.1$), some tentative conclusions concerning the residual strength may be drawn from the results of the present analysis. If the size ratio (of the delamination vs. the laminate), $\bar{a}$, is smaller than the thickness ratio, $\bar{h}$, then the existence of the delamination does not appreciably lower the critical axial load of the laminate, and the latter is a good approximation to the ultimate load capacity of the delaminated plate. On the other hand, if $\bar{a} > \bar{h}$, then the normalized critical axial load is close to $(\bar{h}/\bar{a})^2$. The ultimate load capacity of the delaminted plate is, in general, considerably greater than $(\bar{h}/\bar{a})^2$. Delamination growth starts when the axial load is sufficiently large so that the energy release rate given by Eq. (13) exceeds the fracture toughness of the material. The axial load at the initiation of the delamination growth, or the axial load capacity of the completely delaminated laminate, whichever is greater, is a lower bound and, in general, a good approximation to the residual strengh of the delaminated plate.

Although the foregoing conclusion is mainly based on the analysis of a one-dimensional delamination, the similarity between the curves in Figs. 1

and Fig. 5 supports the validity of the conclusion concerning the critical loads as referred to a circulr plate with a concentric circular delamination. This suggests that the residual strength of a plate with an arbitrarily shaped delamination may be considerd by following a similar line of thinking.

$\left(\frac{\lambda}{3.3317\bar{a}}\right)^2$

$P = \frac{P_{cr}}{P_{cr}^0}$

Fig. 5 Normalized Critical In-plane Load of a Circular Plate with a Concentric Circular Delamination

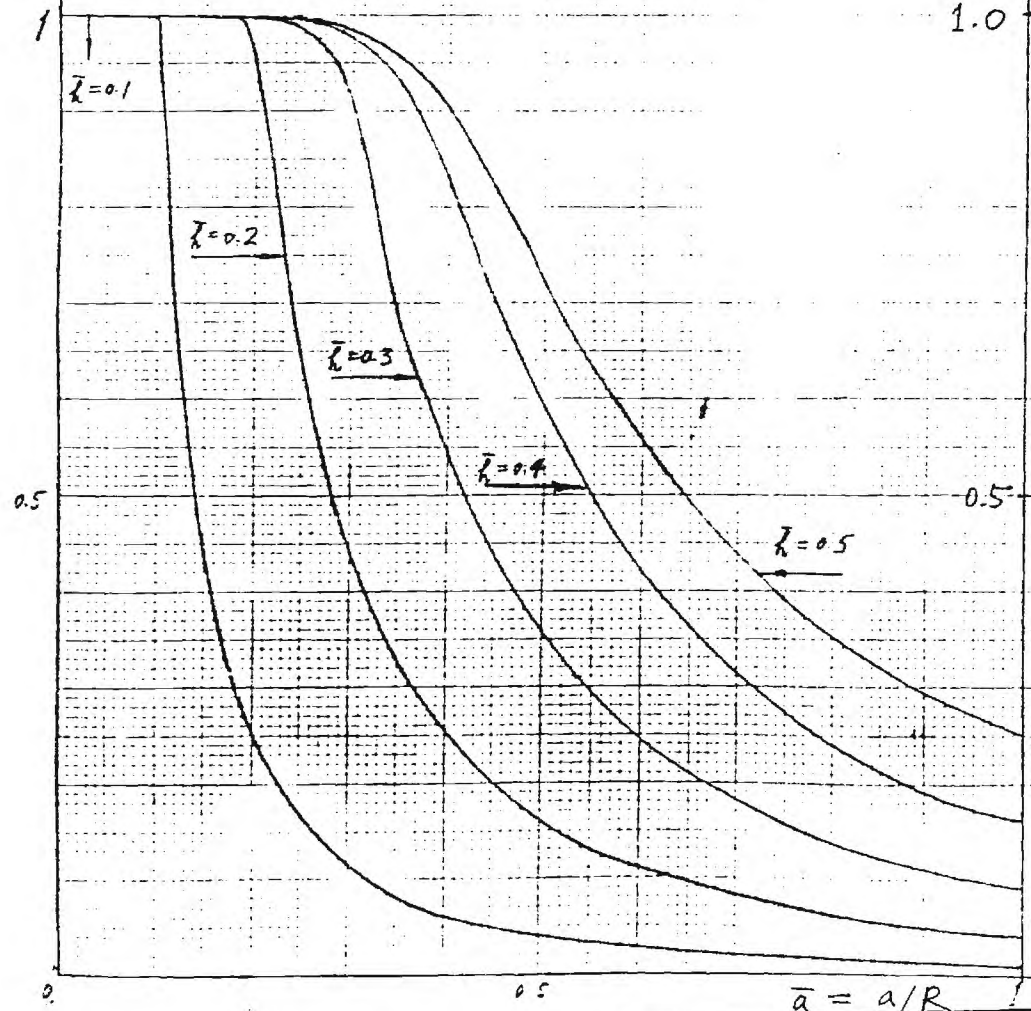

$P = \frac{P_{cr}}{P_{cr}^0}$

Fig. 1 Normalized Critical Axial Load of a Plate with One-Dimensional Delamination

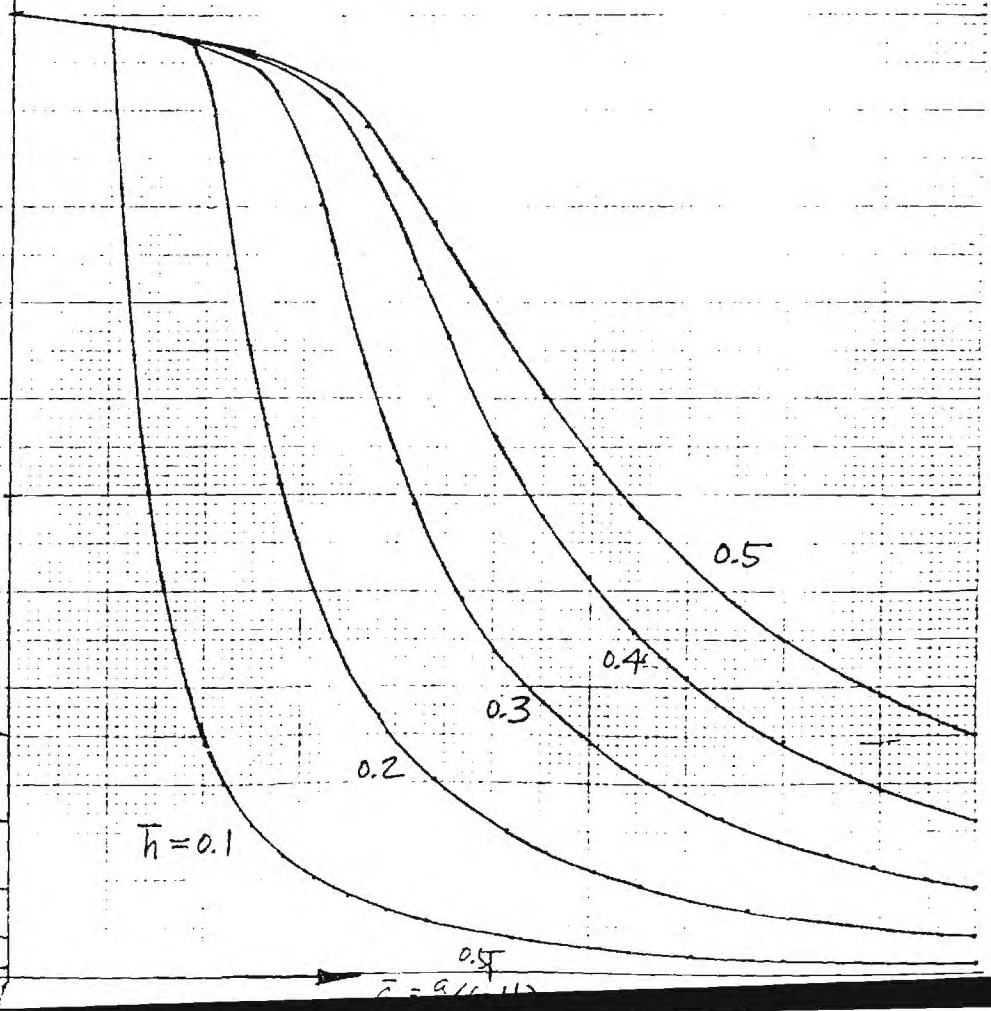

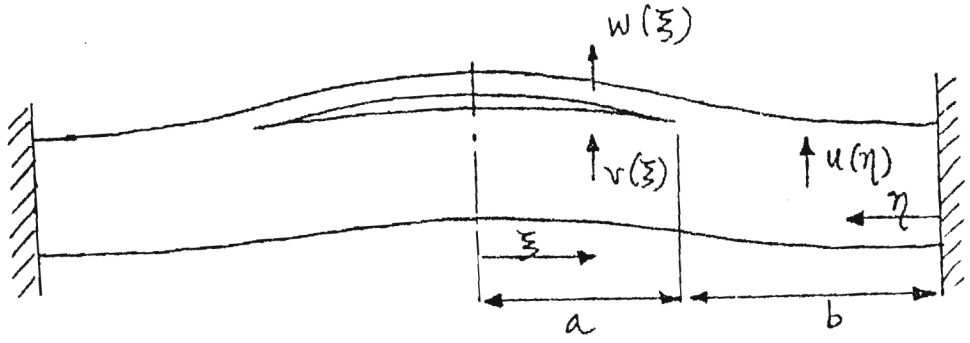

Fig. 2 : One-Dimensional Delamination

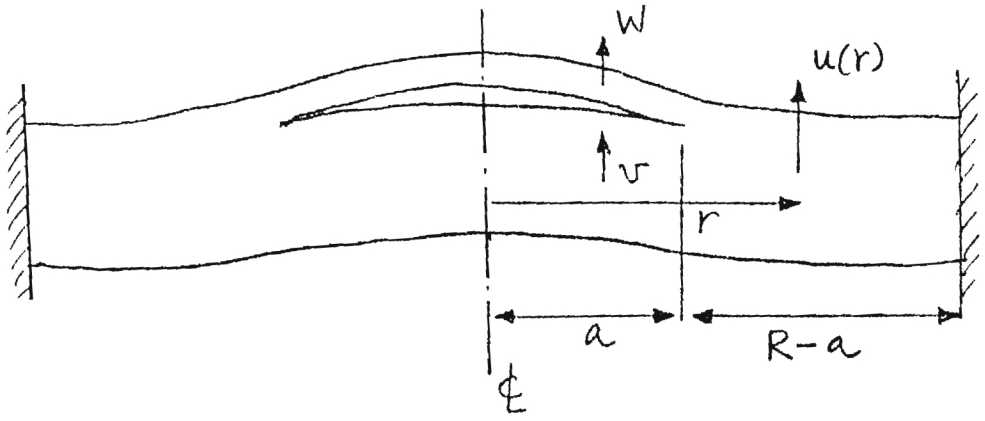

Fig. 4 : Circular Plate with a Concentric Circular Delamination

$\left(\frac{\lambda a}{3.831706\bar{k}}\right)^2$

Fig. 6 Normalized In-Plane Load in the Circular Delamination at the Instant of Buckling

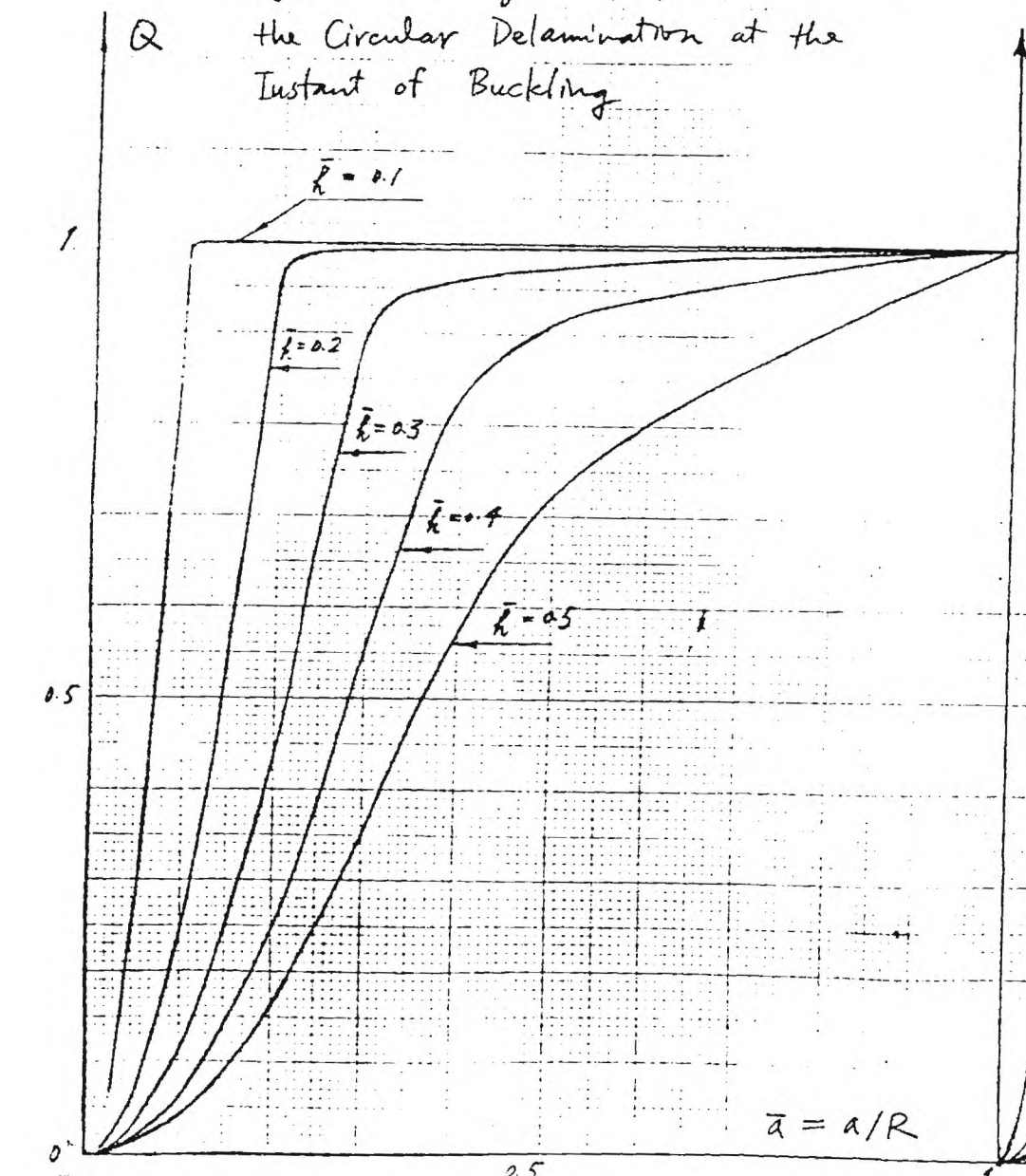

Fig. 3 Normalized Axial Load in the One-Dimensional Delaminated Layer at the Instant of Buckling

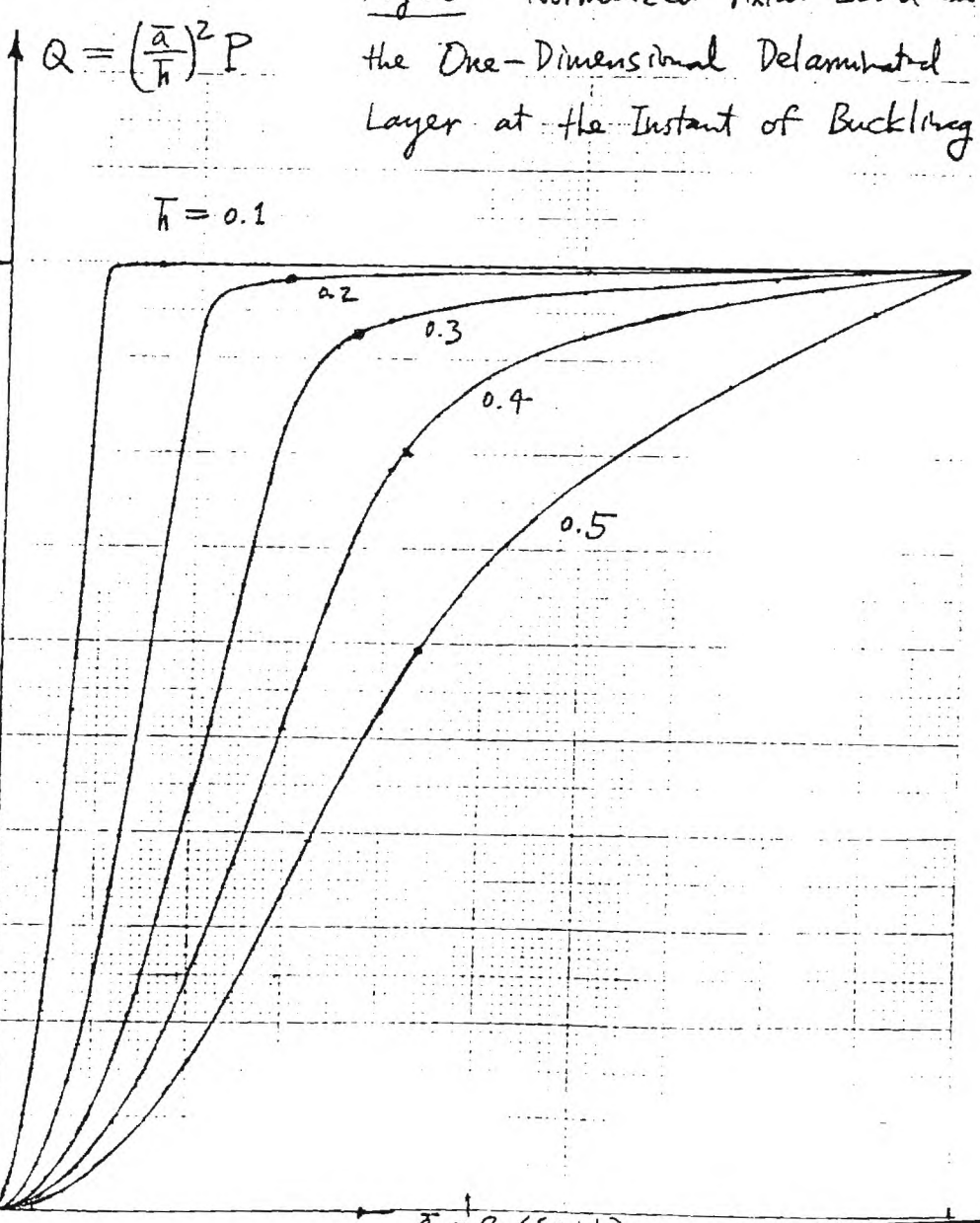

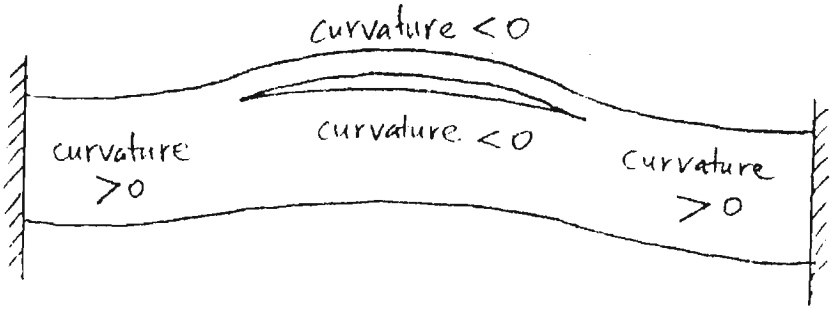

Fig. 7 Postbuckling Deformation : The Initial Phase

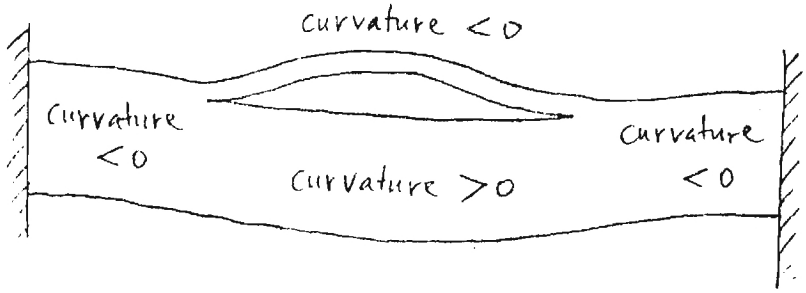

Fig. 8 Postbuckling Deformation : The Later Phase

$P=\frac{P_1 a^2}{\pi^2 \alpha^2 D_1}$	$Q=\frac{P_3 a^2}{\pi^2 D_3}$	$\frac{w(0)-v(0)}{t}$	$\frac{v(0)}{t}$	$\frac{a^2 w''(a)}{2t}$	$\frac{\alpha^2 r''(a)}{2t}$	$\frac{(n+1)^4}{E h^5} G$
.997517	.249229	$.8126 \times 10^{-6}$	.000480	$-.0115 \times 10^{-6}$	-2.98×10^{-6}	8.3842×10^{-6}
.997520	.236738	.000064	.040430	-.000016	-.000251	.054194
.997525	.212383	.000162	.118322	-.000133	-.000735	.386924
.997530	.180643	.000246	.219832	-.000442	-.001366	1.055981
.997535	.129073	.000288	.384772	-.001291	-.002390	2.263526
.997536	.110078	.000277	.445526	-.001702	-.002767	2.704190
.9975365	.095235	.000259	.493004	-.002059	-.003061	3.054541
.9975368	.076710	.000227	.552258	-.002545	-.003430	3.517319
.99753682	.073165	.000220	.563607	-.002643	-.003500	3.611032
.99753682 5	.071000	.000215	.570531	-.002704	-.003543	3.669258
.99753682 8	.069706	.000212	.574672	-.002740	-.003569	3.704493
.99753682 8	.069385	.000211	.575699	-.002749	-.003575	3.713276
.99753682 5	.067500	.000207	.581728	-.002803	-.003613	3.765248
.99753682	.065747	.000203	.587336	-.002853	-.003647	3.814225
.9975368	.062158	.000194	.598819	-.002958	-.003719	3.916590
.9975365	.042843	.000141	.660614	-.003546	-.004102	4.525354
.997536	.026688	.000088	.712301	-.004072	-.004423	5.133046
.997535	.005073	6.75×10^{-6}	.781466	-.004825	-.004852	6.140779

Table 1: Postbuckling Solutions for $\bar{h} = 0.1$, $\bar{a} = 0.05$

$P=\frac{P_1 a^2}{\pi^2 \bar{a}^2 D_1}$	$Q=\frac{P_3 a^2}{\pi^2 D_3}$	$\frac{w(0)-v(0)}{t}$	$\frac{v(0)}{t}$	$\frac{a^2 w''(a)}{2t}$	$\frac{a^2 v''(a)}{2t}$	$\frac{(h+b)^4}{E h^5} G$
.638223	.997223	5.265×10^{-6}	$.244\times10^{-6}$	.000013	$-.0174\times10^{-6}$	3.175×10^{-6}
.638250	.997236	.000169	7.80×10^{-6}	.000417	$-.554\times10^{-6}$	0.003268
.6383	.997261	.000467	21.3×10^{-6}	.001152	-1.516×10^{-6}	0.024931
.6390	.997569	.004084	.000166	.010084	-11.8×10^{-6}	1.910076
.64	.997917	.008187	.000285	.020211	−.000020	7.673758
.643	.998690	.017293	.000379	.042682	−.000027	34.2423
.645	.999097	.022066	.000334	.054458	−.000024	55.7679
.65	.999937	.031835	.000034	.078551	-2.4×10^{-6}	116.1779
.651	1.000086	.033546	−.000048	.082770	3.4×10^{-6}	129.0297
.655	1.000635	.039852	−.000430	.098314	.000030	182.2539
.66	1.001254	.046834	−.001002	.115522	.000069	252.0170
.70	1.005141	.087383	−.008056	.215331	.000526	887.4253
.75	1.009603	.124973	−.023045	.307604	.001395	1814.432
.80	1.015183	.160110	−.050328	.393500	.002800	3080.638
.85	1.024515	.202862	−.111660	.497280	.005654	5052.002
.90	1.051686	.302505	−.378735	.735492	.017250	11821.786
.92	1.115227	.565865	−1.557762	1.345041	.067758	49689.142
.9235	1.223456	1.152835	−5.657719	2.607865	.244173	313540.162
.92365	1.261703	1.400324	−7.808922	3.102346	.336956	533628.863
.92368	1.287605	1.580441	−9.492980	3.448734	.409646	744955.68
.9236824	1.298277	1.657700	−10.242403	3.593922	.442007	850001.91
.9236824	1.298314	1.657966	−10.245018	3.594418	.442120	850380.08
.92368	1.310533	1.748672	−11.144120	3.762315	.480952	985369.64
.92365	1.347491	2.037984	−14.137868	4.279825	.610311	1.505024×10^{6}
.9235	1.448389	2.950877	−24.587775	5.743178	1.062334	4.163009×10^{6}

Table 2: Postbuckling solutions for $\bar{h}=0.1$, $\bar{a}=0.125$

Georgia Institute of Technology
Atlanta, Georgia 30332

E-23-624

College of Engineering
School of Engineering Science and Mechanics

September 28, 1982

Mr. John N. Dickson
Advanced Structures Department
Lockheed Georgia Company
Marietta, GA 30063

SUBJECT: Research Grant P.O. No. CY48335
Georgia Tech Project No. E-23-624

Dear Mr. Dickson:

Enclosed please find a copy of the final progress report for the initial phase of the subject grant ended on September 15, 1982.

Sincerely yours,

clc

Enclosure

Lockheed-Georgia Company

Research Grant P.O. No. CY48335

(Georgia Tech Project No. E-23-624)

DAMAGE OF COMPOSITE STRUCTURES
FINAL REPORT

September, 1982

by

R. K. Kunz
J. T. S. Wang
W. L. Yin

School of Engineering Science and Mechanics
Georgia Institute of Technology
Atlanta, Georgia 30332

Part I

Wave Propagation Due to Impact in Laminated Composite Plates

Wave Propagation Due to Impact in Laminated Composite Plates

During the subject period, an analytical and numerical study of the transient dynamic stresses in composite laminates subject to impact has been continued. Calculations of the transverse and longitudinal propagation of interlaminar stresses is expected to yield valuable information on the initiation of delamination damage to composites resulting from impact loading. Explanations of experimentally observed phenomena and the determination of critical parameters (such as material properties, stacking sequence, and loading function) are primary objectives of this phase of the project.

In previous reports, a description of the analytical techniques used, based on extensions of the work of Kim and Moon [1], has been presented. In this formulation, approximate equations of motion for each layer of the composite are obtained by discretizing all field quantities in the thickness direction, resulting in a set of difference-differential equations for each layer in terms of interfacial displacements and stresses. The equations are then transformed using the Fourier Transformation in space and the Laplace Transformation in time, yielding a set of linear algebraic equations containing as unknowns the transformed interlaminar displacements and stresses, in terms of the Fourier Transform variable k and the Laplace Transform variable s. When boundary conditions on the surfaces of the composite plate corresponding to normal impact loading are incorporated, the result is a set of $6N$ equations for the central impact (three-dimensional) case, or $4N$ equations in the line impact (two-dimensional) case, for a plate containing N layers. The linear algebraic equations form a block-tridiagonal system, for which an efficient solution algorithm was outlined in the previous report.

1. Inversion of Fourier and Laplace Transforms

Using the above-mentioned solution repeatedly, interlaminar stresses and displacements in the transform space may be obtained for discrete values of k and s (wave number and frequency). It then remains to numerically invert the transforms to obtain displacements and stresses as functions of space and time. This is accomplished using the Fast Fourier Transform (FFT) algorithm developed by Cooley and Tukey [2]. The FFT algorithm makes possible efficient machine computation of the so-called discrete Fourier Transform (DFT),

$$H(J) = \sum_{I=0}^{(N-1)} h(I)\, e^{i 2\pi I J/N}, \quad I = 0, 1, \ldots, (N-1), \qquad (1.1)$$

and the inverse discrete Fourier Transform (IDFT),

$$h(J) = \sum_{I=0}^{(N-1)} H(I)\, e^{-i 2\pi I J/N}, \quad I = 0, 1, \ldots, (N-1). \qquad (1.2)$$

It is first necessary, then, to establish the connection between the continuous Fourier and Laplace Transforms, with respect to which the equations of motion were transformed, and the discrete transforms defined by equations (1.1) and (1.2).

In order to numerically invert the Fourier Transform, we must calculate integrals of the form

$$u(x) = \frac{1}{2\pi} \int_{-\infty}^{\infty} U(k)\, e^{-ikx}\, dk, \qquad (1.3)$$

where u(x) represents an interlaminar stress or displacement as a function of position, and U(k) is its Fourier transform (s and t are held constant in this discussion). If significant changes in u(x) are expected to occur only

er distances greater than ?, the largest wave number that need be con-

dered is

$$K = 2\pi/\lambda \quad . \tag{1.4}$$

herefore, (1.3) may be approximated by

$$u(x) \doteq \frac{1}{2\pi} \int_{-K}^{K} U(k)\, e^{-ikx}\, dk ,$$

, shifting the interval of integration,

$$u(x) \doteq \frac{1}{2\pi}\, e^{iKx} \int_{0}^{2K} U(k-K)\, e^{-ikx}\, dk \tag{1.5}$$

w we further approximate the integral by a finite summation over N_F intervals

$$u(x) \doteq \frac{1}{2\pi}\, e^{iKx} \sum_{I=0}^{(N_F-1)} U(k_I - K)\, e^{-ik_I x}\, \Delta k , \tag{1.6}$$

ere

$$\Delta k = \frac{2K}{N_F} , \qquad k_I = \frac{2K}{N_F}\left(\tfrac{1}{2} + I\right) = \frac{4\pi}{N_F \lambda}\left(\tfrac{1}{2} + I\right) \tag{1.7}$$

ation (1.6) may thus be re-written as

$$x) \doteq \frac{K}{\pi N_F}\, e^{iKx(1-1/N_F)} \sum_{I=0}^{(N_F-1)} U(k_I - K)\, e^{-i\frac{2\pi I}{N_F}\frac{2x}{\lambda}} . \tag{1.8}$$

to this point in the discussion, x is a continuous variable. If we now

luate x at the discrete points

$$x = x_J = \frac{\lambda}{2} J , \qquad J = 0, 1, \ldots, (N_F - 1) , \tag{1.9}$$

ation (1.8) becomes, after some rearrangement,

$$x_J) \doteq \frac{K}{\pi N_F}\, e^{i\pi J(N_F-1)/N_F} \sum_{I=0}^{(N_F-1)} U(k_I - K)\, e^{-i2\pi IJ/N_F} ,$$

$$J = 0, 1, \ldots, (N_F - 1) . \tag{1.10}$$

Comparing equation (1.10) with the definition of the IDFT, equation (1.2), we see that

$$u(x_J) = \frac{K}{\pi N_F} e^{i\pi J(N_F-1)/N_F} h(J), \quad J=0,1,\ldots,(N_F-1), \tag{1.11}$$

where h(J) is given by equation (1.2), in which

$$H(I) = U(k_I - K). \tag{1.12}$$

Hence, once λ (and therefore K) is set, the set of algebraic equations for the transformed stresses and displacements are solved using the N_F values of $k = k_I - K$; the FFT is used to compute the N_F values h(J); and the stresses or displacements $u(x_J)$ are obtained from equation (1.12). Stresses and displacements are thus obtained at discrete intervals in x of $\lambda/2$.

It should be noted that the approximation of the IDFT effectively replaces the single impact loading function with an infinite array of sources, periodic in x [3]. As a result, calculated values of $u(x_J)$ represent the true response only up to $x_J = \lambda(N_F/2 - 1)/2$. Hence, N_F must be chosen sufficiently large that disturbances have not propagated past this point. Otherwise, the calculated results will include disturbances emanating from the fictitious sources.

Inversion of the Laplace Transform follows similar steps after noting its similarity to a Fourier Transform. We now consider the interlaminar stress or displacement as a function of time, u(t); U(s) is its Laplace transform, with x now held constant. The Laplace Transform of a function u(t) is defined as

$$U(s) = \int_0^\infty u(t)\, e^{-st}\, dt.$$

Let $s = c + i\omega$, where c is a constant greater than the maximum of the real parts of the poles of U(s); then

$$U(c+i\omega) = \frac{1}{2\pi} \int_0^\infty (2\pi u(t) e^{-ct}) e^{-i\omega t} dt. \qquad (1.13)$$

Equation (1.13) has the form of a continuous inverse Fourier Transform of the function

$$f(t) = 2\pi u(t) e^{-ct}, \quad t > 0$$
$$= 0, \quad t < 0.$$

Inverting back gives

$$2\pi u(t) e^{-ct} = \int_{-\infty}^{\infty} U(c+i\omega) e^{i\omega t} d\omega. \qquad (1.14)$$

As before, U(s) will be known at discrete values of s from solution of the algebraic equations, and we attempt to cast equation (1.14) into a form such that we can calculate u(t) at discrete values of t using the FFT. If significant changes in u(t) are expected to occur over times greater than τ, the largest frequency that need be considered is

$$\Omega = 2\pi/\tau . \qquad (1.15)$$

Then

$$u(t) \doteq \frac{1}{2\pi} e^{ct} \int_{-\Omega}^{\Omega} U(c+i\omega) e^{i\omega t} d\omega.$$

Shifting yields

$$u(t) \doteq \frac{1}{2\pi} e^{ct} e^{-i\Omega t} \int_0^{2\Omega} U(c+i(\omega-\Omega)) e^{i\omega t} d\omega.$$

Replacing the integral by a finite summation leads to

$$u(t) \doteq \frac{\Omega}{\pi N_L} e^{ct} e^{-i\Omega t(N_L-1)/N_L} \sum_{I=0}^{(N_L-1)} U(c + i(\omega_I - \Omega)) e^{i \frac{2\pi I}{N_L} \frac{\Omega}{\pi} t} \tag{1.16}$$

$$\omega_I = \frac{2\Omega}{N_L} (1/2 + I) .$$

If equation (1.16) is evaluated at the discrete times

$$t = t_J = \frac{\tau}{2} J , \qquad J = 0, 1, \ldots, (N_L - 1), \tag{1.17}$$

we get

$$u(t_J) \doteq \frac{\Omega}{\pi N_L} \exp\left(\frac{\pi J}{\Omega} c - i\pi J(N_L-1)/N_L \right) H(J), \qquad J = 0, 1, \ldots, (N_L-1) , \tag{1.18}$$

where H(J) is the DFT defined in equation (1.1), with

$$h(I) = U(c + i(\omega_I - \Omega)) . \tag{1.19}$$

As a result, once c and τ (and therefore Ω) are decided on, the algebraic equations for transformed stresses and displacements are solved for the N_L values of $s = c + i(\omega_I - \Omega)$; the FFT computes the N_L values H(J); and the stresses and displacements $u(t_J)$ are obtained from equation (1.19) at discrete time intervals of $\tau/2$.

Choice of the parameter c affects the accuracy of the computed result. In theory, c must only exceed the real part of the rightmost pole of U(s). However, in conjunction with the FFT, there is a finite range of useful values of c in order to balance round-off errors and aliasing errors for large t in the FFT [4]. It was found in implementation of the computation that a reasonable amount of trial and error yields an acceptable value of c for a given τ. Choices of the parameter τ in the Laplace inversion and of

λ in the Fourier inversion are made simply on the basis of the duration and extent of the impact loading function.

Inversion of both transforms requires a total of $N_F N_L$ combinations of the transform variables k and s. However, the system of algebraic equations need only be solved for $N_F N_L/4$ such combinations. The solutions for the remaining $3N_F N_L/4$ combinations are obtained by taking advantage of symmetries and antisymmetries of the solutions of the algebraic equations about $k = 0$ and $s = c$.

1.2 Computer Program for the Calculation of Interlaminar Stresses

The above analysis has been implemented in a FORTRAN computer program, called IMP2D, for the calculation of interlaminar stresses in a laminated composite subject to line impact loading (two-dimensional case). As noted in the previous report, the 2-D case will be investigated first in order to test the procedures, examine the difficulties, and explore general, qualitative trends before implementing the more general and more complicated central impact (3-D) case.

A documented listing of IMP2D is given in the Appendix. The program accepts as input geometric quantities (number of layers, layer thickness, fiber orientation of each layer), material constants, load parameters, and number of intervals in the discrete Fourier and Laplace inversions. Output lists the interlaminar normal stress and shear stress at each interface as functions of position and time. For the case of a 6-layer plate, using 32 time intervals and 16 spatial intervals, execution time for the program is approximately 20 seconds on Georgia Tech's CDC Cyber 730.

1.3 Results for Line Impact

Results obtained to date for a multi-layered composite plate subject to line-impact loading are summarized below. Figure 1 serves to define some of the nomenclature used in the discussions which follow. At each interface ($n = 1, 2, \ldots, N-1$), interlaminar normal stress ($\sigma_n = \sigma_{22}$) and interlaminar shear stress ($\tau_n = \tau_{12}$) are calculated.

Disturbances due to impact will propagate both transversely (through the thickness) and longitudinally (in the x_1-direction). Due to the significantly different speeds of propagation in the different directions, and because of the nature of the numerical inversion process, the time duration of the loading function determines to some extent which type of propagation may be studied. Hence, to study transverse propagation, a load of short duration is applied in order to facilitate calculations at time intervals small enough to emphasize the details of the rapid propagation of stress waves through the laminate thickness. To investigate the slower longitudinal propagation, a load of relatively longer duration is applied, enabling stresses to be calculated over time intervals long enough to allow the disturbances to propagate in plane sufficiently far from the region of impact loading.

1.3.1 Propagation Through the Thickness. In order to test the computer program, the case of an isotropic steel ($E = 30 \times 10^6$ psi, $\nu = 0.3$) plate was run for the following conditions: $x_o = 1.5$ in., $t_o = 3.4\mu$ sec., layer thickness = 0.2 in., $N = 6$ and 8 layers. Figure 2 shows interlaminar normal stress, normalized with respect to P_o, vs. time at each interface at the point $x_1 = 0$ (directly underneath the center of the loaded region). The results compare favorably to a similar test case in [1]. The initial compressive wave propagates transversely to the bottom surface, from which it is reflected as a tensile wave. Speed of propagation through the thickness

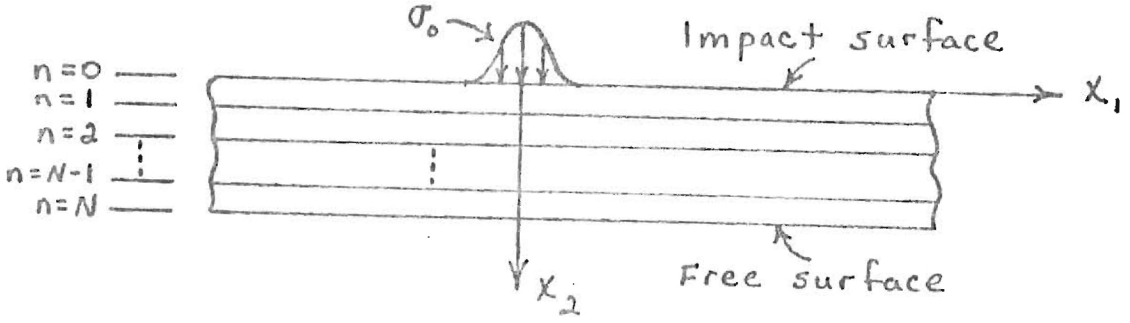

Impact loading function:

$$\sigma_o = -\frac{P_o}{4}\left(1+\cos\frac{\pi x_1}{x_o}\right)\left(1-\cos\frac{2\pi t}{t_o}\right), \quad \begin{matrix} |x_1| < a \\ 0 < t < t_o \end{matrix}$$

$$= 0, \quad \begin{matrix} |x_1| > a \\ t < 0 \\ t > t_o \end{matrix}$$

Figure 1. Multi-layer plate subject to line impact: geometry and nomenclature.

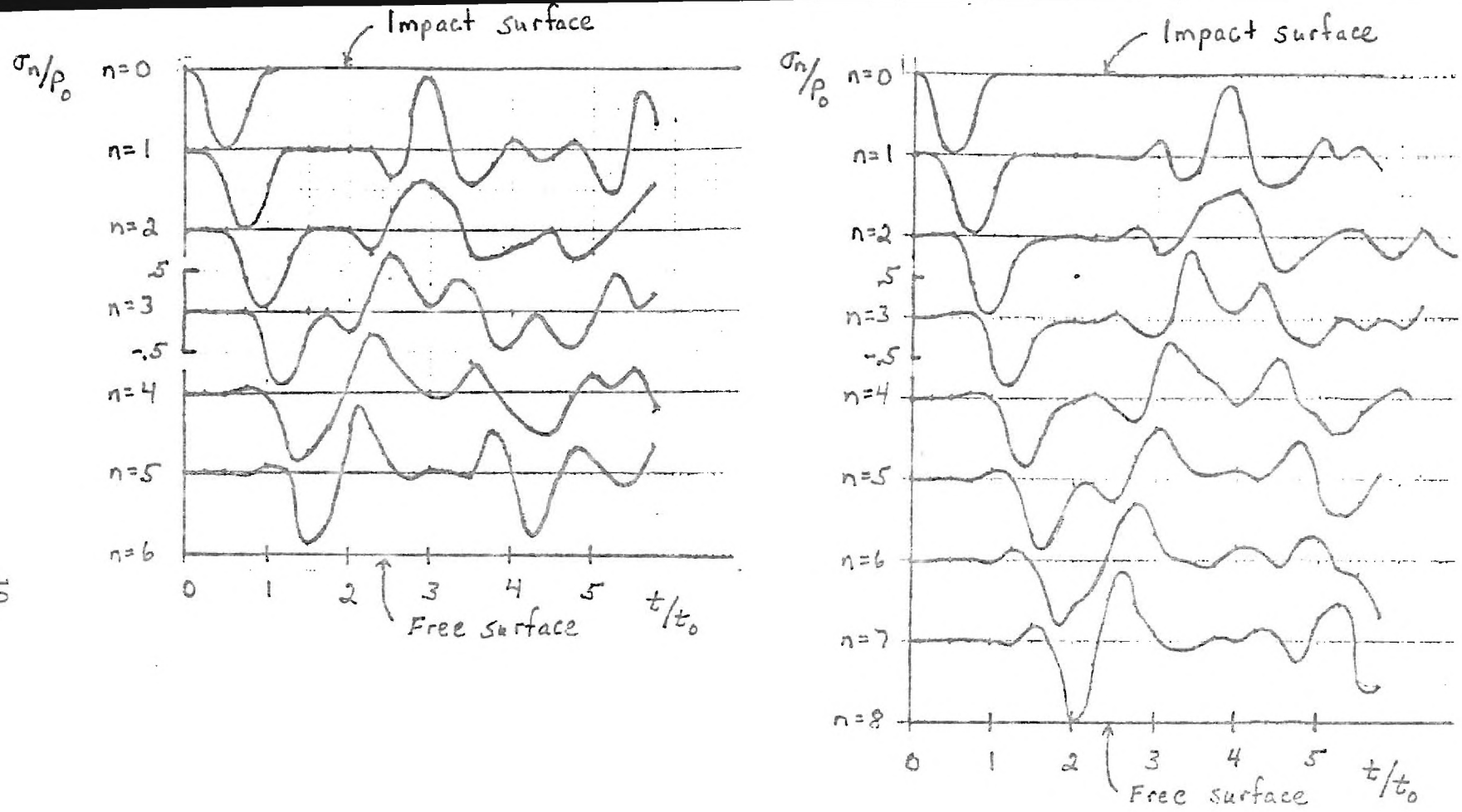

Figure 2. Transverse propagation of normal stress in an isotropic plate: σ_n $(n = 0, 1, \ldots N)$ vs. t at $x_1 = 0$. (Layer thickness = 0.2 in, x_0 = 1.5 in., t_0 = 3.4 μsec.) a) $N = 6$. b) $N = 8$.

is very close to the theoretical dilatational wave speed (2.35×10^5 in./sec.) The shape of the initial compressive pulse is well-preserved during its initial transit through the thickness; distortion becomes more pronounced after reflection and subsequent transmission. This distortion is due to geometric dispersion caused by the presence of the plate boundaries. These results serve to establish confidence in the analytical model and the numerical techniques used.

Through-thickness propagation was next studied for the case of orthotropic layers. Elastic constants used were

$$C_{ij} = \begin{bmatrix} 20.62 & 1.031 & 1.031 & 0 & 0 & 0 \\ & 2.433 & 1.004 & 0 & 0 & 0 \\ & & 2.433 & 0 & 0 & 0 \\ & & & .714 & 0 & 0 \\ & & & & 2.0 & 0 \\ & & & & & 2.0 \end{bmatrix} \times 10^6 \text{ psi}$$

for fibers oriented in the x_1-direction (0^o), where

$$\sigma_i = C_{ij}\, \varepsilon_j$$

These constants correspond to the engineering elastic constants $E_1 = 20 \times 10^6$ psi, $E_2 = E_3 = 2 \times 10^6$ psi, $\nu_{12} = \nu_{13} = 0.3$, $\nu_{23} = 0.4$, $G_{12} = 2 \times 10^6$ psi for a transversely isotropic layer. Program IMP2D was run for a 6-layer plate, with $\Delta = 0.3$ in., $x_o = 0.6$ in., $t_o = 1.53$ μ sec., and several combinations of 0^o and 90^o layers. It was found that transverse propagation of interlaminar normal stresses exhibits the same features as in the isotropic case shown in Figure 2. Stacking sequence has essentially no effect. This result may be anticipated, since the transverse modulus (C_{22}) is unaffected by changes in fiber orientation in the

plane. Maximum tensile and compressive interlaminar stress on all interfaces occurred at $x_1 = 0$ (directly underneath the maximum load). There appeared to be very little longitudinal propagation of σ_{22} over the time interval calculated.

In contrast, interlaminar shear stresses τ_{12} were found to propagate longitudinally as well as transversely. Figure 3 shows a typical result, for a $[0^\circ/0^\circ/90^\circ/90^\circ/0^\circ/0^\circ]$ layer stacking sequence. In this figure, interlaminar shear stress at each interface is plotted vs. x_1 at each time step calculated.

1.3.2 Longitudinal Propagation of Shear Stress. In order to investigate the propagation of stress waves in the x_1-direction, the duration and extent of the loading were increased, with $x_o = 1.2$ in. and $t_o = 10\ \mu$ sec. in the anisotropic calculation. This results in calculation of stresses at longer time intervals, enabling one to observe the propagation of flexural waves. The time duration of the loading is sufficiently long in comparison to transit times of through-thickness stress waves that their presence is not observed.

A typical result for shear stresses at each interface vs. x_1 for several times is shown in Figure 4. Speed of propagation of the peak shear stresses is significantly less than that for dilatational or shear waves, indicating that they are propagating with a flexural wave. It is noted that, for cases of stacking sequences symmetric about the mid-plane (as in the example shown in Figure 4), the interlaminar shear stresses are also very close to symmetric about the mid-plane (i.e., shear stress on interface $n = 2$ equal to that on $n = 4$, and $n = 1$ equal to $n = 5$), further indicating transmission via a flexural wave. As before the interlaminar normal stresses σ_{22} show no tendency to spread in the x_1-direction.

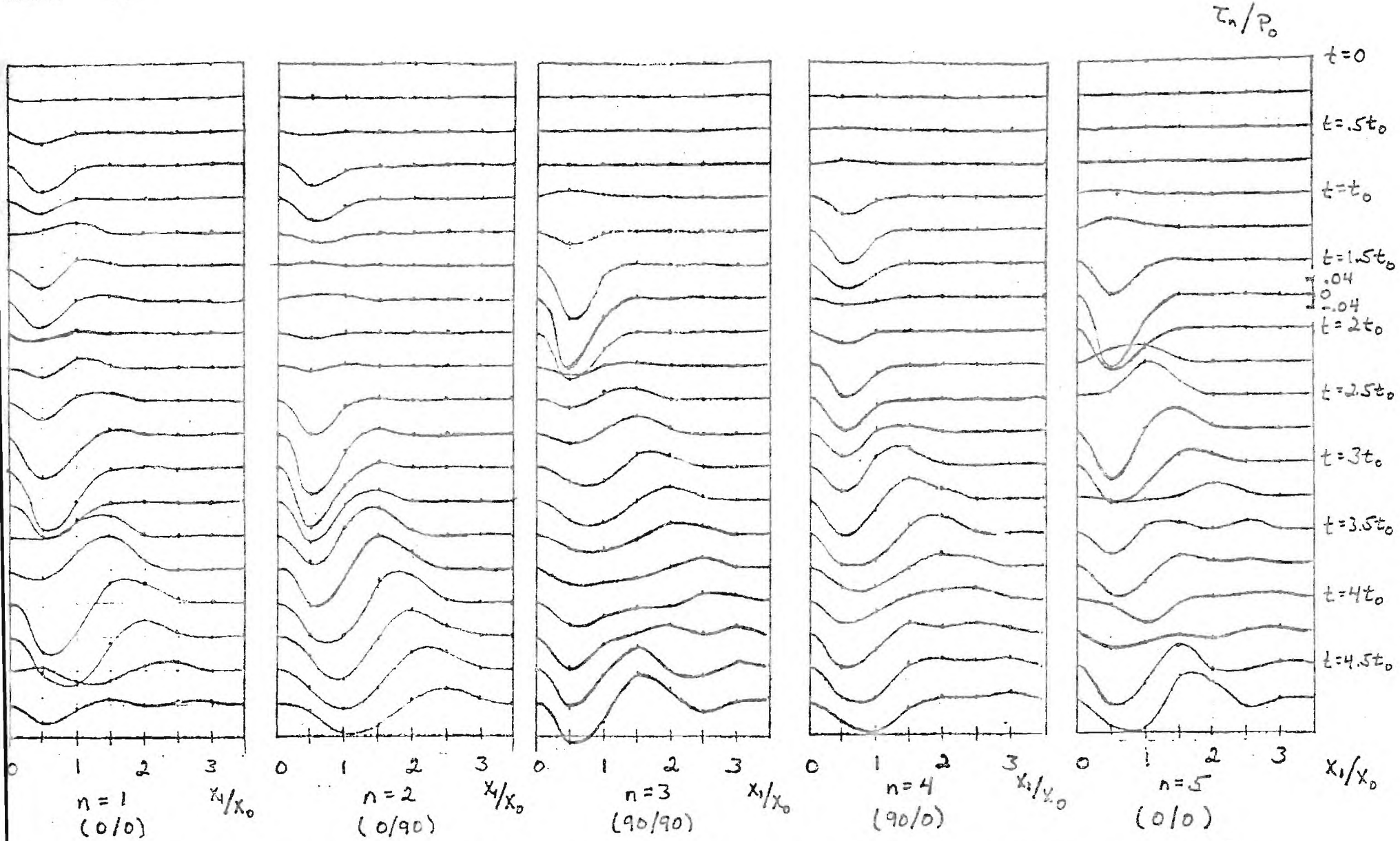

Figure 3. Transverse and longitudinal propagation of shear stress in an anisotropic plate: τ_n vs. X_1 for several times at each interface. ($\Delta = 0.3$ in, $X_0 = 0.6$ in., $t_0 = 1.53$ μsec., [0°/0°/90°/90°,0°,0°]).

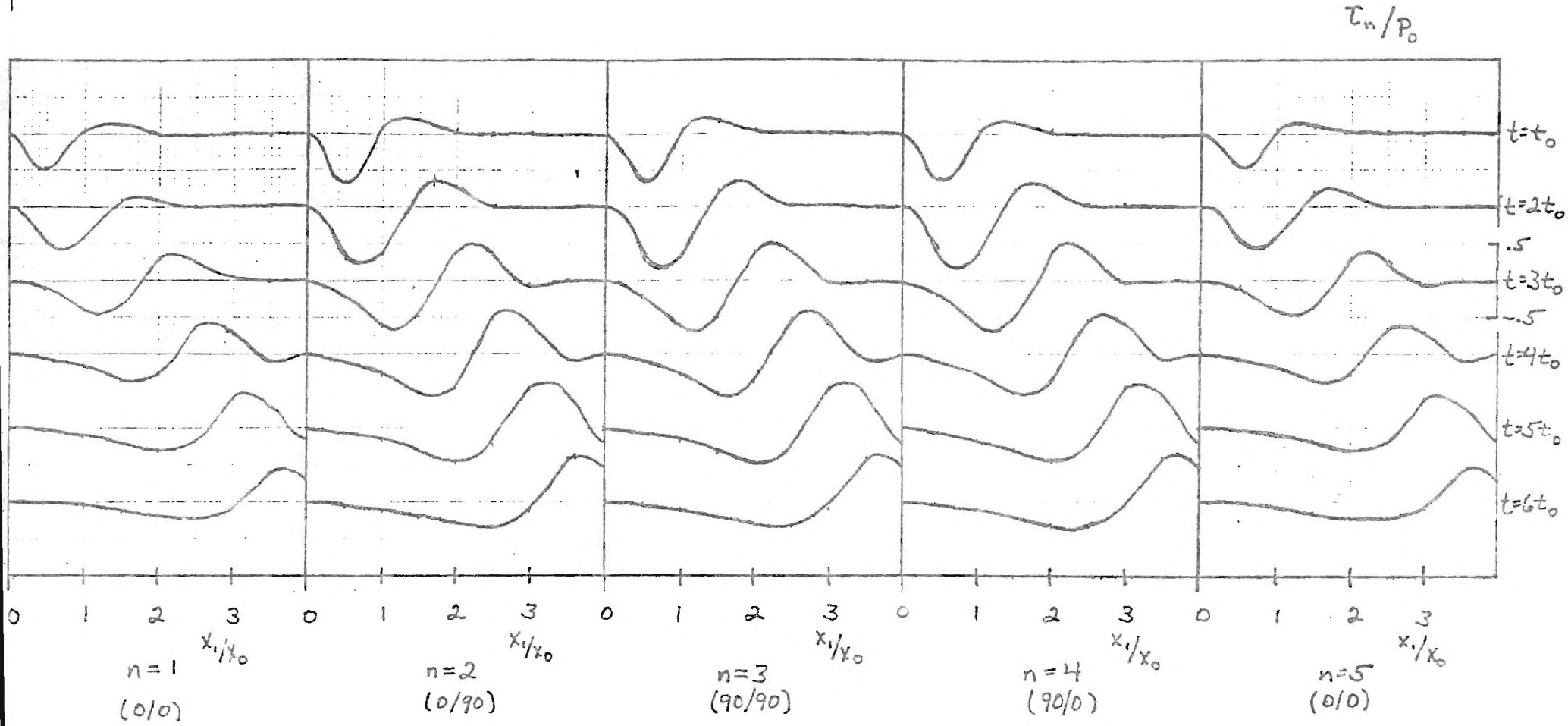

Figure 4. Longitudinal propagation of shear stress in an anisotropic plate: τ_n vs. x_1 for several times at each interface. ($\Delta = 0.3$ in., $x_o = 1.2$ in., $t_o = 10\,\mu$sec., $[0°/0°/90°/90°/0°/0°]$).

1.4 Conclusions and Future Work

Based on the results obtained to date as summarized above, it is possible to arrive at some tentative conclusions concerning the initiation of impact induced delamination, pending further investigation. At this point, it appears likely that delamination is initiated in a small region underneath the loaded area by tensile normal stresses reflected from the bottom free surface (as in Figure 2). Initial delamination would thus occur first at the interface nearest the free surface ($n = N - 1$), followed by subsequent damage at higher interfaces as the tensile wave propagates upwards. It should be noted that the calculation of interlaminar stresses in this work does not take into account any changes in the dynamic response of the laminate once delamination has begun. However, one would expect that, as part of the energy of the tensile wave is absorbed by the delamination process, the amplitude of the tensile wave transmitted onward will be attenuated. Hence, initial damage will be most severe at the interfaces furthest from the impact surface.

Subsequent to this initial delamination occuring in a small region underneath the impact zone, damage may spread in the plane of the interface due to interlaminar shear, as the slower flexural wave develops and propagates longitudinally (Figure 4). Experimental observations by Takeda, Sierakowski, Ross, and Malvern [5] indicate that delamination cracks do in fact propagate with the velocity of flexural waves.

Experimental results further indicate that significant impact-induced delamination damage only occurs between layers with different fiber orientations [5,6]. The calculations summarized above indicate no dramatic differences in interlaminar stress magnitudes between layers with different orientations vs.

layers with like orientations. Hence, it can only be concluded at this point that delamination fracture resistance between like layers is greater than that between unlike layers.

In summary, numerical calculations based on the case of line-impact loading indicate that the multi-layer model used is a promising one for the further investigation of impact-induced delamination in composites. Further work is underway in an attempt to verify the preliminary conclusions stated above. Study of the factors influencing the distribution and maximum values of interlaminar stress, including stacking sequence and impact loading parameters, is continuing in an effort to consider the effective control of such parameters to minimize or contain impact-induced delamination.

The promising results obtained to date indicate both the feasibility and the desirability of extending the calculations to the case of central impact (three-dimensional wave propagation). It is hoped that such an extension will help to explain and quantify experimental observations as to the directional dependence of in-plane delamination propagation on fiber orientation. Further study is also suggested concerning the development of delamination failure criteria in relation both to the calculated dynamic stresses and to experimentally observed delamination patterns.

REFERENCES

1. Kim, B. S. and Moon, F., "Impact Induced Stress Waves in an Anisotropic Plate," AIAA Journal, Oct., 1979, pp. 1126-1133.

2. Cooley, J. W. and Tukey, J. W., "An Algorithm for the Machine Calculation of Complex Fourier Series," Mathematics of Computation, Vol. 90, No. 19, Apr., 1965, pp. 297-301.

3. Brigham, E. O., The Fast Fourier Transform, Prentice-Hall, Englewood Cliffs, N.J., 1974.

4. Cooley, J. W., Lewis, P.A.W., and Welch, P.D., "The Fast Fourier Transform Algorithm: Programming Considerations in the Calculation of Sine, Cosine, and Laplace Transforms," Journal of Sound and Vibration, Vol. 12, 1970, pp. 315-337.

5. Takeda, N., Sierakowski, R. L., Ross, C. A., and Malvern, L. E., "Delamination-crack Propagation in Ballistically Impacted Glass/Epoxy Composite Laminates," Experimental Mechanics, Vol. 22, No. 1, Jan. 1982, pp. 19-25.

6. Dickson, J. N., Private communication, results of experiments run at Lockheed-Georgia Company.

APPENDIX

A listing of the FORTRAN program IMP2D, designed for the calculation of interlaminar stress in a multi-layered composite plate subject to line impact loading, follows. Documentation is included within the program. Notation follows, as closely as possible, that used in this and in previous progress reports.

```
      PROGRAM IMP2D(INPUT,OUTPUT,TAPE5=INPUT,TAPE6=OUTPUT)
C     PROGRAM TO CALCULATE NORMAL AND SHEAR STRESSES ON
C     INTERLAMINAR SURFACES FOR A COMPOSITE LAMINATE SUBJECT
C     TO LINE IMPACT.
      INTEGER IAK(7)
      REAL THETA(6),KK,K,C11(6),C12(6),C22(6),C66(6),DU1(16)
      COMPLEX S,DSS,SIC,CC
      COMPLEX AA(4,4,6),AA1(4,4,6),T22(32,32,6),T12(32,32,6)
      COMPLEX AT22(32),AT12(32)
      COMPLEX A1,A,AN,BB,B,BN,CC,C,CNM1
      COMPLEX DD,D,DN,XXC,XX,XXN
      COMMON/C1/K,S,PI,PO,TL,XL
      COMMON/C3/A1(4,2),A(4,4,6),AN(2,4),BB(2,2),B(4,4,6),BN(2,2)
      COMMON/C4/CC(2,4),C(4,4,6),CNM1(4,2)
      COMMON/C5/DD(2),D(4,6),DN(2),XXC(2),XX(4,6),XXN(2)
C     INPUT PARAMETERS:
C       N = NUMBER OF LAYERS
C       DENS = MASS DENSITY
C       DD = ONE-HALF THICKNESS OF A LAYER
C       THETA(I) = FIBER ORIENTATION IN LAYER I (DEG.)
C       PO = MAXIMUM IMPACT LOAD
C       TL = IMPACT DURATION
C       XL = ONE-HALF OF EXTENT OF IMPACT REGION
C       C11, ETC. = ELASTIC MODULI FOR A 0-DEG. LAYER
C       NL, NF = NUMBER OF INTERVALS IN LAPLACE, FOURIER
C                INVERSIONS (MUST BE EQUAL TO A POWER OF 2)
C       ML, MF = LOG TO BASE 2 OF NL, NF
C       TO = PARAMETER "TAU" IN LAPLACE INVERSION (GENERALLY
C            SET = .5*TL)
C       XO = PARAMETER "LAMBDA" IN FOURIER INVERSION (GENERALLY
C            SET = XL)
C       CC = PARAMETER "C" IN LAPLACE INVERSION
      READ(5,*)N,DENS,DD
      READ(5,*)(THETA(I),I=1,N)
      READ(5,*)PO,TL,XL
      PI=4.*ATAN(1.)
      NM1=N-1
      DO 1 I=1,N
    1 THETA(I)=THETA(I)*PI/180.
      READ(5,*)CC11,CC12,CC13
      READ(5,*)CC22,CC23,CC33
      READ(5,*)CC44,CC55,CC66
C     CALCULATE ELASTIC CONSTANTS OF EACH LAYER IN X1-X2
C     COORDINATE SYSTEM - COORDINATE ROTATION ABOUT X2-AXIS
      DO 2 I=1,N
      CT=(COS(THETA(I)))**2
      ST=(SIN(THETA(I)))**2
      C11(I)=CC11*CT*CT+2.*CT*ST*(CC13+2.*CC55)+CC33*ST*ST
      C12(I)=CC12*CT+CC23*ST
      C22(I)=CC22
    2 C66(I)=CC66*CT+CC44*ST
      READ(5,*)NL,ML,TO,NF,MF,XO,CC
C     KK = PARAMETER "CAPITAL K" = 2*PI/LAMBDA
C     OM = PARAMETER "CAPITAL OMEGA" = 2*PI/TAU
      KK=2.*PI/XO
      OM=2.*PI/TO
      NLM1=NL-1
```

```
      NFM1=NF-1
      NM2=N-2
      NL2=NL/2
      NL3=NL*3/4
      NF2=NF/2
C     CALCULATE COEFFICIENTS IN LINEAR SYSTEM OF EQUATIONS
C     FOR EACH LAYER - DEPEND ON ELASTIC CONSTANTS, K, AND S.
      DO 73 I=1,N
      AA(1,4,I)=CMPLX(-1./BB,0.)
      AA(2,3,I)=AA(1,4,I)
      AA(3,4,I)=CMPLX(-3./DD,0.)
      AA(4,3,I)=AA(3,4,I)
      AA1(1,4,I)=-1.*AA(1,4,I)
      AA1(2,3,I)=-1.*AA(2,3,I)
      AA1(3,4,I)=AA(3,4,I)
      AA1(4,3,I)=AA(4,3,I)
   73 CONTINUE
      DO 3 IF=1,NF2
C     VALUES OF SMALL K AT WHICH EQUATIONS ARE TO BE SOLVED
      K=2.*KK/NF*(IF-.5)-KK
      DO 4 I=1,N
      AA(1,2,I)=CMPLX(0.,C12(I)*K/DD)
      AA(2,1,I)=CMPLX(0.,C66(I)*K/BB)
      AA(3,2,I)=CMPLX(0.,-3.*C66(I)*K/DD)
      AA(3,3,I)=CMPLX(0.,C12(I)*K/C22(I))
      AA(4,1,I)=CMPLX(0.,-3.*C12(I)*K/BB)
      AA(4,4,I)=CMPLX(0.,K)
      AA1(1,2,I)=-1.*AA(1,2,I)
      AA1(2,1,I)=-1.*AA(2,1,I)
      AA1(3,2,I)=AA(3,2,I)
      AA1(3,3,I)=-1.*AA(3,3,I)
      AA1(4,1,I)=AA(4,1,I)
    4 AA1(4,4,I)=-1.*AA(4,4,I)
      DO 55 IL=1,NL2
C     VALUES OF SMALL S AT WHICH EQUATIONS ARE TO BE SOLVED
      S=CMPLX(CC,2.*DM/NL*(IL-.5)-DM)
      DSS=DENS*S*S
      DO 66 I=1,N
      AA(1,1,I)=C11(I)*K*K+DSS
      AA(2,2,I)=C66(I)*K*K+DSS
      AA(3,1,I)=(C11(I)-C12(I)*C12(I)/C22(I))*K*K+3.*C66(I)/(BB*BB)
     1+DSS
      AA(4,2,I)=3.*C22(I)/(DD*DD)+DSS
      AA1(1,1,I)=AA(1,1,I)
      AA1(2,2,I)=AA(2,2,I)
      AA1(3,1,I)=-1.*AA(3,1,I)
   66 AA1(4,2,I)=-1.*AA(4,2,I)
C     FILL SUBMATRIX BLOCKS OF BLOCK-TRIDIAGONAL SYSTEM
C     FILL THE "A" SUBMATRICES
      DO 5 I=1,2
      I2=I+2
      DO 5 J=1,2
    5 A1(I,J)=AA1(I2,J,1)
      IF(N.EQ.2)GO TO 70
      DO 6 L=2,NM1
      DO 6 I=1,2
      I2=I+2
```

```
      DO 6 J=1,4
    6 A(I,J,L)=AA1(I2,J,L)
   70 DO 7 I=1,2
      I2=I+2
      DO 7 J=1,4
    7 AN(I,J)=AA1(I2,J,N)
C   FILL THE "B" SUBMATRICES
      DO 8 I=1,2
      DO 8 J=1,2
    8 BB(I,J)=AA1(I,J,1)
      DO 9 L=1,NM1
      LP1=L+1
      DO 10 I=1,2
      I2=I+2
      DO 10 J=1,4
   10 B(I,J,L)=AA(I2,J,L)
      DO 11 I=3,4
      I2=I-2
      DO 11 J=1,4
   11 B(I,J,L)=AA1(I2,J,LP1)
    9 CONTINUE
      DO 12 I=1,2
      I2=I+2
      DO 12 J=1,2
   12 BN(I,J)=AA(I2,J,N)
C   FILL THE "C" SUBMATRICES
      DO 13 I=1,2
      DO 13 J=1,4
   13 CC(I,J)=AA(I,J,1)
      IF(N.EQ.2)GO TO 71
      DO 14 L=1,NM2
      LP1=L+1
      DO 14 I=3,4
      I2=I-2
      DO 14 J=1,4
   14 C(I,J,L)=AA(I2,J,LP1)
   71 DO 15 I=3,4
      I2=I-2
      DO 15 J=1,2
   15 CNM1(I,J)=AA(I2,J,N)
C   FILL THE "D" SUBVECTORS - RIGHT-HAND SIDE
      CALL LOAD(SIG)
      D(2)=SIG*AA(2,3,1)
      D(1,1)=SIG*AA(3,3,1)
      D(2,1)=-1.*SIG*AA(4,3,1)
C   SOLVE THE SYSTEM OF ALGEBRAIC EQUATIONS FOR A
C   SINGLE PAIR OF K AND S.
C   T22(IF,IL,J) AND T12(IF,IL,J) ARE THE FOURIERFORMS OF
C   THE INTERLAMINAR NORMAL AND SHEAR STRESSES, FOR THE
C   IF-TH VALUE OF K, THE IL-TH VALUE OF S, AND THE J-TH
C   INTERFACE.
      CALL TRIDIB(N)
      DO 16 J=1,NM1
      T22(IF,IL,J)=XX(3,J)
      T12(IF,IL,J)=XX(4,J)
   16 CONTINUE
   55 CONTINUE
```

```
    3  CONTINUE
C   USE SYMMETRIES AND ANTISYMMETRIES IN THE SOLUTION TO
C   CALCULATE T22 AND T12 AT THE REMAINING VALUES OF K AND S.
       DO 75 J=1,NM1
       DO 76 IF=1,NF2
       DO 72 IL=1,NL2
       T22(IF,IL+NL2,J)=CONJG(T22(IF,NL2-IL+1,J))
    72 T12(IF,IL+NL2,J)=-1.*CONJG(T12(IF,NL2-IL+1,J))
       DO 74 IL=1,NL
       T22(NF-IF+1,IL,J)=T22(IF,IL,J)
    74 T12(NF-IF+1,IL,J)=-1.*T12(IF,IL,J)
    76 CONTINUE
    75 CONTINUE
C   INVERT THE FOURIER TRANSFORM OF T22, T12.
       DO 17 J=1,NM1
       DO 18 IL=1,NL
       DO 19 IF=1,NF
       AT22(IF)=CONJG(T22(IF,IL,J))
       AT12(IF)=CONJG(T12(IF,IL,J))
    19 CONTINUE
C   FFT2C IS A SUBROUTINE IN THE INTERNATIONAL MATHEMATICAL
C   AND STATISTICAL LIBRARY (IMSL).
       CALL FFT2C(AT22,NF,IWK)
       CALL FFT2C(AT12,NF,IWK)
       DO 20 IF=1,NF
       JF=IF-1
       BC=CMPLX(0.,PI*JF*(NF-1)/NF)
       T22(IF,IL,J)=KK*CEXP(BC)*CONJG(AT22(IF))/(NF*PI)
       T12(IF,IL,J)=KK*CEXP(BC)*CONJG(AT12(IF))/(NF*PI)
    20 CONTINUE
    15 CONTINUE
C   INVERT THE LAPLACE TRANSFORM OF T22, T12.
       DO 21 IF=1,NF
       DO 22 IL=1,NL
       AT22(IL)=T22(IF,IL,J)
    22 AT12(IL)=T12(IF,IL,J)
       CALL FFT2C(AT22,NL,IWK)
       CALL FFT2C(AT12,NL,IWK)
       DO 23 IL=1,NL
       JL=IL-1
       BC=CMPLX(PI*JL*CC/OM,-1.*PI*JL*(NL-1)/NL)
       T22(IF,IL,J)=OM/(NL*PI)*CEXP(BC)*AT22(IL)
       T12(IF,IL,J)=OM/(NL*PI)*CEXP(BC)*AT12(IL)
    23 CONTINUE
    21 CONTINUE
    17 CONTINUE
C   OUTPUT:
C      AT EACH INTERFACE, INTERLAMINAR NORMAL AND SHEAR
C      STRESSES ARE PRINTED.  EACH LINE OF THE OUTPUT GIVES
C      THE RESULT AS X1 INCREASES FROM ZERO IN STEPS OF X0/2.
C      EACH COLUMN OF THE OUTPUT GIVES THE RESULT AS T
C      INCREASES FROM ZERO IN STEPS OF T0/2.
       DO 90 J=1,NM1
       WRITE(6,150)J
   150 FORMAT(3X,10HINTERFACE NUMBER  ,I1,///)
       WRITE(6,250)
   250 FORMAT(10X,26HINTERLAMINAR NORMAL STRESS,/)
```

```
      DO 91 IL=1,NL
      DO 92 IF=1,NF2
   92 DUM(IF)=REAL(T22(IF,IL,J))
      WRITE(6,350)(DUM(IF),IF=1,NF2)
  350 FORMAT(5X,16(F7.4,1X))
   91 CONTINUE
      WRITE(6,450)
  450 FORMAT(///,10X,25HINTERLAMINAR SHEAR STRESS,/)
      DO 93 IL=1,NL
      DO 94 IF=1,NF2
   94 DUM(IF)=REAL(T12(IF,IL,J))
      WRITE(6,350)(DUM(IF),IF=1,NF2)
   93 CONTINUE
      WRITE(6,550)
  550 FORMAT(////)
   90 CONTINUE
      STOP
      END
```

```
      SUBROUTINE LOAD(SIG)
C   SUBROUTINE TO CALCULATE THE TRANSFORM OF THE IMPACT
C   LOADING FUNCTION FOR A GIVEN VALUE OF K AND S.
      COMPLEX SIG,S
      REAL K
      COMMON/C1/K,S,PI,PO,TL,XL
      PIT=PI/TL
      PIX=PI/XL
      SIG=.5*(1.-CEXP(-1.*S*TL))*(1./S-S/(S*S+4.*PI*PI/(TL*TL)))
      SIG=-.5*PO*SIG*(2./K*SIN(K*XL)+SIN((PIX-K)*XL)/(PIX-K)
     1+SIN((PIX+K)*XL)/(PIX+K))
      RETURN
      END
```

```
      SUBROUTINE TRIDIB(N)
C   SUBROUTINE TO SOLVE THE BLOCK-TRIDIAGONAL SYSTEM OF
C   ALGEBRAIC EQUATIONS
      COMPLEX QQ(2,4),Q(4,4,8),CNM1(4,2),DD(2),D(4,8),DN(2)
      COMPLEX PO(2,2),P(4,4,8),PN(2,2),POI(2,2)
      COMPLEX A1,A,AN,BO,B,BN,CO,C,CNM1,A4,B4,Y
      COMPLEX DD,D,DN,XO,X,XN,DUM,DETPO,DETPN
      COMMON/BSS/A4(4,4),B4(4),Y(4)
      COMMON/C3/A1(4,2),A(4,4,8),AN(2,4),BO(2,2),B(4,4,8),BN(2,2)
      COMMON/C4/CO(2,4),C(4,4,8),CNM1(4,2)
      COMMON/C5/DD(2),D(4,8),DN(2),XO(2),X(4,8),XN(2)
C   FORWARD SOLVE
C   CALCULATE PO
      DO 1 I=1,2
      DO 1 J=1,2
    1 PO(I,J)=BO(I,J)
C   CALCULATE QQ
      DETPO=PO(1,1)*PO(2,2)-PO(1,2)*PO(2,1)
      POI(1,1)=PO(2,2)/DETPO
      POI(1,2)=(-PO(1,2))/DETPO
      POI(2,1)=(-PO(2,1))/DETPO
      POI(2,2)=PO(1,1)/DETPO
      DO 50 I=1,2
      DO 50 J=1,4
      QQ(I,J)=0.
      DO 51 L=1,2
   51 QQ(I,J)=QQ(I,J)+POI(I,L)*CO(L,J)
   50 CONTINUE
C   CALCULATE P(1)
      DO 4 I=1,4
      DO 4 J=1,4
      DUM=(0.,0.)
      DO 5 L=1,2
    5 DUM=DUM+A1(I,L)*QQ(L,J)
    4 P(I,J,1)=B(I,J,1)-DUM
      IF(N.EQ.2)GO TO 52
C   CALCULATE THE Q'S
      NM2=N-2
      DO 6 K=1,NM2
      DO 7 M=1,4
      DO 8 I=1,4
      DO 9 J=1,4
    9 A4(I,J)=P(I,J,K)
    8 B4(I)=C(I,M,K)
      CALL GAUSS4
      DO 10 I=1,4
   10 Q(I,M,K)=Y(I)
    7 CONTINUE
C   CALCULATE THE P'S
      KP1=K+1
      DO 11 I=1,4
      DO 11 J=1,4
      DUM=(0.,0.)
      DO 12 L=1,4
   12 DUM=DUM+A(I,L,KP1)*Q(L,J,K)
   11 P(I,J,KP1)=B(I,J,KP1)-DUM
    6 CONTINUE
```

```
   52 NM1=N-1
C  CALCULATE Q(N-1)
      DO 13 M=1,2
      DO 14 I=1,4
      DO 15 J=1,4
   15 A4(I,J)=P(I,J,NM1)
   14 B4(I)=CNM1(I,M)
      CALL GAUSS4
      DO 16 I=1,4
   16 QNM1(I,M)=Y(I)
   13 CONTINUE
C  CALCULATE P(N)
      DO 17 I=1,2
      DO 17 J=1,2
      DUM=(0.,0.)
      DO 18 L=1,4
   18 DUM=DUM+AN(I,L)*CNM1(L,J)
   17 PN(I,J)=BN(I,J)-DUM
C  CALCULATE THE U'S
      UC(1)=PUI(1,1)*DC(1)+PUI(1,2)*DC(2)
      UC(2)=PUI(2,1)*DC(1)+PUI(2,2)*DC(2)
      DO 25 I=1,4
      DO 25 J=1,4
   25 A4(I,J)=P(I,J,1)
      DO 26 I=1,4
      DUM=(0.,0.)
      DO 27 L=1,2
   27 DUM=DUM+A1(I,L)*UC(L)
   26 B4(I)=D(I,1)-DUM
      CALL GAUSS4
      DO 28 I=1,4
   28 U(I,1)=Y(I)
      IF(N.EQ.2)GO TO 53
      DO 29 K=2,NM1
      KM1=K-1
      DO 30 I=1,4
      DUM=(0.,0.)
      DO 31 L=1,4
   31 DUM=DUM+A(I,L,K)*U(L,KM1)
   30 B4(I)=D(I,K)-DUM
      DO 32 I=1,4
      DO 32 J=1,4
   32 A4(I,J)=P(I,J,K)
      CALL GAUSS4
      DO 33 I=1,4
   33 U(I,K)=Y(I)
   29 CONTINUE
   53 DO 34 I=1,2
      DUM=(0.,0.)
      DO 35 L=1,4
   35 DUM=DUM+AN(I,L)*U(L,NM1)
   34 B4(I)=DN(I)-DUM
      DETPN=PN(1,1)*PN(2,2)-PN(1,2)*PN(2,1)
      UN(1)=(B4(1)*PN(2,2)-B4(2)*PN(1,2))/DETPN
      UN(2)=(B4(2)*PN(1,1)-B4(1)*PN(2,1))/DETPN
C  BACK-SOLVE
C  CALCULATE THE X'S - SOLUTION OF THE SYSTEM
```

```
      XN(1)=UN(1)
      XN(2)=UN(2)
      DO 36 I=1,4
      DUM=(0.,0.)
      DO 37 L=1,2
   37 DUM=DUM+QNM1(I,L)*XN(L)
   36 X(I,NM1)=U(I,NM1)-DUM
      IF(N.EQ.2)GO TO 54
      DO 38 K=2,NM1
      M=N-K
      M1=M+1
      DO 39 I=1,4
      DUM=(0.,0.)
      DO 40 L=1,4
   40 DUM=DUM+Q(I,L,M)*X(L,M1)
   39 X(I,M)=U(I,M)-DUM
   38 CONTINUE
   54 DO 41 I=1,2
      DUM=(0.,0.)
      DO 42 L=1,4
   42 DUM=DUM+Q0(I,L)*X(L,1)
   41 X0(I)=UC(I)-DUM
      RETURN
      END
```

```
      SUBROUTINE GAUSS4
C     SUBROUTINE TO SOLVE A 4X4 LINEAR SYSTEM BY
C     GAUSSIAN ELIMINATION
      COMPLEX A,B,X,C,R
      COMMON/GSS/A(4,4),B(4),X(4)
      DIMENSION C(4)
C     FORWARD SOLVE
      L=1
    4 CONTINUE
      L=L+1
C     PIVOT THE ROWS
      LM1=L-1
      BIG=CABS(A(LM1,LM1))
      K=LM1
      DO 5 I=L,4
      IF(CABS(A(I,LM1)).GT.BIG)GO TO 6
      GO TO 5
    6 CONTINUE
      K=I
      BIG=CABS(A(I,LM1))
    5 CONTINUE
      DO 7 J=LM1,4
      R=A(K,J)
      A(K,J)=A(LM1,J)
    7 A(LM1,J)=R
      R=B(K)
      B(K)=B(LM1)
      B(LM1)=R
C     ELIMINATE
      DO 8 I=L,4
      A(I,LM1)=A(I,LM1)/A(LM1,LM1)
      DO 9 J=L,4
    9 A(I,J)=A(I,J)-A(I,LM1)*A(LM1,J)
    8 B(I)=B(I)-A(I,LM1)*B(LM1)
      IF(L.LE.3)GO TO 4
C     BACK SOLVE
      X(4)=B(4)/A(4,4)
      X(3)=(B(3)-A(3,4)*X(4))/A(3,3)
      X(2)=(B(2)-A(2,3)*X(3)-A(2,4)*X(4))/A(2,2)
      X(1)=(B(1)-A(1,2)*X(2)-A(1,3)*X(3)-A(1,4)*X(4))/A(1,1)
      RETURN
      END
```

THE FOLLOWING SUBROUTINE MAY BE A PROPRIETARY PRODUCT AND HAS BEEN PURCHASED OR SUBSCRIBED TO BY GEORGIA TECH FOR OUR CONTROL DATA USERS. ANY REPRODUCTION OF THIS CODE, AS IN A THESIS OR DISSERTATION FOR DUPLICATION OF RESULTS, SHOULD INCLUDE THE FOLLOWING STATEMENTS:

THE LISTED CODE IS PART OF A PROPRIETARY PRODUCT BELONGING TO -----.

THE LISTINGS ARE REPRODUCED WITH THE PERMISSION OF -----.

THE LISTINGS MAY NOT BE EXTRACTED FOR OTHER PURPOSES, OR USED AS THE BASIS FOR ANY SOFTWARE DEVELOPMENT.

IMSL ROUTINE NAME - FFT2C

COMPUTER - CDC/SINGLE

LATEST REVISION - JANUARY 1, 1978

PURPOSE - COMPUTE THE FAST FOURIER TRANSFORM OF A COMPLEX VALUED SEQUENCE OF LENGTH EQUAL TO A POWER TWO

USAGE - CALL FFT2C (A,M,IWK)

ARGUMENTS
- A - COMPLEX VECTOR OF LENGTH N, WHERE N=2**M. ON INPUT A CONTAINS THE COMPLEX VALUED SEQUENCE TO BE TRANSFORMED. ON OUTPUT A IS REPLACED BY THE FOURIER TRANSFORM.
- M - INPUT EXPONENT TO WHICH 2 IS RAISED TO PRODUCE THE NUMBER OF DATA POINTS, N (I.E. N = 2**M).
- IWK - WORK VECTOR OF LENGTH M+1.

PRECISION/HARDWARE - SINGLE AND DOUBLE/H62
- SINGLE/H60,H70,H80

REQD. IMSL ROUTINES - NONE REQUIRED

NOTATION - INFORMATION ON SPECIAL NOTATION AND CONVENTIONS IS AVAILABLE IN THE MANUAL INTRODUCTION OR THROUGH IMSL ROUTINE UHELP

REMARKS 1. FFT2C COMPUTES THE FOURIER TRANSFORM, X, ACCORDING TO THE FOLLOWING FORMULA;

```
X(K+1) = SUM FROM J = 0 TO N-1 OF
         A(J+1)*CEXP((0.0,(2.0*PI*J*K)/N))
FOR K=0,1,...,N-1 AND PI=3.1415...
```

NOTE THAT X OVERWRITES A ON OUTPUT.

2. FFT2C CAN BE USED TO COMPUTE

```
C                 X(K+1) = (1/N)*SUM FROM J = 0 TO N-1 OF
C                          X(J+1)*CEXP((0.0,-2.0*PI*J*K)/N))
C                 FOR K=0,1,...,N-1 AND PI=3.1415...
C
C               BY PERFORMING THE FOLLOWING STEPS;
C
C                    DO 10 I=1,N
C                       A(I) = CONJG(A(I))
C                 10 CONTINUE
C                    CALL FFT2C (A,M,IWK)
C                    DO 20 I=1,N
C                       A(I) = CONJG(A(I))/N
C                 20 CONTINUE
C
C  COPYRIGHT            - 1978 BY IMSL, INC. ALL RIGHTS RESERVED.
C
C  WARRANTY             - IMSL WARRANTS ONLY THAT IMSL TESTING HAS BEEN
C                         APPLIED TO THIS CODE. NO OTHER WARRANTY,
C                         EXPRESSED OR IMPLIED, IS APPLICABLE.
C-----------------------------------------------------------------------
C
      SUBROUTINE  FFT2C (A,M,IWK)
C                                 SPECIFICATIONS FOR ARGUMENTS
      INTEGER                   M,IWK(1)
      COMPLEX                   A(1)
C                                 SPECIFICATIONS FOR LOCAL VARIABLES
      INTEGER                   I,ISP,J,JJ,JSP,K,K0,K1,K2,K3,K8,KN,MK,MX,MP,N,
     1                          N4,N8,N2,LM,NN,JK
      REAL                      RAD,C1,C2,C3,S1,S2,S3,CK,SK,SQ,A0,A1,A2,A3,
     1                          B0,B1,B2,B3,TWOPI,TEMP,
     2                          ZERO,ONE,Z0(2),Z1(2),Z2(2),Z3(2)
      COMPLEX                   ZA0,ZA1,ZA2,ZA3,AK2
      EQUIVALENCE               (ZA0,Z0(1)),(ZA1,Z1(1)),(ZA2,Z2(1)),
     1                          (ZA3,Z3(1)),(A0,Z0(1)),(B0,Z0(2)),(A1,Z1(1)),
     2                          (B1,Z1(2)),(A2,Z2(1)),(B2,Z2(2)),(A3,Z3(1)),
     3                          (B3,Z3(2))
      DATA                      SQ/.707106781186548/,
     1                          SK/.382683432365090/,
     2                          CK/.923879532511287/,
     3                          TWOPI/6.28318530717959/
      DATA                      ZERO/0.0/,ONE/1.0/
                                SQ=SQRT(2)/2,SK=SIN(PI/8),CK=COS(PI/8)
                                TWOPI=2*PI
                                FIRST EXECUTABLE STATEMENT
      MP = M+1
      N = 2**M
      IWK(1) = 1
      MX = (M/2)*2
      KN = N+1
C                                 INITIALIZE WORK VECTOR
      DO 5  I=2,MP
         IWK(I) = IWK(I-1)+IWK(I-1)
    5 CONTINUE
      RAD = TWOPI/N
      MK = M - 4
      K8 = 1
```

```
      IF (MM .EQ. M) GO TO 15
      K2 = KN
      KO = IWK(MM+1) + KB
   10 K2 = K2 - 1
      KO = KO - 1
      AK2 = A(K2)
      A(K2) = A(KO) - AK2
      A(KO) = A(KO) + AK2
      IF (KO .GT. KB) GO TO 10
   15 C1 = ONE
      S1 = ZERO
      JJ = 0
      K = MM - 1
      J = 4
      IF (K .GE. 1) GO TO 30
      GO TO 70
   20 IF (IWK(J) .GT. JJ) GO TO 25
      JJ = JJ - IWK(J)
      J = J-1
      IF (IWK(J) .GT. JJ) GO TO 25
      JJ = JJ - IWK(J)
      J = J - 1
      K = K + 2
      GO TO 20
   25 JJ = IWK(J) + JJ
      J = 4
   30 ISP = IWK(K)
      IF (JJ .EQ. 0) GO TO 40
C                                     RESET TRIGONOMETRIC PARAMETERS
      C2 = JJ * ISP * RAD
      C1 = COS(C2)
      S1 = SIN(C2)
   35 C2 = C1 * C1 - S1 * S1
      S2 = C1 * (S1 + S1)
      C3 = C2 * C1 - S2 * S1
      S3 = C2 * S1 + S2 * C1
   40 JSP = ISP + KB
C
CC                                    DETERMINE FOURIER COEFFICIENTS
                                        IN GROUPS OF 4
      DO 50 I=1,ISP
         KO = JSP - 1
         K1 = KO + ISP
         K2 = K1 + ISP
         K3 = K2 + ISP
         ZA0 = A(KO)
         ZA1 = A(K1)
         ZA2 = A(K2)
         ZA3 = A(K3)
         IF (S1 .EQ. ZERO) GO TO 45
         TEMP = A1
         A1 = A1 * C1 - B1 * S1
         B1 = TEMP * S1 + B1 * C1
         TEMP = A2
         A2 = A2 * C2 - B2 * S2
         B2 = TEMP * S2 + B2 * C2
         TEMP = A3
         A3 = A3 * C3 - B3 * S3
```

```
      B3 = TEMP * S2 + B3 * C3
45    TEMP = A0 + A2
      A2 = A0 - A2
      A0 = TEMP
      TEMP = A1 + A3
      A3 = A1 - A3
      A1 = TEMP
      TEMP = B0 + B2
      B2 = B0 - B2
      B0 = TEMP
      TEMP = B1 + B3
      B3 = B1 - B3
      B1 = TEMP
      A(K0) = CMPLX(A0+A1,B0+B1)
      A(K1) = CMPLX(A0-A1,B0-B1)
      A(K2) = CMPLX(A2-B3,B2+A3)
      A(K3) = CMPLX(A2+B3,B2-A3)
50    CONTINUE
      IF (K .LE. 1) GO TO 55
      K = K - 2
      GO TO 30
55    KB = K3 + ISP
C                                     CHECK FOR COMPLETION OF FINAL
C                                       ITERATION
      IF (KN .LE. K3) GO TO 70
      IF (J .NE. 1) GO TO 60
      K = 3
      J = MK
      GO TO 20
60    J = J - 1
      C2 = C1
      IF (J .NE. 2) GO TO 65
      C1 = C1 * CK + S1 * SK
      S1 = S1 * CK - C2 * SK
      GO TO 35
65    C1 = (C1 - S1) * SQ
      S1 = (C2 + S1) * SQ
      GO TO 35
70    CONTINUE
C                                     PERMUTE THE COMPLEX VECTOR IN
C                                       REVERSE BINARY ORDER TO NORMAL
C                                       ORDER
      IF(M .LE. 1) GO TO 9005
      MP = M+1
      JJ = 1
C                                     INITIALIZE WORK VECTOR
      IWK(1) = 1
      DO 75  I = 2,MP
        IWK(I) = IWK(I-1) * 2
75    CONTINUE
      N4 = IWK(MP-2)
      IF (M .GT. 2) N8 = IWK(MP-3)
      N2 = IWK(MP-1)
      LM = N2
      NN = IWK(MP)+1
      MP = MP-4
C                                     DETERMINE INDICES AND SWITCH A
```

```
      J = 2
   80 JK = JJ + N2
      AK2 = A(J)
      A(J) = A(JK)
      A(JK) = AK2
      J = J+1
      IF (JJ .GT. N4) GO TO 85
      JJ = JJ + N4
      GO TO 105
   85 JJ = JJ - N4
      IF (JJ .GT. N8) GO TO 90
      JJ = JJ + N8
      GO TO 105
   90 JJ = JJ - N8
      K = MP
   95 IF (IwK(K) .GE. JJ) GO TO 100
      JJ = JJ - IwK(K)
      K = K - 1
      GO TO 95
  100 JJ = IwK(K) + JJ
  105 IF (JJ .LE. J) GO TO 110
      K = NN - J
      JK = NN - JJ
      AK2 = A(J)
      A(J) = A(JJ)
      A(JJ) = AK2
      AK2 = A(K)
      A(K) = A(JK)
      A(JK) = AK2
  110 J = J + 1
C
C                                        CYCLE REPEATED UNTIL LIMITING NUMBER
C                                          OF CHANGES IS ACHIEVED
      IF (J .LE. LM) GO TO 80
C
 9000 RETURN
      END
```

Part II

Analytical Models of Delamination Growth

Part II

Analytical Models of Delamination Growth

Abstract Two new analytical models of one-dimensional delamination -- the merged delamination and the stepped-layer delamination -- are proposed. Single or multiple delaminations of uniform thickness may change into states described by the new models in an advanced stage of growth. For each model, algebraic equations are obtained whose solutions characterize the buckled state of delamination. A simple expression of the strain energy release rate, valid for all one-dimensional models, is derived by the method of J-integral. Furthermore, a theory of separating the strain energy release rate into its mode I and mode II components is developed on the basis of the invariance of solutions under similarity transformations. The theoretical results are in agreement with the finite element analysis results in the literature.

Table of Contents

1. Introduction

The principal types of damage caused by foreign object impact on a composite laminate are delamination, fiber breaking and matrix cracking. It is often observed that delamination occurs in one or more interlaminar planes near that surface of the laminate which is opposite to the side of impact, and at positions directly below the point of impact. This observation suggests that delamination is generated by tensile normal stress waves reflected from the free surface. Analytical prediction of the number and size of delamination or of the location and extent of fiber breaks and matrix cracks, on the basis of various impact parameters and the geometrical and material properties of the laminate, is an exceedingly difficult task. Calculation of the dynamic normal stress generated by impact requires detailed solutions of through-the-thickness stress-wave propagation in a layered structure. Such detailed solutions can be obtained by using the powerful method of integral transforms at the expense of ignoring the changes in the geometry of the laminate produced by the initiation and growth of damage. But in reality damage does occur and occurs continually, creating surfaces of separation that interfere with the phenomena of wave propagation. Furthermore, a tested and accepted dynamic fracture criterion appropriate to fast delamination growth in a composite laminate under impulsive stresses of very short duration is not yet available. In view of these throretical difficulties, the correlation of the impact parameters and the geometrical and material parameters of the laminate with the impact-induced damage relies at the present time more on curve-fitting the experimental data than on theoretical or numerical analysis of dynamic stress and damage growth.

In the analysis of this report, we assume that the impact-induced damage in a laminate is already known -- it is either measured or predicted by an

empirical formula. The scope of our analysis is to investigate one-dimensional buckling of a thin layer of delamination near the surface of the laminate and the energy release rates associated with the growth of delamination when the laminate is subsequently subjected to an in-plane compresseive load. The results of this analysis can be used to infer the residual strength of an impact-damaged laminate, hence the analysis has an important function in charaterizing the impact-damage tolerance of a composite laminate.

Our exclusive concern with delamination damage is justified by two reasons. First, delamination has been generally considered as the main energy-absorption mechanism in low velocity impact of laminates [1]. Delamination occurs whenever a sufficiently large amount of impact energy is imparted to the laminate to produce significant structural damage. Secondly, when the laminate is later subjected to an in-plane compresssive load, a surface delamination may buckle and the delamination may grow when the bad produces a sufficiently large stress intensity factor (or, equivalently, strain energy release rate) at the front of delamination. Thus, delamination governs the residual strength of the laminate because it may lead to catastrophic failure of the laminate in subsequent loading.

Although foreign object impact generally produces two-dimensional delamination, the growth of such delamination can only be studied by numerical methods because closed-form analytical solutions of the buckled state and the associated energy release rates are not available. However, understanding of delamination growth can be gained by considering one-dimensional models in which the delamination runs through the entire width of the laminate. In such models, delamination grows along the perpendicular in-plane direction under a compressive load applied in that direction. Throughout this report,

the laminate is considered as a homogeneous orthotropic body whose three orthotropic axes are parallel to the coordinate axes of the laminate.

In part 1 of this report, we introduced two analytical models of delamination -- the merged delamination and the stepped-layer delamination--which may replace single or multiple delaminations of uniform thickness in their later stages of growth. For each model, we obtain algebraic equations whose solutions determine the buckling load, the buckled shape and the end forces and moments of the delaminated layer. The analysis of this part gives results which are required in the subsequent calculation of the strain energy release rates.

In part 2, we show that the path-independent J-integral provides a simple and efficient method for calculating the strain energy release rates of all one-dimensional models of delamination. For a uniform-thickness delamination, the calculated result reduces to the formula derived by Chai, Babcock and Knauss [2], who used the method of differentiation. Next, a theory of separating the strain energy release rate into its mode I and mode II components is developed on the basis of the invariance of solutions under similarity transformations (dimensional rescalings). The resulting expression for the mode I energy release rate formally belongs to an empirical formula proposed by Whitcomb [3] for a laminate with finite bending stiffness, and our expression for the mode II energy release rate shows the same trend and the same relation of magnitude to the mode I energy release rate as indicated by the finite-element analysis result of Whitcomb [4].

Finally, the use of critical values of the total strain energy release rate or of the mode I component of the energy release rate as the criteria of delamination growth is examined in Part 3 of the report.

Part 1: Analytical Models of One-dimensional Delamination

2. One-dimensional delamination of a surface layer

2.1 Governing equations

Consider a laminated plate with its two faces parallel to the x-z plane and subjected to a compressive strain ϵ_o along the x-direction. For simplicity we assume that the laminate is made of a homogeneous orthotropic material whose three planes of symmetry are parallel to the coordinate planes. Then throughout the laminate the components of stress are given by

$$\sigma_x = -E_1 \epsilon_o , \quad \sigma_y = \sigma_z = \tau_{xy} = \tau_{xy} = \tau_{yz} = 0. \tag{2.1}$$

Furthermore, the strain component in the z-direction has the value

$$\epsilon_z = \nu_{13} \epsilon_0 . \tag{2.2}$$

If a thin surface layer of uniform thickness h and width ℓ is delaminated from the main body of the laminate and the delamination runs across the entire z-direction (one-dimensional model of delamination, see Fig. 1), and if the compressive strain ϵ_0 is sufficiently large to cause the buckling of the delaminated layer, then the deformation of the layer may be investigated in the following manner.

It is assumed that the delamination of the surface layer has negligible effects upon the stress and the strain in the main body of the laminate, that the stress and strain components in the buckled surface layer are independent of the coordinate z and that Eq. (2.2) remains valid. Let v denote the lateral deflection and P, Q and M the axial compressive force, the shearing force and the bending moment (per unit width in the z-direction) of the buckled layer. The equations of equilibrium for the layer are

$$\begin{aligned} M' + Q + P\, v' &= 0, \\ P' &= 0, \\ Q' &= 0, \end{aligned} \tag{2.3}$$

where the prime indicates differentiation with respect to x. The axial strain and axial stress in the layer are given by

$$\epsilon_x = -\nu_{13}\,\nu_{31}\,\epsilon_0 - (1 - \nu_{13}\,\nu_{31})\,\frac{P}{E_1 h} - \frac{M}{K}\,y,$$

$$\sigma_x = -P/h - \frac{12My}{h^3}, \tag{2.4}$$

where

$$K = \frac{E_1 h^3}{12(1 - \nu_{13}\,\nu_{31})} \tag{2.5}$$

is the bending stiffness per unit width of the buckled layer. In the case of small lateral deflection, the moment-curvature relation may be approximated by

$$M = K\,v''. \tag{2.6}$$

Substituting (2.6) into Eq. (2.3a), and differentiating the result, one obtains

$$v'''' + (P/K)\,v'' = 0. \tag{2.7}$$

If the surface layer is composed of two or more segments with different thicknesses (and hence different stiffnesses K), then an equation of the form (2.7) holds in each segment.

2.2 The Chai-Babcock-Knauss thin film model

Chai, Babcock and Knauss [2] studied several one-dimensional models of delamination in which the delaminated layer is assumed to have a constant thickness. Although they also considered buckled layers that were not necessarily thin compared to the laminate, the results for such cases were not qualitatively different from the corresponding results for the delamination of a thin surface layer (the "thin film model"), and the latter results can

be expressed in simple analytical forms. These expressions were presented by Chai et al. for the simple case of isotropic materials. If the material is orthotropic, and if the planes of orthotropy are parallel to the coordinate planes, then, by going through a similar but more laborious derivation, it is found that the corresponding expressions are the same, except that the isotropic moduli E and $1-\nu^2$ are replaced by the orthotropic moduli E_1 and $1-\nu_{13}\,\nu_{31}$:

$$P = \frac{E_1 h\,\pi^2}{3(1-\nu_{13}\,\nu_{31})}\left(\frac{h}{\ell}\right)^2, \qquad Q = 0,$$

$$M(x) = \frac{KA}{2}\left(\frac{2\pi}{\ell}\right)^2 \cos\frac{2\pi x}{\ell}, \tag{2.8}$$

$$v(x) = \frac{A}{2}\left(1 - \cos\frac{2\pi x}{\ell}\right),$$

where,

$$A^2 = (\epsilon_0 - \epsilon_{cr})\left(\frac{2\ell}{\pi}\right)^2 (1-\nu_{13}\,\nu_{31}),$$

$$\epsilon_{cr} = \frac{P}{hE_1} = \frac{\pi^2}{3(1-\nu_{13}\,\nu_{31})}\left(\frac{h}{\ell}\right)^2. \tag{2.9}$$

Chai et al. obtained the energy release rate associated with the growth of delamination by comparing the total strain energies of the system before and after an infinitesimal growth of the delamination. Applying the same method to the orthotropic case, one obtains the result:

$$G_a = 1/2\, E_1 h\,(1-\nu_{13}\,\nu_{31})\,(\epsilon_0 - \epsilon_{cr})\,(\epsilon_0 + 3\epsilon_{cr}). \tag{2.10}$$

If the delaminated surface layer is relatively short or thick so that ϵ_{cr} as defined by Eq. (2.9b) is greater than the given compressive strain ϵ_0 in the main body of the laminate, then the layer does not buckle and the energy release rate is zero:

$$G_a = 0 \qquad \text{if} \qquad \epsilon_0 < \epsilon_{cr}.$$

On the other hand, if the delamination is sufficiently long, so that G_a as given by Eq. (2.10) exceeds the critical value for the growth of delamination, then fracture occurs at the tip of delamination and the length of the delaminated layer increases. The initial phase of delamination growth is accompanied by a rapid increase in the energy release rate, until the latter reaches a peak value. Afterwards G_a decreases monotonically and approaches the limiting value

$$G_\infty = \tfrac{1}{2}(1 - \nu_{13}\nu_{31})\, E_1 h\, \epsilon_0^2$$

as ℓ increases. This latter phrase is accompanied by the decreases of the buckling load P and of the maximum bending moment M in the buckled layer. If G_a falls below the critical value for the growth of delamination, then the growth may be arrested when the kinetic energy carried by the system (due to the accumulated excess of the released energy over the critical fracture energy) is completely absorbed by the fracture mechanism.

3. Coalescence of parallel delaminations

3.1 Physical considerations

The analysis of the Chai-Babcock-Knauss thin film model yields the following conclusion: with a given compressive strain applied to the laminate, a one-dimensional surface delamination will buckle if the thickness-to-length ratio is so small that ϵ_{cr} as defined by Eq. (2.9b) is less than ϵ_0 and, furthermore, the delamination will grow if the thickness h is sufficiently large so that G_a as defined by Eq. (2.10) exceeds the critical value for fracture (notice that G_a is proportional to h). Hence a very thin delaminated film will buckle under a relatively small compressive strain but either the delamination cannot grow because G_a is small or it grows at first but is subsequently arrested as G_a falls below the critical value. On the other hand, a relatively thick delaminated layer would not buckle under the given

compressive strain ϵ_0 if the initial delamination length ℓ is not sufficiently large.

However, in the case of impact-induced defects in laminates, it is not uncommon for two or more parallel delamination faces to coexist in a region near the surface opposite to the location of impact. Each one of the delaminated layers is sufficiently thin to buckle under the given compressive strain ϵ_0. And although the energy release rate associated with any single delamination may be less than the critical value for fracture, two or more delaminated layers taken as a whole may generate a sufficiently large energy release rate to initiate and sustain the growth of that delamination flaw which is farthest away from the surface. Thus the existing delaminations of several parallel layers may coalesce into the delamination of a single thick layer and this delamination growth may continue without arrest until the laminate is severely damaged.

In order to investigate this possible phenomena of delamination growth, we study the one-dimensional buckling problem of a merged delamination model consisting of two identical layers of length a and thickness h joined with a single layer of length b and thickness 2h. In Sec. 3.2, we formulate the equations governing the buckling load and the transverse deflection. Although the buckling load is uniquely determined by the characteristic equation as its lowest root, the equation and the end conditions for the transverse deflection determine the shape of deflection but not its magnitude. An undetermined multiplication factor is obtained in Sec. 3.3 by considering the axial strain of the middle plane of the delaminated layer. Then the shearing forces and the bending moments at the two ends of the delamination can be calculated. In part 2 of this report, this solution is used to obtain the strain energy release rates associated with the growth of a merged delamination.

3.2 Governing equations and buckling load of a merged delamination

Figure 2 shows two identical parallel layers of thickness h joining with a single layer of thickness 2h. If the ratio of lengths b/a is small, then the deflection and the slope at the junction are both small. Hence the two identical thin layers on the left hand side are subjected to approximately the same boundary conditions. As a first approximation, we may assume that they deflect independently and in the same manner, so that the deflection is described by a single function v:

$$v = v(\xi), \qquad 0 \le \xi \le a. \tag{3.1}$$

Strictly speaking, this assumption is valid only if $b = 0$. For $b > 0$, the lower thin layer always carries a larger compressive load than the upper thin layer, tends to show larger lateral deflection, and hence always pushes against the upper layer and cannot deflect independently of the upper layer.

The deflection of the relatively thick layer on the right hand side is described by another function

$$w = w(\eta), \qquad 0 \le \eta \le b. \tag{3.2}$$

The left and right ends of the whole delaminated strip are designated by the coordinates $\xi = 0$ and $\eta = 0$, respectively, where the deflection functions satisfy the boundary conditions

$$v(0) = 0, \quad v'(0) = 0, \quad w(0) = 0, \quad w'(0) = 0. \tag{3.3}$$

The continuity of the deflection, the slope, the bending moment and the shearing force at the junction $\xi = a(\eta = b)$ requires that

$$\begin{aligned} &v(a) = w(b), \quad v'(a) = -w'(b), \\ &2h^3 v''(a) = (2h)^3 w''(b), \\ &2h^3 v'''(a) = -(2h)^3 w'''(b). \end{aligned} \tag{3.4}$$

Furthermore, the deflection of each segment is governed by a system of equations of the form (2.3). Hence

$$\frac{d^4v}{d\xi^4} + \lambda^2 \frac{d^2v}{d\xi^2} = 0, \qquad 0 \le \xi \le a$$
$$\frac{d^4w}{d\eta^4} + \mu^2 \frac{d^2w}{d\eta^2} = 0, \qquad 0 \le \eta \le b \tag{3.5}$$

where

$$\lambda^2 = \frac{P}{2} \frac{1}{K_1} = \frac{P}{2} \frac{12(1 - \nu_{13}\nu_{31})}{E_1 h^3},$$
$$\mu^2 = P/K_2 = P \frac{12(1 - \nu_{13}\nu_{31})}{E_1 (2h)^3} = \frac{\lambda^2}{4}, \tag{3.6}$$

and P is the axial load in the right segment and is equal to twice the axial load in each thin layer of the left segment.

Equation (3.5) together with the end conditions (3.3) and the conditions (3.4) admit non-trivial solutions if the following characteristic equation is satisfied:

$$\Delta \equiv 1 - \cos x \cos y + \frac{5}{4} \sin x \sin y - \left(\frac{x}{2} + y\right)\left(\sin x \cos y + \frac{1}{2} \cos x \sin y\right)$$
$$= 0, \tag{3.7}$$

where

$$x \equiv \lambda a = 2\mu a, \quad y \equiv \mu b.$$

The characteristic equation (3.7) determines the buckling load P. When the lowest buckling load is used to evaluate the parameters μ, $\lambda = 2\mu$, x and y, we obtain the non-trivial solutions of the buckling problem (3.3) - (3.5) in the following form

$$v(\xi) = A\left[\frac{\cos x - \cos y}{2}\left(\sin 2\mu\xi - 2\mu\xi\right) + \left\{\frac{1}{2}\sin x + \sin y - \left(\frac{x}{2} + y\right)\cos y\right\}(1-\cos 2\mu\xi)\right.$$

$$0 \le \xi \le a;$$

$$v(\eta) = A\left[-(\cos x - \cos y)(\sin \mu\eta - \mu\eta) + \left\{\frac{1}{2}\sin x + \sin y - \left(\frac{x}{2} + y\right)\cos x\right\}(1-\cos\mu\eta)\right]$$

$$0 \le \eta \le b, \tag{3.8}$$

where A is a constant to be determined later. The bending moment and shearing force at the two ends may be obtained by differentiation. The results at the right end are

$$M_B = K_2 W''(0) = PA\left\{\frac{1}{2}\sin x + \sin y - \left(\frac{x}{2} + y\right)\cos x\right\}, \tag{3.9}$$

$$Q_B = K_2 W'''(0) + P W'(0) = \mu PA(\cos x - \cos y)$$

Similarly, the two thin layers on the left are each subjected to a shearing force and a bending moment

$$Q_A = Q_B/2, \quad M_A = \frac{PA}{2}\left\{\frac{1}{2}\sin x + \sin y - \left(\frac{x}{2} + y\right)\cos y\right\} \tag{3.10}$$

at the left end $\xi = 0$.

In the special case $b = 0$, the problem reduces to that of the thin film model. Since $y = \mu b = 0$, the characteristic equation (3.7) reduces to

$$1 - \cos \lambda a - \frac{\lambda a}{2}\sin \lambda a = 0.$$

This yields the lowest buckling load

$$\frac{P}{2} = K_1 \lambda^2 = K_1\left(\frac{2\pi}{a}\right)^2,$$

in agreement with the result for a thin film model.

3.3 Calculation of the amplitude of the buckling solution.

The factor A occuring in the expressions (3.8), (3.9) and (3.10) is related to the amplitude of the buckling solution. This factor can be determined by considering the change of the total arc length of the delamination from its initial state to the buckled state. As in the case of Chai-Babcock-Knauss thin film model, the length increases because buckling reduces the axial compressive loads carried by the delaminated layers.

When the main body of the laminate is subjected to a compressive strain ϵ_0, the two ends of the delaminated strip approach each other with a relative displacement $(a + b)\epsilon_0$. But since the delaminated strip has buckled and is subjected to the buckling load P, its axial strain ϵ_x is determined by the following two equations

$$\epsilon_x = \frac{-P}{2hE_1} - \frac{\nu_{31}}{E_3}\,\sigma_z,$$

$$\epsilon_z = \nu_{13}\,\epsilon_0 = \frac{\sigma_z}{E_3} - \frac{\nu_{13}}{E_1}\left(-\frac{P}{2h}\right),$$

where Eq. (2.2) has been used. Consequently,

$$\epsilon_x = -(1 - \nu_{13}\,\nu_{31})\,\frac{P}{2hE_1} - \nu_{13}\,\nu_{31}\,\epsilon_0. \qquad (3.11)$$

The total shortening of the delaminated strip from its undeformed state to its buckled state is $-(a + b)\,\epsilon_x$. This contraction is smaller than the relative approach of the two ends of the strip, $(a + b)\,\epsilon_0$. The difference is due to the curvature effect in the buckled state. Thus,

$$(a + b)\epsilon_0 - \left\{-(a + b)\epsilon_x\right\}$$

$$= \frac{1}{2}\int_0^a \left\{v'(\xi)\right\}^2 d\xi + \frac{1}{2}\int_0^b \left\{w'(\eta)\right\}^2 d\eta$$

$$= \frac{\mu^2 A^2}{2} \int_0^a \Big[(\cos x - \cos y)^2 (1 - \cos 2\mu\xi)^2 + \Big\{ \sin x + 2 \sin y - (x + 2y)\cos y \Big\}^2 \sin^2 2$$

$$-2(\cos x - \cos y) \Big\{ \sin x + 2 \sin y - (x + 2y)\cos y \Big\} \sin 2\mu\xi (1 - \cos 2\mu\xi) \Big] d\xi$$

$$+ \frac{\mu^2 A^2}{2} \int_0^b \Big[(\cos x - \cos y)^2 (1 - \cos \mu\eta)^2 + \frac{1}{4} \Big\{ \sin x + 2\sin y - (x + 2y)\cos \Big\}^2 \sin^2 \mu$$

$$+ (\cos x - \cos y) \Big\{ \sin x + 2 \sin y - (x + 2y)\cos x \Big\} \sin \mu\eta (1 - \cos \mu\eta) \Big] d\eta,$$

or

$$\left(1 - \nu_{13}\nu_{31}\right) \left(\epsilon_0 - \frac{P}{2hE_1}\right) (a + b)$$

$$= \frac{\mu A^2}{8} \Big[(\cos x - \cos y)^2 \Big\{ 3(x + 2y) - 4(\sin x + 2 \sin y) + \frac{1}{2} (\sin 2x + 2 \sin 2y) \Big\}$$

$$+ \Big\{ \sin x + 2 \sin y - (x + 2y) \cos y \Big\}^2 \left(x - \frac{\sin 2x}{2} \right)$$

$$+ \Big\{ \sin x + 2 \sin y - (x + 2y) \cos x \Big\}^2 \left(\frac{y}{2} - \frac{\sin 2y}{4} \right)$$

$$- 2 (\cos x - \cos y) \Big\{ \sin x + 2 \sin y - (x + 2y) \cos y \Big\} (1 - \cos x)^2$$

$$+ 2 (\cos x - \cos y) \Big\{ \sin x + 2 \sin y - (x + 2y) \cos x \Big\} (1 - \cos y)^2 \Big].$$

(3.12)

With the lowest buckling load solved from Eq. (3.7), the factor A occurring in the expressions (3.8), (3.9) and (3.10) can be evaluated by means of Eq. (3.12). The solution of the buckling problem corresponding to a merged delamination is complete.

The energy release rate associated with the extension of a merged delamination will be calculated in Part 2 of this report.

4. The stepped-layer model

4.1 Governing equations

Low velocity impact on composite laminates may cause delamination, fiber breaking and matrix cracking. When the laminate is later subjected to static or cyclic compressive loads, an impact-generated delamination may grow in an interlaminar plane until it intersects an existing transverse crack in the matrix. Subsequently the delamination growth may cease to continue along the original interlaminar plane, and instead may shift to a neighboring interlaminar plane. This is because when the delamination growth shifts to an inner interlaminar plane, more strain energy may be released for each unit of increase in the area of delamination.

In this section, a one-dimensional stepped-layer model (Fig. 3) is proposed for the analysis of a surface delamination that has shifted from one interlaminar plane to an inner plane. As in the previous analysis, the laminate is considered as a homogeneous orthotropic body, with the three orthotropic axes parallel to the coordinate axes.

The left segment (length a, thickness h_1) and the right segment (length b, thickness h_2) transmit the same axial force P per unit length in the z-direction. The differential equations governing the transverse deflections still have the form of Eq. (3.5). However, the parameters λ^2 and μ^2 are now defined by

$$\lambda^2 = P/K_1 = \frac{12(1-\nu_{13}\nu_{31})\ P}{E_1 h_1^3}, \qquad (4.1)$$

$$\mu^2 = P/K_2 = \frac{12(1-\nu_{13}\nu_{31})\ P}{E_2 h_2^3},$$

Whereas the end conditions (3.3) remain valid, one of the continuity condition at the junction $\xi = a$ ($\eta = b$) is changed:

$$v(a) = w(b), \quad v'(a) = -w'(b),$$

$$v''(a) + \lambda^2 \frac{h_2 - h_1}{2} = \frac{\lambda^2}{\mu^2} w''(b), \tag{4.2}$$

$$v'''(a) = -\frac{\lambda^2}{\mu^2} w'''(b).$$

The continuity condition for the bending moment includes a term proportional to $(h_2 - h_1)/2$ because the middle planes of the two segments are not the same, so that the axial compressive force P produces a discontinuity of the bending moment at the junction of the segments. The presence of the eccentricity has the effect that the stepped layer will deflect laterally under any axial compressive load P, no matter how small. As deflection increases (due to increased relative approach of the two ends, i.e., due to increased ε_0), the axial load P also increases but always remains smaller than a limiting value which is determined by the lowest root of the characteristic equation. This limiting value of P will never be reached.

Let

$$x = \lambda a, \; y = \mu b, \quad \beta = \frac{\mu}{\lambda} = \left(\frac{h_1}{h_2}\right)^{3/2}. \tag{4.3}$$

Then the upper limit of P is the lowest root of the equation

$$\Delta = 0,$$

where

$$\Delta \equiv 2\beta\,(1-\cos x \cos y) + (1+\beta^2) \sin x \sin y - (\beta x + y)(\sin x \cos y + \beta \cos x \sin y). \tag{4.4}$$

Since the upper limit of P is never attained, Δ as defined by Eq. (4.4) never vanishes regardless of the value of the compressive strain ϵ_0 in the main body of the laminate, so long as the Euler buckling theory remains valid for the stepped layer.

Equation (3.5) together with the end conditions (3.3) and the continuity conditions (4.2) possess the following solutions

$$v(\xi) = C_1(\sin \lambda\xi - \lambda\xi) - C_2(1 - \cos\lambda\xi), \quad 0 \le \xi \le a,$$
$$w(\eta) = D_1(\sin \mu\eta - \mu\eta) - D_2(1 - \cos\mu\eta), \quad 0 \le \xi \le b, \tag{4.5}$$

where the coefficients C_1, C_2, D_1 and D_2 depend on the axial load P according to the following expressions

$$\frac{2\Delta}{h_2 - h_1} D_1 = -(\sin x + \beta \sin y) + \sin x \cos y + \beta \cos x \sin y,$$

$$\frac{2\Delta}{h_2 - h_1} D_2 = (\beta x + y) \sin x + \beta(\cos x - \cos y - 1) - \sin x \sin y + \beta \cos x \cos$$

$$\frac{2\Delta}{h_2 - h_1} C_1 = -\beta \frac{2\Delta}{h_2 - h_1} D_1 ,$$

$$\frac{2\Delta}{h_2 - h_1} C_2 = \beta \{-(\beta x + y) \sin y + \cos x - \cos y + 1 - \beta \sin x \sin y - \cos x \cos$$

(4.6)

4.2 Determination of the axial load P

The axial load P is always smaller than the lowest root of the characteristic equation $\Delta = 0$. The value of P depends on the compressive strain ϵ_0. It can be determined by considering the change of the total arc length of the layer from its initial state to the deformed state. The method is identical to that of Section 3.3. However, whereas in the previous case of a merged delamination the axial load is simply the lowest root of the characteristic equation and the method of Section 3.3 determines the amplitude of deflection, in the present case of a stepped delamination the amplitude is a known function of the unknown axial load, and it is this unknown axial load that is to be solved by the method of Section 3.3.

The relation between P and ϵ_0 is given by the equality

$$\begin{aligned}
&\left(1-\nu_{13}\nu_{31}\right)\left\{\epsilon_0\ (a+b) - \frac{P}{E_1}\left(\frac{a}{h_1}+\frac{b}{h_2}\right)\right\} \\
&= \frac{1}{2}\int_0^a \left\{v'(\xi)\right\}^2 d\xi + \frac{1}{2}\int_0^b \left\{w'(\eta)\right\}^2 d\eta \\
&= \frac{\lambda}{2}\left[\left(\frac{3}{2}x - 2\sin x + \frac{\sin 2x}{4}\right)C_1^2 + \left(x - \frac{\sin 2x}{2}\right)\frac{C_2^2}{2} + (1-\cos x)^2\, C_1C_2\right] \\
&+ \frac{\mu}{2}\left[\left(\frac{3}{2}y - 2\sin y + \frac{\sin 2y}{4}\right)D_1^2 + \left(y - \frac{\sin 2y}{2}\right)\frac{D_2^2}{2} + (1-\cos y)^2\, D_1D_2\right],
\end{aligned} \tag{4.7}$$

where λ, μ, β, x, y, C_1, C_2, D_1 and D_2 are defined in terms of the axial load P and the geometrical and material constants by Eqs. (4.1), (4.3) and (4.6). We note that Eq. (4.7) yields an explicit expression for ϵ_0 in terms of P and the geometrical and material constants. However, if ϵ_0 is specified, the determination of the axial load P involves numerical solution of a complicated algebraic equation.

When the axial load P is solved from Eq. (4.7) and the coefficients C_1, C_2, D_1 and D_2 are evaluated by means of the expressions (4.6), Eq. (4.5) delivers the lateral deflection of the stepped layer. The reaction forces and moments at the end supports can be easily obtained. We have,

$$M_A = -PC_2, \qquad Q_A = \lambda PC_1 \text{ at } \xi = 0,$$
$$M_B = -PD_2, \qquad Q_B = \lambda PC_1 \text{ at } \eta = 0. \tag{4.8}$$

Part 2: Calculation of the Strain Energy Release Rate and Its Mode I and Mode II Components

5. The method of differentiation and the method of J-integral

In this part of the report, the strain energy release rates associated with the growth of delamination are calculatee for the various types of analytical models introduced in Part I. For the thin film model, Chai et al. obtained the strain energy release rate by differentiating the total strain energy of the system with respect to the length of delamination. Equation (2.10) of this report gives the result for an orthotropic laminate. The formula is only approximate because the underlying theory assumes no rotation of the two ends of the delaminated layer and because it ignores the bending deformation of the main body of the laminate.

The method of differentiation may be applied to the merged-delamination model and the stepped-layer model. However, when the delamination grows in these models under a given compressive strain ϵ_0 in the laminate, the axial load P carried by the delaminated layer is a complicated function of the length b. This functional relation is defined implicitly by the characteristic equation (in the case of the merged-delamination model) or by the relation between the deformed and undeformed arc lengths of the delaminated layer (in the case of the stepped-layer model). Thus, when differentiating the total strain energy of the system with respect to the length b, the method of implicit differentiation must be used. For the total strain energy depends on b as well as on P and the latter is an implicit function of b. Although this method does yield closed-form analytical expressions of the strain energy release rates, these expressions are very complicated. On the other hand, the method works well when it is implemented with computer programs to evaluate the strain energy release rate at each stage of delamination growth. The results of computation show that, with appropriate combinations of the existing

delamination geometry and laminate loading, coalescence of multiple delaminations or bifurcation from constant-thickness delamination to stepped-layer delamination does generate a larger strain energy release rate (Fig. 4). Therefore, these results confirm the possibility of new modes of damage growth which otherwise would have been arrested.

A simpler and more efficient method to obtain analytic expression of the energy release rates associated with delamination growth is the evaluation of a path-independent integral (the J-integral method). This task is accomplished in the following section. We obtain a simple expression of the strain energy release rate (Eq. (6.13)) in terms of the bending moment at the moving end of the delamination and the difference between the laminate strain ϵ_0 and the axial strain of the delaminated layer (averaged over a cross-section close to the moving end). For the Chai-Babcock-Knauss thin film model, this expression reduces to Eq. (2.10). Consequently, once the buckling problem associated with a merged delamination or a stepped-layer model has been solved following the method of Sections 3 and 4, the strain energy release rate can be immediately obtained.

6. Calculation of the energy release rate by the method of J-integral

In order to calculate the strain energy release rates associated with the various types of one-dimensional delamination models by the method of J-integral, we consider the free body shown in Fig. 5. This free body is obtained by removing the delaminated layer from the main body of the laminate. The figure also shows the actual loading on the free body. In Fig. 6, we show two component loading systems whose combination is equivalent to the actual loading of Fig. 5. Notice that the far-field compressive stress $E_1\epsilon_0$ is present only in Fig. 6a but not in Fig. 6b.

Let $\hat{\sigma}_{ij}^{(0)}$ and $\hat{\sigma}_{ij}$ denote the stress fields in the free body associated with the component loading systems of Fig. 6a and Fig. 6b, respectively. Then $\sigma_{ij}^{(0)}$ is a constant stress field:

$$\sigma_x^{(0)} = -E_1\epsilon_0, \quad \sigma_y^{(0)} = \tau_{xy}^{(0)} = 0. \tag{6.1}$$

Equations (2.2) and (6.1) imply the following expressions for the actual stress and strain in the main body of the laminate:

$$\epsilon_z = \nu_{13}\epsilon_0$$

$$\sigma_x = -E_1\epsilon_0 + \hat{\sigma}_x, \quad \sigma_y = \hat{\sigma}_y, \quad \tau_{xy} = \hat{\tau}_{xy}. \tag{6.2}$$

Using the stress-strain relation of an orthotropic material, we obtain

$$\sigma_z = \nu_{13}\frac{E_3}{E_1}\hat{\sigma}_x + \nu_{23}\frac{E_3}{E_2}\hat{\sigma}_y,$$

$$\epsilon_x = -\epsilon_0 + \frac{1-\nu_{13}\nu_{31}}{E_1}\hat{\sigma}_x - \frac{\nu_{31}\nu_{23}+\nu_{21}}{E_2}\hat{\sigma}_y, \tag{6.3}$$

$$\epsilon_y = \nu_{12}\epsilon_0 + \frac{1-\nu_{23}\nu_{32}}{E_2}\hat{\sigma}_y - \frac{\nu_{32}\nu_{13}+\nu_{12}}{E_1}\hat{\sigma}_x.$$

The path-independent integral

$$J = \int_\Gamma dJ = \int_\Gamma U\, dy - \sigma_{ij}\, n_j \frac{\partial u_i}{\partial x}\, ds, \tag{6.4}$$

may be evaluated along any counter-clockwise contour which circles around the moving end of the delamination. The particular contour we shall use is shown in Fig. 7. This contour starts from a boundary point A of the main body of the laminate near the moving end of the delamination and goes vertically downward to the bottom of the laminate. The upward vertical path CE is assumed to be at a large distance away from the delamination so that the stress field on CE is described by Eq. (6.1).

In the integral (6.4), s denotes the arc length along the contour and n_j is the outward normal vector. Along the horizontal paths BC and EF, dJ vanishes because dy = 0 and $\sigma_{ij} n_j = 0$. Along the vertical path AB, we have

$$dJ = \frac{1}{2}\left\{\sigma_x \varepsilon_x - \sigma_y \varepsilon_y - \sigma_z \varepsilon_z + \tau_{xy}\left(\frac{\partial v}{\partial x} - \frac{\partial u}{\partial y}\right)\right\} ds. \tag{6.5}$$

From Eqs. (6.2) and (6.3) we obtain

$$\sigma_x \varepsilon_x = E_1 \varepsilon_0^2 - (2 - \nu_{13}\nu_{31})\varepsilon_0 \hat{\sigma}_x + (\nu_{31}\nu_{23} + \nu_{21})\frac{E_1}{E_2}\varepsilon_0 \hat{\sigma}_y + \frac{1 - \nu_{13}\nu_{31}}{E_1}\hat{\sigma}_x^2 - \frac{\nu_{31}\nu_{23} + \nu_{21}}{E_2}\hat{\sigma}_x \hat{\sigma}_y,$$

$$-\sigma_y \varepsilon_y = -\nu_{12}\varepsilon_0 \hat{\sigma}_y - \frac{1 - \nu_{23}\nu_{32}}{E_2}\hat{\sigma}_y^2 + \frac{\nu_{32}\nu_{13} + \nu_{12}}{E_1}\hat{\sigma}_x \hat{\sigma}_y$$

$$-\sigma_z \varepsilon_z = -\nu_{13}\nu_{31}\varepsilon_0 \hat{\sigma}_x - \nu_{13}\nu_{23}\frac{E_3}{E_2}\varepsilon_0 \hat{\sigma}_y.$$

Using the well-known identities $\nu_{21} E_1 = \nu_{12} E_2$, etc., we find that

$$\frac{1}{2}\left(\sigma_x \varepsilon_x - \sigma_y \varepsilon_y - \sigma_z \varepsilon_z\right) = \frac{E_1 \varepsilon_0^2}{2} - \varepsilon_0 \hat{\sigma}_x + \frac{1 - \nu_{13}\nu_{31}}{2E_1} \sigma_x^2 - \frac{1 - \nu_{23}\nu_{32}}{2E_2} \hat{\sigma}_y^2. \tag{6.6}$$

Along the vertical path CE, dJ reduces to $-\frac{1}{2} E_1 \varepsilon_o^2 \, ds$. This result together with (6.5) and (6.6) yield

$$\int_{ABCD} dJ = \int_A^B dJ + \int_C^D dJ$$

$$= -\varepsilon_0 \int_A^B \hat{\sigma}_x \, ds + \int_A^B \frac{1 - \nu_{13}\nu_{31}}{2E_1} \sigma_x^2 \, ds - \int_A^B \frac{1 - \nu_{23}\nu_{32}}{2E_2} \hat{\sigma}_y^2 \, ds$$

$$+ \int_A^B \hat{\tau}_{xy} \left(\frac{\partial v}{\partial x} - \frac{\partial u}{\partial y}\right) ds. \tag{6.7}$$

The equilibrium of the free body enclosed by the contour Γ requires that

$$-\int_A^B \sigma_x \, ds - \int_C^E E_1 \varepsilon_0 \, ds + P = 0,$$

or

$$\int_A^B \hat{\sigma}_x \, ds = -\int_D^E E_1 \varepsilon_0 \, ds + P = -\left(E_1 \varepsilon_o h_2 - P\right). \tag{6.8}$$

Hence, along the path AB we have

$$\hat{\sigma}_x = -\frac{E_1 \varepsilon_0 h_2 - P}{H} + \frac{M_{AB}\left(S - \frac{H}{2}\right)}{E_1 H^3/12} \tag{6.9}$$

where H is thickness of the laminate and

$$M_{AB} = \left(E_1 \varepsilon_0 h_2 - P\right) \frac{H + h_2}{2} - M_B + Q(a + b)/2$$

is the bending moment in the cross-section AB. Substituting (6.8) and (6.9) into (6.7), we find that the second term on the right hand side of Eq. (6.7) is of the order h_2/H compared to the first term. The third and fourth terms are expected to be not greater than the second terms, according to the classical beam theory. Consequently, by neglecting terms of order $(E\,\epsilon_0^2 h_2)\,h_2/H$ in the strain energy release rate, we obtain the following approximation

$$\int_{ABCD} dJ = \left(E_1\,\epsilon_0\,h_2 - P\right)\epsilon_0. \tag{6.10}$$

It remains to calculate the integral $\int dJ$ along the path FG (a cross-section of the delaminated layer close to the moving end of the delamination). Let η denote the vertical coordinate from the middle plane of the layer. Then, on the path FG

$$\sigma_x = -\frac{P}{h_2} + \frac{12\,M_B\eta}{h_2^3}, \quad \tau_{xy} = -\frac{6Q}{h_2}\left\{\frac{1}{4} - \left(\frac{\eta}{h_2}\right)^2\right\},$$

$$\sigma_y = 0, \quad \sigma_z = \nu(E_1\,\epsilon_0 + \sigma_x), \quad \epsilon_x = \left(1 - \nu_{13}\nu_{31}\right)\frac{\sigma_x}{E_1} - \nu_{13}\nu_{31}\epsilon_0,$$

$$\frac{\partial v}{\partial x} = 0, \quad \frac{\partial u}{\partial y} = \frac{\tau_{xy}}{G_{13}}.$$

These expressions yield the following result:

$$\int_F^G dJ = \frac{1}{2}\int_F^G \left\{\sigma_x\,\epsilon_x - \sigma_z\epsilon_x + \tau_{xy}\left(\frac{\partial v}{\partial x} - \frac{\partial u}{\partial y}\right)\right\} ds$$

$$= -\frac{1}{2}E_1\nu_{13}\nu_{31}\epsilon_0^2\,h_2 + \nu_{13}\nu_{31}\,\epsilon_0\,P + \frac{1 - \nu_{13}\nu_{31}}{2E_1}\,\frac{P^2}{h_2}$$

$$+ \frac{1 - \nu_{13}\nu_{31}}{2E_1}\,\frac{12M_B^2}{h_2^3} - \frac{3}{5}\,\frac{Q^2}{G_{13}\,h_2}. \tag{6.11}$$

Taking the sum of Eqs. (6.10), (6.11) and

$$\int_D^E dJ = -\frac{1}{2} E_1 \epsilon_o^2 h_2,$$

we obtain

$$\int_\Gamma dJ = \int_{ABCD} dJ + \int_D^E dJ + \int_F^G dJ$$

$$= \frac{1 - \nu_{13}\nu_{31}}{2 E_1 h_2} \left\{ \left(E_1 \epsilon_o h_2 - P \right)^2 + 12 \left(\frac{M_B}{h_2} \right)^2 \right\} - \frac{3}{5} \frac{Q^2}{G_{13} h_2} . \qquad (6.12)$$

However, the equilibrium of the delaminated layer requires that

$$(a + b)Q + M_B - M_A = 0.$$

Therefore, on the right hand side of Eq. (6.12) the term involving Q^2 is of the order $\left\{ h_2/(a + b) \right\}^2$ compared to the term involving M^2. The smaller term should be ignored since we have already neglected terms of order $(E \epsilon_0^2 h_2) h_2/H$ in the approximate result (6.10). Thus Eq. (6.12) yields the strain energy release rate

$$G = \int_\Gamma dJ = \frac{1 - \nu_{13}\nu_{31}}{2 E_1 h_2} \left\{ \left(E_1 \epsilon_0 h_2 - P \right)^2 + 12 \left(\frac{M_B}{h_2} \right)^2 \right\}. \qquad (6.13)$$

This result is applicable to all types of one-dimensional delamination models considered in Part 1 of this report. The buckling load P and the bending moment M_B at the moving end of the delamination should be solved according to the methods of Sections 3 and 4.

For the Chai-Babcock-Knauss thin-film model, we have $h_2 = h$ and Eqs. (2.8) and (2.9) yield

$$P = h E_1 \epsilon_{cr}, \quad M_B^2 = \left(\frac{KA}{2} \right)^2 \left(\frac{2\Gamma}{\ell} \right)^4 = \frac{1}{3} E_1^2 (\epsilon_0 - \epsilon_{cr}) \epsilon_{cr}.$$

Substituting these results into Eq. (6.13), we obtain the same expression (2.10) which was derived earlier by the method of differentiation.

7. Separation into the mode I and mode II components -- a discussion of Whitcomb's approximate theory

The critical value of the strain energy release rate associated with the initiation or continuation of fracture at the tip of an existing delamination generally depends on the relative significance of the symmetric and anti-symmetric modes of fracture. Therefore, in order to obtain a measure of the residual strength of a laminate containing an existing surface delamination, it is important to separate the strain energy release rate into its mode I and mode II components.

Partition of the strain energy release rate was not considered by Chai et al. in their analysis of one-dimensional models of delamination growth. However, in the case of a graphite/epoxy layer of small and uniform thickness bonded to a relatively thick aluminum plate, where the bonding contains an artificially introduced discontinuity strip of width ℓ, Whitcomb [4] has calculated the mode I and mode II energy release rates corresponding to various combinations of delamination thickness, length, and axial compression. His calculation was based on finite-element computation of the crack closure integral, and non-linear strain-displacement relations were used in the modelling of the buckled layer.

In a subsequent report [3], Whitcomb developed an approximate analysis to obtain analytical expressions of the mode I and mode II energy release rates. The expressions involved two undetermined constant coefficients which could be evaluated by a small number of finite-element computations.

The reasoning in Whitcomb's approximate theory was guided by the well-known formula for the energy release rate of a double-cantilever beam. In analogy with that situation, Whitcomb assumed that the mode I energy release

rate of delamination is given by an expression of the form

$$G_I = C_2 \frac{M^2}{K}, \tag{7.1}$$

where K is the bending stiffness per unit width of the delaminated layer, C_2 is an undetermined coefficient, and M is the algebraic sum of the bending moment M_B at the moving end of the delamination, which tends to open the crack, and a "restoring moment" M_C due to the difference between the axial forces in the delaminated and the bonded segments of the thin film, which tends to close the crack:

$$M = M_B + M_C = M_B - C_1 \frac{h}{2}(E \varepsilon_0 h - P). \tag{7.2}$$

Substitution of Eq. (7.2) into (7.1) yields the expression

$$G_I = \frac{C_2}{K}\left\{M_B - C_1 \frac{h}{2}(E \varepsilon_0 h - P)\right\}^2, \tag{7.3}$$

where C_1 and C_2 are undetermined coefficients.

In Whitcomb's approximate theory, the expression (7.1) for the mode I energy release rate in terms of an effective peeling moment M is an a priori assumption rather than a derived result from more general principles. Although this expression is suggested by the known result for a double cantilever beam, there remains the question as to whether a close analogy can be truly established (by introducing an effective restoring moment) between the phenomena of delamination growth involving mode II behavior and the fracture of a symmetric double cantilever in which the mode II behavior is entirely absent. Hence the intuitively appealing assumption behind Eqs. (7.1) and (7.3) requires further justification on theoretical grounds, and such a justification is given in the following section of this report. A similar question arises

when Eq. (7.1) or (7.3) is used in conjunction with Eq. (6.13) to obtain an expression for $G_{II} = G - G_I$. Although an analytical expression for G_{II} was not attempted in Whitcomb's work, it will be given subsequently in this report.

Within Whitcomb's approximate theory, the ultimate justification of the assumption underlying Eq. (7.1) is the success and effectiveness of that equation in generating results which agree well with the results of established and more refined methods. Whitcomb found that good agreement could be obtained with the results of finite-element analysis if the delaminated layer was sufficiently thin, that the coefficients C_1 and C_2 were independent of the delamination length and laminate loading, and finally that C_1 was also independent of the thickness of delamination. Again, these attributes of the coefficients were empirical conclusions inductively drawn from the results of extensive computation, rather than theoretical conclusions deduced from general principles. Hence, if the validity of Eq. (7.3) is to be extended to more general cases such as the merged-delamination model and the stepped-layer model, more extensive and elaborate finite element analysis would be required to confirm the prediction. However, this task can be avoided because separate expressions of G_I and G_{II} can be derived on the basis of certain invariance relations under dimensional rescaling, as will be shown in the next section.

8. Partition of the energy release rate - a theory based on dimensional analysis

8.1 The stress intensity facorts

In the present section, we use dimensional analysis to study the functional forms of the mode I and mode II stress intensity factors associated with a buckled delamination. The functional forms of the mode I and mode II energy release rates are then obtained by using the well-known relations between these quantities and the corresponding stress intensity factors, and furthermore by using Eq. (6.13) which represents the combined energy release rate. This theory of partitioning the energy release rate is based on the invariance of the stress field near the crack tip under similarity transformations and it is applicable to all one-dimensional models of delamination including the merged-lamination model and the stepped-layer model. As in the previous analysis, the ratio of the thickness of the layer to that of the laminate, h/H, is assumed to be small, so that terms of order $E\,\epsilon_0^2 h(h/H)$ and higher are neglegible in the expressions of the strain energy release rates.

Our analysis yields an expression for the mode I energy release rate which is formally identical to Eq. (7.3). It is shown that both coefficients C_1 and C_2 are independent of the loading on the laminate and of the geometry of delamination, and furthermore that one coefficient determines the other (the relation between C_1 and C_2 depends on the elastic moduli of the orthotropic material). Thus for the case of constant-thickness delamination, our theory yields a formula for G_I which is more special than Whitcomb's approximate theory. This is because our theory ignores the bending deformation of the main body of the laminate, in agreement with the assumption of the thin-film model.

Whitcomb's approximate theory did not propose a formula for the mode II energy release rate, although for the thin film model such a formula could be

obtained by subtracting the mode I energy release rate from Eq. (2.10). On the other hand, the formula for G_{II} derived in the following analysis, when applied to the film model, does agree with the trends and behavior observed by Whitcomb on the basis of the results of finite element analysis. In general, the value of G_{II} is much larger than that of G_I during the growth of delamination.

Our formulae for G_I and G_{II} contain a single undetermined parameter which depends only on the elastic moduli of the material and does not depend on the thickness or the length of the delaminated layer nor on the axial loading in the laminate. This undetermined parameter may be evaluated by executing a finite-element calculation or by performing an experiment.

In Fig. 8, we show the force and moment system which produces the stress concentration at the tip of the delamination. This system includes a clockwise moment M, a leftward horizontal force $E_1 \varepsilon_o h - P$, and a vertical shearing force Q which is small compared to the horizontal force.

Let us first consider the effect of the horizontal force $E_1 \varepsilon_o h - P$ (see Fig. 9a). This force produces a normal stress $\sigma = \sigma_y$ and a shearing stress $\tau = \tau_{xy}$ ahead of the crack tip. Within a neighborhood of the tip, these stresses are asympotically proportional to $r^{-\frac{1}{2}}$, where r is the distance from the crack tip. Since the material is linear, the stresses are also proportional to the horizontal force $E_1 \varepsilon_0 h - P$.

Hence

$$\sigma(r; h) = \frac{f(h)}{r^{\frac{1}{2}}} (E_1 \varepsilon_0 - P), \tag{8.1}$$

where the proportionality factor f depends on the layer thickness h as well as on the elastic moduli. A similar formula holds for the shearing stress τ.

We next consider a delamination of thickness αh in a laminate of the same

material subjected to a leftward horizontal force $\alpha(E\,\epsilon_0\,h - P)$, as shown in Fig. 9b. The normal stress for this case is given by

$$\sigma(r;\,\alpha h) = \frac{f(\alpha h)}{r^{\frac{1}{2}}}\;\alpha(E_1\,\epsilon_0\,h - P).$$

Now the latter case is related to the former case by a change of the length scale if the thickness of the laminate is much larger than that of the layer; the boundary tractions and the boundary strains in the two cases are the same (stress $\sigma_x = -P/h$ from the delaminated layer and strain $\epsilon_x = -\epsilon_0$ in the remote region of the laminate). Therefore, the stress fields $\sigma(.;\,h)$ and $\sigma(.\,;\,\alpha h)$ must also be related by merely a change of the length scale:

$$\sigma(r\,;\,h) = \sigma(\alpha r;\,\alpha h). \tag{8.2}$$

From the last three equations we obtain

$$\frac{f(h)}{r^{\frac{1}{2}}}\left(E_1\,\epsilon_0\,h - P\right) = \frac{f(\alpha h)}{(\alpha r)^{\frac{1}{2}}}\,\alpha\left(E_1\,\epsilon_0\,h - P\right),$$

or,

$$f(\alpha h) = \frac{f(h)}{\alpha^{\frac{1}{2}}}\ .$$

Assuming f is a differentiable function of its argument, we obtain by differentiating the last equation with respect to α:

$$h\,f'\,(\alpha h) = -\frac{f(h)}{2\alpha^{3/2}}\ .$$

Setting $\alpha = 1$, we have

$$\frac{f'(h)}{f(h)} = -\frac{h}{2}\ .$$

Hence

$$f(h) = \frac{f_0}{h^{\frac{1}{2}}}\ ,$$

where f_0 depends only on the elastic moduli of the material. Equation (8.1) now reduces to

$$\sigma(r;\ h) = \frac{f_0}{(hr)^{\frac{1}{2}}}(E_1\ \varepsilon_0\ h - P). \tag{8.3}$$

A similar expression holds for the shearing stress τ:

$$\tau(r;\ h) = \frac{f_1}{(hr)^{\frac{1}{2}}}(E_1\ \varepsilon_0\ h - P), \tag{8.4}$$

where the factor f_1 also depends on the material moduli only.

The applied moment M also produces stress concentration ahead of the crack tip. Let the near-field normal stress due to the moment M be represented by

$$\sigma(r;\ h) = \frac{g(h)}{r^{\frac{1}{2}}}\ M\ . \tag{8.5}$$

Then, a rescaled problem is obtained if the thickness of the delamination is changed from h to αh and the applied moment is changed from M to $\alpha^2 M$. Here the far-field strain of the laminate is taken to be zero in the original and in the rescaled problem. The relation (8.2) now yields

$$\frac{g(h)}{r^{\frac{1}{2}}}\ M = \frac{g(\alpha h)}{(r\alpha)^{\frac{1}{2}}}\ \alpha^2 M.$$

Following a line of reasoning similar to that leading to the expression (8.3), we obtain

$$\sigma(r;\ h) = \frac{g_0}{(h^3 r)^{\frac{1}{2}}}\ M.$$

Finally, the vertical force Q produces near-field stress singularities of the form (8.3) and (8.4), except that $E_1\varepsilon_0 h - P$ is replaced by Q. Combining the effects of the moment M and of the horizontal and vertical forces, we obtain the mode I and mode II stress intensity factors

$$K_I = a_1 \frac{E_1 \varepsilon_0 h - P}{h^{\frac{1}{2}}} + a_2 \frac{M}{h^{3/2}} + a_3 \frac{Q}{h^{\frac{1}{2}}},$$

$$K_{II} = b_1 \frac{E_1 \varepsilon_0 h - P}{h^{\frac{1}{2}}} + b_2 \frac{M}{h^{3/2}} + b_3 \frac{Q}{h^{\frac{1}{2}}}, \tag{8.6}$$

where the coefficients a_i and b_i ($i = 1, 2, 3$) depend only on the elastic moduli of the material but not on the thickness of the delamination nor on the loading.

8.2 The energy release rates

In the case of an orthotropic material, the mode I and mode II energy release rates are related to the corresponding stress intensity factors according to [5]

$$G_I = \frac{K_I^2}{E_1} \gamma^2 \delta, \quad G_{II} = \frac{K_{II}^2}{E_1} \delta, \tag{8.7}$$

where γ and δ are dimensionles constant given by

$$\gamma = \left(\frac{E_1}{E_2}\right)^{\frac{1}{4}}, \quad \delta = \frac{1}{\sqrt{2}} \left(\gamma^2 + \frac{E_1}{2G_{12}} - \nu_{12}\right)^{\frac{1}{2}} \tag{8.8}$$

Substituting (8.6) into (8.7), we have

$$\frac{E_1 h}{\delta} G_I = \gamma^2 \left\{a_1 (E_1 \varepsilon_0 h - P) + a_2 \frac{M}{h} + a_3 Q\right\}^2,$$

$$\frac{E_1 h}{\delta} G_{II} = \left\{b_1 (E_1 \varepsilon_0 h - P) + b_2 \frac{M}{h} + b_3 Q\right\}^2. \tag{8.9}$$

Taking the sum of the last two expressions, and comparing with Eq. (6.13), we obtain the following identity:

$$\frac{1 - \nu_{13}\nu_{31}}{2\delta} \left\{\left(E_1 \varepsilon_0 h - P\right)^2 + 12 \left(\frac{M}{h}\right)^2\right\}$$

$$= \left\{(\gamma a_1)^2 + b_1^2\right\}\left(E_1 \epsilon_0 h - P\right)^2 + \left\{(\gamma a_2)^2 + b_2^2\right\}\left(\frac{M}{h}\right)^2 + \left\{(\gamma a_2)^2 + b_3^2\right\}Q^2$$

$$+ 2\left(\gamma^2 a_1 a_2 + b_1 b_2\right)\left(E_1 \epsilon_0 h - P\right)\frac{M}{h} + 2\left(\gamma^2 a_2 a_3 + b_2 b_3\right)\frac{M}{h} Q$$

$$+ 2\left(\gamma^2 a_1 a_3 + b_1 b_3\right)\left(E_1 \epsilon_0 h - P\right)Q. \qquad (8.10)$$

We recall that in deriving Eq. (6.13) by the J-integral method, the applied forces and moment could in principle assume arbitrary values independently of one another, and not necessarily those particular combinations representing the boundary values of the delaminated layer. Likewise, Eq. (8.9) is valid for arbitrary combinations of forces and moments. Hence Eq. (8.10) is an identity. Setting $E_1 \epsilon_0 h - P = 0$, $M = 0$ and $Q \neq 0$ in (8.10), we obtain

$$(\gamma a_3)^2 + b_3^2 = 0,$$

or,

$$a_3 = b_3 = 0. \qquad (8.11)$$

We recall that Eq. (6.13) is an approximate result obtained by neglecting terms involving Q which are known to be small compared to the retained terms. The present result of Eq. (8.11) is therefore also valid to the same order of approximation.

Further study of the identity (8.10) yields

$$\begin{aligned} \gamma a_1 &= \varkappa \sin\omega, \quad \gamma a_2 = 12\ \varkappa \cos\omega, \\ b_1 &= \varkappa \cos\omega, \quad b_2 = 12\ \varkappa \sin\omega, \end{aligned} \qquad (8.12)$$

where ω is an undetermined quantity and

$$\varkappa = \left(\frac{1 - \nu_{13}\nu_{31}}{2\delta}\right)^{\frac{1}{2}}.$$

Equation (8.6) now reduces to

$$K_I = \frac{1}{\gamma}\sqrt{\frac{1 - \nu_{13}\nu_{31}}{2\delta}}\left(- \sin\omega \ \frac{E_1 \varepsilon_0 h - P}{h^{\frac{1}{2}}} + \sqrt{12} \ \cos\omega \ \frac{M}{h^{3/2}}\right),$$

$$K_{II} = \sqrt{\frac{1 - \nu_{13}\nu_{31}}{2\delta}}\left(\cos\omega \ \frac{E_1 \varepsilon_0 h - P}{h^{\frac{1}{2}}} + \sqrt{12} \sin\omega \ \frac{M}{h^{3/2}}\right), \tag{8.13}$$

and the corresponding energy release rates are

$$G_I = \frac{1 - \nu_{13}\nu_{31}}{2E_1 \, h^3/12}\left\{\frac{- \sin\omega}{\sqrt{12}}(E_1 \varepsilon_0 h - P)h + \cos\omega \, M\right\}^2,$$

$$G_{II} = \frac{1 - \nu_{13}\nu_{31}}{2E_1 \, h^3/12}\left\{\frac{\cos\omega}{\sqrt{12}}(E_1 \varepsilon_0 h - P)h + \sin\omega \, M\right\}^2 . \tag{8.14}$$

8.3 Comparison with Whitcomb's finite-element solutions

The expression (8.14a) for the mode I energy release rate is of the form of Eq. (7.3). The coefficients C_1 and C_2 are given by:

$$C_1 = \frac{\tan\omega}{\sqrt{3}}, \qquad C_2 = \frac{1 - \nu_{13}\nu_{31}}{2} \cos^2\omega.$$

By eliminating the undetermined quantity ω from these expressions, we find that the coefficients C_1 and C_2 are directly related:

$$\omega = \tan^{-1}(\sqrt{3}\, C_1) = \cos^{-1}\left(\frac{2 C_2}{1 - \nu_{13}\nu_{31}}\right)^{\frac{1}{2}} .$$

The undetermined quantity ω depends only on the elastic moduli of the material. It can be evaluated by executing a finite element analysis or by performing an experiment. The experimental method is described in the subsequent section. ω is expected to be a positive quantity because if the moment M vanishes, the leftward horizontal force $E_1 \varepsilon_0 h - P$ should produce a negative stress intensity factor K_I at the crack tip.

The expressions of G_I and G_{II} given by Eq. (8.14) are valid for any one-dimensional model of delamination, including the merged-delamination model and the stepped-layer model. When these expressions are applied to the Chai-Babcock-Knauss thin film model, we obtain

$$G_I = \tfrac{1}{2}\left(1 - \nu_{13}\,\nu_{31}\right) E_1\, h \left(\epsilon_0 - \epsilon_{cr}\right)\left(-\sqrt{\epsilon_0 - \epsilon_{cr}}\,\sin\omega + 2\sqrt{\epsilon_{cr}}\,\cos\omega\right)^2,$$

$$G_{II} = \tfrac{1}{2}\left(1 - \nu_{13}\,\nu_{31}\right) E_1\, h \left(\epsilon_0 - \epsilon_{cr}\right)\left(\sqrt{\epsilon_0 - \epsilon_{cr}}\,\cos\omega + 2\sqrt{\epsilon_{cr}}\,\sin\omega\right)^2,$$

where

$$\epsilon_{cr} = \frac{P}{E_1 h} = \frac{\pi^2}{3(1 - \nu_{13}\nu_{31})}\left(\frac{h}{\ell}\right)^2. \tag{2.9}$$

If we introduce a non-dimensionalized length of delamination

$$\hat{\ell} = \left(\frac{\epsilon_0}{\epsilon_{cr}}\right)^{\frac{1}{2}} = \sqrt{3(1 - \nu_{13}\nu_{31})}\;\frac{\ell}{\pi h},$$

then Eq. (8.15) becomes

$$G_I = \tfrac{1}{2}\left(1 - \nu_{13}\nu_{31}\right)\cos^2\omega\, E_1\, h\, \epsilon_0^{\,2}\,\hat{\ell}^{-4}\,(\hat{\ell}^2 - 1)\left(2 - \tan\omega\sqrt{\hat{\ell}^2 - 1}\right)^2,$$

$$G_{II} = \tfrac{1}{2}\left(1 - \nu_{13}\nu_{31}\right)\cos^2\omega\, E_1\, h\, \epsilon_0^{\,2}\,\hat{\ell}^{-4}\,(\hat{\ell}^2 - 1)\left(2\tan\omega + \sqrt{\hat{\ell}^2 - 1}\right)^2. \tag{8.16}$$

For a given compressive strain ϵ_0 in the laminate, G_{II} is positive whenever $\hat{\ell} > 1$ whereas G_I at first increases and then decreases to zero when $\hat{\ell} = \sqrt{1 + 4\,\mathrm{ctn}^2\omega}$. The maximum value of G_I is attained when $\hat{\ell}$ equals

$$\ell_1 = \left\{2 - \tan^2\omega\left(\sqrt{\tfrac{1}{4} + \mathrm{ctn}^2\omega} - \tfrac{1}{2}\right)\right\}^{\frac{1}{2}},$$

and

$$(G_I)_{max} = \frac{1 - \nu_{13}\nu_{31}}{2}\, E_1\, h\, \epsilon_0^{\,2}\left\{\cos^2\omega - \sin^2\omega\left(\sqrt{\tfrac{1}{4} + \mathrm{ctn}^2\omega} - \tfrac{1}{2}\right)\right\}.$$

G_{II} attains its maximum value

$$\left(G_{II}\right)_{max} = \frac{1 - \nu_{13}\nu_{31}}{2} E_1 \, h \, \epsilon_0^2 \left\{\sin^2 \omega + \cos^2 \omega \left(\sqrt{\tfrac{1}{4} + \tan^2 \omega} + \tfrac{1}{2}\right)\right\}$$

when $\hat{\ell}$ equals

$$\ell_2 = \left\{2 + \operatorname{ctn}^2 \omega \left(\tfrac{1}{4} + \tan^2 \omega + \tfrac{1}{2}\right)\right\}^{\frac{1}{2}} ,$$

and thereafter G_{II} falls off slowly.

The results of the present analysis is based on the assumption of a homogeneous orthotropic laminate. Whitcomb has evaluated the coefficients C_1 and C_2 of Eq. (7.3) by fitting the formula with the results of finite-element analysis of graphite-epoxy layers bonded to an aluminum plate. His value for the first coefficient, $C_1 = 0.504$, corresponds to

$$\omega = \tan^{-1} \left(\sqrt{3}\, C_1\right) = 41.1^{\circ}.$$

If we ignore the effect of non-homogeneity due to the presence of the aluminum plate, and substitute $\omega = 41.1^{\circ}$ and the elastic moduli of graphite-epoxy into Eq. (8.14a), we obtain

$$C_2 = \left(1 - \nu_{13}\nu_{31}\right) \cos^2 \omega = (1 - 0.21 \times 0.021) \cos^2 41.1^{\circ} = 0.565 .$$

According to Whitcomb, comparison with the results of finite element analysis yields the values 0.330, 0.412 and 0.478, respectively, corresponding to the thickness of delamination 0.762 mm, 0.508 mm and 0.254 mm. Since our theory is based on the assumption of an infinitesimally small ratio of the thickness of delamination to that of the laminate, and since it does not take into account the different elastic moduli of the aluminum plate, the predicted value $C_2 = 0.565$ may be considered as satisfactory in the limit of vanishing thickness of delamination.

For $\omega = 41.1^{\circ}$, the relative magnitudes of G_{II} versus G_I for a thin-film delamination as given by Eq. (8.16) are plotted in Fig. 10. Both curves have the features shown by the results of Whitcomb's finite element analysis (see Fig. 15 of Witcomb's earlier paper [4]). In particular, G_{II} is numerically much larger than G_I and, as delamination progresses under a constant load on the laminate, G_I first increases rapidly to a maximum value and thereafter decreases to zero.

8.4 Experimental determination of the material constant ω.

The undetermined quantity ω is a material constant and therefore it can be evaluated experimentally. Let a laminate with a thin delaminated layer be subjected to a compressive strain ϵ_0, as shown in Fig. 11. The delaminated portion of the thin layer is not subjected to an axial force (i.e., $P = 0$) but is subjected to an applied pure bending moment M. The moment M is adjusted until the normal stress σ_y ahead of the crack tip vanishes. According to Eq. (8.13a), this moment satisfies the equation

$$\tan \omega = \frac{\sqrt{12}\, M}{E_1 \epsilon_0 h^2} \quad . \tag{8.17}$$

Now, if K_I vanishes ahead of the crack, then the near-field stress is purely of the mode II type. The horizontal line ahead of the crack is a line of shearing stress, i.e., a 45° isocline. When this state is achieved by adjusting the applied moment M, the material constant ω can be calculated from Eq. (8.17).

The 45° isocline may be observed with a reflection polariscope by applying photo-elastic coating to the exposed section of the specimen. However transparent lateral restraints should be provided to ensure that the assumption of Eq. (2.2) is satisfied in an approximate sense.

Part 3. Energy Release Rates as the Criteria of Delamination Growth

9. Criteria based on the total energy release rate

The simplest criterion of delamination growth is based on the value of the strain energy release rate without discriminating its components associated with mode I and mode II behavior. Under a static loading, this criterion asserts that the growth of delamination or its arrest depends on whether G, the sum of G_I and G_{II}, is greater or less than a critical value. Under a constant-range cyclic loading, the rate of delamination growth is assumed to be a function of the range and the peak of G. The work of Chai, Babcock and Knauss on one-dimensional models of delamination and its extension to two-dimensional models [6] were essentially based on the criterion of a critical energy release rate in static loading. Furthermore, they assumed that the growth of a two-dimensional elliptical delamination progresses in such a manner as to maximize the energy release rate at each stage of growth.

In the present section, we show that if delamination growth follows a pattern that maximizes the total energy release rate at each stage of growth, then, with appropriate geometry of the delamination and sufficient strain in the laminate, a delamination of uniform thickness will change into a stepped delamination and parallel multiple delaminations will merged into the delamination of a single thick layer, as described in Secs. 3 and 4 of this report.

The energy release rate of a thin-film delamination with a uniform thickness h is, according to Eq. (6.13)

$$G = \frac{1 - \nu_{13}\nu_{31}}{2 E_1 h}\left\{\left(E_1 \epsilon_0 h - P\right)^2 + 12\left(\frac{M}{h}\right)^2\right\}, \tag{9.1}$$

Where P and M may be obtained from Eqs. (2.8) and (2.9) :

$$P = E_1 h \varepsilon_{cr} = E_1 h \frac{\pi^2}{3(1 - \nu_{13}\nu_{31})} \left(\frac{h}{\ell}\right)^2 ,$$
$$M = \frac{E_1 h^2}{\sqrt{3}} \sqrt{\varepsilon_{cr} (\varepsilon_0 - \varepsilon_{cr})}. \tag{9.2}$$

If the uniform-thickness delamination changes to a stepped delamination with $h_1 = h$ and $h_2 = 2h$, then immediately after the change the force P remains the same whereas h and M are replaced by 2h and M + Ph/2, respectively. Hence the new energy release rate is

$$G' = \frac{1 - \nu_{13}\nu_{31}}{4 E_1 h} \left\{\left(2 E_1 \varepsilon_0 h - P\right)^2 + 12\left(\frac{M + Ph/2}{2h}\right)^2\right\}. \tag{9.3}$$

The sudden change in the energy release rate is

$$G' - G = \frac{1 - \nu_{13}\nu_{31}}{2} \left\{\left(\varepsilon_0 - \frac{7}{4}\varepsilon_{cr}\right)^2 + \frac{5}{16}\varepsilon_{cr}^2 + \frac{3}{2}\varepsilon_{cr}^{3/2}\sqrt{\varepsilon_0 - \varepsilon_{cr}}\right\} ,$$

Since this quantity is always positive regardless of the delamination length ℓ, the simple criterion of a critical energy release rate implies that a shift from uniform-thickness delamination to a stepped delamination will occur whenever such an opportunity arises due to the existence of a transverse matrix crack.

Similarly, consider two parallel uniform-thickness delaminations of thickness h and length ℓ. The energy release rate associated with each delamination is given by Eq. (9.1). If the delaminations merge into a single layer of thickness 2h, the energy release rate of the merged delamination immediately after the coalescence is

$$G'' = \frac{1 - \nu_{13}\nu_{31}}{4 E_1 h} \left\{\left(2 E_1 \varepsilon_0 h - 2P\right)^2 + 12\left(\frac{2M}{2h}\right)^2\right\}.$$

The sudden increase in the energy release rate is given by

$$G'' - G = \tfrac{1}{2}\left(1 - \nu_{13}\nu_{31}\right) E_1 h (\varepsilon_0 - \varepsilon_{cr}) (\varepsilon_0 - 3\varepsilon_{cr}).$$

Since

$$\epsilon_{cr} = \frac{\pi^2}{3\left(1 - \nu_{13}\nu_{31}\right)} \left(\frac{h}{\ell}\right)^2 ,$$

the increase $G'' - G$ is positive if the delamination length and axial strain ϵ_0 are sufficiently large so that

$$\ell\sqrt{\epsilon_0} > \pi h \left(1 - \nu_{13}\nu_{31}\right)^{-\frac{1}{2}} .$$

10. Criteria based on the mode II energy release rate

Whitcomb has performed a rather limited number of experiments to investigate the growth rate of delamination under cyclic loading [4]. It is observed that the growth rate decreases as delamination progresses, in close correlation with the change of G_I, and in spite of the much larger magnitude and the continued increase of G_{II}. He therefore suggested that "delamination growth is dominated by G_I, even though G_{II} may be numerically much larger".

In this section, we calculate the sudden changes in G_I that accompany the transition from a uniform-thickness delamination to a stepped delamination or from parallel delaminations to merged delamination. It is found that the jump in G_I accompanying the latter case is always negative whenever the mode I stress intensity factor K_I at the stage of transition is positive. Therefore, if a growth criterion involving G_I alone is valid, then a transition from parallel delaminations to merged delamination can never occur. The jump in G_I accompanying the transition to a stepped delamination is more complicated and may assume either a positive or a negative value. Hence a growth criterion involving G_I alone implies that as delamination shifts from one interlaminar plane to another plane, it may either shift inward or outward, i.e., h_2 may either be greater or smaller than h_1. This conclusion suggests an experimental method to determine whether a delamination growth criterion

based on G is more realistic than a criterion based on G_I. Let a delamination be introduced near the surface of a laminate and let it branch off into two very short delaminations, one closer and the other farther away from the boundary than the main branch of the delamination. The geometrical parameters may be so selected that when the specimen is subjected to a sufficiently large axial loading, the two growth criteria would yield different conclusions as to whether the delamination growth shifts to the inner branch or the outer branch. The observer phenomenon could be used to reject one criterion and partially support the other criterion.

The mode I energy release rate of a uniform-thickness delamination is given by Eq. (8.14a). When two parallel delaminated layers merge and delamination growth continues along the lower plane, the mode I energy release rate abruptly changes to

$$G_I'' = \frac{1 - \nu_{13}\nu_{31}}{4E_1 h}\left\{-\sin\omega\left(2E_1\epsilon_0 h - 2P\right) + 12\cos\omega\left(\frac{2M}{2h}\right)\right\}^2 .$$

The difference

$$G_I'' - G_I = \frac{3(1 - \nu_{13}\nu_{31})}{4E_1 h}\left\{\sin^2\omega\,(E_1\epsilon_0 h - P)^2 - 12\cos^2\omega\left(\frac{M}{h}\right)^2\right\}$$

$$= \frac{3}{4}(1 - \nu_{13}\nu_{31})\,E_1 h\sin^2\omega\,(\epsilon_0 - \epsilon_{cr})\left\{\epsilon_0 - (1 + 4\,\mathrm{ctn}^2\omega)\epsilon_{cr}\right\} \tag{10.1}$$

is negative in the range of the delamination length corresponding to positive K_I:

$$1 \le \epsilon/\epsilon_{cr} \le 1 + 4\,\mathrm{ctn}^2\omega.$$

Hence, the occurrence of a merged delamination is impossible according to a growth criterion based entirely on the consideration of G_I.

In a transition from a delamination of uniform thickness h to a stepped delamination of new thickness h_2, the mode I energy release rate changes abruptly from G_I of Eq. (8.14a) or (8.16a) to

$$G_I' = \frac{1 - \nu_{13}\nu_{31}}{2E_1 h_2}\left\{-\sin\omega\,(E_1 \epsilon_0 h_2 - P) + \sqrt{12}\cos\omega\left(\frac{M}{h_2} + P\,\frac{h_2 - h_1}{2h_2}\right)\right\}^2.$$

Let

$$\hat{\ell} = \left(\frac{\epsilon_0}{\epsilon_{cr}}\right)^{\frac{1}{2}}, \qquad r = (h_2/h)^{\frac{1}{2}}. \tag{10.2}$$

Then,

$$\frac{G_I' - G_I}{(1 - \nu_{13}\nu_{31})\,E_1 h}$$

$$= \frac{\cos^2\omega}{2\hat{\ell}^4}(r^2 - 1)\left\{\left(\hat{\ell}^2 - \frac{1}{r}\right)\tan\omega - \frac{\sqrt{3}}{r^3}(r - 1) - \frac{2}{r^3}(1 - r + r^2)\sqrt{\hat{\ell}^2 - 1}\right.$$

$$\left.\times\left\{\left(\hat{\ell}^2 + \frac{1}{r}\right)\tan\omega - \frac{\sqrt{3}}{r^3}(r + 1) - \frac{2}{r^3}(1 + r + r^2)\sqrt{\hat{\ell}^2 + 1}\right\},\right.$$

and this may be either positive or negative depending on the particular combination of the values of ω, r and $\hat{\ell}$.

References

[1] Takeda, N., Sierakowski, R.L., Ross, C. A. and Malvern. L.E., "Delamination-crack propagation in ballistically impacted glass/epoxy composite laminates," Exp. Mech., Jan. 1982. 1982, 19-25.

[2] Chai, H., Babcock, C.D. and Knauss, W.G., "One dimensional modelling of failure in laminated plates by delamination buckling," Int. J. Solids Structures, 17, 1069-1083 (1981).

[3] Whitcomb, J.D., "Approximate analysis of postbuckled through-width delaminations", NASA Technical Memorandum TM-83147 (1981).

[4] Whitcomb, J.D., "Finite element analysis of instability related delamination growth," J. Composite Materials, 15, 403-426 (1981).

[5] Sih, G.C. and Liebowitz, H., "Mathematical theories of brittle fracture," in Fracture, vol. II (H. Liebowitz, Ed.) Academic Press, New York, 1968.

[6] Chai, H., Ph.D. Thesis, The Growth of Impact Damage in Compressively Loaded Laminates, California Institute of Technology, Pasadena, California, 1982.

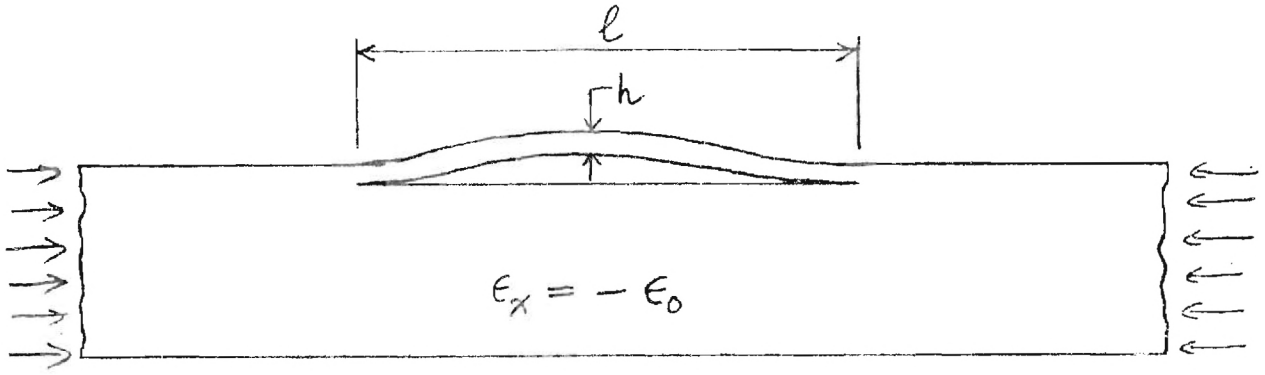

Fig. 1 Buckling of a one-dimensional delaminated layer

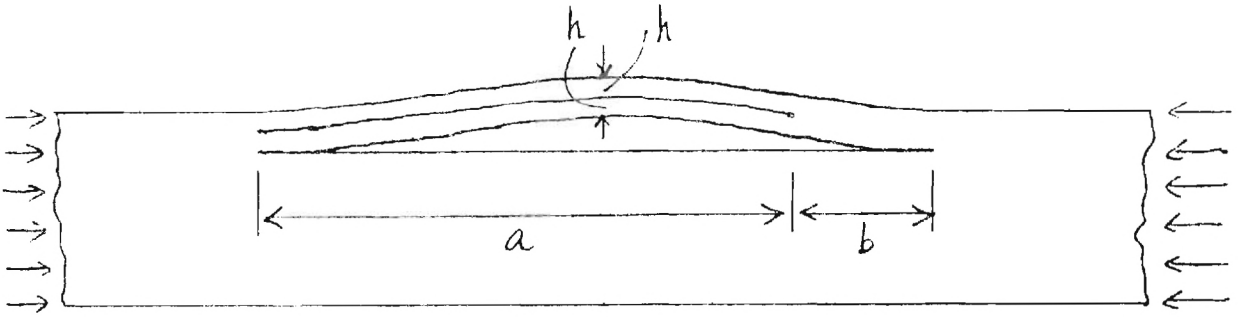

Fig. 2 A merged delamination

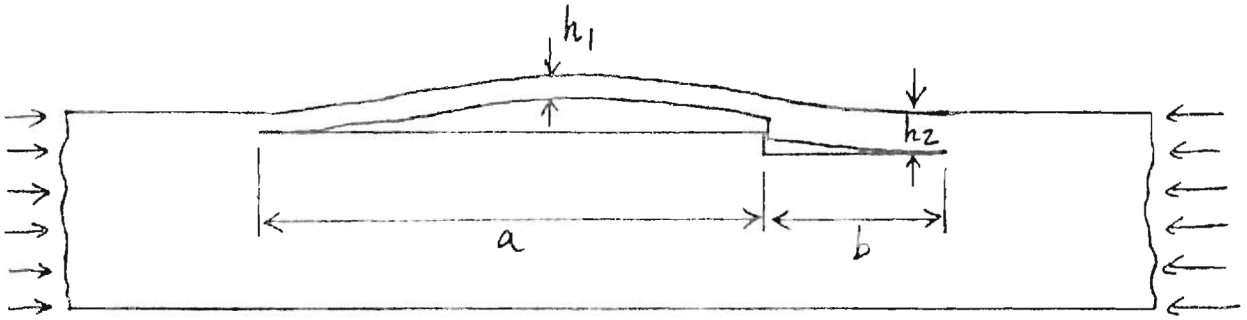

Fig. 3 A stepped-layer delamination

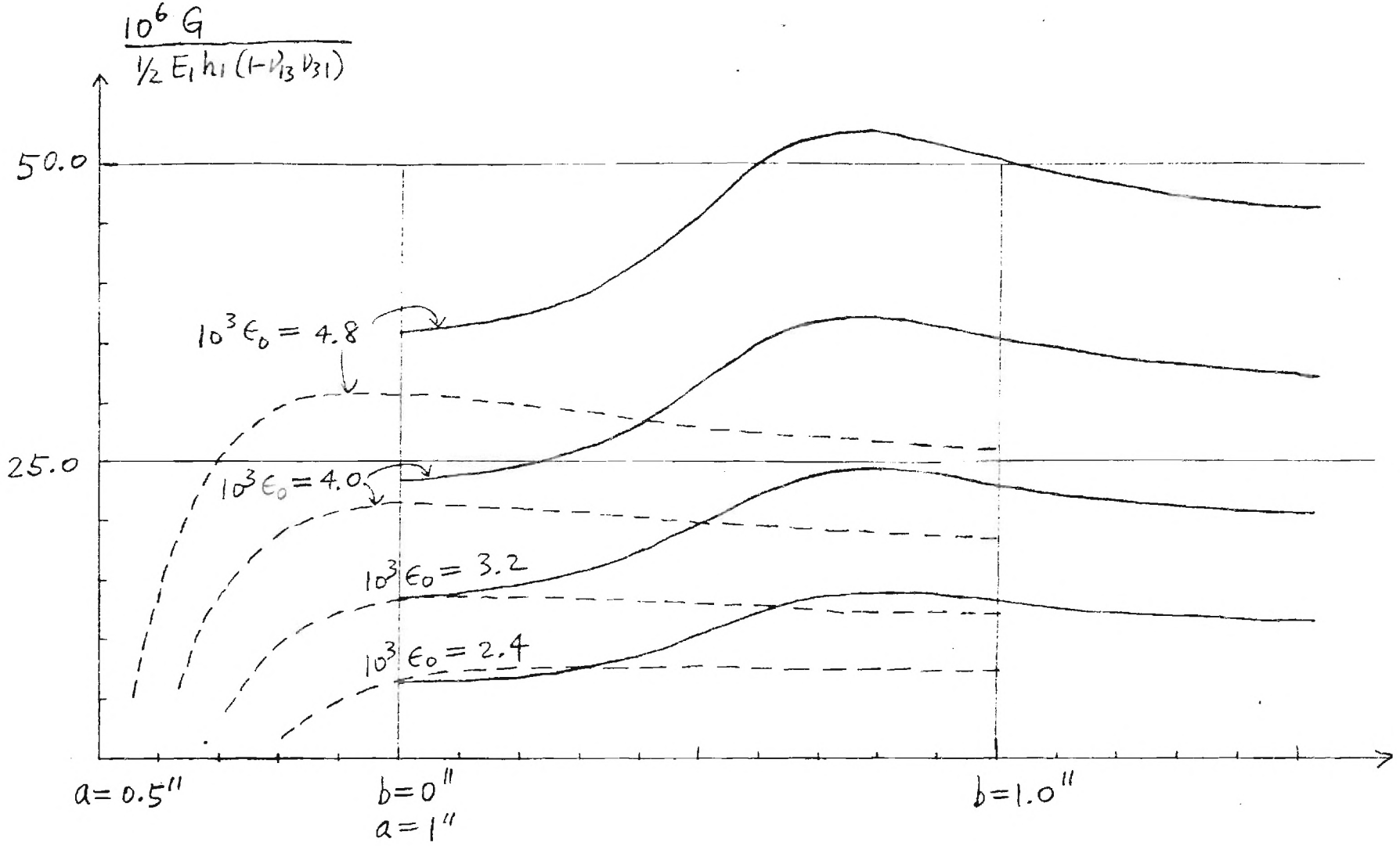

Fig. 4 Energy release rate of a stepped delamination ($h_1 = h_2/2 = 0.02''$, $a = 1''$)

Note: The energy release rates of a uniform-thickness delamination ($h = .02''$) under the same laminate strain are shown by broken curves.

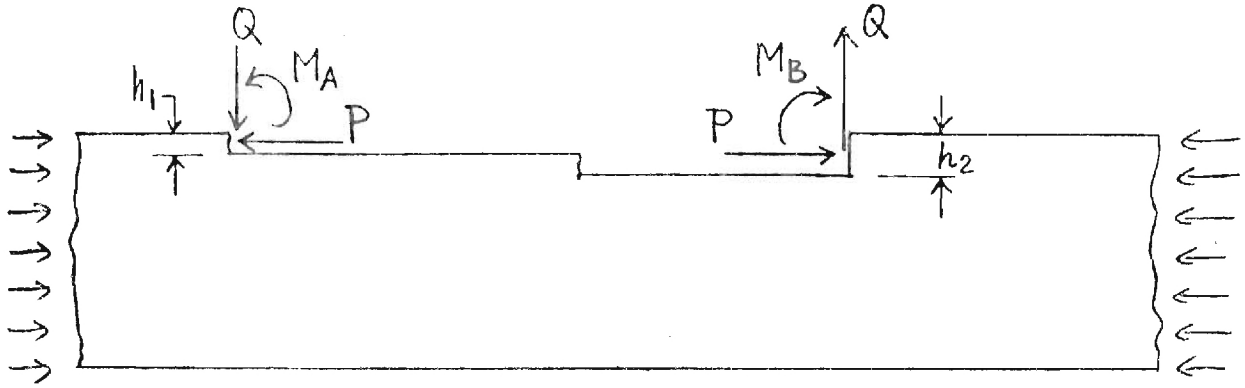

Fig. 5

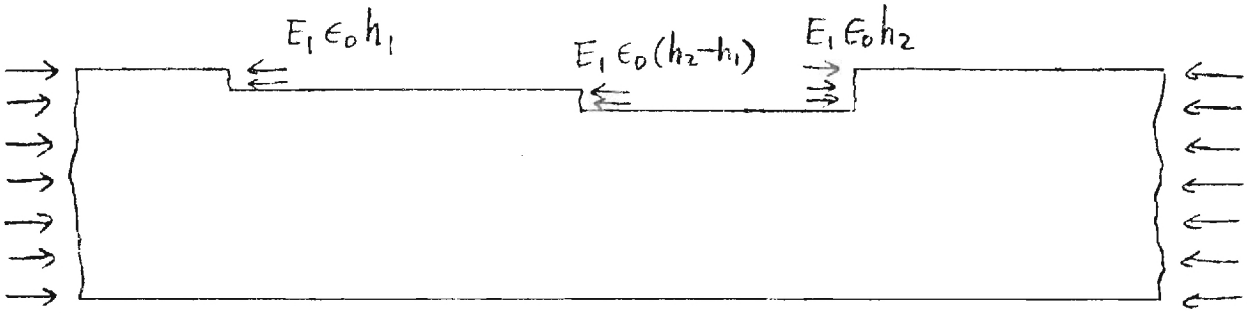

Fig. 6a

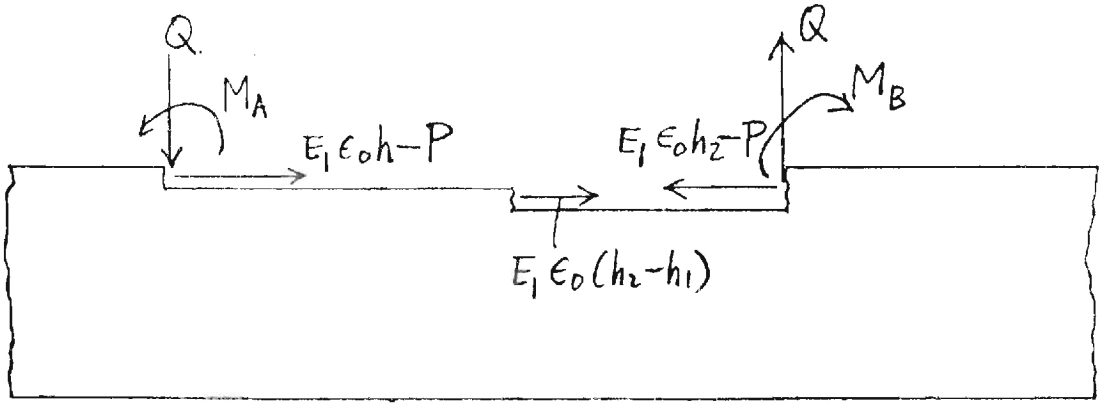

Fig. 6b

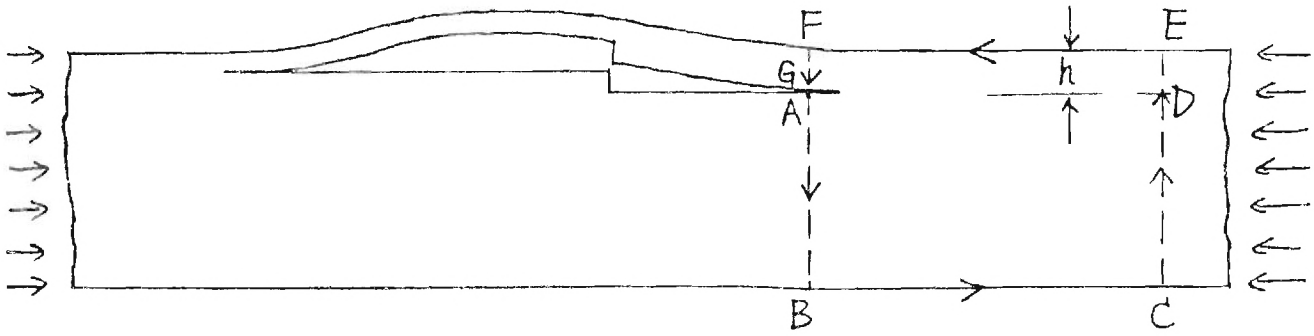

Fig. 7 Path of integration for evaluating the J-integral

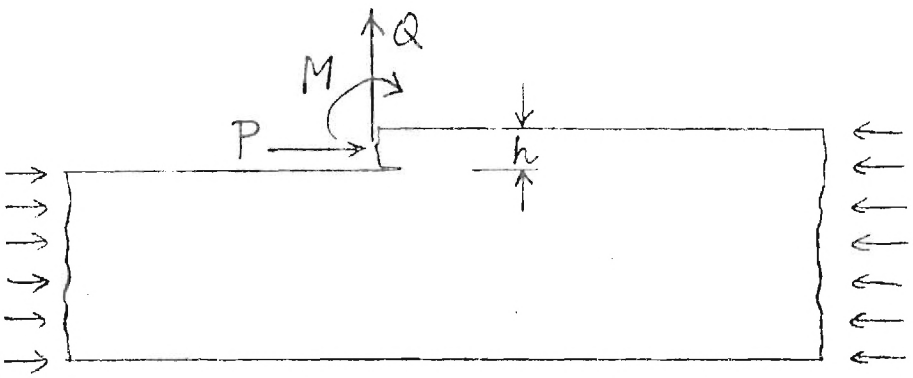

Fig. 8

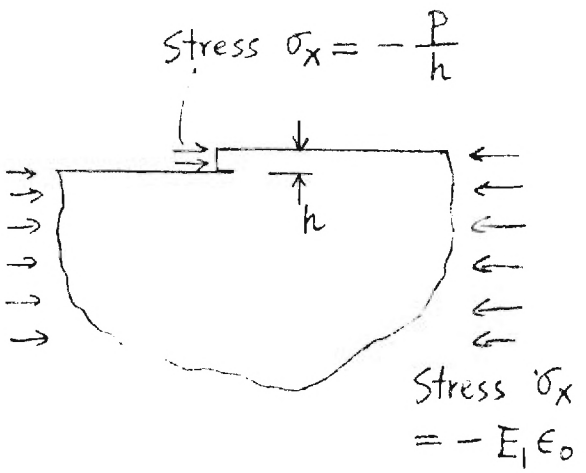

Fig. 9a

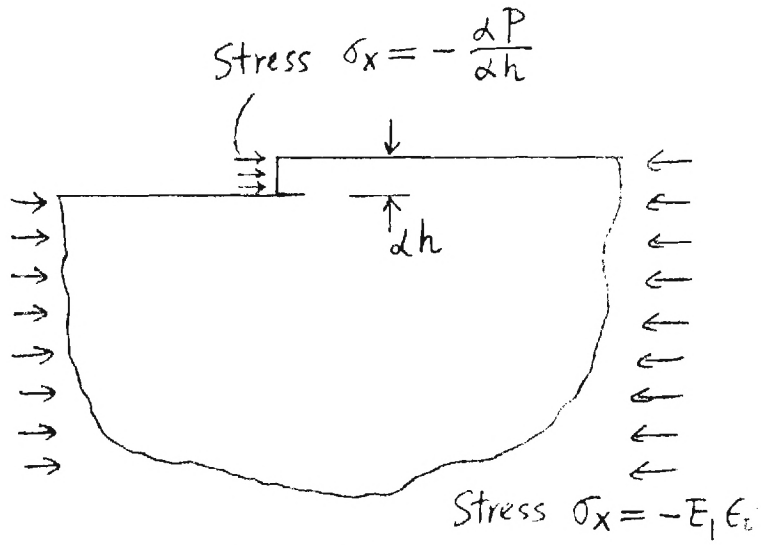

Fig. 9b

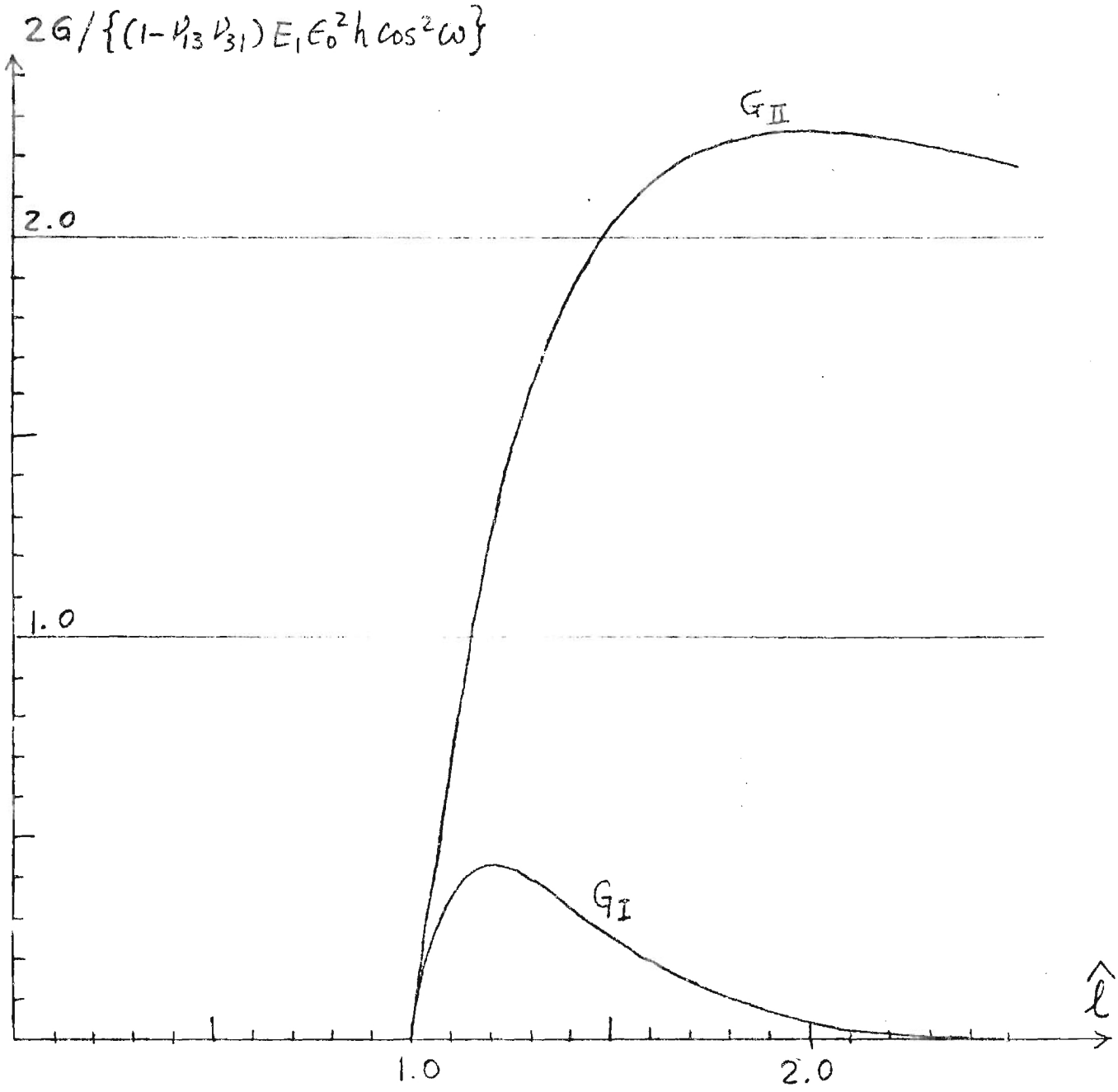

Fig. 10 G_{II} vs. G_I for $\cos\omega = 0.754$

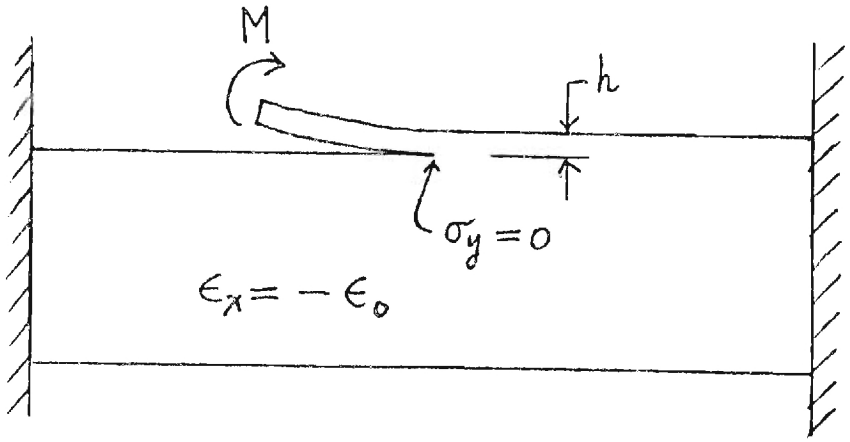

Fig. 11

Georgia Institute of Technology
Atlanta, Georgia 30332

College of Engineering
School of Engineering Science and Mechanics

January 23, 1984

Mr. John N. Dickson
Department 72-77
Mail Zone 399
Lockheed-Georgia Company
Marietta, Georgia 30063

Subject: Research Grant P. O. No. CA08738
Georgia Tech Project No. E-23-624
Summary Report for year 1983

Dear Mr. Dickson:

As the major research effort under the subject grant for the year 1983 has been made during the first three quarters, analytical and computational results have been reported in the previous three quarterly progress reports. A summary of accomplishments with discussions is enclosed. A listing of the computer program used for calculating the interlaminar stress in composite plates subject to central impact loading is included.

Sincerely yours,

R. K. Kunz, Assistant Professor

J.T.S. Wang, Professor

W. L. Yin, Associate Professor

Enclosure(s)
bjm

Lockheed-Georgia Company
Research Grant P. O. No. CA08738
(Georgia Tech Project No. E-23-624)

Damage of Composite Structures

Summary Report for Year 1983

January, 1984

by

R. K. Kunz
J. T. S. Wang
W.-L. Yin

School of Engineering Science and Mechanics
Georgia Institute of Technology
Atlanta, Georgia 30332

Part I

Wave Propagation Due to Impact in Laminated Composite Plates

R. K. Kunz

1. Introduction

During the past year, efforts have been focused on the development and implementation of Fortran computer code for the purpose of determining the dynamic interlaminar stresses in a laminated composite plate subject to central normal impact loading on a free surface. This study is motivated by the conviction that impact-induced delamination is initiated as a result of the stresses which act on interlaminar surfaces exceeding a critical value. Hence, a study of the three-dimensional propagation of stress waves in the vicinity of the impact loading zone will potentially yield valuable information as to the nature of, and the parameters affecting, the delamination phenomenon. By making the analysis sufficiently general, dynamic interlaminar stresses may be calculated for arbitrary geometrical and material parameters, and for arbitrary layer stacking sequences. As a result, the effects of these parameters on interlaminar stress levels, and therefore on the initiation of delamination, may be studied.

Results previously reported for the case of a composite plate subject to line impact loading, and the ensuing two-dimensional propagation of stress waves, have served to verify the analytical and numerical models employed in this work, and to suggest some preliminary conclusions as to the mechanisms involved in the onset of delamination. These results are summarized in [3]. How-

ever, due to the nature of the two-dimensional analysis, only certain stacking sequences may be employed, and some fundamental questions remain unanswered. The present work is aimed toward the more general and realistic case of central impact loading and the resulting three-dimensional wave propagation. Therefore, the limitations inherent in the two-dimensional analysis have been removed, and it is expected that the results obtained will yield additional information on the critical parameters affecting the generation of impact-induced delaminations.

2. Problem Formulation and Numerical Solution Procedure

The geometry of the problem under consideration is shown in Figure 1. The plate consists of N orthotropic layers, each with its principal orthotropic axes at an arbitrary orientation in the $x_1 - x_3$ plane. There are M = N + 1 interlaminar planes, with m = 0 corresponding to the impact surface, and m = N corresponding to the bottom free surface. A general layer n is bounded by interfaces m = n - 1 and m = n.

The analysis leading up to the numerical calculations has been developed in detail in previous reports [1,2], and will be summarized here for the sake of completeness:

i) A set of six approximate equations of motion for layer n are obtained. These are cast in the form of differential equations in terms of the interlaminar stresses and displacements on the bounding surfaces m = n - 1 and m = n. Hence, the unknowns are the three displacement components u_1, u_2, u_3 and the three stress components τ_{22}, τ_{12}, τ_{23} on each of the two surfaces. Each of the unknowns is a function of x_1, x_3, and t.

Figure 1. Plate Geometry

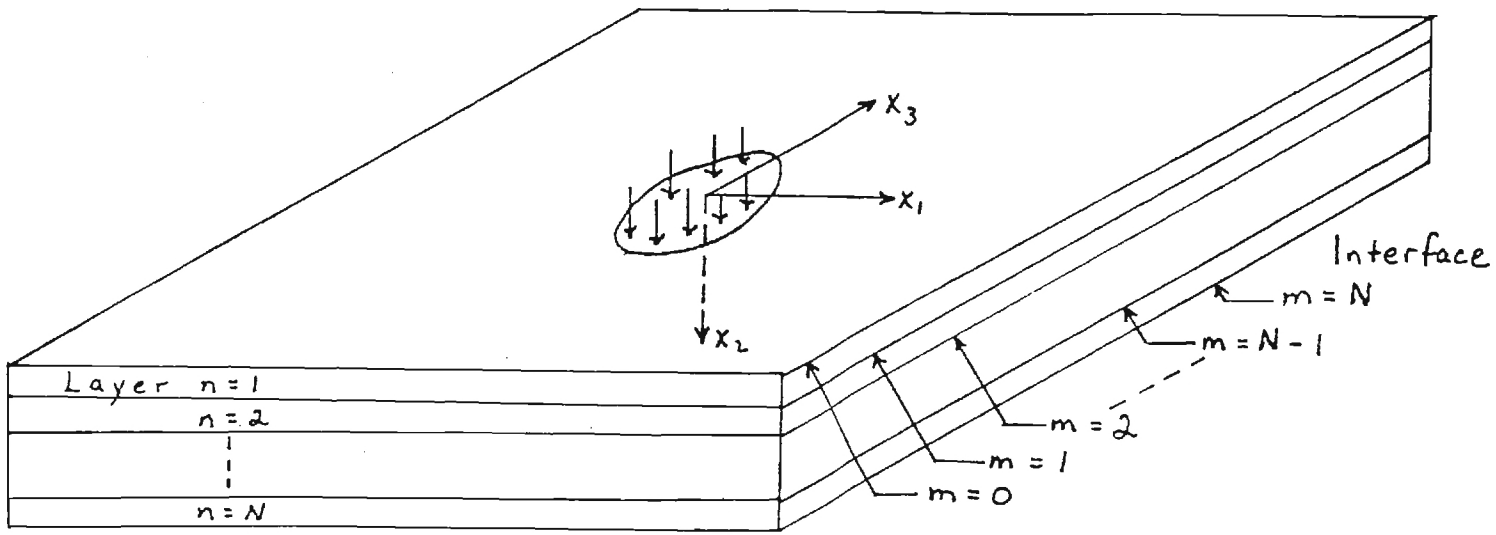

ii) This set of differential equations is transformed using the Laplace transformation in time, and the Fourier transformation in both the x_1 and x_3 directions. The result is a set of six linear algebraic equations corresponding to layer n for the transformed interlaminar stresses and displacements on surfaces m = n - 1 and m = n. The transformed unknowns are related to the physical stresses and displacements through transformations of the form

$$U(k_1, k_3, s) = \int_0^\infty \int_{-\infty}^{\infty} \int_{-\infty}^{\infty} u(x_1, x_3, t) \exp[-st + i(k_1 x_1 + k_3 x_3)] dx_1 \, dx_3 \, dt \qquad (1)$$

where k_1, k_3, s are the transform variables. It should be noted that, during the process of transforming the equations, boundary conditions at x_1 and $x_3 = \pm\infty$ (stresses and displacements vanish) and initial conditions at t = 0 (stresses, displacements, and velocities zero) are explicitly satisfied.

iii) The sets of equations for all N layers are assembled, resulting in a set of 6N algebraic equations for the 6(N + 1) transformed interlaminar stresses and displacements. Continuity of stresses and displacements at the internal interfaces (m = 1 to N - 1) are automatically satisfied.

iv) Boundary conditions at the top and bottom surfaces are appended. These are: on m = N, transformed stresses $T_{22} = 0$, $T_{12} = T_{23} = 0$; on m = 0, $T_{12} = T_{23} = 0$, $T_{22} = \sigma$, where σ is the transform of the impact loading function.

At this point, the problem is completely formulated, and numerical methods must be employed to determine the interlaminar stresses as functions of position and time. These may be briefly summarized as follows:

v) The set of linear algebraic equations is solved repeatedly for the transformed interlaminar stresses and displacements at selected discrete combinations of the transform variables k_1, k_3, and s.

vi) The inverse transforms of the transformed interlaminar stresses are numerically calculated to yield the true interlaminar stresses at discrete values of x_1, x_3, and t.

3. Implementation of Numerical Procedures

3.1 Loading Function. The function chosen to model the applied surface traction on the free surface m = 0 due to normal impact is

$$\sigma(x_1, x_3, t) = \begin{cases} -p_o (1 - 2r^2/a^2 + r^4/a^4)[1 - \cos(2\pi t/t_o)]/2, \\ \qquad 0 < r < a;\ 0 < t < t_o \\ 0, \quad r > a;\ t_o > t;\ t < 0. \end{cases} \tag{2}$$

where $r^2 = x_1^2 + x_3^2$. By inspection, the maximum normal compressive load is p_o, which occurs at r = 0, $t = t_o/2$. For numerical reasons, the function was chosen to have continuous first derivatives with respect to both position and time at its boundaries (r = a, t = 0 and t_o). It is expected that this function will adequately model the applied load due to foreign object impact normal to the plate surface. When transformed by equation (1), the result is

$$\sum(k_1, k_3, t) = 8\pi p_o \{4J_o(ak)/(ak)^2 + [1/(ak) - 8/(ak)^3]J_1(ak)\} * \tag{3}$$

$$(1 - e^{-st_o})[1/s - s/(s^2 + (2\pi/t_o)^2)]/k^2$$

where $k^2 = k_1^2 + k_3^2$, and J_o and J_1 are Bessel functions of the first kind of order zero and one.

3.2 Solution of equations. The set of linear algebraic equations to be solved is in so-called block-tridiagonal form; each group of six equations for a given layer contains only the six unknowns on each of its corresponding bounding surfaces. Because of this form, an efficient algorithm is available for their solution, as discussed in [2]. This is fortunate, since the set of equations must be solved repeatedly in order to obtain the transformed interlaminar stresses for all combinations of the chosen values of k_1, k_3, and s. (Considerations necessary for the selection of the discrete values of the transform variables are defined in the next sub-section). Specifically, if it is desired to obtain values for the stresses at the nodes of an $N_F \times N_F$ grid in the x_1-x_3 plane, for N_L time intervals, solutions to the algebraic equations must be obtained for $N_F^2 N_L$ combinations of k_1, k_3, and s. However, the following symmetries and antisymmetries were observed in the solutions of the equations:

$$T_{22}(k_1, k_3, s) = \bar{T}_{22}(k_1, k_3, \bar{s})$$
$$T_{12}(k_1, k_3, s) = -\bar{T}_{12}(k_1, k_3, \bar{s})$$
$$T_{23}(k_1, k_3, s) = -\bar{T}_{23}(k_1, k_3, \bar{s})$$
$$T_{22}(k_1, k_3, s) = T_{22}(-k_1, -k_3, s)$$
$$T_{12}(k_1, k_3, s) = -T_{12}(-k_1, -k_3, s)$$
$$T_{23}(k_1, k_3, s) = -T_{23}(-k_1, -k_3, s)$$

where $\bar{}$ denotes the complex conjugate. Hence, the set of algebraic equations need be solved only $N_F^2 N_L/4$ times; the solutions for the remaining $3N_F^2 N_L/4$ combinations of the transform are obtained through the above symmetries.

3.3 Transform Inversion. In order to obtain the inter-laminar stresses as functions of position and time, the inverse transforms of the solutions to the algebraic systems must be obtained. By theorems of Fourier and Laplace transforms, the inverses of transformations (1) may be written as

$$u(x_1, x_3, t) = \frac{1}{8\pi^3}\int_{-\infty}^{\infty}\int_{-\infty}^{\infty}\int_{c-i\infty}^{c+i\infty} U(k_1, k_3, s)\exp[st - i(k_1 x_1 + k_3 x_3)]\,ds\,dk_1\,dk_3 \qquad (4)$$

where the Laplace transform variable $s = c - i\omega$ with c a positive constant greater than the real part of the rightmost pole of U. Since the transformed stresses, represented in (4) by U, may be obtained as outlined above at discrete values of k_1, k_3 and s, a discrete form of (4) must be obtained; specifically one which casts the inversion problem into a form for which Fast-Fourier transform methods may be used.

If changes of significance are expected to occur only over distances greater than λ and over times greater than τ, then the largest wave numbers k_1 and k_3 and frequencies ω which need be considered are, respectively

$$Q = 2\pi/\lambda \qquad\qquad \Omega = 2\pi/\tau \qquad (5)$$

and equation (4) may be approximated by an integral over finite ranges:

$$u(x_1, x_3, t) = \frac{1}{8\pi^3} e^{ct}\int_{-Q}^{Q}\int_{-Q}^{Q}\int_{-\Omega}^{\Omega} U(k_1, k_3, s)\exp[-i(\omega t + k_1 x_1 + k_3 x_3)]\,d\omega\,dk_1\,dk_3$$

We shift the intervals of integration to get

$$u(x_1, x_3, t) = \frac{1}{8\pi^3}\exp[ct + i(\Omega t + Q(x_1 + x_3))]\int_0^{2Q}\int_0^{2Q}\int_0^{2\Omega} U(k_1 - Q, k_3 - Q, s + i\Omega) *$$
$$\exp[-i(\omega t + k_1 x_1 + k_3 x_3)]\,d\omega\,dk_1\,dk_3$$

Now we further approximate the integral by a finite summation over N_F intervals in both k_1 and k_3, and N_L intervals in ω; i.e.

$$u(x_1,x_3,t) \doteq \frac{1}{8\pi^3}\exp[ct+i(\Omega t+Q(x_1+x_3))]\sum_{K=0}^{N_L-1}\sum_{I=0}^{N_F-1}\sum_{J=0}^{N_F-1}U(k_I-Q,k_J-Q,s_K+i\Omega)* \exp[-i(\omega t+k_1x_1+k_3x_3)](\Delta k)^2\Delta\omega \tag{6}$$

where $\quad \Delta k = 2Q/N_F \qquad k_I = 2Q(I+.5)/N_F$

$\quad \Delta\omega = 2\Omega/N_F \qquad s_K = c-i2\Omega(I+.5)/N_L$

Equation (6) may hence be written as

$$u(x_1,x_3,t) = \frac{Q^2\Omega}{\pi^3N_F^2N_L}\exp[ct+i[\Omega(1-1/N_L)t+Q(1-1/N_F)(x_1+x_3)]]* \sum_{I=0}^{N_F-1}\sum_{J=0}^{N_F-1}\sum_{K=0}^{N_L-1}U(k_I-Q,k_J-Q,s_K+i\Omega)\exp[-i(\frac{2\Omega}{N_L}Kt+\frac{2Q}{N_F}(Ix_1+Jx_3))] \tag{7}$$

Up to this point x_1, x_3, and t are continuous variables. If we now evaluate these quantities at the discrete points

$$x_1 = x_L = \pi L/Q, \qquad x_3 = x_M = \pi M/Q; \qquad L,M = 0,1,\ldots,N_F-1$$

$$t = t_N = \pi N/\Omega \qquad N = 0,1,\ldots,N_L-1$$

equation (7) becomes, after some rearrangement,

$$u(x_L,x_M,t_N) = \frac{Q^2\Omega}{\pi^3}\exp[c\pi N/\Omega+i\pi[N(1-1/N_L)+(L+M)(1-1/N_F)]]H(L,M,N) \tag{8}$$

where

$$H(L,M,N) = \frac{1}{N_F^2N_L}\sum_{I=0}^{N_F-1}\sum_{J=0}^{N_F-1}\sum_{K=0}^{N_L-1}U(k_I-Q,k_J-Q,s_K+i\Omega)\exp[-i2\pi(KN/N_L+IL/N_F+ +JM/N_F)], \qquad L,M=0,1,\ldots,N_F-1;\ N=0,1,\ldots,N_L-1 \tag{9}$$

Equation (9) has the form of the Inverse Discrete Fourier Transform (IDFT) of the discrete three-dimensional array U. The Fast Fourier Transform algorithm developed by Cooley and Tukey (4) provides an efficient means for calcualting the summations of

equation (9) to yield the array H(L,M,N). The function u is then obtained from equation (8) at discrete values of x_1, x_3 and t.

The above discussion indicates the required values of k_1, k_3, and s for which solutions of the algebraic equations for the transformed interlaminar stresses and displacements must be obtained. Once λ and τ are determined (through consideration of the duration and extent of the loading function and the theoretical wave speeds in the medium), solutions are obtained for all combinatins of

$$k_1,\ k_3 = \frac{4\pi}{\lambda N_F}(I+.5)-2\pi/\lambda, \quad I = 0,1,\ldots,N_F-1$$
$$s = c - i\left[\frac{4\pi}{\tau N_L}(I+.5)-2\pi/\tau\right], \quad I = 0,1,\ldots,N_L-1$$

The inversion procedure then yields the interlaminar stresses at the discrete values

$$x_1,\ x_3 = \lambda J/2, \quad J = 0,1,\ldots,N-1$$
$$t = \tau J/2, \quad J = 0,1,\ldots,N-1.$$

It should be noted that the approximation of the IDFT over the infinite interval effectively replaces the single impact loading function with an infinite array of sources periodic in x_1 and x_3. As a result, calculated values represent the true response only up to

$$x_1,\ x_3 = \lambda(N_F/2-1)/2. \tag{10}$$

That is, true stresses due to the single point source are obtained for only one-half of the values of x_1 and x_3; at values past

the points given by equation (10), disturbances propagating from the fictitious sources are included in the results. Hence, N must be chosen sufficiently large that disturbances have not propagated past this point during the time span of the calculation.

Choice of the parameter c affects the accuracy of the computed result. In theory, c must only exceed the real part of the rightmost pole of U. However, in the numerical calculation, there is a finite range of useful values of c in order to balance round-off errors and aliasing errors for large t in the FFT [5]. It was found that a reasonable amount of trial and error yields an acceptable value of c.

3.4 Programming considerations. The principal effort during the period of this report has been in the development, testing, and refinemem of a Fortran computer program, IMP3D, to carry out the numerical procedures described above. This program is similar in principle to IMP2D, the program for the case of line impact reported previously [3]. However, certain major modifications to the original program were necessitated by the additional complexity of the three-dimensional problem. In particular, computer storage limitations, which were not a critical factor in the two-dimensional case, became a prime consideration in the development of the present program. At this writing, development and testing of IMP3D are completed, several test cases have been run, and a parametric study has been initiated; some of the preliminary results are summarized in the next

section. In its present form, IMP3D can perform the necessary interlaminar stress calculations for a plate of up to six layers ($N = 6$), with up to 8 steps in the x_1 and x_3 directions ($N_F = 16$), and 16 steps in time ($N_L = 16$). While it is acknowledged that most composites contain far more than 6 layers, the purposes of this study should be adequately served by consideration of a relatively small number of layers. For the limiting values of N, N_F, and N_L, approximately 200 K of computer core is required, with an execution time of 300 CPU seconds on Georgia Tech's Cyber computer system.

A documented source listing of IMP3D is included as an Appendix to this report.

4. Preliminary Results and Future Work

The table on the following page summarizes a sampling of the results obtained in a typical run of IMP3D. The results presented are for the interlaminar normal stress τ_{22} on each interface at the location $x_1 = x_3 = 0$ (directly underneath the center of the impact region). These results are consistent with those of the two-dimensional case reported previously. As can be observed from examination of the table, a compressive wave propagates through the thickness to the bottom surface, and is reflected back as a tensile wave. As before, the calculated speed of propagation is very close to the theoretical dilatational wave velocity. This sample of numerical results serves to establish some measure of confidence in the numerical techniques and in their implementation in IMP3D.

At this writing, a parametric study has been initiated in order to determine the effects of plate geometry, material properties, stacking sequence, and load duration and extent on calculated interlaminar normal and shear stress magnitudes. The purpose of thes study is two-fold - first, to identify those parameters which may be adjusted to minimize the critical interlaminar stresses; and second, to determine precisely what are the critical conditions of stress which lead to delamination damage; that is, to arrive at an appropriate stress criterion for failure due to delamination. The identification of such a failure criterion is of primary interest, and will be aided by the following experimental observations:

i) The delaminated area is generally largest at the in-

Table 1

Transverse Propagation of Normal Stress

$\frac{\tau_{12}}{p_0}$	Interface Number						
Time Step	0	1	2	3	4	5	6
0	0.00	0.02	0.07	0.11	0.04	-0.03	0.00
1	-0.50	0.03	0.08	0.06	0.10	0.10	0.00
2	-1.00	-0.51	0.04	0.09	0.11	0.11	0.00
3	-0.50	-1.06	-0.57	0.11	0.13	-0.01	0.00
4	0.00	-0.44	-0.95	-0.61	0.00	0.06	0.00
5	0.00	0.03	-0.37	-0.99	-0.74	0.01	0.00
6	0.00	-0.02	-0.10	-0.39	-0.88	-0.90	0.00
7	0.00	-0.12	-0.09	-0.10	-0.53	-0.72	0.00
8	0.00	-0.48	-0.13	-0.32	0.01	0.49	0.00
9	0.00	-0.03	-0.30	0.05	0.70	0.59	0.00
10	0.00	-0.30	0.27	0.75	0.56	0.19	0.00
11	0.00	0.37	0.67	0.69	0.31	0.01	0.00
12	0.00	0.92	0.78	0.25	0.18	0.17	0.00
13	0.00	0.25	0.54	0.34	0.10	0.18	0.00
14	0.00	-0.34	-0.20	0.36	0.38	-0.09	0.00
15	0.00	-0.42	-0.46	-0.22	0.11	0.32	0.00

Calculations based on the following:

Material constants $E_1 = 20 \times 10^6$ psi $E_2 = 2 \times 10^6$ psi
$\nu_{12} = 0.30$ $\nu_{23} = 0.40$
G_{12} 2×10^6 psi $\ell = 0.055$ lb/in^3

Loading function Duration of load = 1.53 μsec
Radius of loaded region = 0.60 in.

Time step = 0.38 μsec.

terfaces furthest removed from the impact site [6].

ii) After initiation, the delamination spreads longitudinally at the speed of flexural waves [7].

iii) At a given interface, the shape of the delaminated region is elongated in the direction of the fibers in the layer on the side further from the impact site [6,7].

iv) Significant delamination damage only occurs between layers with different fiber orientations [7].

By correlating the computational results for interlaminar stresses from several cases covering a range of parameters with the above qualitative experimental observations, it is hoped that a suitable failure criterion may be ascertained.

Based on preliminary results obtained to date and on experimental observations (i) and (ii) above, the most probable sequence of events for the initiation and spread of the delamination is as follows: damage is initiated directly beneath the impact loading site by tensile normal stresses reflected from the bottom (free) surface of the plate. Delamination spreads longitudinally due to interlaminar shear stress propagating in the plane of the plate as the slower flexural waves develop and spread outward from the impact site.

At this point in the project, some qualitative conclusions and some suggestions for further investigation may be set forth based on early results from the parametric studies. The magnitudes of the interlaminar tensile stresses underneath the impact site have been shown, from the numerical results

obtained so far, to be insensitive to the stacking sequence; regardless of the fiber orientation, the through-thickness modulus (C_{22}) is uniform through the thickness. However, it has been found that maximum tensile stress decreases as the plate thickness increases, for the same impact loading function; by the time the compressive pulse reaches the free surface and is reflected as a tensile wave, the pulse has spread out longitudinally so that, while the total energy contained in the pulse remains constant, it has spread over a larger region resulting in a lower peak tensile stress. While the designer has some control over the overall thickness of the plate, he has no control over the magnitude, size, and extent of the loading function. Further analytical work needs to be done to estimate these loading parameters for a foreign object of given size and kinetic energy impacting a plate with known properties. To this point, the load parameters are input to IMP3D as arbitrary quantities selected by the user. This analysis should be possible as a separate calculation based on a simplified model.

Additional details of the propagation of shear stresses with flexural waves need investigation as the parametric study continues. Due to the nature of the numerical algorithms, and to the wide differences in the speeds of propagation of the different types of waves, it is difficult to see in a single run of IMP3D the effects of both through-thickness and longitudinal propagation. The longer time spans required to see the flexural waves mask the more rapid transverse propagation. Hence, the

immediate continuation of the parametric study will be focused on the shear stresses which develop and propagate longitudinally. Of particular interest will be the directional dependence of the propagation of the largest shear stresses compared with the fiber orientation. It is hoped that this study will exhibit some correlation with one or more of the experimental observations mentioned above, and aid in the identification of a critical stress failure criterion for delamination.

If the preliminary conclusion mentioned above is correct, that delamination is initiated due to the reflected tensile pulse propagating upward from the free surface, two additional areas of extension to the present investigation merit some study. First, it has been suggested that a thin layer of material exhibiting elastic-plastic behavior could be added to the surface to be impacted, thus absorbing some of the impact energy before it is transmitted to the laminate. It should be possible to modify the existing analysis to study the effects on the interlaminar stresses of the addition of such an energy-absorbing layer. This study would require determining an adequate, simple constitutive model for the additive layer, and analysis of how a known impact load on this layer is transmitted to the plate itself. Once this is known, the calculations could proceed unchanged from the present case. Intuitively it would seem that the major factor limiting the effectiveness of this idea of adding an absorbing layer would be the requirement that this layer be relatively thin in practice.

A second possible area of investigation aimed at reducing the effect of the through-thickness normal stresses lies in the insertion within the plate of one or more layers of material with elastic modulus in the thickness direction different from that of the rest of the layers. These additional layers could simply consist of a composite material having a different type of fiber. The addition of such layers could have the effect of attenuating the magnitude of a normal stress pulse propagating through the thickness, for the following reason. When such a pulse reaches a free surface, it is entirely reflected; however, when it reaches an interface between two materials of differing moduli, part of the pulse is reflected and part is transmitted onward into the new material. Hence, the additional layers could have the effect of degrading the intensity of the initial compressive pulse before it reaches the bottom surface and is reflected as a tensile wave. The numerical investigation of this idea could be implemented as a straightforward extension to the current analysis.

In summary, the numerical program for the study of stress wave propagation in composite plates due to impact has been successfully implemented. A parametric study is in progress and will continue. Based on the preliminary results of this study, several qualitative conclusions, as mentioned above, can be made, subject to further verification by the completion of the study. Additional possibilities for areas of investigation have also been suggested and may merit further consideration.

References

1. Kunz, R. K., Wang, J. T. S., and Yin, W.-L., "Damage of Composite Structures", Progress Report for Lockheed Research Grant P.O. No. CY48335, April, 1982.

2. Kunz, R. K., Wang, J. T. S., and Yin, W.-L., "Damage of Composite Structures", Progress Report for Lockheed Research Grant P.O. No. CY48335, June, 1982.

3. Kunz, R. K., Wang, J. T. S., and Yin, W.-L., "Damage of Composite Structures", Final Report for Lockheed Research Grant P.O. No. CY48335, September, 1982.

4. Cooley, J. W., and Tukey, J. W., "An Algorithm for the Machine Calculation of Complex Fourier Series", Mathematics of Computation, Vol. 90, No. 19, April, 1965, pp.297-301.

5. Cooley, J. W., Lewis, P. A. W., and Welch, P. D., "The Fast Fourier Transform Algorithm: Programming Considerations in the Calculation of Sine, Cosine, and Laplace Transforms", Journal of Sound and Vibraion, Vol. 12, 1970, pp. 315-337.

6. Takeda, N., Sierakowsky, R. L., Ross, C. A., and Malvern, L. E., "Delamination-crack Propagation in Ballistically Impacted Glass/Epoxy Composite Laminates", Experimental Mechanics, Vol. 22, No. 1, Jan. 1982, pp 19-25.

7. Dickson, J. N., Private communication, results of experiments run at Lockheed-Georgia Company.

Appendix

A source listing of the Fortran program IMP3D, designed for the calculation of interlaminar stress in a multi-layered composite plate subject to central impact loading, follows. Documentation is included within the program. Notation and variable names follow, as closely as practical, those used in this and in previous reports [1-3].

```
      PROGRAM IMP3D(INPUT,OUTPUT,TAPE5=INPUT,TAPE6=OUTPUT)
C   PROGRAM TO CALCULATE NORMAL AND SHEAR STRESSES ON
C   INTERLAMINAR SURFACES FOR A COMPOSITE LAMINATE
C   SUBJECT TO CENTRAL IMPACT.
      REAL K1,K3,K11,K13,K33,KK,TO(8)
      COMPLEX S,DSS,AA,SIG
      COMPLEX A1,A,AN,BO,B,BN,CO,C,CNM1
      COMPLEX DO2,D1,XO,X,XN,DDO2,DD1(3)
      COMPLEX U,T22(1024,7),T12(1024,7),T23(1024,7)
      COMMON/C1/THETA(8),CC11,CC12,CC13,CC22,CC23,CC33,CC44,CC55,CC66
      COMMON/C2/AA(6,6),BB,K1,K3,K11,K13,K33,DSS,S
      COMMON/C3/A1(3,3),A(3,6,6),AN(3,6),BO(3,3),B(6,6,7),BN(3,3)
      COMMON/C4/CO(3,6),C(3,6,6),CNM1(3,3)
      COMMON/C5/DO2,D1(3),XO(3),X(6,7),XN(3)
      COMMON/C6/C11(8),C12(8),C22(8),C66(8),C13(8),C15(8),C23(8),
     1C25(8),C33(8),C35(8),C44(8),C46(8),C55(8)
      COMMON/C7/C11H(8),C15H(8),C55H(8),C13H(8),C35H(8),C33H(8)
      COMMON/C8/KK,UM,AO,TO,PO,SIG
      COMMON/C9/U(16,16,16),NF,NL,NF2,NL2,MF,ML
C
C   INPUT PARAMETERS
C
C     N = NUMBER OF LAYERS
C     DENS = MASS DENSITY
C     BB = ONE-HALF THICKNESS OF A LAYER
C     THETA(I) = FIBER ORIENTATION IN LAYER I (DEG.)
C     PO = MAXIMUM IMPACT LOAD
C     AO = RADIUS OF IMPACT REGION
C     TO = TIME DURATION OF IMPACT LOAD
C     CC11, ETC. = ORTHOTROPIC ELASTIC CONSTANTS FOR
C                  A LAYER
C     NF, NL = NUMBER OF INTERVALS IN FOURIER AND
C              LAPLACE INVERSIONS (MUST BE EQUAL TO A
C              POWER OF TWO)
C     MF, ML = LOG TO BASE 2 OF NF, NL
C     XS = PARAMETER "LAMBDA" IN FOURIER INVERSIONS
C          (USUALLY SET = AO)
C     TS = PARAMETER "TAU" IN LAPLACE INVERSIONS
C          (USUALLY SET = .5*TO)
C     CC = PARAMETER "C" IN LAPLACE INVERSION
      READ(5,*)N,DENS,BB
      READ(5,*)(THETA(I),I=1,N)
      READ(5,*)PO,AO,TO
      READ(5,*)CC11,CC12,CC13
      READ(5,*)CC22,CC23,CC33
      READ(5,*)CC44,CC55,CC66
      READ(5,*)NF,MF,XS,NL,ML,TS,CC
C   PRINT INPUT VALUES
      BB2=2.*BB
      XS2=XS/2.
      TS2=TS/2.
      WRITE(6,1060)
      WRITE(6,1070)N
      WRITE(6,1080)BB2
      WRITE(6,1090)(THETA(I),I=1,N)
      WRITE(6,1100)AO
      WRITE(6,1110)TO
```

```
      WRITE(6,1120)PO
      WRITE(6,1130)DENS
      WRITE(6,1140)
      WRITE(6,1150)CC11,CC12,CC13
      WRITE(6,1150)CC22,CC23,CC33
      WRITE(6,1170)CC44,CC55,CC66
      WRITE(6,1180)
      WRITE(6,1190)XS2
      WRITE(6,1200)NF
      WRITE(6,1210)TS2
      WRITE(6,1220)NL
      WRITE(6,1230)CC
 1060 FORMAT(1X,11HINPUT DATA:,/)
 1070 FORMAT(3X,19HNUMBER OF LAYERS = ,I1)
 1080 FORMAT(3X,18HLAYER THICKNESS = ,F5.1)
 1090 FORMAT(3X,20HSTACKING SEQUENCE = ,6(F4.0))
 1100 FORMAT(3X,26HRADIUS OF LOADED REGION = ,F8.1)
 1110 FORMAT(3X,19HDURATION OF LOAD = ,F7.2)
 1120 FORMAT(3X,15HMAXIMUM LOAD = ,F5.1)
 1130 FORMAT(3X,10HDENSITY = ,1PE12.4)
 1140 FORMAT(3X,30HORTHOTROPIC ELASTIC CONSTANTS:)
 1150 FORMAT(5X,6HC11 = ,0PF9.4,2X,6HC12 = ,F9.4,2X,6HC13 = ,F9.4)
 1160 FORMAT(5X,6HC22 = ,F9.4,2X,6HC23 = ,F9.4,2X,6HC33 = ,F9.4)
 1170 FORMAT(5X,6HC44 = ,F9.4,2X,6HC55 = ,F9.4,2X,6HC66 = ,F9.4,/)
 1180 FORMAT(1X,24HCOMPUTATIONAL CONSTANTS:,/)
 1190 FORMAT(3X,25HLONGITUDINAL STEP SIZE = ,F8.1)
 1200 FORMAT(3X,28HNO. OF LONGITUDINAL STEPS = ,I2)
 1210 FORMAT(3X,17HTIME STEP SIZE = ,F8.3)
 1220 FORMAT(3X,20HNO. OF TIME STEPS = ,I2)
 1230 FORMAT(3X,5HCC = ,F6.2)
      NF2=NF/2
      NL2=NL/2
C  CALL ROUTINE TO FIND ELASTIC CONSTANTS FOR EACH
C  LAYER IN GLOBAL COORDINATE SYSTEM THROUGH
C  COORDINATE TRANSFORMATION.
      CALL CONST(N)
C  CALCULATE THOSE COEFFICIENTS OF BLOCK-TRIDIAGONAL
C  SYSTEM WHICH ARE INDEPENDENT OF K1, K3, S.
      AA(1,5)=-1./BB
      AA(2,4)=AA(1,5)
      AA(3,6)=AA(1,5)
      AA(4,5)=-3./BB
      AA(5,4)=AA(4,5)
      AA(6,6)=AA(4,5)
      CO(1,5)=AA(1,5)
      CO(2,4)=AA(2,4)
      CO(3,6)=AA(3,6)
      CO(1,4)=(0.,0.)
      CO(1,6)=(0.,0.)
      CO(2,5)=(0.,0.)
      CO(2,6)=(0.,0.)
      CO(3,4)=(0.,0.)
      CO(3,5)=(0.,0.)
      B(1,6,1)=(0.,0.)
      B(3,5,1)=(0.,0.)
      B(1,5,1)=AA(4,5)
      B(2,4,1)=AA(5,4)
```

```
      B(3,6,1)=AA(6,6)
      DOO2=AA(2,4)
      DO1(2)=-AA(5,4)
      NM1=N-1
      IF(N.EQ.2)GO TO 101
      DO 10 I=2,NM1
      IM1=I-1
      B(4,5,IM1)=-AA(1,5)
      B(5,4,IM1)=-AA(2,4)
      B(6,6,IM1)=-AA(3,6)
      B(4,4,IM1)=(0.,0.)
      B(4,6,IM1)=(0.,0.)
      B(5,5,IM1)=(0.,0.)
      B(5,6,IM1)=(0.,0.)
      B(6,4,IM1)=(0.,0.)
      B(6,5,IM1)=(0.,0.)
      C(1,5,IM1)=AA(1,5)
      C(2,4,IM1)=AA(2,4)
      C(3,6,IM1)=AA(3,6)
      C(1,4,IM1)=(0.,0.)
      C(1,6,IM1)=(0.,0.)
      C(2,5,IM1)=(0.,0.)
      C(2,6,IM1)=(0.,0.)
      C(3,5,IM1)=(0.,0.)
      C(3,4,IM1)=(0.,0.)
      A(1,5,IM1)=AA(4,5)
      A(2,4,IM1)=AA(5,4)
      A(3,6,IM1)=AA(6,6)
      A(1,6,IM1)=(0.,0.)
      A(3,5,IM1)=(0.,0.)
      B(1,6,I)=(0.,0.)
      B(3,5,I)=(0.,0.)
      B(1,5,I)=AA(4,5)
      B(2,4,I)=AA(5,4)
   10 B(3,6,I)=AA(6,6)
  101 B(4,5,NM1)=-AA(1,5)
      B(5,4,NM1)=-AA(2,4)
      B(6,6,NM1)=-AA(3,6)
      B(4,4,NM1)=(0.,0.)
      B(4,6,NM1)=(0.,0.)
      B(5,5,NM1)=(0.,0.)
      B(5,6,NM1)=(0.,0.)
      B(6,4,NM1)=(0.,0.)
      B(6,5,NM1)=(0.,0.)
      AN(1,6)=(0.,0.)
      AN(3,5)=(0.,0.)
      AN(1,5)=AA(4,5)
      AN(2,4)=AA(5,4)
      AN(3,6)=AA(6,6)
      KK=6.2831853/XS
      OM=6.2831853/TS
C     OUTER LOOP - FOR ALL VALUES OF K1 TO BE USED
      DO 400 IF1=1,NF
      K1=2.*KK/NF*(IF1-.5)-KK
      K11=K1*K1
C     MIDDLE LOOP - FOR HALF THE VALUES OF K3 TO
C     BE USED.
```

```
      DO 401 IF3=1,NF2
      K3=2.*KK/NF*(IF3-.5)-KK
      K33=K3*K3
C  CALCULATE THOSE COEFFICIENTS OF BLOCK-TRIDIAGONAL
C  SYSTEM WHICH DEPEND ON K1, K3 ONLY.
      K13=K1*K3
      CALL FAA2(1)
      BO(1,2)=-AA(1,2)
      BO(1,3)=AA(1,3)
      BO(2,1)=-AA(2,1)
      BO(2,3)=-AA(2,3)
      BO(3,1)=AA(3,1)
      BO(3,2)=-AA(3,2)
      CO(1,2)=AA(1,2)
      CO(1,3)=AA(1,3)
      CO(2,1)=AA(2,1)
      CO(2,3)=AA(2,3)
      CO(3,1)=AA(3,1)
      CO(3,2)=AA(3,2)
      A1(1,2)=AA(4,2)
      A1(1,3)=-AA(4,3)
      A1(2,1)=AA(5,1)
      A1(2,3)=AA(5,3)
      A1(3,1)=-AA(6,1)
      A1(3,2)=AA(6,2)
      B(1,2,1)=AA(4,2)
      B(1,3,1)=AA(4,3)
      B(1,4,1)=AA(4,4)
      B(2,1,1)=AA(5,1)
      B(2,3,1)=AA(5,3)
      B(2,5,1)=AA(5,5)
      B(2,6,1)=AA(5,6)
      B(3,1,1)=AA(6,1)
      B(3,2,1)=AA(6,2)
      B(3,4,1)=AA(6,4)
      DD1(3)=AA(6,4)
      DD1(1)=AA(4,4)
      IF(N.EQ.2)GO TO 202
      DO 20 I=2,NM1
      CALL FAA2(I)
      IM1=I-1
      B(4,2,IM1)=-AA(1,2)
      B(4,3,IM1)=AA(1,3)
      B(5,1,IM1)=-AA(2,1)
      B(5,3,IM1)=-AA(2,3)
      B(6,1,IM1)=AA(3,1)
      B(6,2,IM1)=-AA(3,2)
      C(1,2,IM1)=AA(1,2)
      C(1,3,IM1)=AA(1,3)
      C(2,1,IM1)=AA(2,1)
      C(2,3,IM1)=AA(2,3)
      C(3,1,IM1)=AA(3,1)
      C(3,2,IM1)=AA(3,2)
      A(1,2,IM1)=AA(4,2)
      A(1,3,IM1)=-AA(4,3)
      A(1,4,IM1)=-AA(4,4)
      A(2,1,IM1)=AA(5,1)
```

```
      A(2,3,IM1)=AA(5,3)
      A(2,5,IM1)=-AA(5,5)
      A(2,6,IM1)=-AA(5,6)
      A(3,1,IM1)=-AA(6,1)
      A(3,2,IM1)=AA(6,2)
      A(3,4,IM1)=-AA(6,4)
      B(1,2,I)=AA(4,2)
      B(1,3,I)=AA(4,3)
      B(1,4,I)=AA(4,4)
      B(2,1,I)=AA(5,1)
      B(2,3,I)=AA(5,3)
      B(2,5,I)=AA(5,5)
      B(2,6,I)=AA(5,6)
      B(3,1,I)=AA(6,1)
      B(3,2,I)=AA(6,2)
   20 B(3,4,I)=AA(6,4)
  202 CALL FAA2(N)
      B(4,2,NM1)=-AA(1,2)
      B(4,3,NM1)=AA(1,3)
      B(5,1,NM1)=-AA(2,1)
      B(5,3,NM1)=-AA(2,3)
      B(6,1,NM1)=AA(3,1)
      B(6,2,NM1)=-AA(3,2)
      CNM1(1,2)=AA(1,2)
      CNM1(1,3)=AA(1,3)
      CNM1(2,1)=AA(2,1)
      CNM1(2,3)=AA(2,3)
      CNM1(3,1)=AA(3,1)
      CNM1(3,2)=AA(3,2)
      AN(1,2)=AA(4,2)
      AN(1,3)=-AA(4,3)
      AN(1,4)=-AA(4,4)
      AN(2,1)=AA(5,1)
      AN(2,3)=AA(5,3)
      AN(2,5)=-AA(5,5)
      AN(2,6)=-AA(5,6)
      AN(3,1)=-AA(6,1)
      AN(3,2)=AA(6,2)
      AN(3,4)=-AA(6,4)
      BN(1,2)=AA(4,2)
      BN(1,3)=AA(4,3)
      BN(2,1)=AA(5,1)
      BN(2,3)=AA(5,3)
      BN(3,1)=AA(6,1)
      BN(3,2)=AA(6,2)
C     INNER LOOP - FOR HALF THE VALUES OF S TO
C     BE USED.
      DO 402 IL=1,NL2
      S=CMPLX(CC,OM-2.*OM/NL*(IL-.5))
      DSS=DENS*S*S
C     CALCULATE THOSE COEFFICIENTS OF BLOCK-TRIDIAGONAL
C     SYSTEM WHICH DEPEND ON K1, K3, S.
      CALL FAA3(1)
      DO 31 J=1,3
      BO(J,J)=AA(J,J)
      CO(J,J)=AA(J,J)
      JP3=J+3
```

```
      A1(J,J)=-AA(JP3,J)
   31 B(J,J,1)=AA(JP3,J)
      IF(N.EQ.2)GO TO 303
      DO 30 I=2,NM1
      CALL FAA3(I)
      IM1=I-1
      DO 32 J=1,3
      JP3=J+3
      B(JP3,J,IM1)=AA(J,J)
      C(J,J,IM1)=AA(J,J)
      A(J,J,IM1)=-AA(JP3,J)
   32 B(J,J,I)=AA(JP3,J)
   30 CONTINUE
  303 CALL FAA3(N)
      DO 33 J=1,3
      JP3=J+3
      B(JP3,J,NM1)=AA(J,J)
      CNM1(J,J)=AA(J,J)
      AN(J,J)=-AA(JP3,J)
   33 BN(J,J)=AA(JP3,J)
      CALL LOAD
      DD2=DD02*SIG
      DO 55 I=1,3
   55 D1(I)=DD1(I)*SIG
C  SOLVE BLOCK-TRIDIAGONAL SYSTEM FOR A SINGLE
C  COMBINATION OF K1, K3, S.  STORE SOLUTION FOR
C  TRANSFORMED STRESSES AT EACH INTERFACE IN ARRAYS
C  T22, T12, T23.
      CALL TRIDIB(N)
      IND1=NL2*(NF2*(IF1-1)+IF3-1)+IL
      DO 403 I=1,NM1
      T22(IND1,I)=X(4,I)
      T12(IND1,I)=X(5,I)
      T23(IND1,I)=X(6,I)
  403 CONTINUE
C  CLOSE INNER LOOP.
  402 CONTINUE
C  CLOSE MIDDLE LOOP.
  401 CONTINUE
C  CLOSE OUTER LOOP.
  400 CONTINUE
      F=8./(TS*XS*XS*NF*NF*NL)
C  THIS SECTION CALLS THE ROUTINE TRANS TO INVERT
C  THE TRANSFORMS OF THE STRESSES.  WHEN COMPLETED,
C  THE ARRAYS T22, T12, T23 CONTAIN THE TRUE STRESSES
C  AT DISCRETE VALUES OF X1, X3, T AT EACH INTERFACE.
      DO 404 L=1,NM1
      DO 405 I=1,NF
      DO 405 J=1,NF2
      DO 405 K=1,NL2
  405 U(I,J,K)=CONJG(T22(NL2*(NF2*(I-1)+J-1)+K,L))
      CALL TRANS(1)
      DO 406 I=1,NF2
      DO 406 J=1,NF2
      DO 406 K=1,NL
  406 T22(NL*(NF2*(1-1)+J-1)+K,L)=F*
     1CEXP(CMPLX(CC*TS*(K-1.)/2.,3.141592654*((NF-1.)/NF*(I+J-2.)+
```

```
     2(NL-1.)/NL*(K-1.))))*CONJG(U(I,J,K))
      DO 407 I=1,NF
      DO 407 J=1,NF2
      DO 407 K=1,NL2
  407 U(I,J,K)=T12(NL2*(NF2*(I-1)+J-1)+K,L)
      CALL TRANS(-1)
      DO 408 I=1,NF2
      DO 408 J=1,NF2
      DO 408 K=1,NL
  408 T12(NL*(NF2*(I-1)+J-1)+K,L)=F*
     1CEXP(CMPLX(CC*TS*(K-1.)/2.,3.141592654*((NF-1.)/NF*(I+J-2.)+
     2(NL-1.)/NL*(K-1.))))*CONJG(U(I,J,K))
      DO 409 I=1,NF
      DO 409 J=1,NF2
      DO 409 K=1,NL2
  409 U(I,J,K)=T23(NL2*(NF2*(I-1)+J-1)+K,L)
      CALL TRANS(-1)
      DO 410 I=1,NF2
      DO 410 J=1,NF2
      DO 410 K=1,NL
  410 T23(NL*(NF2*(I-1)+J-1)+K,L)=F*
     1CEXP(CMPLX(CC*TS*(K-1.)/2.,3.141592654*((NF-1.)/NF*(I+J-2.)+
     2(NL-1.)/NL*(K-1.))))*CONJG(U(I,J,K))
  404 CONTINUE
C  OUTPUT THE INTERLAMINAR STRESSES.
      WRITE(6,1030)
      DO 500 L=1,NM1
      WRITE(6,1010)L
      DO 501 K=1,NL
      KM1=K-1
      WRITE(6,1020)KM1
      DO 502 J=1,NF2
      DO 503 I=1,NF2
  503 TO(I)=REAL(T22(NL*(NF2*(I-1)+J-1)+K,L))
      WRITE(6,1000)(TO(I),I=1,NF2)
  502 CONTINUE
      WRITE(6,*)
  501 CONTINUE
  500 CONTINUE
      WRITE(6,1040)
      DO 504 L=1,NM1
      WRITE(6,1010)L
      DO 505 K=1,NL
      KM1=K-1
      WRITE(6,1020)KM1
      DO 506 J=1,NF2
      DO 507 I=1,NF2
  507 TO(I)=REAL(T12(NL*(NF2*(I-1)+J-1)+K,L))
      WRITE(6,1000)(TO(I),I=1,NF2)
  506 CONTINUE
      WRITE(6,*)
  505 CONTINUE
  504 CONTINUE
      WRITE(6,1050)
      DO 508 L=1,NM1
      WRITE(6,1010)L
      DO 509 K=1,NL
```

```
      KM1=K-1
      WRITE(6,1020)KM1
      DO 510 J=1,NF2
      DO 511 I=1,NF2
  511 TO(I)=REAL(T23(NL*(NF2*(I-1)+J-1)+K,L))
      WRITE(6,1000)(TO(I),I=1,NF2)
  510 CONTINUE
      WRITE(6,*)
  509 CONTINUE
  508 CONTINUE
 1000 FORMAT(7X,8(F9.4))
 1010 FORMAT(3X,14HINTERFACE NO. ,I2,/)
 1020 FORMAT(5X,11HTIME STEP  ,I2,/)
 1030 FORMAT(1X,17HNORMAL STRESS T22,/)
 1040 FORMAT(1X,16HSHEAR STRESS T12,/)
 1050 FORMAT(1X,16HSHEAR STRESS T23,/)
      STOP
      END
```

```
      SUBROUTINE TRANS(L)
C   ROUTINE TO:
C     A) APPLY SYMMETRY CONDITIONS TO DETERMINE VALUES
C        OF TRANSFORMED STRESSES AT THE REMAINING
C        COMBINATIONS OF K1, K3, S  AND
C     B) INVERT THE TRANSFORMS USING THE FAST FOURIER
C        TRANSFORM ALGORITHM.
      INTEGER IWK(5)
      COMPLEX U,CWK(16)
      COMMON/C9/U(16,16,16),NF,NL,NF2,NL2,MF,ML
C   APPLY SYMMETRY CONDITIONS TO FILL OUT ARRAY U.
      DO 1 I=1,NF
      DO 1 J=1,NF2
      DO 1 K=1,NL2
    1 U(I,J,NL-K+1)=CONJG(U(I,J,K))*L
      DO 2 K=1,NL
      DO 2 I=1,NF
      DO 2 J=1,NF2
    2 U(NF-I+1,NF-J+1,K)=U(I,J,K)*L
C   INVERT THE THIRD SUBSCRIPT (S-INVERSION)
      DO 25 I=1,NF
      DO 25 J=1,NF
      DO 15 K=1,NL
      CWK(K)=U(I,J,K)
   15 CONTINUE
      CALL FFT2C(CWK,ML,IWK)
      DO 20 K=1,NL
      U(I,J,K)=CWK(K)
   20 CONTINUE
   25 CONTINUE
C   INVERT THE SECOND SUBSCRIPT (K3-INVERSION)
      DO 40 I=1,NF
      DO 40 K=1,NL
      DO 30 J=1,NF
      CWK(J)=U(I,J,K)
   30 CONTINUE
      CALL FFT2C(CWK,MF,IWK)
      DO 35 J=1,NF
      U(I,J,K)=CWK(J)
   35 CONTINUE
   40 CONTINUE
C   INVERT THE FIRST SUBSCRIPT (K1-INVERSION)
      DO 45 J=1,NF
      DO 45 K=1,NL
      CALL FFT2C(U(1,J,K),ML,IWK)
   45 CONTINUE
      RETURN
      END
```

```
      SUBROUTINE LOAD
C     ROUTINE TO CALCULATE THE TRANSFORM OF THE
C     LOADING FUNCTION AT PARTICULAR VALUES OF
C     K1, K3, S.  MMBSJ0 AND MMBSJ1 ARE IMSL
C     FUNCTION SUBPROGRAMS TO CALCULATE THE
C     BESSEL FUNCTIONS.
      COMPLEX SIG,S,DSS,AA
      REAL K1,K3,K11,K33,K13,K,KK,MMBSJ0,MMBSJ1
      COMMON/C2/AA(6,6),BB,K1,K3,K11,K13,K33,DSS,S
      COMMON/C8/KK,OM,A0,T0,P0,SIG
      K=SQRT(K11+K33)
      AK=A0*K
      SIG=25.13274123*P0/(K*K)*(4./(AK*AK)*MMBSJ0(AK,IER)+
     1(1./AK-8./(AK*AK*AK))*MMBSJ1(AK,IER))*(1.-CEXP(-S*T0))*
     2(1./S-S/(S*S+39.47842/(T0*T0)))
      RETURN
      END
```

```
      SUBROUTINE CONST(N)
C   ROUTINE TO APPLY COORDINATE TRANSFORMATIONS
C   TO CALCULATE THE ELASTIC CONSTANTS FOR THE
C   X1, X2, X3 COORDINATE SYSTEM FOR EACH OF THE
C   N LAYERS.
      COMMON/C1/THETA(8),CC11,CC12,CC13,CC22,CC23,CC33,CC44,CC55,CC66
      COMMON/C6/C11(8),C12(8),C22(8),C66(8),C13(8),C15(8),C23(8),
     1C25(8),C33(8),C35(8),C44(8),C46(8),C55(8)
      COMMON/C7/C11H(8),C15H(8),C55H(8),C13H(8),C35H(8),C33H(8)
      PI=4.*ATAN(1.)
      DO 1 I=1,N
      THETA(I)=THETA(I)*PI/180.
      CT=COS(THETA(I))
      ST=SIN(THETA(I))
      CS=CT*ST
      CT=CT*CT
      ST=ST*ST
      C11(I)=CC11*CT*CT+2.*CT*ST*(CC13+2.*CC55)+CC33*ST*ST
      C12(I)=CC12*CT+CC23*ST
      C22(I)=CC22
      C66(I)=CC66*CT+CC44*ST
      C13(I)=CT*ST*(CC11-4.*CC55+CC33)+CC13*(CT*CT+ST*ST)
      C15(I)=CT*CS*(CC13-CC11+2.*CC55)+ST*CS*(CC33-CC13-2.*CC55)
      C23(I)=CC12*ST+CC23*CT
      C25(I)=CS*(CC23-CC12)
      C33(I)=CC11*ST*ST+ST*CT*(2.*CC12+4.*CC55)+CC33*CT*CT
      C35(I)=ST*CS*(CC13-CC11+2.*CC55)+CT*CS*(CC33-CC13-2.*CC55)
      C44(I)=CC66*ST+CC44*CT
      C46(I)=CS*(CC44-CC66)
      C55(I)=CT*ST*(CC11-2.*CC13-2.*CC55+CC33)+CC55*(CT*CT+ST*ST)
      C11H(I)=C11(I)-C12(I)*C12(I)/C22(I)
      C15H(I)=C15(I)-C12(I)*C25(I)/C22(I)
      C55H(I)=C55(I)-C25(I)*C25(I)/C22(I)
      C13H(I)=C13(I)-C12(I)*C23(I)/C22(I)
      C35H(I)=C35(I)-C23(I)*C25(I)/C22(I)
    1 C33H(I)=C33(I)-C23(I)*C23(I)/C22(I)
      RETURN
      END
```

```
      SUBROUTINE FAA2(I)
C   ROUTINE TO CALCULATE CERTAIN COEFFICIENTS (I.E.,
C   THOSE DEPENDING ON K1, K3 ONLY) OF THE EQUATIONS
C   OF MOTION FOR LAYER I.  THESE ARE THEN PASSED TO
C   THE MAIN PROGRAM FOR INSERTION INTO THE BLOCK-
C   TRIDIAGONAL SYSTEM.
      COMPLEX AA
      REAL K1,K3,K11,K13,K33
      COMMON/C2/AA(6,6),BB,K1,K3,K11,K13,K33
      COMMON/C6/C11(8),C12(8),C22(8),C66(8),C13(8),C15(8),C23(8),
     1C25(8),C33(8),C35(8),C44(8),C46(8),C55(8)
      COMMON/C7/C11H(8),C15H(8),C55H(8),C13H(8),C35H(8),C33H(8)
      AA(1,2)=CMPLX(0.0,(C12(I)*K1+C25(I)*K3)/BB)
      AA(1,3)=C15(I)*K11+(C13(I)+C55(I))*K13+C35(I)*K33
      AA(2,1)=CMPLX(0.0,(C66(I)*K1+C46(I)*K3)/BB)
      AA(2,3)=CMPLX(0.0,(C46(I)*K1+C44(I)*K3)/BB)
      AA(3,1)=C15(I)*K11+(C55(I)+C13(I))*K13+C35(I)*K33
      AA(3,2)=CMPLX(0.0,(C25(I)*K1+C23(I)*K3)/BB)
      AA(4,2)=CMPLX(0.0,-3.*(C46(I)*K3+C66(I)*K1)/BB)
      AA(4,3)=C15H(I)*K11+(C13H(I)+C55H(I))*K13+C35H(I)*K33+
     13.*C46(I)/(BB*BB)
      AA(4,4)=CMPLX(0.0,(C12(I)*K1+C25(I)*K3)/C22(I))
      AA(5,1)=CMPLX(0.0,-3.*(C12(I)*K1+C25(I)*K3)/BB)
      AA(5,3)=CMPLX(0.0,-3.*(C23(I)*K3+C25(I)*K1)/BB)
      AA(5,5)=CMPLX(0.0,K1)
      AA(5,6)=CMPLX(0.C,K3)
      AA(6,1)=C15H(I)*K11+(C55H(I)+C13H(I))*K13+C35H(I)*K33+
     13.*C46(1)/(BB*BB)
      AA(6,2)=CMPLX(0.0,-3.*(C44(I)*K3+C46(I)*K1)/BB)
      AA(6,4)=CMPLX(0.0,(C25(I)*K1+C23(I)*K3)/C22(I))
      RETURN
      END
```

```
      SUBROUTINE FAA3(I)
C   ROUTINE TO CALCULATE CERTAIN COEFFICIENTS (I.E.,
C   THOSE DEPENDING ON K1, K3, AND S) OF THE EQUATIONS
C   OF MOTION FOR LAYER I.  THESE ARE THEN PASSED TO
C   THE MAIN PROGRAM FOR INSERTION INTO THE BLOCK-
C   TRIDIAGONAL SYSTEM.
      COMPLEX AA,DSS
      REAL K1,K3,K11,K13,K33
      COMMON/C2/AA(6,6),BB,K1,K3,K11,K13,K33,DSS
      COMMON/C6/C11(8),C12(8),C22(8),C66(8),C13(8),C15(8),C23(8),
     1C25(8),C33(8),C35(8),C44(8),C46(8),C55(8)
      COMMON/C7/C11H(8),C15H(8),C55H(8),C13H(8),C35H(8),C33H(8)
      AA(1,1)=C11(I)*K11+3.*C15(I)*K13+C55(I)*K33+DSS
      AA(2,2)=C66(I)*K11+C46(I)*K13+C44(I)*K33+DSS
      AA(3,3)=C55(I)*K11+3.*C35(I)*K13+C33(I)*K33+DSS
      AA(4,1)=C11H(I)*K11+3.*C15H(I)*K13+C55H(I)*K33+
     13.*C66(I)/(BB*BB)+DSS
      AA(5,2)=3.*C22(I)/(BB*BB)+DSS
      AA(6,3)=C55H(I)*K11+3.*C35H(I)*K13+C33H(I)*K33+
     13.*C44(I)/(BB*BB)+DSS
      RETURN
      END
```

```
      SUBROUTINE TRIDIB(N)
C  ROUTINE TO SOLVE THE BLOCK-TRIDIAGONAL SYSTEM OF
C  EQUATIONS.
      COMPLEX QO(3,6),Q(6,6,6),QNM1(6,3)
      COMPLEX P(6,6,7),PN(3,3)
      COMPLEX A1,A,AN,BO,B,BN,CO,C,CNM1,A6,B6,Y
      COMPLEX DO2,D1,XO,X,XN,DUM
      COMMON/GSS/A6(6,6),B6(6),Y(6)
      COMMON/C3/A1(3,3),A(3,6,6),AN(3,6),BO(3,3),B(6,6,7),BN(3,3)
      COMMON/C4/CO(3,6),C(3,6,6),CNM1(3,3)
      COMMON/C5/DO2,D1(3),XO(3),X(6,7),XN(3)
C  FORWARD SOLVE
C  PO = BO
C  CALCULATE QO.
      DO 48 M=1,6
      DO 49 I=1,3
      DO 50 J=1,3
   50 A6(I,J)=BO(I,J)
   49 B6(I)=CO(I,M)
      CALL GAUSS(3)
      DO 51 I=1,3
   51 QO(I,M)=Y(I)
   48 CONTINUE
C  CALCULATE P(1)
      DO 4 I=1,3
      DO 4 J=1,6
      DUM=(0.,0.)
      DO 5 L=1,3
    5 DUM=DUM+A1(I,L)*QO(L,J)
    4 P(I,J,1)=B(I,J,1)-DUM
      DO 400 I=4,6
      DO 400 J=1,6
  400 P(I,J,1)=B(I,J,1)
      IF(N.EQ.2)GO TO 52
      NM2=N-2
C  CALCULATE THE Q'S
      DO 6 K=1,NM2
      DO 7 M=1,6
      DO 8 I=1,6
      DO 8 J=1,6
    8 A6(I,J)=P(I,J,K)
      DO 9 I=1,3
    9 B6(I)=(0.,0.)
      DO 900 I=1,3
  900 B6(I+3)=C(I,M,K)
      CALL GAUSS(6)
      DO 10 I=1,6
   10 Q(I,M,K)=Y(I)
    7 CONTINUE
C  CALCULATE THE P'S
      KP1=K+1
      DO 11 I=1,3
      DO 11 J=1,6
      DUM=(0.,0.)
      DO 12 L=1,6
   12 DUM=DUM+A(I,L,K)*Q(L,J,K)
   11 P(I,J,KP1)=B(I,J,KP1)-DUM
```

```
      DO 110 I=4,6
      DO 110 J=1,6
  110 P(I,J,KP1)=B(I,J,KP1)
    6 CONTINUE
   52 NM1=N-1
C  CALCULATE Q(N-1)
      DO 13 M=1,3
      DO 14 I=1,6
      DO 14 J=1,6
   14 A6(I,J)=P(I,J,NM1)
      DO 15 I=1,3
   15 B6(I)=(0.,0.)
      DO 150 I=1,3
  150 B6(I+3)=CNM1(I,M)
      CALL GAUSS(6)
      DO 16 I=1,6
   16 QNM1(I,M)=Y(I)
   13 CONTINUE
C  CALCULATE P(N)
      DO 17 I=1,3
      DO 17 J=1,3
      DUM=(0.,0.)
      DO 18 L=1,6
   18 DUM=DUM+AN(I,L)*QNM1(L,J)
   17 PN(I,J)=BN(I,J)-DUM
C  CALCULATE THE U'S (STORED IN ARRAYS XO, X, XN)
      B6(1)=(0.,0.)
      B6(2)=DO2
      B6(3)=(0.,0.)
      DO 65 I=1,3
      DO 69 J=1,3
   69 A6(I,J)=BO(I,J)
   65 CONTINUE
      CALL GAUSS(3)
      DO 68 I=1,3
   68 XO(I)=Y(I)
      DO 25 I=1,6
      DO 25 J=1,6
   25 A6(I,J)=P(I,J,1)
      DO 26 I=1,3
      DUM=(0.,0.)
      DO 27 L=1,3
   27 DUM=DUM+A1(I,L)*XO(L)
   26 B6(I)=D1(I)-DUM
      DO 260 I=4,6
  260 B6(I)=(0.,0.)
      CALL GAUSS(6)
      DO 28 I=1,6
   28 X(I,1)=Y(I)
      IF(N.EQ.2)GO TO 53
      DO 29 K=2,NM1
      KM1=K-1
      DO 30 I=1,3
      DUM=(0.,0.)
      DO 31 L=1,6
   31 DUM=DUM+A(I,L,KM1)*X(L,KM1)
   30 B6(I)=-DUM
```

```
      DO 300 I=4,6
  300 B6(I)=(0.,0.)
      DO 32 I=1,6
      DO 32 J=1,6
   32 A6(I,J)=P(I,J,K)
      CALL GAUSS(6)
      DO 33 I=1,6
   33 X(I,K)=Y(I)
   29 CONTINUE
   53 DO 34 I=1,3
      DUM=(0.,0.)
      DO 35 L=1,6
   35 DUM=DUM+AN(I,L)*X(L,NM1)
   34 B6(I)=-DUM
      DO 72 I=1,3
      DO 72 J=1,3
   72 A6(I,J)=PN(I,J)
      CALL GAUSS(3)
      DO 73 I=1,3
   73 XN(I)=Y(I)
C  BACKSOLVE
C  CALCULATE THE X'S (WRITTEN OVER THE U'S)
      DO 36 I=1,6
      DUM=(0.,0.)
      DO 37 L=1,3
   37 DUM=QNM1(I,L)*XN(L)+DUM
   36 X(I,NM1)=X(I,NM1)-DUM
      IF(N.EQ.2)GO TO 54
      DO 38 K=2,NM1
      M=N-K
      M1=M+1
      DO 39 I=1,6
      DUM=(0.,0.)
      DO 40 L=1,6
   40 DUM=DUM+Q(I,L,M)*X(L,M1)
   39 X(I,M)=X(I,M)-DUM
   38 CONTINUE
   54 DO 41 I=1,3
      DUM=(0.,0.)
      DO 42 L=1,6
   42 DUM=DUM+Q0(I,L)*X(L,1)
   41 X0(1)=X0(I)-DUM
      RETURN
      END
```

```
      SUBROUTINE GAUSS(N)
C   ROUTINE TO SOLVE AN N*N LINEAR SYSTEM BY
C   GAUSSIAN ELIMINATION.
      COMPLEX A,B,X,R,DUM
      COMMON/GSS/A(6,6),B(6),X(6)
C   FORWARD SOLVE
      DO 1 L=2,N
      LM1=L-1
C   PIVOT THE ROWS
      BIG=CABS(A(LM1,LM1))
      K=LM1
      DO 5 I=L,N
      IF(CABS(A(I,LM1)).GT.BIG)GO TO 6
      GO TO 5
    6 CONTINUE
      K=I
      BIG=CABS(A(I,LM1))
    5 CONTINUE
      DO 7 J=LM1,N
      R=A(K,J)
      A(K,J)=A(LM1,J)
    7 A(LM1,J)=R
      R=B(K)
      B(K)=B(LM1)
      B(LM1)=R
C   ELIMINATE
      DO 8 I=L,N
      A(I,LM1)=A(I,LM1)/A(LM1,LM1)
      DO 9 J=L,N
    9 A(I,J)=A(I,J)-A(I,LM1)*A(LM1,J)
    8 B(I)=B(I)-A(I,LM1)*B(LM1)
    1 CONTINUE
C   BACK SOLVE
      X(N)=B(N)/A(N,N)
      NM1=N-1
      DO 10 II=1,NM1
      I=N-II
      DUM=(0.,0.)
      DO 11 JJ=1,II
      J=N-JJ+1
   11 DUM=DUM+A(I,J)*X(J)
   10 X(I)=(B(I)-DUM)/A(I,I)
      RETURN
      END
```

THE FOLLOWING SUBROUTINE MAY BE A PROPRIETARY PRODUCT AND HAS BEEN PURCHASED OR SUBSCRIBED TO BY GEORGIA TECH FOR OUR CONTROL DATA USERS. ANY REPRODUCTION OF THIS CODE, AS IN A THESIS OR DISSERTATION FOR DUPLICATION OF RESULTS, SHOULD INCLUDE THE FOLLOWING STATEMENTS:

THE LISTED CODE IS PART OF A PROPRIETARY PRODUCT BELONGING TO -----.

THE LISTINGS ARE REPRODUCED WITH THE PERMISSION OF -----.

THE LISTINGS MAY NOT BE EXTRACTED FOR OTHER PURPOSES, OR USED AS THE BASIS FOR ANY SOFTWARE DEVELOPMENT.

IMSL ROUTINE NAME - FFT2C

COMPUTER - CDC/SINGLE

LATEST REVISION - JANUARY 1, 1978

PURPOSE - COMPUTE THE FAST FOURIER TRANSFORM OF A COMPLEX VALUED SEQUENCE OF LENGTH EQUAL TO A POWER TWO

USAGE - CALL FFT2C (A,M,IWK)

ARGUMENTS
- A - COMPLEX VECTOR OF LENGTH N, WHERE N=2**M. ON INPUT A CONTAINS THE COMPLEX VALUED SEQUENCE TO BE TRANSFORMED. ON OUTPUT A IS REPLACED BY THE FOURIER TRANSFORM.
- M - INPUT EXPONENT TO WHICH 2 IS RAISED TO PRODUCE THE NUMBER OF DATA POINTS, N (I.E. N = 2**M).
- IWK - WORK VECTOR OF LENGTH M+1.

PRECISION/HARDWARE - SINGLE AND DOUBLE/H32
- SINGLE/H36,H48,H60

REQD. IMSL ROUTINES - NONE REQUIRED

NOTATION - INFORMATION ON SPECIAL NOTATION AND CONVENTIONS IS AVAILABLE IN THE MANUAL INTRODUCTION OR THROUGH IMSL ROUTINE UHELP

REMARKS 1. FFT2C COMPUTES THE FOURIER TRANSFORM, X, ACCORDING TO THE FOLLOWING FORMULA;

```
X(K+1) = SUM FROM J = 0 TO N-1 OF
         A(J+1)*CEXP((0.0,(2.0*PI*J*K)/N))
FOR K=0,1,...,N-1 AND PI=3.1415...
```

NOTE THAT X OVERWRITES A ON OUTPUT.

2. FFT2C CAN BE USED TO COMPUTE

```
X(K+1) = (1/N)*SUM FROM J = 0 TO N-1 OF
         A(J+1)*CEXP((0.0,(-2.0*PI*J*K)/N))
FOR K=0,1,...,N-1 AND PI=3.1415...
```

BY PERFORMING THE FOLLOWING STEPS;

```
DO 10 I=1,N
```

```
            A(I) = CONJG(A(I))
         10 CONTINUE
            CALL FFT2C (A,M,IWK)
            DO 20 I=1,N
               A(I) = CONJG(A(I))/N
         20 CONTINUE
```

```
      SUBROUTINE  FFT2C (A,M,IWK)
                                  SPECIFICATIONS FOR ARGUMENTS
      INTEGER                     M,IWK(1)
      COMPLEX                     A(1)
                                  SPECIFICATIONS FOR LOCAL VARIABLES
      INTEGER                     I,ISP,J,JJ,JSP,K,K0,K1,K2,K3,KB,KN,MK,MM,MP,N,
     1                            N4,N8,N2,LM,NN,JK
      REAL                        RAD,C1,C2,C3,S1,S2,S3,CK,SK,SQ,A0,A1,A2,A3,
     1                            B0,B1,B2,B3,TWOPI,TEMP,
     2                            ZERO,ONE,Z0(2),Z1(2),Z2(2),Z3(2)
      COMPLEX                     ZA0,ZA1,ZA2,ZA3,AK2
      EQUIVALENCE                 (ZA0,Z0(1)),(ZA1,Z1(1)),(ZA2,Z2(1)),
     1                            (ZA3,Z3(1)),(A0,Z0(1)),(B0,Z0(2)),(A1,Z1(1)),
     2                            (B1,Z1(2)),(A2,Z2(1)),(B2,Z2(2)),(A3,Z3(1)),
     3                            (B3,Z3(2))
      DATA                        SQ/.707106781186557,
     1                            SK/.382683432365097,
     2                            CK/.923879532511297,
     3                            TWOPI/6.28318530717967
      DATA                        ZERO/0.0/,ONE/1.0/
                                  SQ=SQRT2/2,SK=SIN(PI/8),CK=COS(PI/8)
                                  TWOPI=2*PI
                                  FIRST EXECUTABLE STATEMENT
      MP = M+1
      N = 2**M
      IWK(1) = 1
      MM = (M/2)*2
      KN = N+1
                                  INITIALIZE WORK VECTOR
      DO 5  I=2,MP
         IWK(I) = IWK(I-1)+IWK(I-1)
    5 CONTINUE
      RAD = TWOPI/N
      MK = M - 4
      KB = 1
      IF (MM .EQ. M) GO TO 15
      K2 = KN
      K0 = IWK(MM+1) + KB
   10 K2 = K2 - 1
      K0 = K0 - 1
      AK2 = A(K2)
      A(K2) = A(K0) - AK2
      A(K0) = A(K0) + AK2
      IF (K0 .GT. KB) GO TO 10
   15 C1 = ONE
      S1 = ZERO
      JJ = 0
      K = MM - 1
      J = 4
```

```
      IF (K .GE. 1) GO TO 30
      GO TO 70
   20 IF (IWK(J) .GT. JJ) GO TO 25
      JJ = JJ - IWK(J)
      J = J-1
      IF (IWK(J) .GT. JJ) GO TO 25
      JJ = JJ - IWK(J)
      J = J - 1
      K = K + 2
      GO TO 20
   25 JJ = IWK(J) + JJ
      J = 4
   30 ISP = IWK(K)
      IF (JJ .EQ. 0) GO TO 40
                                    RESET TRIGONOMETRIC PARAMETERS
      C2 = JJ * ISP * RAD
      C1 = COS(C2)
      S1 = SIN(C2)
   35 C2 = C1 * C1 - S1 * S1
      S2 = C1 * (S1 + S1)
      C3 = C2 * C1 - S2 * S1
      S3 = C2 * S1 + S2 * C1
   40 JSP = ISP + KB
                                    DETERMINE FOURIER COEFFICIENTS
                                      IN GROUPS OF 4
      DO 50 I=1,ISP
         K0 = JSP - I
         K1 = K0 + ISP
         K2 = K1 + ISP
         K3 = K2 + ISP
         ZA0 = A(K0)
         ZA1 = A(K1)
         ZA2 = A(K2)
         ZA3 = A(K3)
         IF (S1 .EQ. ZERO) GO TO 45
         TEMP = A1
         A1 = A1 * C1 - B1 * S1
         B1 = TEMP * S1 + B1 * C1
         TEMP = A2
         A2 = A2 * C2 - B2 * S2
         B2 = TEMP * S2 + B2 * C2
         TEMP = A3
         A3 = A3 * C3 - B3 * S3
         B3 = TEMP * S3 + B3 * C3
   45    TEMP = A0 + A2
         A2 = A0 - A2
         A0 = TEMP
         TEMP = A1 + A3
         A3 = A1 - A3
         A1 = TEMP
         TEMP = B0 + B2
         B2 = B0 - B2
         B0 = TEMP
         TEMP = B1 + B3
         B3 = B1 - B3
         B1 = TEMP
         A(K0) = CMPLX(A0+A1,B0+B1)
         A(K1) = CMPLX(A0-A1,B0-B1)
         A(K2) = CMPLX(A2-B3,B2+A3)
         A(K3) = CMPLX(A2+B3,B2-A3)
   50 CONTINUE
      IF (K .LE. 1) GO TO 55
      K = K - 2
      GO TO 30
```

```
55 KB = K3 + ISP
                                        CHECK FOR COMPLETION OF FINAL
                                          ITERATION
   IF (KN .LE. KB) GO TO 70
   IF (J .NE. 1) GO TO 60
   K = 3
   J = MK
   GO TO 20
60 J = J - 1
   C2 = C1
   IF (J .NE. 2) GO TO 65
   C1 = C1 * CK + S1 * SK
   S1 = S1 * CK - C2 * SK
   GO TO 35
65 C1 = (C1 - S1) * SQ
   S1 = (C2 + S1) * SQ
   GO TO 35
70 CONTINUE
                                        PERMUTE THE COMPLEX VECTOR IN
                                          REVERSE BINARY ORDER TO NORMAL
                                          ORDER
   IF(M .LE. 1) GO TO 9005
   MP = M+1
   JJ = 1
                                        INITIALIZE WORK VECTOR
   IWK(1) = 1
   DO 75  I = 2,MP
      IWK(I) = IWK(I-1) * 2
75 CONTINUE
   N4 = IWK(MP-2)
   IF (M .GT. 2) N8 = IWK(MP-3)
   N2 = IWK(MP-1)
   LM = N2
   NN = IWK(MP)+1
   MP = MP-4
                                        DETERMINE INDICES AND SWITCH A
   J = 2
80 JK = JJ + N2
   AK2 = A(J)
   A(J) = A(JK)
   A(JK) = AK2
   J = J+1
   IF (JJ .GT. N4) GO TO 85
   JJ = JJ + N4
   GO TO 105
85 JJ = JJ - N4
   IF (JJ .GT. N8) GO TO 90
   JJ = JJ + N8
   GO TO 105
90 JJ = JJ - N8
   K = MP
95 IF (IWK(K) .GE. JJ) GO TO 100
   JJ = JJ - IWK(K)
   K = K - 1
   GO TO 95
100 JJ = IWK(K) + JJ
105 IF (JJ .LE. J) GO TO 110
   K = NN - J
   JK = NN - JJ
   AK2 = A(J)
   A(J) = A(JJ)
   A(JJ) = AK2
   AK2 = A(K)
   A(K) = A(JK)
```

```
      A(JK) = AKZ
  110 J = J + 1
                                    CYCLE REPEATED UNTIL LIMITING NUMBER
                                      OF CHANGES IS ACHIEVED
      IF (J .LE. LM) GO TO 80

 9005 RETURN
      END
```

PART II: Delamination Growth and Residual Strength

by W.-L. Yin, J. T. S. Wang and Z.-Z Fei

A. Summary of Results

The analytical and computational results obtained within the scope of the present project in the year 1983 have been reported in three progress reports (April 1983, July 1983 and October 1983). The major achievements in the subject of delamination growth and residual strength are the following:

(1) The energy-release rate in the growth of a general one-dimensional delamination (i.e., the case in which the thickness of the delaminated layer is not necessarily small in comparison with that of the laminate) has been expressed in terms of the axial forces and bending moments of the postbuckling solution. This algebraic expression generalizes our previous results for a thin-film delamination and it is also based on the method of the J-integral.

(2) On the basis of dimensional analysis, i.e., the invariance of the crack-tip stress field under spatial rescaling, the energy-release rate in the growth of a one-dimensional delamination is separated into its Mode I and Mode II components. The expressions for the two components involve an undetermined function of the thickness ratio of the delamination vs. the laminate. The form of this function depends on the material and should be ascertained either experimentally or by comparison with the closure integrals of finite-element solutions.

(3) Our analysis of the general one-dimensional delamination model is based on the Euler-Bernoulli theory of beam-plates. In order to test the validity and accuracy of the present analysis, we calculate the postbuckling solutions and energy-release rates of a specific delamination model which was previously studied by Whitcomb. The model consists of thin layers of

graphite-epoxy bonded to a relatively thick aluminum plate except for a detached segment of specified length. The postbuckling solutions and the energy-release rates are obtained according to the present theory and the results are compared with Whitcomb's finite-element solutions. Excellent agreement is found in the total energy-release rate.

(4) The unknown material function of the thickness ratio which characterizes the separation of Mode I and Mode II energy-release rates in our theory is also determined by comparison of the present results with the closure integrals of Whitcomb's finite-element analysis. Comparison of several sets of data corresponding to different lengths of delamination yields essentially the same material function. Hence the validity and accuracy of the present analysis is demonstrated, and it is computationally far more economical than the finite-element analysis.

(5) The characteristic equation governing the critical buckling load of a general one-dimensional delamination model is solved for various combinations of thickness ratios and length ratios of the delamination vs. the laminate. These buckling loads are normalized with respect to the corresponding critical loads of perfect beam-plates and the results are presented in graphical form. For a beam-plate with clamped ends, it is found that the presence of a thin or moderately thick delamination significantly reduces the critical buckling load if and only if the length ratio exceeds the thickness ratio.

(6) The change of postbuckling solution with the increase of axial load is studied. Immediately after buckling, the deflections of the upper and lower delaminated layers have the same algebraic sign. For a relatively short delamination, the deflections increase with the axial load until they become excessively large or until delamination growth starts with a sufficiently large energy-release rate. However, if the initial delamination is relatively long,

then as the axial load continues to increase the postbuckling deformation enters into a second phase in which the two delaminated layers deflect in opposite directions. The energy-release rate increases monotonically with theaxial load or with the relative approach of the two ends of the beam-plate. Stability characteristics of delamination growth is determined by the initial length of the delamination and the fracture toughness of the material.

(7) For a clamped circular plate with a concentric circular delamination of arbitrary thickness, the characteristic equation governing the critical axisymmetric buckling load is derived and the solutions are obtained in terms of Bessel functions and their inverse functions. The critical loads are computed for various combinations of the thickness ratios and the radius ratios of the delamination vs. the plate. The non-dimensionalized results are presented in graphical form and the curves are very similar to the corresponding curves of a one-dimensional delamination.

(8) The equations governing the postbuckling deformation of a thin-film circular delamination are derived on the basis of von Karman's nonlinear theory of plates. The system consists of two second order nonlinear ordinary differential equations. With proper non-dimensionalization, all solutions of the problem are reducible to a one-parameter family of numerical solutions. Once started, the growth of a circular thin-film delamination is always catastrophic regardless of whether the in-plane compression is forced-controlled or displacement controlled.

(9) The energy-release rate associated with uniform-expansion growth of a two-dimensional delamination of an arbitrary shape is obtained by means of the surface-independent M-intergral. The result is expressed in terms of a line integral of various terms involving the in-plane normal and shearing forces and

the bending and twisting moments along the boundary of delamination. The formula is applied to the special case of a circular delamination.

B. Implications on Residual Strength

Although the preceding results were obtained for certain delamination models with special geometry and structure and for special types of in-plane loading, they enhance the general understanding of the nature and characteristics of delamination buckling and growth because both the similarities and the differences among the various groups of results can be attributed to the underlying assumptions of the respective models. Our results suggest a few tentative conclusions whose general validity must require further confirmation. These conclusions have special significance with regard to the residual strength of a damaged laminate.

(1) For a thin or moderately thick delamination in a plate with clamped boundary, if the size ratio of the delamination vs. the laminate is smaller than the thickness ratio, then the critical buckling load of the delaminated plate is very close to the critical buckling load of a perfect plate without delamination. Furthermore, once the delaminated plate starts to buckle under the critical buckling load, the plate can sustain only a negligible amount of additional in-plane load before the occurrence of excessive deflection or of catastrophic delamination growth. Hence the failure of a homogeneous plate containing a relatively small and thick delamination is essentially governed by the initiation of buckling, and the critical buckling load is a close lower bound of the residual strength of the damaged laminate.

(2) On the other hand, if the size ratio is greater than the thickness ratio, then the failure of the delaminated plate is generally governed by delamination growth which in turn depends on the fracture toughness of the

material. Postbuckling analysis of an axisymmetrically loaded circular plate with a concentric circular thin-film delamination shows that the growth of a delamination, once started, is always catastrophic, regardless of whether the in-plane load is force-controlled or displacement controlled. Although stable growth of delamination is sometimes found in a one-dimensional delamination model subjected to a displacement-controlled loading, this case is considered rather exceptional because the postbuckling equations of a one-dimensional delamination model is based on the linear plate theory. For a two-dimensional delamination, the governing equations must be based on von Karman's nonlinear theory of plates, and our results for a circular delamination suggest that the in-plane load corresponding to the initiation of delamination growth is the failure load of the laminate. This critical in-plane load depends on the fracture toughness of the material and may be considerably greater than the critical buckling load if the size of the existing delamination is large.

(3) Hence for a laminate containing a relatively large or thin delamination, the estimation of the residual strength requires the solution of the postbucklng problem and the evaluation of the energy-release rates corresponding to various alternative modes of growth. If under a specified in-plane load one can find a mode of delamination growth whose energy-release rate equals the fracture toughness of the material, then this specified in-plane load indicates the residual strength of the laminate.

(4) In contrast to a homogeneous plate, a laminate with a layered structure generally has no prebuckling states. Transverse deflection and bending moments set in as soon as any in-plane load is applied, and delamination growth invariably precedes the failure of the laminate. However, ordinarily the laminate shows weak coupling between membrane and bending behavior, and in such

cases the dependence of the energy-release rate upon the axial load may be close to the corresponding relation for an equivalent homogeneous plate.

(5) As a more realistic modelling of the fracture behavior, it may be necessary to separate the energy-release rate into the Mode I, Mode II and Mode III components and adopt a delamination growth criterion which discriminates the effects of the three components of energy-release rates. Such a program can be developed on the basis of our results because tha separation of the energy-release rate into its model components has been considered in our previous reports.